



UNIVERSITÀ DEGLI STUDI DI MILANO

Scuola di Dottorato in Scienze Biologiche e Molecolari

XXVII Ciclo

# THE ROLE OF MICROTUBULES IN GENE- AND TOXIN- BASED NEURODEGENERATION UNDERLYING PARKINSON'S DISEASE

**Francesca Casagrande**

PhD Thesis

**Scientific tutor: Prof. Graziella Cappelletti**

Academic year: 2014-2015

SSD: BIO/06

Thesis performed at the Department of Biosciences,
Università degli Studi di Milano.

Cover:

NGF-differentiated PC12 cells exposed to 20 mM 2,5-HD:
immunostained for tyrosinated tubulin (red), detyrosinated tubulin (green) and DAPI (blue).

*"An expert is a person who has made all the mistakes*
*that can be made in a very narrow field."*
*Niels Bohr*

*In loving memory of Vittoria Bellucci,*
*whose heart is still beating in our lives.*

*To my brother Luca,*
*who, like every patient, struggles every day*
*hoping in and supporting our efforts in the research.*

# *Index*

## PART III

**Contents**

**Manuscript in preparation**: (Casagrande et al.)

"*PARK2* haploinsufficiency affects microtubule stability in mice"

## SIDE RESEARCHES:

**Published Paper 2**: (Cartelli et al., *Sci Rep*. 2013)

"Microtubule alterations occur early in experimental parkinsonism and the microtubule stabilizer Epothilone D is neuroprotective"

**Manuscript 3**: (Cartelli et al., submitted)

"α-Synuclein is a novel microtubule dynamase"

# *Abbreviation*

| | |
|---|---|
| +TIP | Plus end-tracking protein |
| 2,5-HD (or HD) | 2,5-hexanedione |
| 6-OHDA | 6-hydroxydopamine |
| AR-JP | Autosomal recessive juvenile parkinsonism |
| ATP | Adenosine triphosphate |
| BBB | Blood brain barrier |
| CNS | Central nervous system |
| CS | *Corpus striatum* |
| DA | Dopamine |
| DAT | Dopamine transporter |
| GDP | Guanosine diphosphate |
| GTP | Guanosine triphosphate |
| IBR | In between ring |
| KIF | Kinesin superfamily motor proteins |
| KO | Knockout |
| LB | Lewy body |
| L-dopa | L-3,4-dihydroxyphenylalanine |
| LRRK2 | Leucine-rich repeat kinase 2 also called dardarin protein |
| MAO-B | Monoamine oxidase B |
| MAP | Microtubule associated protein |
| MPP+ | 1-methyl-4-phenylpyridinium |
| MPTP | 1-methyl-4-phenyl-1,2,3,6-tetrahydropyridine |
| MT | Microtubule |
| MTOC | Microtubule-organizing center |
| NF | Neurofilament |
| NF-H | Neurofilament high subunit |
| NF-L | Neurofilament light subunit |
| NF-M | Neurofilament medium subunit |
| NGF | Nerve growth factor |
| *PARK2* | Gene coding for parkin protein |
| $PARK2^{+/-}$ | Heterozygous condition for *PARK2* gene |

| | |
|---|---|
| PD | Parkinson’s disease |
| PINK1 | PTEN-induced putative kinase 1 |
| PTM | Post-translational modification |
| RING | Really interesting new gene |
| ROS | Reactive oxygen specie |
| α-syn | α-synuclein protein |
| PNS | Peripheral nervous system |
| SNpc | *Substantia nigra pars compacta* |
| SNpr | *Substantia nigra pars reticulata* |
| α-Tub | α-tubulin |
| β-Tub | β-tubulin |
| γ-Tub | γ-tubulin |
| Δ2 Tub | Δ2 tubulin |
| Ac Tub | Acetylated tubulin |
| deTyr Tub | Detyrosinated tubulin |
| Tyr Tub | Tyrosinated tubulin |
| TH | Tyrosine hydroxylase |
| TTL | Tubulin tyrosine ligase |
| TTLL | TTL-like proteins |
| UBL | Ubiquitin-like domain |
| UCH-L1 | Ubiquitin carboxyl-terminal hydrolase isoenzyme L1 |
| UPS | Ubiquitin-proteasome system |
| wt | Wild type |

# *Abstract*

Currently, there are just symptomatic treatments available for Parkinson's disease (PD), that is the second most common neurodegenerative disease after Alzheimer's disease and is predicted to increase in prevalence as the world population ages. Its central pathological features is the selective degeneration of dopaminergic neurons in the *Substantia nigra* (SN) *pars compacta* projecting to the *Corpus striatum* (CS), leading to a striatal dopamine deficiency resulting in the typical movement disorders of parkinsonism. Even though the majority of PD cases are sporadic, mutations in a number of genes have been associated with familial PD. It's also known that parkinsonism can be induced by exposure to environmental toxins such as pesticide, chemical compounds and hydrocarbon solvents, including 2,5-hexanedione (2,5-HD), the toxic metabolite of *n*-hexane. 2,5-HD has been shown to induce parkinsonism in animals and humans and to affect directly the cytoskeletal proteins. In particular, microtubules (MTs) have been found to interact with some of the proteins mutated in PD, such as α-synuclein, LRRK2 and parkin, and to be affected by the action of some PD toxins like $MPP^+$ and rotenone. Therefore, in the last years, the MT dysfunction has become an emerging hypothesis in PD pathogenesis. In this scenario, our goal was to investigate the MT dysfunction in neuronal cells, primary skin fibroblasts from PD patients and transgenic mice, taking advantage of both a gene- (using *PARK2* mutations) and toxin- (using 2,5-HD) based models of PD neurodegeneration.

In the first part of the project, nerve growth factor (NGF)-differentiated PC12 cell line has been used as a model of dopaminergic neurons in culture using three different concentrations of toxin (0,2 mM; 2 mM and 20 mM 2,5-HD) for 24 hours, in order to study the early events of neurodegeneration. Thus, the characterization of the effects of 2,5-HD on cytoskeleton has been carried out through both western blot analysis and immunofluorescence techniques, revealing an impact on all its components (actin, neurofilaments and MTs). Subsequently, I focused on MT system through the analysis of different post-translational modified forms of α-tubulin, showing significative MT stabilizing effects of 2,5-HD in both levels and distribution, in particular it could increase the levels of stable MTs that appeared fragmented or accumulated in the cell body. In accordance with these results, the analysis of tubulin polymerization *in cell* revealed a higher content of MT mass caused by 2,5-HD. On the contrary, from our *in vitro* data no significant effects of 2,5-HD emerged in the tested conditions and also the ultrastructure of MTs obtained in the presence of toxin resulted conventional. Interestingly, the first signs of mitochondrial damage, in our experimental

conditions, seemed to be induced only at the highest concentration of 2,5-HD, while strong effects on cytoskeleton came up earlier at lower doses in our cellular model. Following, the effect of 2,5-HD has been tested on skin fibroblasts, obtained from healthy donors and PD patients carrying mutation in *PARK2* gene, since it encodes for parkin, an E3 ubiquitin ligase that is supposed to bind and stabilize MTs. Cell viability was not affected by 2,5-HD whereas cell morphology appeared significantly modified just in PD patient fibroblasts. Moreover, we found that cytoskeletal organization and stability were affected, with a consequent alteration of cell morphology and behaviour, in PD patient cells already at baseline conditions without the addition of any stressor: all parkinsonian fibroblasts showed a reduced MT mass and displayed significant changes in MT stability-related signalling pathways, without any activation of autophagy or apoptosis. This shows for the first time that MT dysfunction occurs in patients and not only in experimental models of PD. The PD fibroblasts were also much more susceptible to 2,5-HD effects than healthy controls, suggesting that the genetic background may really make the difference in MT susceptibility to environmental factors. Consistent with this hypothesis, we observed the increase of fragmentation of stable MTs in *PARK2* patient-derived ventral midbrain neurons.

The second part of the project has been dedicated to *in vivo* experiments in wild type and *PARK2* heterozygous ($PARK2^{+/-}$) mice. In fact, although *PARK2* mutations are responsible for a familial early-onset autosomal recessive form of PD, some individuals carrying heterozygous mutations, usually asymptomatic, have been found to present nigrostriatal abnormalities, making *PARK2* haploinsufficiency a possible risk factor for developing the late-onset disease or other neurological disorder. Biochemical analysis of the cytoskeletal protein level in lysates from SN and CS and confocal microscopy on immunostained brain slices have revealed that the MT system is more dynamic in $PARK^{+/-}$ mice respect to wt ones. In addition, we evaluated the motor behaviour of these mice using a video-tracking system mounted above open field cages. Surprisingly, we found the heterozygous mice were significantly more active than wt ones. Finally, we have found no cell loss in both genetic backgrounds or terminal loss in the CS after treatment. The imbalance of post-translationally modified tubulins, that are associated with differences in MT stability, occurs also in *PARK2* knockout mice and precedes the block of mitochondrial transport.

Our data showed that *PARK2* mutations or haploinsufficiency impacts MT system *in vivo*, unravelling parkin as a regulator of MT stability in neurons and suggesting a key role for MT dysfunction in the PD selectively dopaminergic neurodegeneration.

# PART I

# State of art

## 1.1 Microtubule function and dysfunction in neurons

The ability of eukaryotic cells to adopt a variety of shapes and to carry out coordinated and directed movements depends on a complex network of protein filaments that extends throughout the cytoplasm. This network is called the cytoskeleton, although, unlike a skeleton made of bone, it is highly dynamic structure that reorganizes continuously as the cell changes shape, divides and responds to its environment. The cytoskeleton was once thought to be a feature only of eukaryotic cells, but homologues to all the major proteins of the eukaryotic cytoskeleton have been found also in prokaryotes (Shih and Rothfield 2006). The diverse activities of the cytoskeleton depend on three types of protein filaments: microfilaments, intermediate filaments and microtubules. Each type of filament is formed from a different protein subunit: actin for microfilaments, tubulin for microtubules, and a family of related fibrous proteins for intermediate filaments.

Actin filaments (also known as microfilaments) are two-stranded helical polymers of the protein actin. They appear as flexible structures, with a diameter of 5–9 nm. Actin filaments are also dynamic structures, but they normally exist in bundles or networks rather than as single filaments. A layer called the cortex is formed just beneath the plasma membrane from actin filaments and a variety of actin-binding proteins. This actin-rich layer controls the shape and surface movements of most animal cells, especially through the interaction with specific motor proteins like myosins (Alberts et al. 2008). Different isoforms, each codified by a different gene, exist, but in neurons the most abundant isoform is the β-actin (42 kDa) (Kandel et al., 2003).

Intermediate filaments are strong rope-like polymers of fibrous polypeptides with a diameter of around 10 nm that differ in the type of polypeptide they contain. Their function is to resist stretch and to play a structural or tension-bearing role in the cell. A variety of cell- and tissue-specific forms of intermediate filament proteins, which constitute a large and heterogeneous family, are known. Nerve cells contain a variety of unique intermediate filaments, which are expressed in different regions of the nervous system or at specific stages of development. By far the most abundant are the neurofilaments (NFs), which extend along the length of an axon and form its primary cytoskeletal component, especially in mature nerve cells. In mammals, three NF proteins have long been recognized: termed NF-L, NF-M, and NF-H, for low (70 kDa), middle (160 kDa), and high (200 kDa) molecular weight, respectively. In each NF, all

three subunits are usually present. NFs in axons are linked side by side by their carboxyl-terminal tail domains to provide a continuous rope of filaments that can be a meter or more in length. NF proteins are synthesized within the cell body, and hence they must travel along the axon to reach their final destination (Alberts et al. 2008).

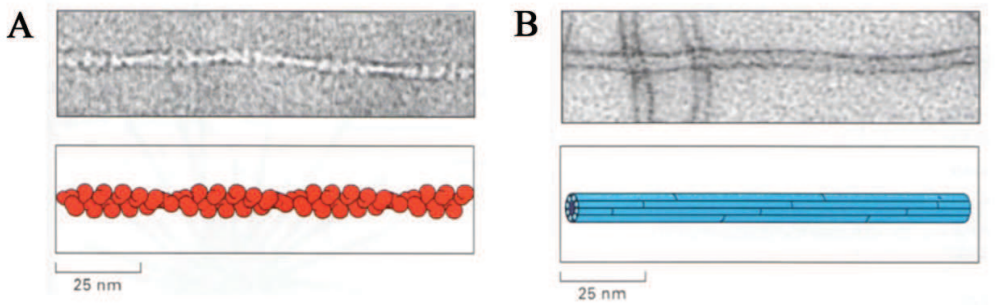


**Figure 1. Actin and intermediate filaments structure.**
Ultrastructure of (A) microfilaments and (B) intermediate filaments by electron microscopy and a schematic drawing. (modified from Alberts et al., 2008)

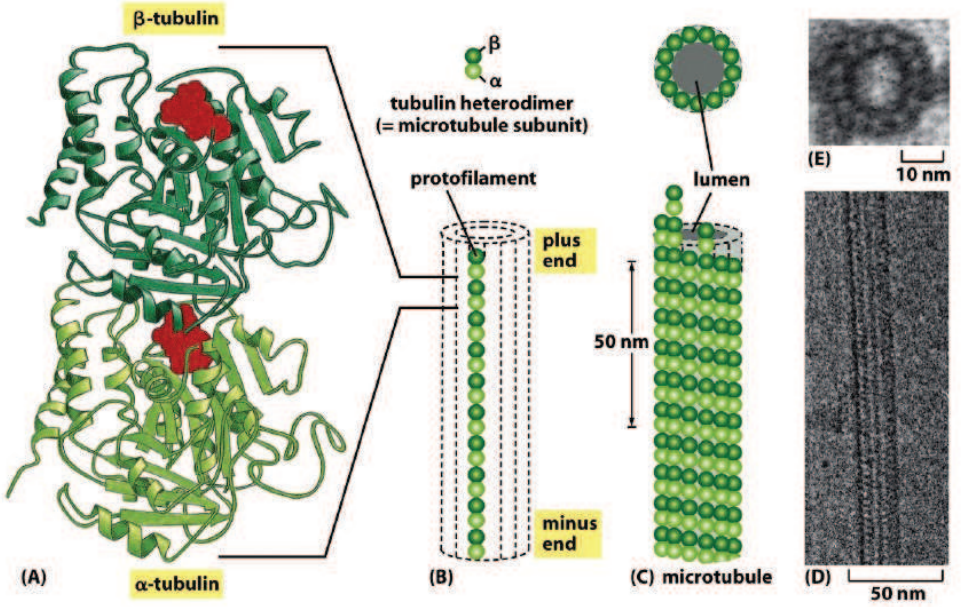


**Figure 2. From tubulin molecules to a microtubule.**
Schematic representation of (A) α/β-tubulin heterodimer, that is the building block of (B) protofilaments that, in turn, associate laterally to form a (C) MT as a hollow tube. Also the ultrastructure by electron microscopy is shown (D). (from Alberts et al., 2008)

Microtubules (MTs) are non-covalent cytoskeletal polymers, that are involved in mitosis, cell motility, intracellular transport, secretion, maintenance of cell shape and cell polarization. They are polarized structures composed of α- and β-tubulin heterodimer subunits assembled

into linear protofilaments in a head-to-tail fashion. The sequence and structure of tubulins have been especially highly conserved throughout the evolution, resulting in a molecular weight of 50 kDa for each monomer that is linked to one another in a non-covalent manner. A single MT is comprised of 10–15 protofilaments (usually 13 in mammalian cells) that associate laterally to form a 25 nm wide hollow cylinder (figure 2) (Desai and Mitchison 1997). The head-to-tail association of the α/β heterodimers makes MTs polar structures, and they have different polymerization rates at the two ends. In each protofilament, the α/β heterodimers are oriented with their β-tubulin monomer pointing towards the faster-growing end (plus end) and their α-tubulin monomer exposed at the slower-growing end (minus end). The lateral interaction between subunits of adjacent protofilaments has been described as a B-type lattice with a seam.

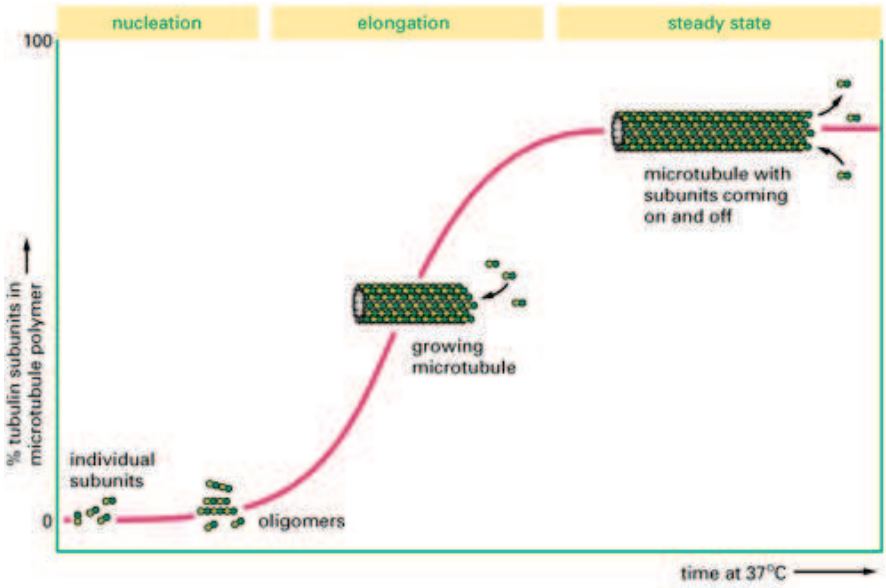


**Figure 3. The polymerization curve of pure tubulin *in vitro*.**
The amount of MT polymers, measured by light scattering, follows a sigmoidal curve. The three typical phase of polymerization are specified: nucleation, elongation and steady state. For simplicity, subunits are shown coming on and off the MT at only one end. (from Alberts et al., 2008)

The assembly of a protein into a long helical polymer such as a cytoskeletal filament typically shows the particular time course. MT polymerization and depolymerization are complex and interesting processes with important biological roles. It's possible to follow the kinetics of pure tubulin polymerizing into MTs *in vitro* at 37°C as long as $Mg^{2+}$ and GTP are present by light scattering measurements. The resulting polymerization curve shows an initial lag phase, that corresponds to time taken for nucleation, after which MTs form rapidly (elongation) until

a plateau level (steady state) of polymerization is reached (Fig. 3). During the lag phase individual tubulin molecules associate to form metastable aggregates, some of which act as a nucleus for polymerization. The assembly of a nucleus is relatively slow, which explains the lag phase seen during polymerization. The lag phase reflects a kinetic barrier to the nucleation process and can be reduced or abolished entirely by adding pre-made nuclei, such as fragments of already polymerized MTs. During the rapid elongation phase, subunits add to the free ends of existing MTs. When the plateau of polymerization is reached, however, not all the heterodimers of the tubulin will have polymerized because subunits are dissociating (depolymerizing) from the ends of MTs as well as adding to them. The rate of polymerization drops with time because this rate is proportional to the concentration of free tubulin; during the plateau phase, polymerization and depolymerization are balanced because the amount of free tubulin has dropped to the point where a critical concentration has been reached (Alberts et al. 2008). A third tubulin isoform, γ-tubulin, functions as a template for the correct assembly of microtubules (Erickson 2000), being the major constituent of the microtubule-organizing-center (MTOC), the structure from which MTs emerge (Fig. 4a). The most important MTOC in most animal cells is the centrosome, a cloud of poorly defined pericentriolar material associated with a pair of centrioles. MTs are associate to this nucleating structures with their minus end, while the plus end are favoured to assembly.

A characteristic property of MTs is their ability to undergo cycles of rapid growth and disassembly, known as dynamic instability (Fig. 4b) (Mitchison and Kirschner 1984), that has been observed both *in vitro* and *in vivo* (Desai and Mitchison 1997; Burbank and Mitchison 2006). This behaviour enables them to reorganize rapidly according to changing conditions and needs of the cell. Conversion from growth to shrinkage is called catastrophe while switch from shrinkage to growth is termed rescue. The dynamic instability depends on a delicate equilibrium between the polymerization and depolymerization that require an input of energy, coming from hydrolysis of GTP. GTP binds to the nucleotide exchangeable site (E site) of β-tubulin subunit of the heterodimer and when a new dimer adds to the plus end of the MT, this GTP is hydrolyzed to GDP. The α-tubulin subunit also carries GTP, but this cannot be exchanged and is not hydrolyzed, so it can be considered a fixed part of the tubulin protein structure. MTs grow by addition of GTP-tubulin subunits. After they are incorporated into the MT, subunits are hydrolysed to become GDP-tubulin, thus, the microtubule lattice is predominantly composed of GDP–tubulin that is most stable in a curved state. The curving can only begin at the ends. While the ends are stable, a MT will grow, but once an end begins to come apart, the splaying propagates down the MT, that rapidly shrinks (Burbank and

Mitchison 2006). The plus end generally has a minimum GTP cap of one tubulin layer that stabilizes the MT structure. When this GTP cap is lost, the protofilaments splay apart and the MT rapidly depolymerizes. At the minus end, GTP cap is not present but it's replaced by different capping proteins (Conde and Cáceres 2009).

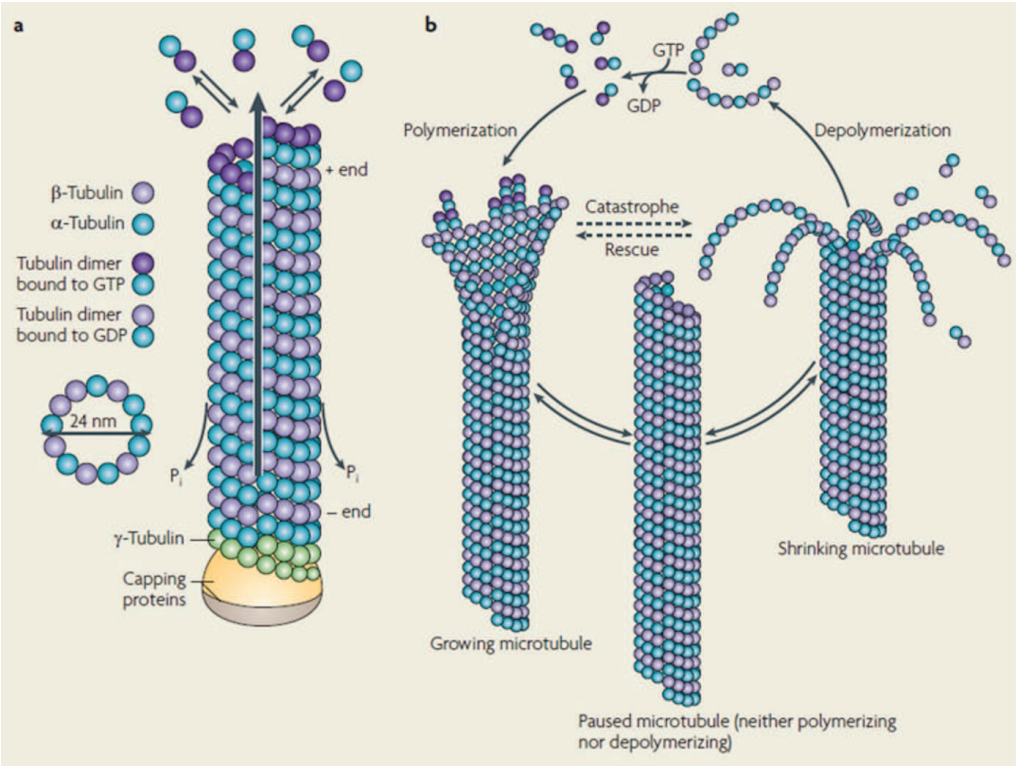


**Figure 4. Representation of dynamic instability of microtubules.**
(a) Structure of a MT and (b) a representative scheme of typical dynamic instability of MTs. (from Conde and Cáceres, 2009)

MT dynamics and functions are modulated by interaction with other proteins: the MT motor proteins and (non-motor) MT associated proteins (MAPs). The motor proteins that move along MTs belong to two major families: the plus-end directed kinesins involved in anterograde cargo transport and the minus-end directed dyneins involved in retrograde transport (Fig. 5). Motor proteins generate force upon interaction with MTs and these forces are used for various intracellular functions, most obviously intracellular transport. MT-dependent transport takes place in almost all cell type, but of course neurons, in which cargoes need to be transported over long distances from the cell body to synapses, are particularly dependent on this crucial task.

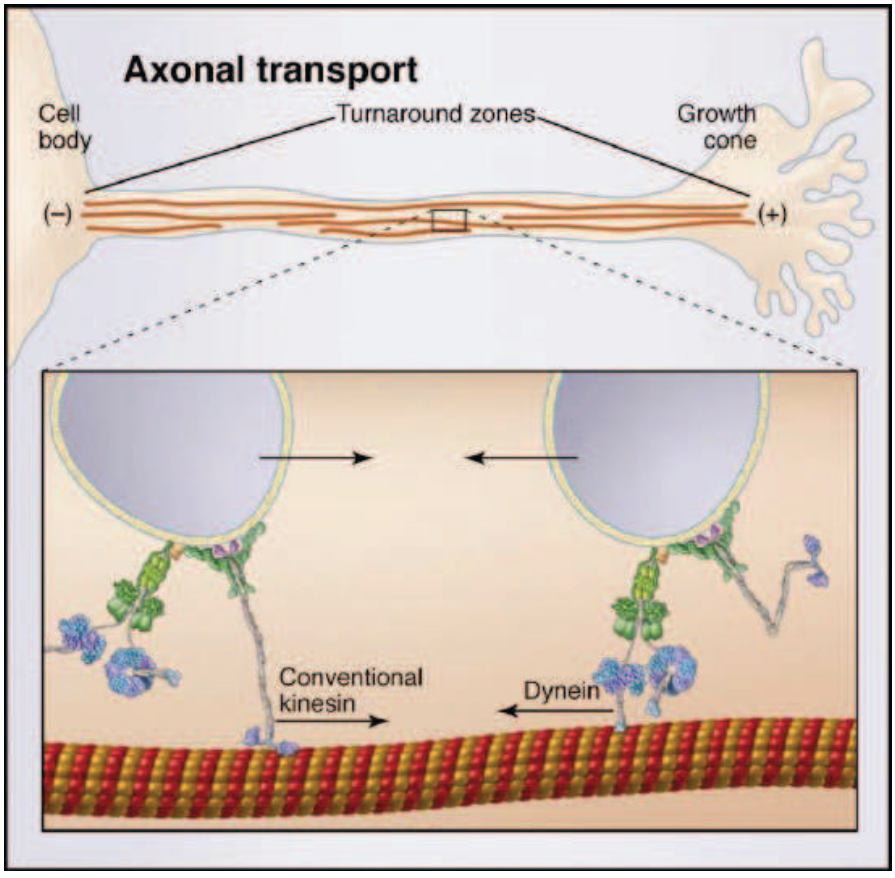


**Figure 5. Coordination of opposite polarity motors in the axon.**
Kinesin motors carry cargo along a unipolar array of microtubule toward the plus ends. Dynein is carried along with this anterograde cargo in a repressed form, and reversals in the direction of movement are infrequent. At a "turnaround" zone at the tip of these structures, dynein is activated and kinesin is repressed, and the processed cargo then can be transported back toward the cell body. The opposite activation/inactivation of the motors is believed to occur at the base near the cell body. (modified from Vale, 2003)

The heterogeneous group of non-motor MAPs comprises not only many proteins that stabilize MTs (such as tau, MAP1 and MAP2), but also severing proteins (such as spastin and katanin) which destabilize MT lattice (Roll-Mecak and McNally 2010). Another group of intensely studied MAPs is that of the MT plus end-tracking proteins (+TIPs), which help to control MT dynamics and interactions with other cellular organelles and subcellular domains (Akhmanova and Steinmetz 2008). Thus, many, if not all, functions of MTs are mediated by a highly complex and diverse set of MT-interacting proteins.

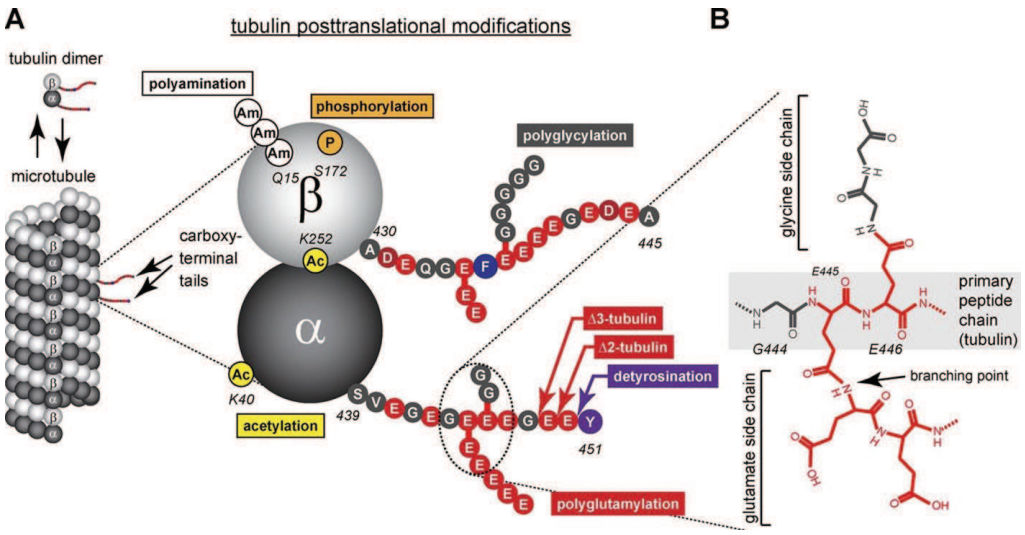


**Figure 6. Tubulin heterogeneity generated by PTMs.**
(A) Schematic representation of the distribution of different PTMs of tubulin on the α/β-tubulin dimer with respect to their position in the MT lattice. Acetylation (Ac), phosphorylation (P), and polyamination (Am) are found within the tubulin bodies that assemble into the MT lattice, whereas polyglutamylation, polyglycylation, detyrosination, and C-terminal deglutamylation take place within the C-terminal tubulin tails that project away from the lattice surface. (B) Chemical structure of the branched peptide formed by polyglutamylation and polyglycylation, using the γ-carboxyl groups of the modified glutamate residues as acceptor sites for the isopeptide bonds. (from Janke, 2014)

Although the structure of MTs is conserved among cell types and organisms, they can be adapted to highly divergent tasks thanks to two intrinsic regulators and sources of variability of MTs: the incorporation of different tubulin isoforms, codified by different genes, and on how they have been altered by various forms of post-translational modification (PTM) (Janke and Kneussel 2010). Furthermore, tubulin modifications alone or in combination have the potential to generate complex molecular signals creating a code on MTs that can be read by MAPs (Verhey and Gaertig 2007). The probable downstream effectors of this code are the intracellular transport machinery and other molecular players that mediate neuronal differentiation and polarization, in fact, tubulin PTMs influence the preferences of some molecular motors and MAPs (Janke and Kneussel 2010). Tubulin is subject to a large range of PTMs (Fig. 6, 7), from well-known ones, such as acetylation or phosphorylation, to others that have been very recently discovered; some of them are unique to tubulin, while others are shared with other proteins (Janke and Bulinski 2011). PTMs of tubulin subunits mark subpopulations of MTs and generate chemical differences that are sufficient to confer specific cellular functions on MTs. Although they are not directly involved in determining the

dynamic properties of MTs, specific PTMs of tubulin correlate well with the half-life and spatial distribution of MTs (Conde and Cáceres 2009).

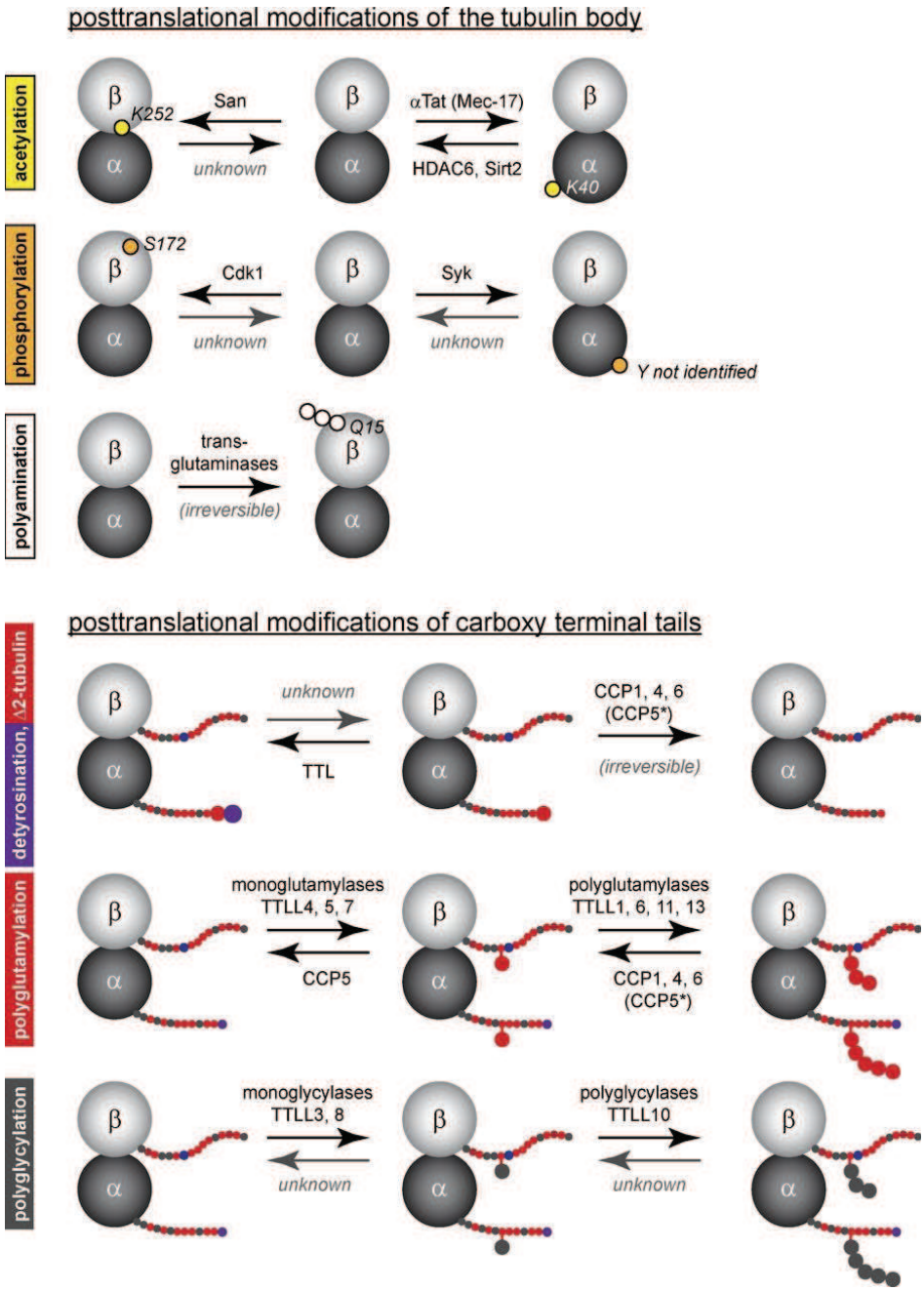


**Figure 7. Enzymes involved in PTM of tubulin.**
Schematic representation of known enzymes (mammalian enzymes are shown) involved in the generation and removal of PTMs shown in Fig. 5. Note that some enzymes still remain unknown, and some modifications are irreversible. (*CCP5 preferentially removes branching points; however, the enzyme can also hydrolyse linear glutamate chains). (from Janke, 2014)

Tubulin may be modified as a soluble dimer or in a MT, and some PTMs occur on both, even though most of the modifying enzymes act preferentially on tubulin subunits that are already incorporated into microtubules (Conde and Cáceres 2009). The variable C-terminal domains of α-tubulin represent a hot spot for modification, while fewer modifications appear to associate with the C-termini of b-tubulin. Studies have revealed that MTs are modified in a heterogeneous manner, with PTMs being coextensive or concentrated in distinct domains on MTs, thereby adding an additional level of complexity. Indeed, assigning specific functions to a given modification *in vivo* is complicated by the heterogeneity of modifications found in the MT as well as the multiple modifications that may be present on the individual tubulin dimers themselves (Song and Brady 2015).

Most α-tubulin genes in different species encode a C-terminal tyrosine residue. This tyrosine can be enzymatically removed and religated, as occurs for the first modification discovered by Barra and colleagues (Barra et al. 1973). As detyrosination was mostly found on stable and long-lived MTs especially in neurons, it was assumed that this modification promotes or correlates with MT stability. The modification itself probably has no direct stabilizing ability, but more likely causes a lower preference of MT-depolymerizing factor for MTs. The carboxypeptidase catalysing detyrosination of α-tubulin has yet to be identified and acts preferentially on polymerized MTs. In contrast, the reverse enzyme, tubulin tyrosine ligase (TTL), is known and modified non polymerized tubulin dimers exclusively to re-convert them into the native tyrosinated tubulin (Janke 2014). In most organisms, only one unique gene for TTL exists and is strictly tubulin specific (Prota et al. 2013). Detyrosinated tubulin can be further converted to the so-called Δ2 tubulin by the removal of its C-terminal glutamate residue (for two C-terminal amino acids missing). Δ2 Tubulin cannot undergo retyrosination by TTL, thus is considered an irreversible PTM (Janke and Bulinski 2011). This modification is typical only for very stable MTs and is very frequent in neurons, in fact, it occurs in about 35% of brain tubulin. Its function seems to simply lock MTs in the detyrosinated state (Janke 2014). The enzymes responsible for Δ2 tubulin generation are members of a family of cytosolic carboxypeptidases (CCPs) and most of them also remove polyglutamylation from tubulin (Rogowski et al. 2010). These enzymes are also able to generate Δ3 tubulin, but the functional significance of this event is unknown.

The second discovered tubulin PTM was acetylation (Hernault and Rosenbaumt 1985). It takes place on MT polymer, like detyrosination, and occurs most commonly on lysine 40 of α-tubulin, but recently additional acetylation sites on both α- and β-tubulin have been

identified (Janke and Bulinski 2011). Acetylation is generally enriched on stable MTs in cells, but it is rather unlikely that it directly stabilizes MTs. As a result of its localization at the inner face of MTs, lysine 40 acetylation might affect the binding of MT inner proteins, moreover it seems also to regulate intracellular transport by regulating the traffic of kinesin motors (Janke 2014). The enzymes involved in lysine 40 acetylation are the acetyl transferase α-Tat1 (α-tubulin N-acetyltransferase 1) that specifically acetylates α-tubulin lysine 40, and two deacetylating enzymes, HDAC6 (histone deacetylase 6) and SIRT2 (sirtuin 2), both of them deacetylate also other substrates (Janke and Bulinski 2011). Another acetylation event has been described at lysine 252 of β-tubulin. This modification is catalysed by the acetyltransferase San and might regulate the assembly efficiency of MTs as a result of its localization at the polymerization face. In contrast with lysine 40 acetylation, this one was reported to take place preferentially on non-polymerized tubulin (Chu et al. 2011).

Tubulin polyglutamylation and polyglycylation are two similar and reversible PTMs, that are the progressive addition of mono or poly residues of glutamine or glycine respectively, onto one or more glutamine residues near to the C-terminal of tubulin within the MTs. Glycylation and glutamylation are more heterogeneous than other known PTMs, as both can occur on either α- or β-tubulin and both can form long or short side chains. Moreover, both PTMs use similar or overlapping modification sites and can thus compete with one another. The enzymes able to catalyse both the glutamylation and glycylation belong to the TTLL (tubulin tyrosine ligase-like) family and each displays defined reaction preferences, that is, for modifying α- and β-tubulin and for generating short and long side chains. Deglutamylases were identified as members of the CCP family and, similar to the glutamylated TTLL enzymes, can be distinguished by their reaction preference, they can not only remove polyglutamylation from tubulin but also from an extensive group of other proteins. Polyglutamylation is a major PTM in the brain, whereas glycylation seems to be restricted to cilia and flagella in most organisms analysed so far. Their role in regulation of MT function is mostly unknown (Rogowski et al. 2010; Janke and Bulinski 2011; Janke 2014)

Early studies identified tubulin phosphorylation, however, no specific functions were found. The best-studied phosphorylation event on tubulin takes place at serine 172 of β-tubulin, is catalysed by Cdk1 and might regulate MT dynamics during cell division (Janke 2014).

Very recently, has been discovered a new modification on brain tubulin, the polyamination. Among several glutamine residues of α- and β-tubulin that can be polyaminated, glutamine 15 of β-tubulin is considered the primary modification site. Polyamination is catalysed by

transglutaminases, which modify the free tubulin as well as MTs in an irreversible manner, and most likely contribute directly to the stabilization of MTs (Song et al. 2013).

Several other PTMs have been found on tubulin, but they have mostly been reported without follow-up studies, and some of them are only found in specific cell types or organisms and/or under specific metabolic conditions, so further studies will be necessary.

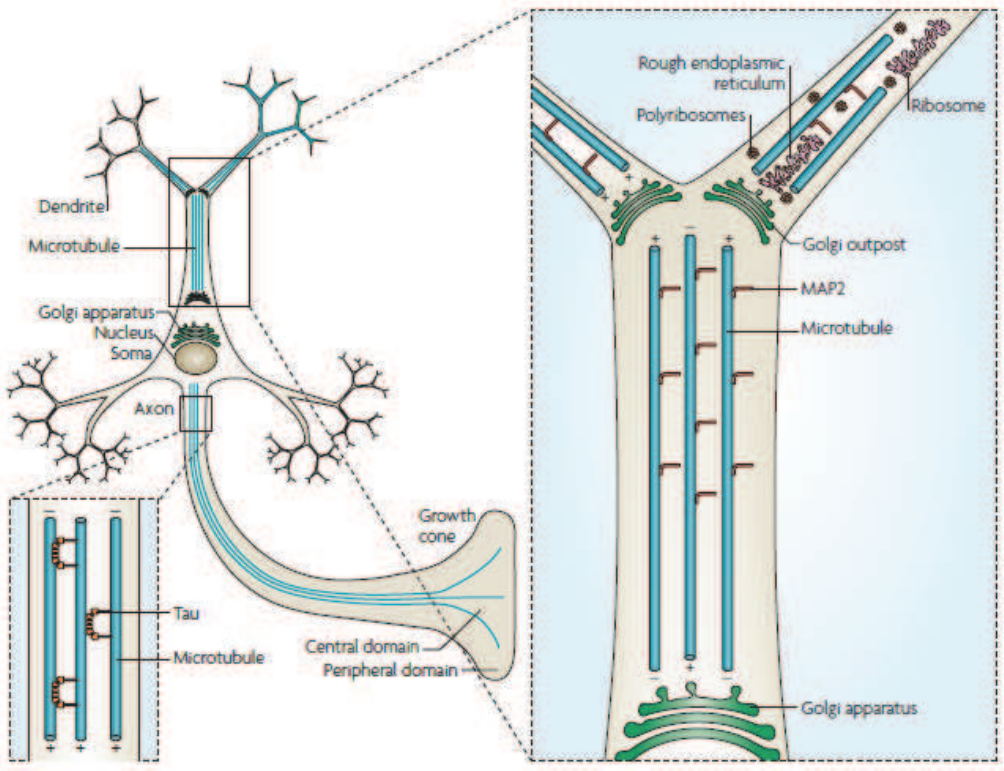


**Figure 8. Microtubule organization and organelle distribution in axons and dendrites.**
Axons have tau bound microtubules of uniform orientation, whereas dendrites have microtubule associated protein 2 (MAP2)-bound microtubules of mixed orientation. Dendrites also contain organelles that are not found in axons, such as rough endoplasmic reticulum, polyribosomes and Golgi outposts. (from Conde and Cáceres, 2009)

Neurons are unique among cell types as they are highly polarized and excitable cells, with two molecularly and functionally distinct domains that emerge from the cell body: a single thin, long axon, which transmits signals, and multiple shorter dendrites, which are specialized to receive signals. The ability of neurons to polarize is crucial for synaptic transmission, and it has become clear that loss of polarity correlates with characteristic changes in MT organization and dynamics (Baas 2002). In fact, changing MT dynamics is sufficient to alter axon and dendrite specification and development. In neurons, MTs actively participate in the

initial steps of neuronal polarization, the organization of intracellular compartments, the remodeling of dendritic spines and the trafficking of cargo molecules to pre-, post- or extra-synaptic domains (Janke and Kneussel 2010). MTs form dense parallel bundles in neurites that are required for their growth and maintenance, but the MT organization differs between axon and dendrites in at least two major aspects (Fig. 8). First, orientation: axonal MTs have uniform orientation, with their plus ends facing the axonal tip, whereas dendritic MTs have mixed orientation, with their plus ends facing either the cell body or the dendritic tip (Baas et al. 1988). Second, MTs differ in their complements of MAPs: for example, MAP2 is found mostly in dendrites, while tau is found mainly in the axons (Matus 1994).

First of all, in the cell body neuronal MTs are nucleated at the centrosome, rapidly release by the action of the MT-severing protein katanin and then transported as short polymers into neurites by molecular motors (Vale 2003). Then, MTs actively participate in axon specification during neuronal polarization; in fact, axonal MTs show increased stability. On the other hand, MTs in proximal dendrites display a mixed orientation with equal amounts of plus-ends pointing to growth cones/synapses and the cell body, whereas MTs in distal dendrites are unipolar, as in axons (Baas et al. 1988). On the contrary, in the growth cones MTs are highly dynamic: their rapid and constant reorganization and remodeling is required for persistent growth cone advance, axonal elongation and the recognition of guidance cues. During branch formation, MTs are locally disrupted by severing enzymes such as spastin and katanin (Janke and Kneussel 2010).

Differentiated neurons form neuronal circuits, grow synaptic contacts and propagate information in a unidirectional fashion; to do that they are provided of MTs carrying elevated levels and unique PTMs, depending on the specific sub-localization (Fig. 9) (Janke and Bulinski 2011). Tubulin PTMs are dynamic and must be regulated during development and differentiation and in response to injury and stress. Just as MTs can be dynamic or long-lived, both the distribution and levels of a given PTM may be changed in response to physiological and pathological cues (Song and Brady 2015). In the developing neuron (Fig. 9 upper), when the axon is extending but the dendrites have not yet differentiated, MTs in all neurites are plus end out. Modification levels for detyrosination, Δ2 tubulin, glutamylation, and polyamination in the neuronal perikaryon are relatively low. Acetylation, glutamylation, and detyrosination are elevated in the growing axon, but all three are reduced in the growth cone. Little or no acetylation is seen in the MTs of the growth cone, consistent with the presence of highly dynamic MTs. The minor neurites at this stage are lower in acetylation, but relatively rich in detyrosinated and glutamylated/polyglutamylated MTs. Polyamination may be detectable in

the growing axon at a low level. In a mature neuron (Fig. 9 lower), as both dendrites and synaptic specializations form, tubulin modifications change both quantitatively and qualitatively. Dendritic MTs exhibit mixed polarity as dendrites form, while axonal MTs remain plus end out. Polyamination of axonal MTs increases with maturation, but may be relatively low or absent from dendritic domains. Detyrosinated and Δ2 tubulin levels remain relatively high in differentiated dendrites and axons, while acetylation increases in both axon shafts and dendrites. Acetylation is also detectable in the distal axon and presynaptic regions, consistent with reduced numbers of highly dynamic microtubules in stable connections. During the differentiation and maturation of neurons, there are also changes in MAPs in different neuronal subcellular domains (Song and Brady 2015). Tubulin PTMs are involved, in some way, in regulating most of the processes in which MTs function, and aberrations in the normal pattern of PTMs could directly or indirectly lead to disease. The prime candidate for such diseases are those connected to malfunctions of MTs that normally exhibit high levels of PTMs, such as neurodegeneration (Janke and Bulinski 2011).

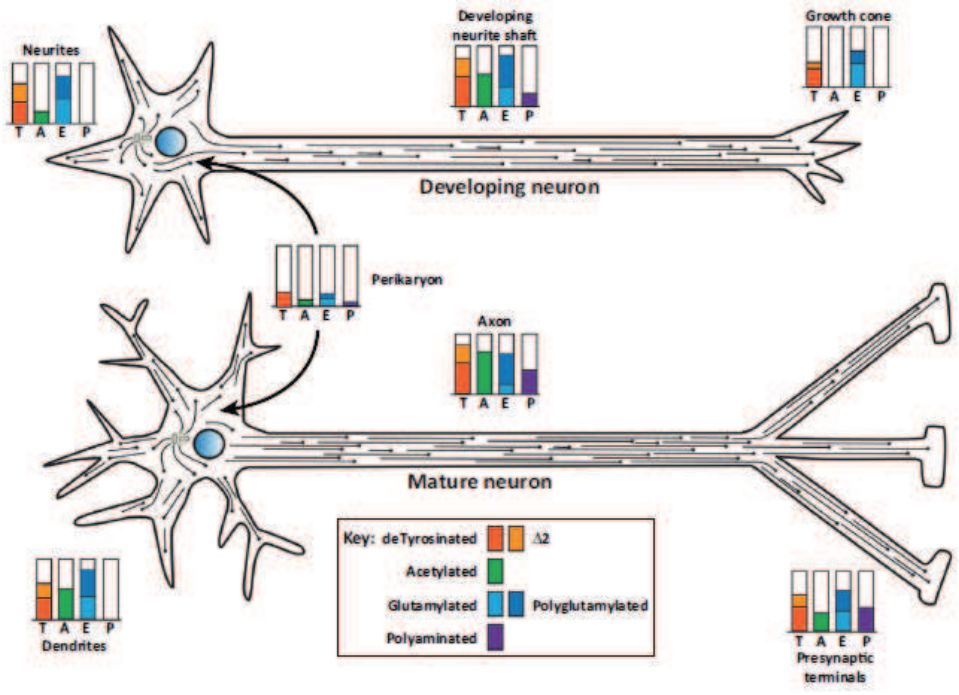


**Figure 9. PTMs of tubulin and microtubules vary in different regions of a neuron and change during neuronal differentiation.**
Modification levels for detyrosination (T), Δ2 tubulin (Δ2), acetylation (A), glutamylation (E), and polyamination (P) are shown in both a developing neuron (upper) and a mature neuron (lower). Tubulin modifications change both quantitatively and qualitatively as indicated. (from Song and Brady, 2015)

Many major human neurodegenerative diseases, including Alzheimer's disease, Parkinson's disease and amyotrophic lateral sclerosis (ALS), display axonal pathologies including abnormal accumulations of proteins and organelles. Evidence of axonal transport defects in neurodegenerative diseases emerged from microscopy studies showing that, in these disorders, some cargoes that are usually conveyed along the axons, such as cytoskeletal components and mitochondria, can accumulate in the perikaryon, the proximal segment of the axon or the distal part of it. Now, it's known that disruption of axonal transport is an early and perhaps causative event in many of these diseases, since this is an essential process in neurons because of the extreme polarity and size of these cells. In fact, most neuronal proteins are synthesized in the cell body, thus anterograde axonal transport has a role in supplying proteins and lipids to the distal synapse and mitochondria for local energy requirements, whereas retrograde transport is involved in the clearance of misfolded and aggregated proteins from the axon and the intracellular transport of distal trophic signals to the soma. The main mechanism to deliver cellular components to their actions site is long-range MT-based transport. The two major components of this transport machinery are molecular motors and MTs, the rails on which they run. Anyway, the mechanisms by which axonal transport could be disrupted in disease are varied and can occur via damage to the molecular motors, damage to MTs, damage to cargoes and damage to the ATP fuel supply (mitochondria), contributing all of them to the neurodegeneration (De Vos et al. 2008). It is also possible that various axonal transport insults could lead to a convergent neurodegenerative pathway that affects the most vulnerable neurons. The identification of mutations in genes encoding proteins that are known to be involved in axonal transport, together with the observation that chronic exposure to some chemicals can provoke axonal transport disturbances and subsequent neurodegeneration, strongly support the view that defective intracellular transport can directly trigger neurodegeneration (Millecamps and Julien 2013). Even if the mechanisms by which axonal transport is disrupted in disease are varied, the principal system to be investigate should be the MT-based transport, being this one the most important transport system in the cells and particularly in neurons. Interestingly, in tauopathies, a group of clinically heterogeneous neurodegenerative disease showing alterations in the MT-associated protein tau, some mutations in MAPT gene, coding for tau, compromise the MT-binding function of tau, thereby reducing MT stability leading to impairment in axonal transport (Forman et al. 2004). In accordance with this, also mutation in SNCA gene, coding for the small presynaptic protein α-synuclein, leading to neurodegenerative diseases called α-synucleinopathies, affects MT stability and MT-based transport, resulting in protein aggregates inclusion bodies, known

as Lewy bodies. Moreover, in an axonal transport deficits-related disorder as Charcot-Marie-Tooth disease, a pharmacological approach to increase tubulin acetylation by HDAC6 inhibitors has succeeded in correcting the axonal transport defects and consequently rescuing disease-related phenotypes in mouse model of the disease (d'Ydewalle et al. 2011). According to these evidences, axonal transport defects and in particular MTs should be considered as a suitable therapeutic targets in neurodegenerative diseases.

## *1.2 Parkinson's disease*

Parkinson's disease (PD) is the second most common age-related neurodegenerative disorder after Alzheimer's disease and affects 1% of the population worldwide after the age of 65 years (Forman et al. 2004). Clinically, PD is characterized by motor impairment and some non-motor symptoms such as mood, sleep and cognitive disturbances (Fahn 2003). Its central pathological feature is the selective degeneration of dopaminergic neurons of the *Substantia nigra pars compacta* (SNpc) that have their projections in the *Corpus striatum* (CS). This degeneration leads to a severe dopamine (DA) deficiency in the CS, the brain region controlling voluntary locomotor activities, resulting in the typical symptoms of parkinsonism as tremor, rigidity and bradykinesia (Dauer and Przedborski 2003).

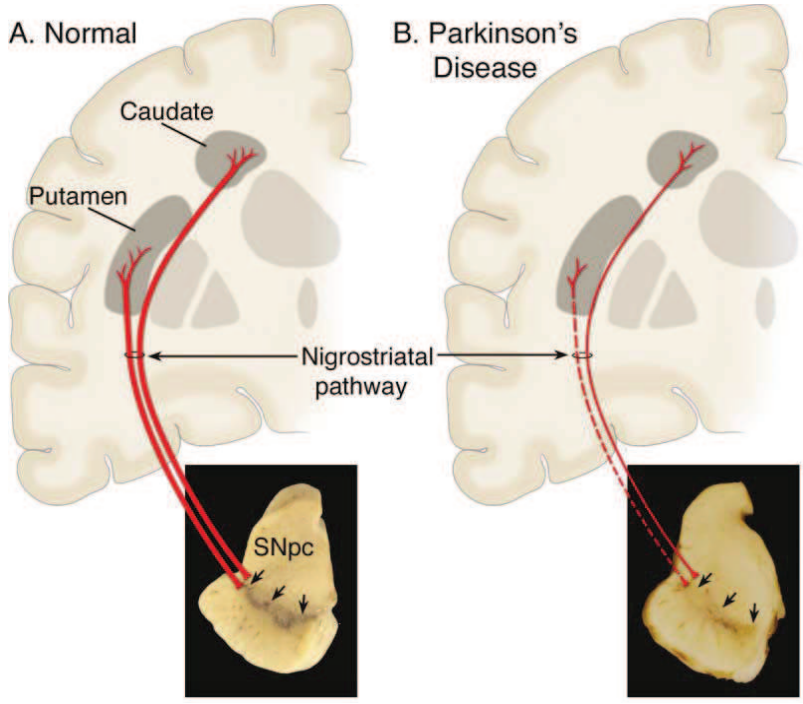


**Figure 10. Neuropathology of Parkinson's disease.**
(A) Schematic representation of the normal nigrostriatal pathway (in red). It is composed of dopaminergic neurons whose cell bodies are located in the *Substantia nigra pars compacta* (SNpc; see arrows). These neurons project (thick solid red lines) to the basal ganglia and synapse in the *Corpus striatum*. The photograph highlights the normal pigmentation of the SNpc, produced by neuromelanin within the dopaminergic neurons. (B) Schematic representation of the diseased nigrostriatal pathway (in red). There is a marked loss of dopaminergic neurons that project to the putamen (dashed line) and a much more modest loss of those that project to the caudate (thin red solid line). The photograph demonstrates depigmentation (i.e., loss of dark-brown pigment neuromelanin; arrows) of the SNpc due to the marked loss of dopaminergic neurons. (modified from Dauer and Przedborski, 2003)

The nigral damage, however, is always accompanied by extensive extranigral pathology, involving also a number of other neuronal populations in brain region as cortex, thalamus and subthalamic nuclei (Braak et al. 2003). Thus, a new definition of PD should acknowledges the disease as a multisystem synucleinopathy with pathology extending beyond the confines of the central nervous system and clinical manifestation extending beyond dopamine cell loss in the SNpc (Stern et al. 2012). The other pathological hallmark of PD is the presence of specific inclusion bodies, which develop as thread-like Lewy neurites (LNs) in cellular processes, and in the form of globular Lewy bodies (LBs) in neuronal perikarya (Braak et al. 2003), composed predominantly of the presynaptic protein α-synuclein (α-syn) (Spillantini et al. 1997).

The bases for such degeneration are presently unknown and current therapies offer just the management of symptoms rather than prevention of neuron death and block or reverse of the disease progression. Although in the majority of PD cases are sporadic, genetic studies have uncovered a number of genes that, when mutated, are associated with familial PD or increased risk of the disorder as well as polymorphisms that enhance disease susceptibility (Hardy 2010). These PD-related proteins include α-syn, parkin, DJ-1, PINK1 and LRRK2, and are responsible for less than 10% of PD cases (Dawson and Dawson 2010). In spite of the etiology of PD is still unclear, both genetic and environmental components are considered to contribute to the disease (Greenamyre et al. 2003; Vance et al. 2010; Cannon and Greenamyre 2013). It's well known that parkinsonism can also be induced by exposure to environmental toxins, such as pesticide, chemical compounds and hydrocarbon solvents. Among them, 2,5-hexanedione (2,5-HD), the toxic metabolite of n-hexane, has been shown to induce parkinsonism in animals and humans (Spencer and Schaumburg 1985; Pezzoli et al. 1990; Pezzoli et al. 2000) and to affect the cytoskeleton *in vitro* and *in vivo* models (LoPachin and DeCaprio 2004; Song et al. 2007; Wang et al. 2008). So far the most studied PD-toxins have been resulted to be potent inhibitors of complex I of electron transport chain, thus mitochondrial dysfunction has been considered for long time the principal culprit of neuronal death in PD (Yao and Wood 2009; Malkus et al. 2009). The best studied PD-toxin is surely MPTP, that was associated with PD in 1982, when some young drug users developed an acute permanent parkinsonian syndrome (Langston et al. 1983). Later on, it was confirmed that MPTP could induce parkinsonism also in primates and rodents, since it could easily surpass the blood-brain barrier and then be converted by astrocytes into its active metabolite $MPP^+$, that is selectively up-taken by dopaminergic neurons through the dopamine transporter (DAT) rendering these neurons particularly vulnerable (Dauer and Przedborski 2003) (Fig. 11).

$MPP^+$ is a potent inhibitor of mitochondrial complex I, but it also alters MT dynamics and can act on different organelles.

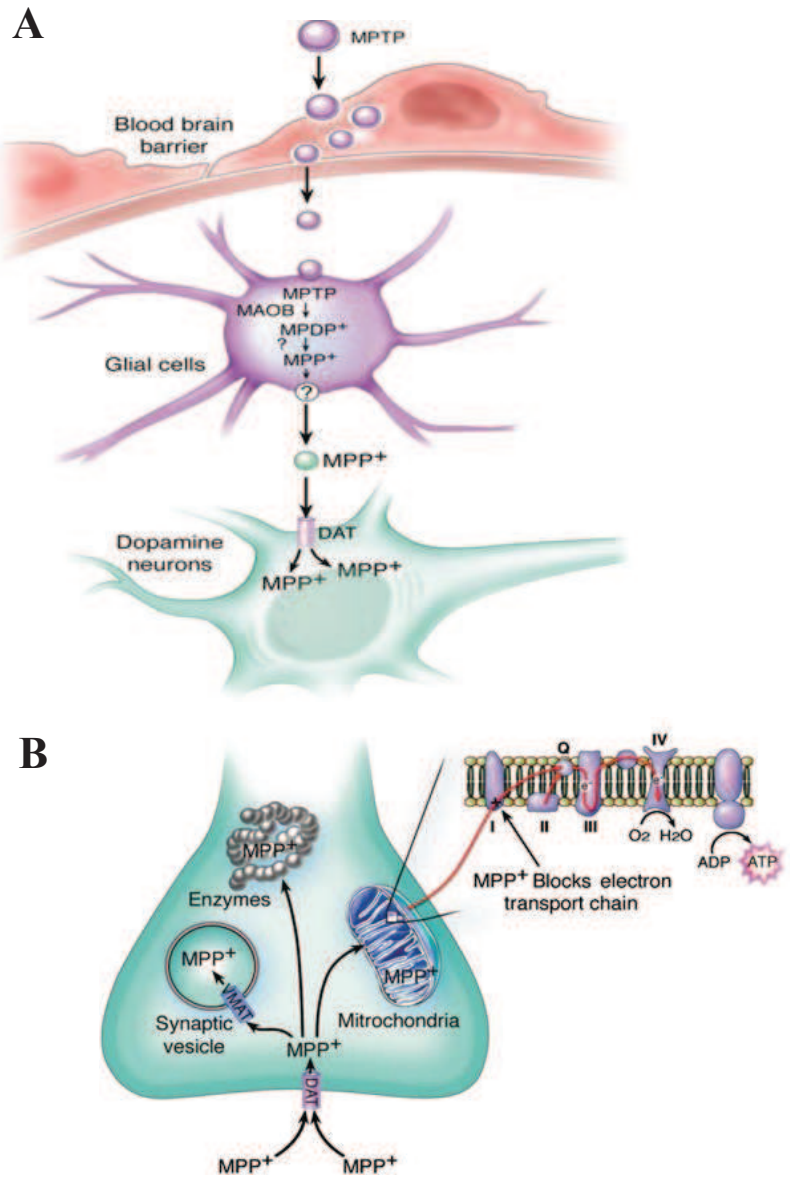


**Figure 11. Schematic representation of MPTP metabolism.**
(A) After systemic administration, MPTP crosses the blood-brain barrier. Once in the brain, MPTP is converted within non-dopaminergic cells, such as glial cells, to $MPP^+$ by monoamine oxidase B (MAO-B) and further unknown mechanism (?). Thereafter, $MPP^+$ is released into the extracellular space. $MPP^+$ is concentrated into dopaminergic neurons via the dopamine transporter (DAT). (B) Inside dopaminergic neurons, MPP+ can follow one of three routes: (1) block the complex I of mitochondrial electron transport chain; (2) interaction with cytosolic enzymes; (3) sequestration into synaptic vesicles via the vesicular monoamine transporters (VMAT). The interaction also with MTs has been proved (not shown).(modified from Dauer and Przedborski, 2003)

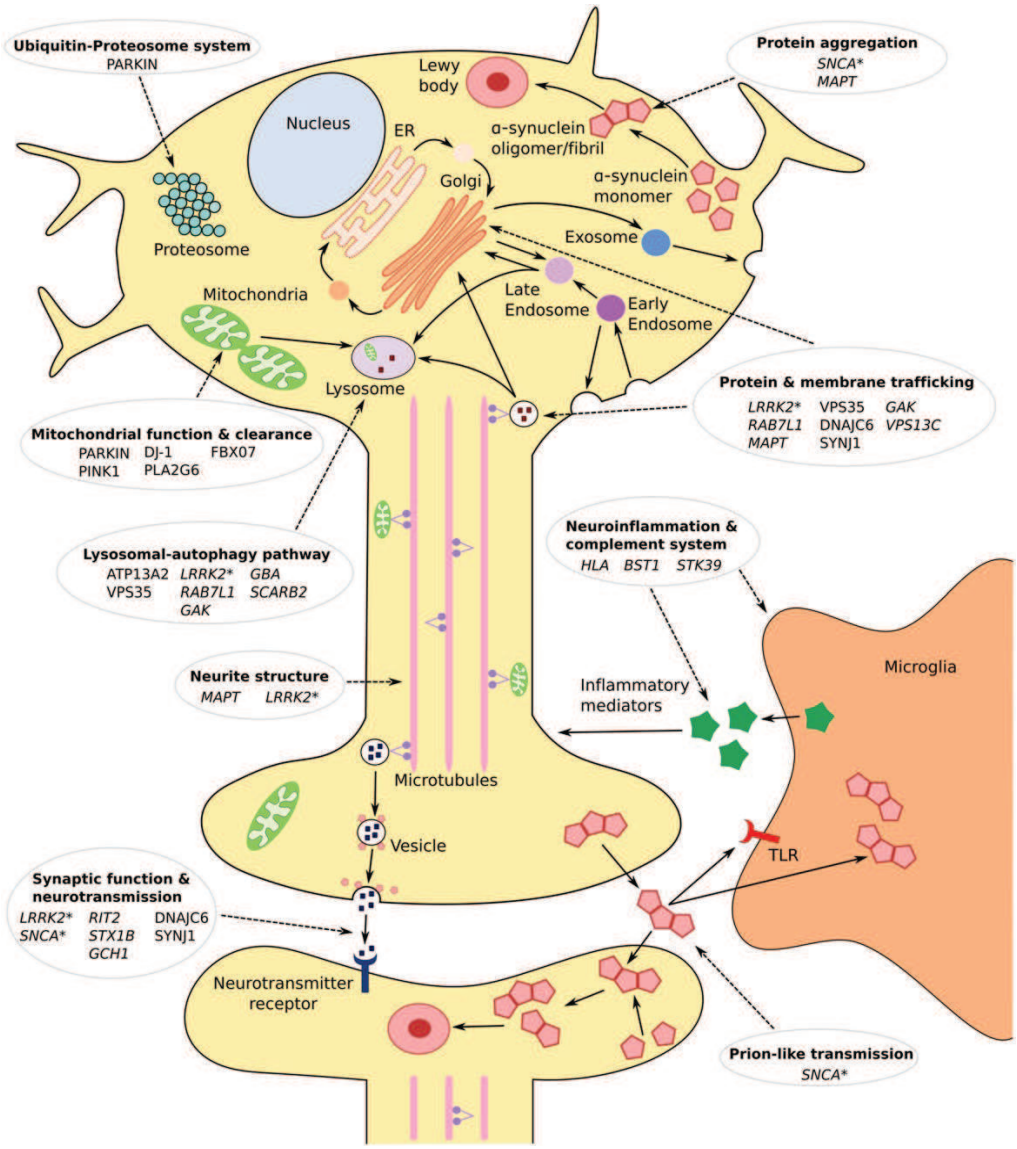


**Figure 12.** Molecular processes involved in PD pathogenesis as highlighted by genetic findings. Using genes recently nominated as risk factors for idiopathic PD along with those responsible for familial PD, it is possible to extrapolate a number of cellular processes that may underlie disease development. Each large gray circle represents a biological process and details the genes linked to it. Genes listed in italics represent nominated risk factors for idiopathic PD, identified through GWAS, whereas those in normal font are associated with familial PD. An asterisk denotes that the gene is linked to both forms of the disorder. Some genes like SNCA and LRRK2 are associated with multiple processes. While the majority of cellular pathways contribute to both familial and sporadic forms of the disease, neuroinflammations likely plays a more prominent role the latter. Conversely, mitochondrial dysfunction shows a greater association with familial PD. (from Kumaran and Cookson, 2015)

Interestingly, MTs interact with some of the proteins mutated in PD, like α-syn (Alim et al. 2002) and parkin (Ren et al. 2003), and they are involved in the mechanism of action of

model PD toxins as MPP+ and rotenone (Feng 2006). In particular, $MPP^+$ is able to influence the state of tubulin polymerization in cultured neuron-like cells (Cappelletti et al. 1999) and to act directly on MTs *in vitro* by affecting their assembly and dynamics (Cappelletti et al. 2005), while rotenone is known to induce MT depolymerization *in vitro*. MPP+ has been also proven to decrease anterograde and increase retrograde axonal transport of membranous vesicles in squid axoplasm (Morfini et al. 2007). There is a limited range of acceptable MT dynamic behaviours in neurons, outside of which MTs cannot function normally and the cells cannot survive (Feinstein and Wilson 2005). Moreover, dopaminergic neurons, appears to be particularly sensitive to any insults that could damage the MT cytoskeleton because of their peculiar architecture, characterized by an extremely widespread arborization and particularly long axons, that made their function and survival strongly dependent on intracellular trafficking (Hunn et al. 2015).

PD can be defined as a disease of impaired intracellular trafficking, selectively leading to the dopaminergic neurons death. The typical hallmark lesions of the disease are the LB inclusion, which are mainly composed of hyperphosphorylated α-syn. Mutations in the gene coding α-syn cause familial autosomal dominant PD, and revealed a reduced transport rates of the mutants, with the consequent disruption of α-syn transport that may contribute to the accumulation of this protein in LB (Saha et al. 2004). Even analysis of post-mortem patient brains showed that kinesin and cytoplasmic dynein subunit levels are decreased in sporadic PD, with kinesin levels being affected early on in the disorder, before dopaminergic loss (Chu et al. 2012). Consistent with these observations, dysfunction of MT system is emerging as a novel contributing factor in several neurodegenerative processes, including PD (Hunn et al. 2015; Kumaran and Cookson 2015).

## *1.3 PARK2 gene*

Mutations in the *PARK2* gene are the most frequent known cause of early-onset (<40–50 years) PD (10–20% worldwide) with a percentage of about 50% of all recessive familial forms); however, the frequency of mutations decreases significantly with increasing age at disease onset (Corti et al. 2011). Exonic deletions in this gene were first reported in Japanese families with autosomal recessive juvenile-onset parkinsonism (ARJP) (Kitada et al. 1998). In fact, dysregulation of this gene leads to the selective loss of dopaminergic neurons in the SNpc, together with loss of noradrenergic neurons in *Locus coeruleus*. Even if AR-JP patients display an onset frequently occurring before the age of 20, they present a clinical phenotype similar to that of sporadic PD patients, but also a number of specific clinical features, such as the lack of LB pathology in the most of cases (Feany and Pallanck 2003).

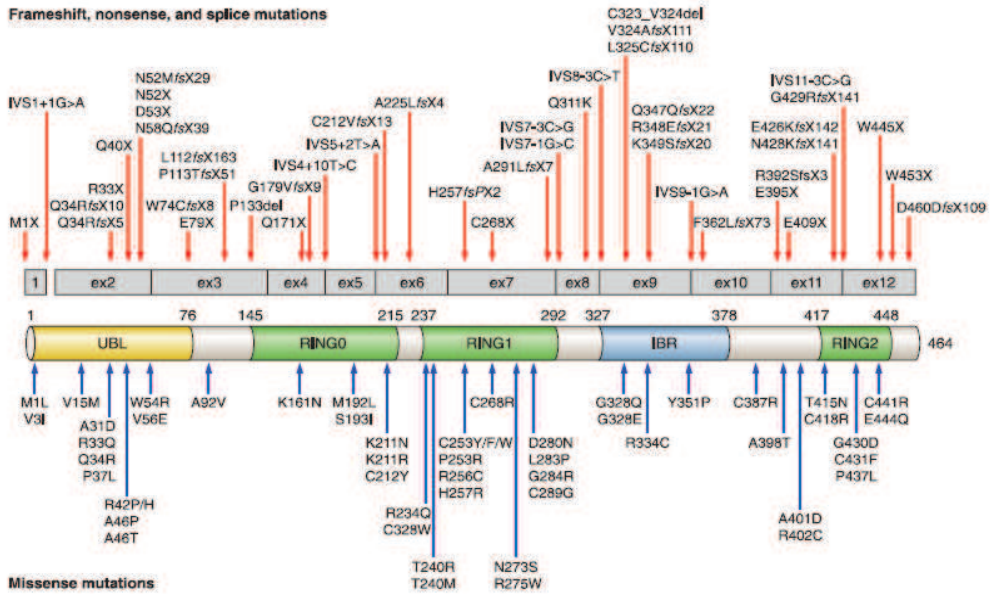


**Figure 13. Schematic representation of parkin on transcript level and the functional domains of the protein.** Are shown the pathogenic frameshift mutations above the transcript and protein organizations and missense mutations below. Parkin is a 465-amino acid protein that contains an $NH_2$-terminal ubiquitin-like (UBL) domain followed by three RING (really interesting new gene) finger domains (RING 0–2) separated by a IBR (in-between-ring) domain in the COOH-terminal part. Numbers under the protein line indicate the boundaries of each domain. (modified from Corti et al., 2011)

Interestingly, despite the recessive inheritance pattern of *PARK2* mutations induced familial PD, heterozygous mutations have been found in some cases of idiopathic PD; furthermore,

evidences of nigro-striatal abnormalities in individuals with heterozygous mutations have been observed, even if asymptomatic. This suggests that *PARK2* haploinsufficiency might be a risk factor for developing the disease (Khan et al. 2005). Later on, more than 170 different mutations have been identified throughout the sequence of this particularly large gene (1.35 Mb) made up of 12 exons, including large deletions or multiplications, small deletions/insertions as well as missense mutations, often resulting in exon rearrangements (Corti et al. 2011) (Fig. 13). *PARK2* gene encodes for a 465-amino acids protein with a molecular weight of about 52 kDa, containing an $NH_2$-terminal ubiquitin-like domain (UBL) followed by three RING (really interesting new gene) finger domains (RING 0–2) separated by a 51-residue IBR (In-Between-Ring) domain in the COOH-terminal part (Corti et al. 2011) (Fig. 13).

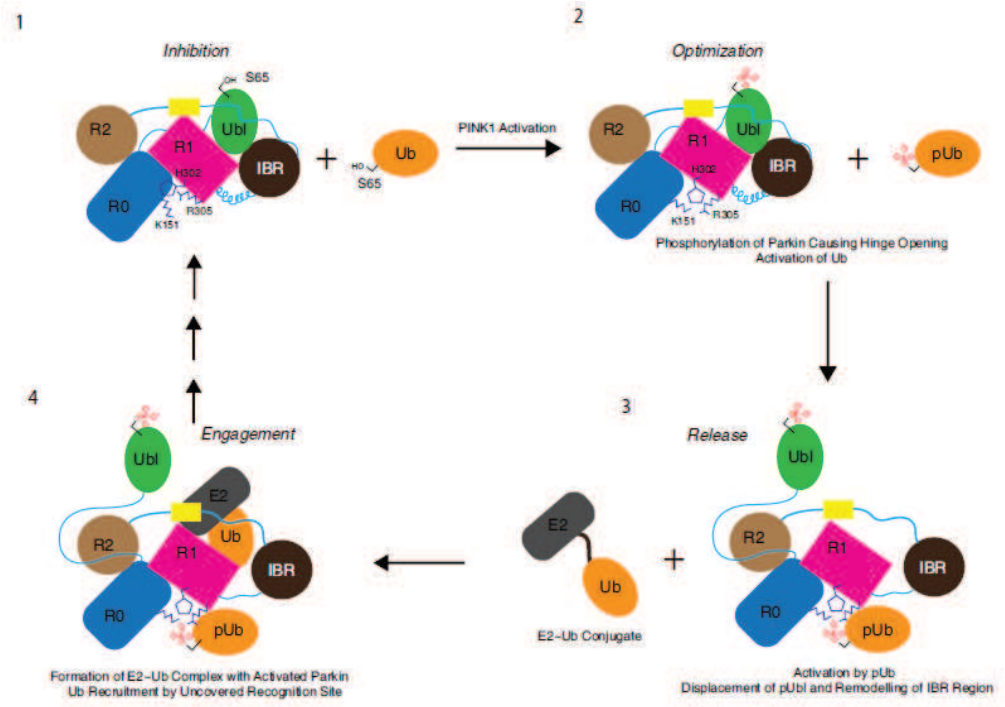


**Figure 14. Model of parkin inhibition and activation.**
(1) Inhibition: wt parkin is auto-inhibited in the absence of phospho-ubiquitin. PINK1 activation leads to phosphorylation of the accessible S65 in both parkin and ubiquitin. (2) Optimization: Parkin phosphorylation stabilizes the flipped-out conformation of H302, thus optimizing the phosphate-binding site. (3) Release: Phospho-ubiquitin binds to helix H3 of the RING1 domain, leading to displacement of the Ubl domain and loss of structure near the RING1/IBR interface. (4) Engagement: The ubiquitin and E2 binding surfaces uncovered by displacement of the Ubl domain engage with charged E2~Ub conjugate poised for ubiquitin transfer. (from Kumar et al., 2015)

Functionally, parkin is an E3 ubiquitin ligases (Shimura et al. 2000), thus together with ubiquitin-activating (E1) and ubiquitin-conjugating (E2) enzymes confers substrate specificity in the ubiquitination pathway, being responsible for the final transfer of activated ubiquitin molecules to a protein substrate. This process, termed ubiquitination, may have various biological significances, including signaling and proteasomal degradation of the modified or misfolded protein. In the ubiquitination process the RING finger domains are required to recruit E2 enzymes, while the UBL domain serves to interact with the substrate and 26S proteasome facilitating the degrading process (Shimura et al. 2000). Very recently, the molecular regulation of parkin E3 ligase activity has been unraveled, showing that parkin exists in an autoinhibited state. It is activated by phosphorylation of its N-terminal UBL domain, that primes parkin for optimal phospho-ubiquitin binding, that in turn leads to a consequent displacement of the Ubl domain, unveiling the ubiquitin-binding site used by the E2~Ub conjugate, thus leading to active parkin (Kumar et al. 2015) (Fig. 14).

In addition to its ligase activity, parkin seems to participate in other cellular functions (Alves da Costa and Checler 2012); in fact, it is robustly expressed in many tissues, including brain, skeletal muscle, heart and liver tissues, which suggests that it has a widespread physiological role (Youle and Narendra 2011). Parkin is also able to interact with two target involved in the pathogenesis of PD: mitochondria and MTs. It's already well known that parkin is involved through PINK1 pathway in mitochondrial dynamics, maintenance and mitophagy (Youle and Narendra 2011; Scarffe et al. 2014), regulating also the transport of damaged mitochondria before their degradation (Wang et al. 2011). Parkin as E3 ubiquitin ligase has specificity for a wide range of different substrates, such as Pael-R, CDCrel1, glycosylated α-syn, synphilin-1 and many others. Very recently, it has also been reported that parkin interacts with the kainate receptor GluK2 subunit, regulating the receptor functions *in vitro* and *in vivo* (Maraschi et al. 2014). Moreover, different studies have demonstrated the role of parkin in protecting neurons from diverse insults: α-syn toxicity, proteasomal inhibition, Pael-R accumulation and kainate-induced excito-toxicity (Feany and Pallanck 2003).

Interestingly, parkin is able to ubiquitinate α- and β- tubulin, regulating their degradation by the 26S proteasome (Ren et al. 2003). Moreover, it can bind tubulin/MTs through strong redundant and independent interactions mediated by three RING domain of parkin, resulting in MT stabilization (Yang et al. 2005). In fact, some *PARK2* mutation can abolish the MT-binding ability of the protein, making parkin unable to protect midbrain dopaminergic neurons from MT-depolymerizing toxins, such as rotenone or colchicine (Ren et al. 2009). Interestingly, in human iPSCs-derived neurons the complexity of neuronal processes was

greatly reduced in both dopaminergic and non-dopaminergic neurons from PD patients with *PARK2* mutations and that MT stability was significantly decreased as demonstrated by the reduction in MT mass (Ren et al. 2015).

Several parkin knockout (KO) mice have been developed, although none has shown substantial dopaminergic or behavioural abnormalities, except for subtle nigrostriatal and *Locus coeruleus* alterations. These mice show a higher susceptibility both to neurotoxins and inflammatory stimuli, suggesting that parkin mutations may sensitize dopaminergic neurones to cellular insults (Blandini and Armentero 2012). On the other hand, transgenic mice overexpressing the Q311X parkin mutation selectively in dopaminergic neurones developed progressive motor deficits and age-dependent nigrostriatal degeneration, as well as a-synuclein pathology, thereby suggesting that mutant parkin proteins may act a dominant-negative modulators (Lu et al. 2009).

In conclusion, parkin acts as a multipurpose neuroprotective agent against a variety of toxic insults, resulting necessary for neuronal functionality and survival, especially for dopaminergic neurons, through different pathways, especially MT stabilization.

## *1.4 2,5-Hexanedione*

The neurotoxic property of certain hexacarbon solvents was discovered in Japan in the early 1960s, when workers exposed to hexanes in the laminating industry developed a sensorimotor polyneuropathy. Similar outbreaks of neuropathy were subsequently reported in Japan, Europe, and the U.S.A. (Spencer et al. 1980). After cessation of exposure, the severity of the neurological deficit has been observed to progress from 1 to 4 months, followed by recovery. The degree of recovery is inversely related to the severity of the neuropathy, and is complete in mild cases, while in most severely affected workers the damage persists (Graham et al. 1995). Japanese physicians also identified the first case of neurological disease in individuals inhaling solvent vapours for their euphoric properties, a practise which subsequently let to the discovery of "glue-sniffers" neuropathy in other countries. The common thread linking the industrial and glue-sniffers neuropathies was repetitive exposure to normal hexane (*n*-hexane). Since this compound had enjoyed wide usage, it was generally regarded as having a low toxicity potential, but this idea was finally overthrown when unequivocal neuropathological damage was demonstrated in exposed rats similar to that reported from examination of nerve biopsies from those patients (Spencer et al. 1980).

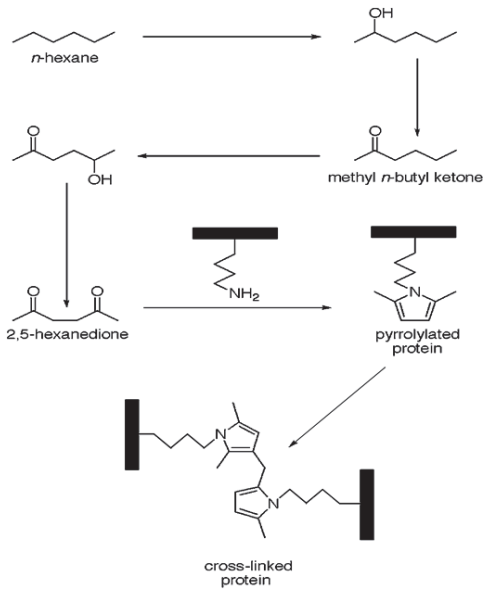


**Figure 15. The reactions of *n*-hexane in cell leading to cross-linked proteins.**
The common solvents *n*-hexane and methyl *n*-butyl methane are converted to the ultimate toxicant, 2,5-hexanedione (2,5-HD). 2,5-HD reacts with lysyl ε-amines of proteins (*black rectangle*) to form pyrrolylated proteins, which undergo intra- and inter-molecular cross-linking reactions, including dimer formation. (Boekelheide et al. 2003)

Thus nowadays, it's well-known that exposure to occupational and environmental solvent mixture containing *n*-hexane, cause peripheral neuropathy and damage to central nervous system, inducing axon atrophy and subsequent axonal swellings (LoPachin and DeCaprio 2004). *n*-Hexane is metabolized in animals and humans to the γ-diketone 2,5-HD, a compound with substantially greater neurotoxic potency than the parent alkane (Spencer and Schaumburg 1985). In fact, 2,5-HD is able to react with the lysine group of proteins forming pyrrole adducts, which undergo secondary oxidation resulting in crosslinked proteins.

Although this toxicant could potentially react with every protein containing lysine groups, it's certain that 2,5-HD preferentially interacts with various components of the cytoskeleton and in particular with NFs (Graham et al. 1995). This results in the degeneration of the distal extent of the longest axons in the peripheral and central nervous system, preceded by the aggregation of NFs in the axoplasm, with the formation of large NF-filled swellings proximal to nodes of Ranvier (Graham 1999). The resulting neuropathy was termed by Cavanagh (Cavanagh 1964) a "dying back" neuropathy, that has been observed in many neurological diseases, PD included.

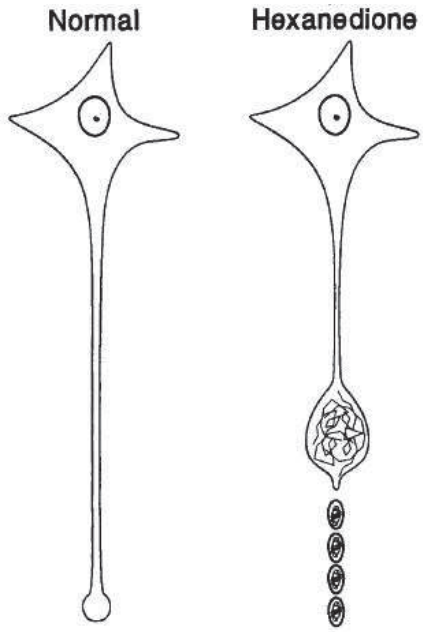


**Figure 16. Typical distal axonopathy following 2,5-HD exposure.**
Chronic exposure to *n*-hexane or their toxic metabolite, 2,5-hexanedione (Hexanedione) results in large swellings of the distal axon filled with NFs. With continued exposure, axonal degeneration develops distal to the axonal swellings. (from Graham et al., 1995)

Since different diseases could have the same pathological mechanism(s), it's crucial to understand the biochemical basis of this toxin-induced neurodegeneration. The crosslinking of NFs and their consequent accumulation in the axonal swellings has been considered the central event in the γ-diketone axonopathy, however, 2,5-HD appeared to affect also the function of MT-associated proteins, such as motor proteins or MAPs (Zhang et al. 2010; Han et al. 2014) and MTs themselves (Boekelheide 1987a; Boekelheide 1987b; Markelewicz et al. 2004), resulting in an impairment of axonal transport, a dysfunction already described in many neurodegenerative diseases (De Vos et al. 2008). The axonal transport defects, in fact, could explain why the NFs are apparently the most affected cytoskeletal component by this compound, since along the length of the axon the NFs appear as a continuous filament that moves down the axon at 1mm/day, the slowest moving component of axoplasm. It follows that it would be vulnerable to progressive derivatization and crosslinking during chronic intoxication, respect to the more dynamic and fast moving MTs and microfilaments (Graham and Gottfried 1984). Moreover, just the accumulation of NFs does not appear to explain the onset distal axonal degeneration, since wt mice and transgenic mice not expressing NFs, revealed similar patterns of distal axonal degeneration in 2,5-HD neuropathy, which is likely to be a consequence of axonal transport impairment (Stone et al. 1999; Stone et al. 2001). The 2,5-HD, like other toxins such as pesticides and chemical compounds, has been clearly correlated also to parkinsonism in occupational exposed humans and in experimental animals (Pezzoli et al. 1990; Pezzoli et al. 2000; Qing-Shan and Xie 2009). Some individuals with particular genotype may have difficulty in metabolizing one or more environmental toxins (Vanacore et al. 2000; Canesi et al. 2003), and this could results in an increased susceptibility to develop PD following toxin exposure. However, in previous studies, the effects of 2,5-HD on intermediate filaments have been extensively described in different cell lines (Durham et al. 1988; Malorni et al. 1989; Sager 1989), but both microfilaments and MTs were poorly investigated. On this purpose, we took advantage of this toxin-induced experimental model of PD neurodegeneration to study in deep the MT dysfunction, also in combination with different genetic backgrounds.

# *Aim of the project*

Many neurodegenerative diseases are characterized by adult-onset, progressive accumulations of specific proteins in different types of neurons. Whether such protein accumulations are the cause or the consequence of axonal transport defects is still a subject of debate. Anyway, it is commonly assumed that disturbances in axonal transport are key pathological events that contribute to neurodegeneration, making them a suitable therapeutic targets in neurodegenerative diseases (Millecamps and Julien 2013). Even if the mechanisms by which axonal transport is disrupted in disease are varied, the principal system to be investigate should be the MT-based transport, being this one the most important transport system in the cells and particularly in neurons.

Among the major human neurodegenerative diseases, also PD can be defined as a disease of impaired intracellular trafficking through the dysfunction of dopaminergic pathway (Hunn et al. 2015). Although, the majority of PD cases are sporadic, both genetic and environmental components are considered to contribute to the disease (Vance et al. 2010; Cannon and Greenamyre 2013). Notably, MTs have been found to interact with some of the proteins mutated in PD and to be affected by the action of some PD toxins (Feng 2006). Therefore, in the last years, the MT dysfunction has become an emerging hypothesis in PD pathogenesis (Feng 2006; Cappelletti et al. 2015).

In this scenario, our aim was to get lines of evidence from different experimental models that could suggest if the early PD pathogenesis is likely to be a consequence of and be defined by MT dysfunction. On this purpose, the role of MTs has been studied in detail, taking advantage of both a gene- (using mainly *PARK2* mutations) and toxin- (using 2,5-HD) based models of PD neurodegeneration. Since dopaminergic neurons, appears to be particularly sensitive to any insult that could damage the MT cytoskeleton because of their peculiar architecture, characterized by an extremely widespread arborization and particularly long axons that made their function and survival strongly dependant by intracellular trafficking (Hunn et al. 2015), NGF-differentiated PC12 cells have been extensively studied as a model of dopaminergic neurons in culture. In addition, MT dysfunction was analysed also *in vitro*, *in vivo* using *PARK2* transgenic mice and human models, including primary skin fibroblasts and post-mortem brain samples from PD patients.

# *Main results*

Cytoskeletal and MT dysfunctions were initially investigated in the context of toxin-based neurodegeneration using NGF-differentiated PC12 cells, as a model of dopaminergic neurons in culture, exposed to 2,5-HD. Thus, the characterization of the cytoskeleton following different concentrations of 2,5-HD (0.2 mM, 2 mM and 20 mM) has been carried out, resulting in a transient increase of actin level and the decrease of both form of NFs investigated, while the tubulin level was unchanged. On the other hand, the immunofluorescence microscopy revealed an impact on all the cytoskeletal components, highlighting actin ruffles, NFs accumulations in the soma and along the neurites and, finally, the fragmentation of the MT network. The analyses of tubulin PTMs also showed an imbalance of MT system, with a different level and distribution of MTs bearing specific PTMs. In fact, acetylated and detyrosinated tubulin levels, associated with stable MTs, were significantly increased and accumulated in the perinuclear zone, while the tyrosinated tubulin, marker of dynamic MT pool, concomitantly decreased. Consistent with these results, also the MT fraction was higher compared to free tubulin fraction in cell, revealing a MT-stabilizing effect of 2,5-HD. Unfortunately, it was no possible to see any effect on tubulin polymerization and MT formation in vitro in the tested conditions, probably because the lacking of a pre-incubation time between tubulin and the toxin. Even some mitochondrial effects observed, in term of increased ROS production and decreased mitochondrial fission/fusion (DRP1 and MFN2, respectively) protein levels, emerged later than those seen for cytoskeleton and tubulin PTMs (Casagrande et al. to be submitted, in PART II). Live cell imaging showed that the absence of parkin in *PARK2*-silenced neuronal-like cells, affected MT system causing a MT destabilization, that consequently lead to altered mitochondria MT-based transport. This axonal transport defects were restored by the MT-stabilizing agent paclitaxel, confirming the importance of modulation of parkin on MT stability (Cartelli et al. to be submitted, in PART II).

In agreement with the data obtained in PC12 cells, the cytoskeleton organization has been investigated and resulted altered also in primary fibroblasts deriving from patients with idiopathic or genetic PD, carrying mutations in *PARK2* and *LRRK2*. All parkinsonian fibroblasts had a reduced MT mass, represented by a higher fraction of unpolymerized tubulin in respect to control cells, and displayed significant changes in MT stability-related signaling pathways, without any activation of autophagy or apoptosis. Furthermore, we show that the reduction of MT mass is so closely related to the alteration of cell morphology and behaviour

that both pharmacological treatment with MT-targeted drugs, and genetic approaches, by transfecting the wt parkin or LRRK2, could restore the proper MT stability and were able to rescue cell architecture. All these data suggest that different mechanisms of neurodegeneration can convergence on the same pathway in both genetic and idiopathic forms of parkinsonism, highlighting, for the first time, that MT dysfunction occurs in patients and not only in experimental models of PD (Cartelli et al. 2012, and Casagrande et al. to be submitted, in PART II). Moreover, fibroblasts from PD patients carrying mutations in *PARK2* resulted much more susceptible to 2,5-HD-dependent MT stabilization than healthy controls, suggesting that the genetic background may really make the difference in MT susceptibility to environmental factors (Casagrande et al. to be submitted, in PART II).

The imbalance of tubulin PTMs, associated with MTs that behave differently, occurred not only in neuronal-like cell model but also in *PARK2* KO mice, preceding the block of mitochondrial transport (Cartelli et al. to be submitted, in PART II). Even in in *PARK2*$^{+/-}$ mice the MT system resulted more dynamic respect to wt ones, revealing by the increased level of tyrosinated tubulin both in lysates from ventral mesencephalon, containing the SNpc, and CS and in immunofluorescence analysis of brain slices. In addition, these heterozygous mice were found surprisingly more active than wt mice, considering the speed, the total distance travelled and the time of immobility (Casagrande et al. manuscript in preparation, in PART III).

More importantly, the increased fragmentation of the acetylated MTs (stable pool) has been reported in iPSC-derived ventral midbrain neurons obtained from *PARK2* PD patients, indicating again parkin as a regulator of MT stability in neurons (Cartelli et al. to be submitted, in PART II).

In conclusion, evidences emerging from the multiple approaches and experimental models employed in this PhD work together with data coming from other laboratories converge on and reinforce the idea that MT dysfunction may be important in the PD pathogenesis (Cappelletti et al. 2015, in PART II).

# *Conclusions*

All the data presented in this thesis clearly indicate that MT system has a key role in neurodegeneration processes. The evidences from both gene- and toxin-based experimental models of PD have revealed that any perturbations of the equilibrium of MT dynamics lead to the impairment of the axonal and intracellular transport with serious consequences on the maintenance and survival of cells, especially of dopaminergic neurons (Cartelli et al., 2012; Casagrande et al., to be submitted, in PART II). Moreover, the genetic background we investigated (*PARK2* mutations) can make the MT cytoskeleton even more susceptible to various environmental insults, probably because of the lacking neuroprotective and MT-stabilizing action of parkin. More importantly, our data also suggests for the first time the direct regulation of parkin on MTs occurs through the modulation of tubulin PTMs in both mice and human neurons, together with the observation that MT system in the PD patients and experimental models is destabilized respect to controls (Cartelli et al., to be submitted, in PART II). We also demonstrated that the other PD-linked protein α-syn is as a novel, foldable, microtubule-dynamase, which organizes the MT cytoskeleton at the presynapse, through its binding to tubulin and its regulation of MT nucleation and dynamics, and lend support to the concept that the α-syn/MT interaction plays a pivotal role in modulating synaptic physiology and its alteration can cause neuronal dysfunction (Cartelli et al., submitted, in PART III). Thus, MT stabilizing strategies may offer an opportunity for treating neurodegenerative diseases. Importantly, we have recently demonstrated that this may be true also in PD showing that Epothilone D, a MT stabilizer drug, exerts neuroprotective effects in a toxin-based murine model of PD (Cartelli et al., 2013, in PART III).

Future work will be focused on further characterization of the molecular mechanisms involved in cytoskeleton dysfunction in PD neurodegeneration, including signalling pathways converging on the regulation of MT system. Since both toxic and transgenic classes of animal PD models have their own specificities and limitations, and above all they do not recapitulate the all the key features of PD, it is more and more crucial to step forward in the study of human samples closer to the real condition of the patients. Thus, we are going to use and analyse more in detail not only the patient brain samples available in the nervous tissue bank, but in particular the powerful cutting-edge model of the pluripotent stem cells (iPSCs)-derived dopaminergic ventral midbrain neurons, obtained from PD patient fibroblasts.

# *References*


Akhmanova A, Steinmetz MO (2008) Tracking the ends: a dynamic protein network controls the fate of microtubule tips. Nat Rev Mol Cell Biol 9:309–322. doi: 10.1038/nrm2369

Alberts B, Johonson A, Lewis J, et al (2008) Molecular Biology of the Cell, Garland Sc.

Alim MA, Hossain MS, Arima K, et al (2002) Tubulin seeds alpha-synuclein fibril formation. J Biol Chem 277:2112–7. doi: 10.1074/jbc.M102981200

Alves da Costa C, Checler F (2012) Parkin: much more than a simple ubiquitin ligase. Neurodegener Dis 10:49–51.

Baas PW (2002) Neuronal polarity: microtubules strike back. Nat Cell Biol 4:E194–E195. doi: 10.1038/ncb0802-e194

Baas PW, Deitch JS, Black MM, Banker G a (1988) Polarity orientation of microtubules in hippocampal neurons: uniformity in the axon and nonuniformity in the dendrite. Proc Natl Acad Sci U S A 85:8335–8339. doi: 10.1073/pnas.85.21.8335

Barra HS, Rodriguez JA, Arce CA, Caputto R (1973) A soluble preparation from rat brain that incorporates into its own proteins (14 C) arginine by a ribonuclease-sensitive system and (14 C)tyrosine by a ribonuclease-insensitive system. J Neurochem 20:97–108. doi: 10.1111/j.1471-4159.1973.tb12108.x

Blandini F, Armentero M-T (2012) Animal models of Parkinson's disease. FEBS J 279:1156–1166. doi: 10.1111/j.1742-4658.2012.08491.x

Boekelheide K (1987a) 2,5-Hexanedione alters microtubule assembly I. Toxicol Appl Pharmacol 88:370–382.

Boekelheide K (1987b) 2,5-Hexanedione alters microtubule assembly II. Toxicol Appl Pharmacol 88:383 – 396.

Boekelheide K, Fleming SL, Allio T, et al (2003) 2,5-Hexanedione-Induced Testicular Injury. Annu Rev Pharmacol Toxicol 43:125–47. doi: 10.1146/annurev.pharmtox.43.100901.135930

Braak H, Tredici K Del, Rüb U, et al (2003) Staging of brain pathology related to sporadic Parkinson's disease. Neurobiol Aging 24:197–211. doi: 10.1016/S0197-4580(02)00065-9

Burbank KS, Mitchison TJ (2006) Microtubule dynamic instability. Curr Biol 16:516–517. doi: 10.1016/j.cub.2006.06.044

Canesi M, Perbellini L, Maestri L, et al (2003) Poor metabolization of n-hexane in Parkinson's disease. J Neurol 250:556–60. doi: 10.1007/s00415-003-1035-y

Cannon JR, Greenamyre JT (2013) Gene-environment interactions in Parkinson's disease:

specific evidence in humans and mammalian models. Neurobiol Dis 57:38–46. doi: 10.1016/j.nbd.2012.06.025

Cappelletti G, Casagrande F, Calogero A, et al (2015) Linking microtubules to Parkinson's disease: the case of parkin. Biochem Soc Trans 43:292–6. doi: 10.1042/BST20150007

Cappelletti G, Maggioni MG, Maci R (1999) Influence of MPP+ on the state of tubulin polymerisation in NGF-differentiated PC12 cells. J Neurosci Res 56:28–35.

Cappelletti G, Surrey T, Maci R (2005) The parkinsonism producing neurotoxin MPP+ affects microtubule dynamics by acting as a destabilising factor. FEBS Lett 579:4781–6. doi: 10.1016/j.febslet.2005.07.058

Cartelli D, Casagrande F, Busceti CL, et al (2013) Microtubule alterations occur early in experimental parkinsonism and the microtubule stabilizer epothilone D is neuroprotective. Sci Rep 3:1837. doi: Artn 1837\rDoi 10.1038/Srep01837

Cartelli D, Goldwurm S, Casagrande F, et al (2012) Microtubule destabilization is shared by genetic and idiopathic Parkinson's disease patient fibroblasts. PLoS One 7:e37467. doi: 10.1371/journal.pone.0037467

Cavanagh J (1964) The significance of "dying back" processes in experimental and human neurological disease. Int Rev Exp Pathol 3:219–267.

Chu C-W, Hou F, Zhang J, et al (2011) A novel acetylation of β-tubulin by San modulates microtubule polymerization via down-regulating tubulin incorporation. Mol Biol Cell 22:448–56. doi: 10.1091/mbc.E10-03-0203

Chu Y, Morfini GA, Langhamer LB, et al (2012) Alterations in axonal transport motor proteins in sporadic and experimental Parkinson's disease. Brain 135:2058–2073. doi: 10.1093/brain/aws133

Conde C, Cáceres A (2009) Microtubule assembly, organization and dynamics in axons and dendrites. Nat Rev Neurosci 10:319–32. doi: 10.1038/nrn2631

Corti O, Lesage S, Brice A (2011) What Genetics Tells us About the Causes and Mechanisms of Parkinson's Disease. Physiol Rev 91:1161–1218. doi: 10.1152/physrev.00022.2010

d'Ydewalle C, Krishnan J, Chiheb DM, et al (2011) HDAC6 inhibitors reverse axonal loss in a mouse model of mutant HSPB1–induced Charcot-Marie-Tooth disease. Nat Med 17:968–974. doi: 10.1038/nm.2396

Dauer W, Przedborski S (2003) Parkinson ' s Disease : Mechanisms and Models. Neuron 39:889–909.

Dawson TM, Dawson VL (2010) The role of parkin in familial and sporadic Parkinson's disease. Mov Disord 25 Suppl 1:S32–9. doi: 10.1002/mds.22798

De Vos KJ, Grierson AJ, Ackerley S, Miller CCJ (2008) Role of axonal transport in neurodegenerative diseases. Annu Rev Neurosci 31:151–73. doi:

10.1146/annurev.neuro.31.061307.090711

Desai A, Mitchison TJ (1997) Microtubule polymerization dynamics. Annu Rev Cell Dev Biol 13:83–117.

Durham H, Pena S, Ecobichon D (1988) Hexahydrocarbon effects on intermediate filament organization in human fibroblasts. Muscle Nerve 11:160–165.

Erickson HP (2000) Gamma-tubulin nucleation: template or protofilament? Nat Cell Biol 2:E93–E96. doi: 10.1038/35014084

Fahn S (2003) Description of Parkinson ' s Disease as a Clinical Syndrome. Ann N Y Acad Sci 991:1–14.

Feany MB, Pallanck LJ (2003) Parkin: a multipurpose neuroprotective agent? Neuron 38:13–16.

Feinstein SC, Wilson L (2005) Inability of tau to properly regulate neuronal microtubule dynamics: a loss-of-function mechanism by which tau might mediate neuronal cell death. Biochim Biophys Acta 1739:268–79. doi: 10.1016/j.bbadis.2004.07.002

Feng J (2006) Microtubule: a common target for parkin and Parkinson's disease toxins. Neuroscientist 12:469–76. doi: 10.1177/1073858406293853

Forman MS, Trojanowski JQ, Lee VM (2004) OUR TENTH YEAR Neurodegenerative diseases : a decade of discoveries paves the way for therapeutic breakthroughs. 10:1055–1063. doi: 10.1038/1113

Graham D (1999) Neurotoxicants and the cytoskeleton. Curr Opin Neurol 12:733–737.

Graham DG, Amarnath V, Valentine WM, et al (1995) Pathogenetic studies of hexane and carbon disulfide neurotoxicity. Crit Rev Toxicol 25:91–112. doi: 10.3109/10408449509021609

Graham DG, Gottfried MR (1984) Cross-species extrapolation in hydrocarbon neuropathy. Neurobehav Toxicol Teratol 6:433–35.

Greenamyre JT, Betarbet R, Sherer TB (2003) The rotenone model of Parkinson's disease: genes, environment and mitochondria. Parkinsonism Relat Disord 9:59–64. doi: 10.1016/S1353-8020(03)00023-3

Han X-Y, Cheng D, Song F-Y, et al (2014) Decelerated transport and its mechanism of 2,5-hexanedione on middle-molecular-weight neurofilament in rat dorsal root ganglia cells. Neuroscience 269:192–198. doi: 10.1016/j.neuroscience.2014.03.044

Hardy J (2010) Genetic analysis of pathways to Parkinson disease. Neuron 68:201–6. doi: 10.1016/j.neuron.2010.10.014

Hernault SWL, Rosenbaumt JL (1985) Clamydomonas alpha-tubulin is posttranslationally modified by acetylation on the €-amino group of a lysine. Biochemistry 24:473–478.

Hunn BHM, Cragg SJ, Bolam JP, et al (2015) Impaired intracellular trafficking defines early Parkinson's disease. Trends Neurosci 38:178–188. doi: 10.1016/j.tins.2014.12.009

Janke C (2014) The tubulin code: Molecular components, readout mechanisms, and functions. J Cell Biol 206:461–472. doi: 10.1083/jcb.201406055

Janke C, Bulinski JC (2011) Post-translational regulation of the microtubule cytoskeleton: mechanisms and functions. Nat Rev Mol Cell Biol 12:773–86. doi: 10.1038/nrm3227

Janke C, Kneussel M (2010) Tubulin post-translational modifications: encoding functions on the neuronal microtubule cytoskeleton. Trends Neurosci 33:362–72. doi: 10.1016/j.tins.2010.05.001

Khan NL, Scherfler C, Graham E, et al (2005) Dysfunction in Unrelated , Asymptomatic Carriers of a Single Parkin. Ann Neurol 7–9.

Kitada T, Asakawa S, Hattori N, et al (1998) Mutations in the parkin gene cause autosomal recessive juvenile parkinsonism. Nature 392:605–608. doi: 10.1038/33416

Kumar A, Aguirre JD, Condos TEC, et al (2015) Disruption of the autoinhibited state primes the E3 ligase parkin for activation and catalysis. EMBO J 34:2506–21.

Kumaran R, Cookson MR (2015) Pathways to Parkinsonism Redux: convergent pathobiological mechanisms in genetics of Parkinson's disease. Hum Mol Genet 24:R32–R44. doi: 10.1093/hmg/ddv236

Langston JW, Ballard P, Tetrud JW, Irwin I (1983) Chronic Parkinsonism in humans due to a product of meperidine-analog synthesis. Science 219:979–980. doi: 10.1126/science.6823561

LoPachin RM, DeCaprio AP (2004) gamma-Diketone neuropathy: axon atrophy and the role of cytoskeletal protein adduction. Toxicol Appl Pharmacol 199:20–34. doi: 10.1016/j.taap.2004.03.008

Lu X-H, Fleming SM, Meurers B, et al (2009) Bacterial Artificial Chromosome Transgenic Mice Expressing a Truncated Mutant Parkin Exhibit Age-Dependent Hypokinetic Motor Deficits, Dopaminergic Neuron Degeneration, and Accumulation of Proteinase K-Resistant -Synuclein. J Neurosci 29:1962–1976. doi: 10.1523/JNEUROSCI.5351-08.2009

Malkus K a, Tsika E, Ischiropoulos H (2009) Oxidative modifications, mitochondrial dysfunction, and impaired protein degradation in Parkinson's disease: how neurons are lost in the Bermuda triangle. Mol Neurodegener 4:24. doi: 10.1186/1750-1326-4-24

Malorni W, Iosi F, Formisano G, Arancia G (1989) Cytoskeletal changes induced in vitro by 2,5-hexanedione: an immunocytochemicalstudy. Exp Mol Pathol 50:50 – 68.

Maraschi A, Ciammola A, Folci A, et al (2014) Parkin regulates kainate receptors by interacting with the GluK2 subunit. Nat Commun 5:5182. doi: 10.1038/ncomms6182

Markelewicz RJ, Hall SJ, Boekelheide K (2004) 2,5-Hexanedione and Carbendazim Coexposure Synergistically Disrupts Rat Spermatogenesis Despite Opposing Molecular Effects on Microtubules. Toxicol Sci 80:92–100. doi: 10.1093/toxsci/kfh140

Matus a. (1994) Stiff microtubules and neuronal morphology. Trends Neurosci 17:19–22. doi: 10.1016/0166-2236(94)90030-2

Millecamps S, Julien J-P (2013) Axonal transport deficits and neurodegenerative diseases. Nat Rev Neurosci 14:161–76. doi: 10.1038/nrn3380

Mitchison T, Kirschner M (1984) Dynamic instability of microtubule growth. Nature 312:237–42. doi: 10.1038/312237a0

Morfini G, Pigino G, Opalach K, et al (2007) 1-Methyl-4-phenylpyridinium affects fast axonal transport by activation of caspase and protein kinase C. Proc Natl Acad Sci U S A 104:2442–2447. doi: 10.1073/pnas.0611231104

Pezzoli G, Canesi M, Antonini a., et al (2000) Hydrocarbon exposure and Parkinson's disease. Neurology 55:667–673. doi: 10.1212/WNL.55.5.667

Pezzoli G, Ricciardi S, Masotto C, et al (1990) N-Hexane Induces Parkinsonism in Rodents. Brain Res 531:355–7.

Prota AE, Bargsten K, Zurwerra D, et al (2013) Molecular mechanism of action of microtubule-stabilizing anticancer agents. Science (80- ) 339:587–590. doi: 10.1126/science.1230582

Qing-Shan W, Xie K-Q (2009) Chronic exposure to n-hexane contributes to induce onset of Parkinson's disease. Med Hypotheses 72:107–8. doi: 10.1016/j.mehy.2008.08.002

Ren Y, Jiang H, Hu Z, et al (2015) Parkin mutations reduce the complexity of neuronal processes in iPSC-derived human neurons. Stem Cells 33:68–78.

Ren Y, Jiang H, Yang F, et al (2009) Parkin protects dopaminergic neurons against microtubule-depolymerizing toxins by attenuating microtubule-associated protein kinase activation. J Biol Chem 284:4009–17. doi: 10.1074/jbc.M806245200

Ren Y, Zhao J, Feng J (2003) Parkin binds to alpha/beta tubulin and increases their ubiquitination and degradation. J Neurosci 23:3316–24.

Rogowski K, van Dijk J, Magiera MM, et al (2010) A Family of Protein-Deglutamylating Enzymes Associated with Neurodegeneration. Cell 143:564–578. doi: 10.1016/j.cell.2010.10.014

Roll-Mecak A, McNally FJ (2010) Microtubule severing enzymes. Curr Opin Cell Biol 22:1–14. doi: 10.1016/j.ceb.2009.11.001.Microtubule

Sager PR (1989) Cytoskeletal effects of acrylamide and 2,5-hexanedione: selective aggregation of vimentin filaments. Toxicol Appl Pharmacol 97:141–155. doi: 10.1016/0041-008X(89)90063-X

Saha AR, Hill J, Utton MA, et al (2004) Parkinson's disease alpha-synuclein mutations exhibit defective axonal transport in cultured neurons. J Cell Sci 117:1017–1024. doi: 10.1242/jcs.00967

Scarffe LA, Stevens DA, Dawson VL, Dawson TM (2014) Parkin and PINK1: much more than mitophagy. Trends Neurosci 37:315–324. doi: 10.1016/j.tins.2014.03.004

Shih Y-L, Rothfield L (2006) The Bacterial Cytoskeleton. Microbiol Mol Biol Rev 70:729–754. doi: 10.1128/MMBR.00017-06

Shimura H, Hattori N, Kubo SI, et al (2000) Familial Parkinson disease gene product, parkin, is a ubiquitin-protein ligase. Nat Genet 25:302–305. doi: 10.1038/77060

Song F, Zhang C, Yu S, et al (2007) Time-dependent alteration of cytoskeletal proteins in cerebral cortex of rat during 2,5-hexanedione-induced neuropathy. Neurochem Res 32:1407–14. doi: 10.1007/s11064-007-9325-x

Song Y, Brady ST (2015) Post-translational modifications of tubulin: pathways to functional diversity of microtubules. Trends Cell Biol 25:125–136. doi: 10.1016/j.tcb.2014.10.004

Song Y, Kirkpatrick LL, Schilling AB, et al (2013) Transglutaminase and polyamination of tubulin: posttranslational modification for stabilizing axonal microtubules. Neuron 78:109–23. doi: 10.1016/j.neuron.2013.01.036

Spencer PS, Schaumburg HH (1985) Organic solvent neurotoxicity: Facts and research needs. Scand J Work Environ Heal 11:53–60.

Spencer PS, Schaumburg HH, Sabri MI, Veronesi B (1980) The enlarging view of hexacarbon neurotoxicity. Crit Rev Toxicol 7:279–356.

Spillantini MG, Schmidt ML, Lee VM-Y, et al (1997) alpha-Synuclein in Lewy bodies. Nature 388:839–840.

Stern MB, Lang A, Poewe W (2012) Toward a redefinition of Parkinson's disease. Mov Disord 27:54–60. doi: 10.1002/mds.24051

Stone JD, Peterson a P, Eyer J, et al (1999) Axonal neurofilaments are nonessential elements of toxicant-induced reductions in fast axonal transport: video-enhanced differential interference microscopy in peripheral nervous system axons. Toxicol Appl Pharmacol 161:50–58. doi: 10.1006/taap.1999.8780

Stone JD, Peterson a P, Eyer J, et al (2001) Neurofilaments are nonessential to the pathogenesis of toxicant-induced axonal degeneration. J Neurosci 21:2278–2287. doi: 21/7/2278 [pii]

Vale RD (2003) The molecular motor toolbox for intracellular transport. Cell 112:467–80. doi: 10.1016/S0092-8674(03)00111-9

Vanacore N, Gasparini M, Brusa L, Meco G (2000) A possible association between exposure to n-hexane and parkinsonism. Neurol Sci 21:49–52.

Vance JM, Ali S, Bradley WG, et al (2010) Gene-environment interactions in Parkinson's disease and other forms of parkinsonism. Neurotoxicology 31:598–602. doi: 10.1016/j.neuro.2010.04.007

Verhey KJ, Gaertig J (2007) The Tubulin Code. Cell Cycle 6:2152–2160.

Wang Q-S, Hou L-Y, Zhang C-L, et al (2008) Changes of cytoskeletal proteins in nerve tissues and serum of rats treated with 2,5-hexanedione. Toxicology 244:166–78. doi: 10.1016/j.tox.2007.11.009

Wang X, Winter D, Ashrafi G, et al (2011) PINK1 and Parkin target miro for phosphorylation and degradation to arrest mitochondrial motility. Cell 147:893–906. doi: 10.1016/j.cell.2011.10.018

Yang F, Jiang Q, Zhao J, et al (2005) Parkin stabilizes microtubules through strong binding mediated by three independent domains. J Biol Chem 280:17154–62. doi: 10.1074/jbc.M500843200

Yao Z, Wood NW (2009) Cell Death Pathways in Parkinson ' s Disease : Role of Mitochondria. Antioxid Redox Signal 11:2135–2149.

Youle RJ, Narendra DP (2011) Mechanisms of mitophagy. Nat Rev Mol Cell Biol 12:9–14. doi: 10.1038/nrm3028

Zhang L, Gavin T, DeCaprio AP, LoPachin RM (2010) Gamma-diketone axonopathy: analyses of cytoskeletal motors and highways in CNS myelinated axons. Toxicol Sci 117:180–9. doi: 10.1093/toxsci/kfq176

# *Acknowledgements*

First of all, I would like to thank my tutor Prof. Graziella Cappelletti, for having given me the opportunity to do my PhD in her lab under her supervision. I am also grateful to her for having introduced me to the exciting field of neuroscience and having sharing her endless passion for science with me.

Secondly, I really want to thank Daniele, for having taught all about neurons and microscopy when I arrived in the lab changing my field of research. Especially, I has been delight from our stimulating discussion on everything and your intellectual curiosity, you've been always a great source of scientific (and also not scientific) inspiration. Thank you also for all the wonderful dinners and evening spend together.

I have to thank Alida, for having taught me almost all I know about mouse brain! You have open me to a new very interesting aspect of neuroscience, that I have really appreciated. Thank you also to all the members of your lab, that help me a lot during these years: in particular Silvia, Francesca and Davide.

Of course I need to thank the Fondazione Grigioni per il Morbo di Parkinson, especially Gianni Pezzoli, for having supporting me, not only financially, but above all for the stimulating ideas and discussion on my project.

A huge thanks to all the member of the lab, in particular to Alessandra and Carmelita.

Many thanks to all my family and friends.

# PART II

# *Contents*

Published Paper 1
Cartelli et al., 2012

OPEN ACCESS Freely available online

PLoS one

# Microtubule Destabilization Is Shared by Genetic and Idiopathic Parkinson's Disease Patient Fibroblasts

**Daniele Cartelli[1], Stefano Goldwurm[2], Francesca Casagrande[1], Gianni Pezzoli[2], Graziella Cappelletti[1]***

**1** Department of Biology, University of Milan, Milan, Italy, **2** Parkinson Institute, Istituti Clinici di Perfezionamento, Milan, Italy

## Abstract

Data from both toxin-based and gene-based models suggest that dysfunction of the microtubule system contributes to the pathogenesis of Parkinson's disease, even if, at present, no evidence of alterations of microtubules *in vivo* or in patients is available. Here we analyze cytoskeleton organization in primary fibroblasts deriving from patients with idiopathic or genetic Parkinson's disease, focusing on mutations in parkin and leucine-rich repeat kinase 2. Our analyses reveal that genetic and likely idiopathic pathology affects cytoskeletal organization and stability, without any activation of autophagy or apoptosis. All parkinsonian fibroblasts have a reduced microtubule mass, represented by a higher fraction of unpolymerized tubulin in respect to control cells, and display significant changes in microtubule stability-related signaling pathways. Furthermore, we show that the reduction of microtubule mass is so closely related to the alteration of cell morphology and behavior that both pharmacological treatment with microtubule-targeted drugs, and genetic approaches, by transfecting the wild type parkin or leucine-rich repeat kinase 2, restore the proper microtubule stability and are able to rescue cell architecture. Taken together, our results suggest that microtubule destabilization is a point of convergence of genetic and idiopathic forms of parkinsonism and highlight, for the first time, that microtubule dysfunction occurs in patients and not only in experimental models of Parkinson's disease. Therefore, these data contribute to the knowledge on molecular and cellular events underlying Parkinson's disease and, revealing that correction of microtubule defects restores control phenotype, may offer a new therapeutic target for the management of the disease.

**Citation:** Cartelli D, Goldwurm S, Casagrande F, Pezzoli G, Cappelletti G (2012) Microtubule Destabilization Is Shared by Genetic and Idiopathic Parkinson's Disease Patient Fibroblasts. PLoS ONE 7(5): e37467. doi:10.1371/journal.pone.0037467

**Editor:** Sara Salinas, CNRS, France

**Received** November 3, 2011; **Accepted** April 23, 2012; **Published** May 22, 2012



**Funding:** This work was supported by Fondazione Grigioni per il Morbo di Parkinson, Milan, Italy (to G.C.) and "Dote ricerca", FSE, Regione Lombardia, Italy (to D.C.). The funders had no role in study design, data collection and analysis, decision to publish, or preparation of the manuscript.

**Competing Interests:** The authors have declared that no competing interests exist.

* E-mail: graziella.cappelletti@unimi.it

## Introduction

Parkinson's disease (PD) is the most common motor neurodegenerative disorder, characterized by the loss of dopaminergic neurons in the substantia nigra. Although it has been extensively studied, its molecular etiopathogenesis is not well understood [1]. Monogenic forms of the disorder account for up to 10% of parkinsonisms, and mutated *parkin* and leucine-rich repeat kinase 2 (*LRRK2*) are responsible for the majority of genetic PD cases [2]. Although parkin and LRRK2 seem to act on different physiological processes, being parkin an E3 ligase catalyzing the addition of ubiquitin to target proteins [3] and LRRK2 a multi-domain protein involved in the regulation of neuronal process elongation [4], their actions converge on microtubules (MTs) [5,6].

MTs are cytoskeletal polymers built up by $\alpha/\beta$ tubulin heterodimers, which participate in many cellular functions, such as morphology acquisition, cell migration and intracellular transport. MTs usually show a dynamic behavior switching between slow growth and rapid depolymerization [7]. α-Tubulin post-translational modifications (PTMs) correlate with subsets of MTs that behave differently: tyrosinated (Tyr) MTs are the most dynamic subset, acetylated (Ac) or detyrosinated (deTyr) MTs are more stable pools [8].

Several recent studies have highlighted the crucial role of MTs during PD progression. Indeed, many PD-linked proteins, such as parkin, LRRK2 and α-synuclein, are able to modulate the stability of MTs [9–11]. However, nothing has been reported about their ability to regulate α-tubulin PTMs. Further evidence has been obtained from neurotoxic models of PD: both rotenone and 1-methyl-4-phenyl-piridinium ($MPP^+$) destabilize MTs *in vitro* [12,13] and in neuronal cells [14,15]. Moreover, we have demonstrated the importance of α-tubulin PTMs in PD pathology, reporting that $MPP^+$ causes an early change in MT stability [15]. All these data highlight the importance of MT dysfunction in PD experimental models, but the demonstration of MT involvement in human disease is still lacking.

Post-mortem analyses of human brain could reveal molecular alterations present in the very late phases of neurodegenerative diseases, with the great disadvantage of working with dead tissues. On the other hand, peripheral tissues are a unique source of human living cells, and in the last few years they have become reliable models for the identification of molecular alterations and possible therapeutic targets in neurodegenerative disorders, including PD [16–19]. As recently highlighted [20], human skin fibroblasts are an easy available and robust PD experimental model, due to some of their peculiarities: they express most of the gene relevant to PD and mirror the polygenic risk factors of specific patient; they comprise the chronological and biological aging other than the environmental exposition, reflecting all the cumulative cell damage of the patient; they make very dynamic contacts as neurons do.

On this basis, here we analyzed fibroblasts from patients with idiopathic PD or from patients carrying mutations in either parkin or LRRK2 to establish whether MT alterations are present in baseline conditions or not. The principal findings we report are the considerable reduction in fibroblast MT mass in PD patients with respect to controls and the rescue resulting from either pharmacological or genetic approaches that stabilize MT system. Thus, our results highlight that MT destabilization occurs in PD patients and it seems to represent a point of convergence of genetic and idiopathic parkinsonisms.

## Materials and Methods

### Ethics Statement and Patients

Primary fibroblasts were obtained by skin biopsies from 25 individuals, whose phenotype and genotype data are summarized in Table 1, and that included 10 healthy volunteers as control group and 15 patients affected by PD, divided into three different pathological groups. Age distribution of each group is reported in the scatter plot (Figure S1), and the statistical analyses did not reveal significant differences in age between control and patient groups. All patients were examined by movement disorder neurologists and clinical diagnosis of PD was established according to the UK Parkinson Disease Society Brain Bank criteria [21,22]. The *LRRK2* G2019S missense mutation and mutations on the parkin (*PRKN*) gene were screened as previously described [23,24].

The study was approved by the local ethics committee (Istituti Clinici di Perfezionamento, July 13th 2010) and all participants gave written informed consent.

### Cell Culture and Morphometric Analyses

Human fibroblasts were cultured in RPMI 1640 (Hyclone, Logan, UT, USA) containing 15% foetal bovine serum (HyClone) supplemented with 2 mM L-glutamine, 100 U/ml penicillin, 100 μg/ml streptomycin, at 37°C in a humidified atmosphere, 5% $CO_2$. For transfection experiments, human fibroblasts were plated at the density of 5000 cells/well. The day after cells were transiently transfected using Lipofectamine 2000 (Invitrogen) (1:3 DNA to Lipofectamine ratio, 1.5 μg of DNA per well) and analyzed 24 h after transfection. All the plasmids for parkin silencing and over-expression (Figure S2) were supplied by Dr. Sassone (IRCCS Istituto Auxologico Italiano, Milano, Italy) The plasmids encoding untagged human parkin was generated by in-frame insertion of a PCR-amplified DNA fragment encoding human parkin into the pcDNA4-Myc-HIS vector. The fragment was then subcloned in the pECFP-C1 vector to produce in frame CFP-tagged parkin. As negative control a plasmid encoding EGFP mRNA was used. Plasmid encoding short hairpin RNA (shRNA) selective for human parkin was generated with the Gateway®

**Table 1.** Phenotype and genotype characterisation of investigated individuals.

| | COD | PHENOTYPE | GENOTYPE | SEX | AGE[a] | AGE OF ONSET [b] |
|---|---|---|---|---|---|---|
| **CONT** | FFF0311991 | HEALTHY | | F | 39 | |
| | FFF0541986 | HEALTHY | | M | 41 | |
| | FFF0191992 | HEALTHY | | M | 43 | |
| | FFF0531978 | HEALTHY | | F | 44 | |
| | FFF0961978 | HEALTHY | | M | 44 | |
| | FFF0401991 | HEALTHY | | F | 46 | |
| | FFF0521978 | HEALTHY | | M | 51 | |
| | FFF0421991 | HEALTHY | | M | 54 | |
| | FFF0422011 | HEALTHY | | M | 69 | |
| | FFF0412011 | HEALTHY | | F | 64 | |
| **PARK** | FFF0302009 | AFFECTED | c.C815G (p.C238W); exon 6–7 del. | F | 57 | 30 |
| | FFF1072009 | AFFECTED | c.del202_203AG (p.Q34/X43); exon 4–6 del. | M | 53 | 40 |
| | FFF0142009 | AFFECTED | c.C924T (p.R275W); exon 3 del. | F | 41 | 22 |
| | FFF0292009 | AFFECTED | exon 3 del (homozygotes) | F | 69 | 39 |
| | FFF0902009 | AFFECTED | c.del202_203AG (p.Q34/X43) (homozygotes) | M | 51 | 20 |
| | FFF0072010 | AFFECTED | c.del202_203AG (p.Q34/X43) (homozygotes) | F | 59 | 39 |
| **LRRK2** | FFF0642009 | AFFECTED | p.G2019S (heterozygotes) | F | 58 | 41 |
| | FFF0962009 | AFFECTED | p.G2019S (heterozygotes) | M | 47 | 40 |
| | FFF0112010 | AFFECTED | p.G2019S (homozygotes) | M | 68 | 63 |
| | FFF0092009 | AFFECTED | p.G2019S (heterozygotes) | M | 46 | 35 |
| | FFF0502009 | AFFECTED | p.G2019S (heterozygotes) | F | 61 | 46 |
| | FFF0452009 | AFFECTED | p.G2019S (heterozygotes) | M | 79 | 72 |
| **PD** | FFF0562009 | AFFECTED | X | M | 71 | 66 |
| | FFF0542009 | AFFECTED | X | M | 68 | 52 |
| | FFF0202010 | AFFECTED | X | M | 50 | 42 |

[a]Age at time of skin biopsy and establishment of fibroblast cell line.
[b]The age at which the patient first noticed a PD-related symptom was considered the age of onset of the disease.
doi:10.1371/journal.pone.0037467.t001

recombination cloning technology (Invitrogen, Carlsbad, CA). The sequence is: sh-183: 5′ CACCGGATCAGCAGAG-CATTGTTCACGAATGAACAATGCTCTGCTGATCC 3′.

The double stranded DNA oligo encoding a sense-loop-antisense sequence to the targeted gene was cloned into the pENTR$^{TM}$/U6 entry vector. The shRNA cassettes was then transferred into the plasmid pBLOCK-iT 3-DEST, suitable for Geneticin® selection. As negative control a plasmid encoding shRNA for bacterial lacZ mRNA was used. LRRK2 constructs [25] were kindly gifted by Dr. Greggio (Department of Biology, University of Padova, Padova, Italy).

For pharmacological treatment, control and patient fibroblasts were plated at the density of 5000 cells/well. The day after cells were incubated 2 h with 10 μM of Paclitaxel dissolved in methanol (Sigma-Aldrich, St Louis, MO), Nocodazole dissolved in methanol (Sigma-Aldrich) or Thiocolchine dissolved in DMSO (provided by Dr. Passarella, Dep. of Industrial and Organic Chemistry, Univ. of Milan, Italy) and then analyzed.

In all assays, the fibroblast passage numbers were matched (<10). For morphometric analyses, 5 to 10 random images per plate were captured using an Axiovert 200 M microscope (Zeiss, Oberkochen, Germany), and analyses were made using digital image processing software (Interactive measurement module, Axiovision, Zeiss). All cells in each image were analyzed.

### Immunofluorescence Microscopy

Cells were fixed with cold methanol or 4% paraformaldehyde and incubated with the following primary antibodies and probes: α-tubulin mouse IgG (clone B-5-1-2, Sigma-Aldrich, St Louis, MO); deTyr tubulin rabbit IgG (Chemicon, Temecula, CA); Tyr tubulin mouse IgG (clone TUB-1A2, Sigma-Aldrich); Ac tubulin mouse IgG (clone 6-11B-1, Sigma-Aldrich); vimentin mouse IgG (clone V6, Sigma-Aldrich); Phalloidin-Tetramethylrhodamine B isothiocyanate and 4′,6-Diamidino-2-phenylindole dihydrochloride (Sigma-Aldrich). As secondary antibodies we used Alexa Fluor$^{TM}$ 568 donkey anti-mouse, and Alexa Fluor$^{TM}$ 488 goat anti-rabbit (Invitrogen, Carlsbad, CA). The coverslips were mounted in Mowiol® (Calbiochem, San Diego, CA)–DABCO (Sigma-Aldrich, St Louis, MO) and examined with the Axiovert 200 M microscope.

### Western Blot Analysis

Whole cell extracts, Triton X-100 soluble and insoluble fractions of human fibroblasts were prepared as previously reported [26]. Equal proportions of each fraction or protein samples from whole cell extracts (25 μg per lane) were separated by 7 or 15% SDS-PAGE and blotted onto PDVF membranes (Immobilon$^{TM}$-P, Millipore, Billerica, MA). Membranes were probed with the following antibodies: α-tubulin mouse IgG (clone B-5-1-2, Sigma-Aldrich, St Louis, MO); β-tubulin mouse IgG (clone Tub 2.1, Sigma-Aldrich); deTyr tubulin rabbit IgG (Chemicon, Temecula, CA); Tyr tubulin mouse IgG (clone TUB-1A2, Sigma-Aldrich); Ac tubulin mouse IgG (clone 6-11B-1, Sigma-Aldrich); microtubule-associated protein 1 light chain 3 rabbit IgG (Sigma-Aldrich); vimentin mouse IgG (clone V6, Sigma-Aldrich); actin mouse IgM (N350, Amersham, Little Chalfont, UK); Caspase 3 rabbit IgG (Enzo Life Sciences Ag., Lausen, Switzerland), GADPH mouse IgG (Biogenesis, Poole, UK); Heat Shock Protein 70 mouse IgG (clone 3A3, Chemicon); Glycogen synthase kinase 3 beta rabbit IgG (Abcam, Cambride, UK); Phospho-Glycogen synthase kinase 3 beta (Ser9) rabbit IgG (Cell Signaling Technology, Beverly, MA); p38 alpha MAP Kinase mouse IgG (clone L53F8, Cell Signaling Technology); Phospho-p38 MAP Kinase (Thr180/Tyr182) rabbit IgG (clone 3D7, Cell Signaling Technology); p44/42 MAPK (Erk1/2) rabbit IgG (clone 137F5, Cell Signaling Technology); Phospho-p44/42 MAPK (Thr202/Tyr204) rabbit IgG (clone D13.14.4E, Cell Signaling Technology); parkin mouse IgG (clone prk8, Sigma-Aldrich). Next, immunoblots were incubated with HRP donkey anti-mouse IgG and HRP goat anti-rabbit IgG (Pierce, Rockfort, IL) or HRP goat anti-mouse IgM (Sigma-Aldrich), and developed using enhanced chemioluminescence (Supersignal West Pico Chemiluminescent, Pierce, Rockford, IL). Immunoblots were scanned with JX-330 color image scanner (Sharp Electronics Europe) and analyzed by ImageJ software (National Institute of Health).

### Statistical Analysis

Statistical analysis was performed using STATISTICA (StatSoft Inc., Tulsa, OK), and significant differences of PD patients versus control fibroblasts, or between groups in rescue experiments, were assessed by one-way ANOVA with Tukey HSD *post hoc* test. Data are expressed as means ± SEM.

## Results

### Morphological Alterations Characterize PD Fibroblasts

We observed striking differences between the cultured human fibroblasts collected from PD patients and those collected from controls in terms of morphology and behavior. Looking at the general morphology of the cells, control fibroblasts were elongated and flanked each other, whereas fibroblasts from PD patients were wider, larger, and partly overlapped, as they lost the ability to sense each other (Figures 1 and 2). Morphometric analyses underlined the decrease of the ratio between maximum and minimum axis (Figure 1B), and the measurement of the area corroborated the idea that PD fibroblasts were larger than control cells (Figure 1C), at least in the presence of mutated parkin or LRRK2. Furthermore, parkinsonian fibroblasts showed a different spatial organization, being much more enshrouded, as pointed out by the increase in overlapping regions (Figure 1D). These data highlight that fibroblasts deriving from PD patients are characterized by altered morphology.

### PD Fibroblasts Show Subtle Cytoskeleton Differences

Since changes in cell morphology are likely mediated by rearrangements of cytoskeletal architecture, we investigated the levels (Figure 2A–B) and organization (Figure 2C) of all the three cytoskeletal polymers: intermediate filaments (IFs), MTs and actin filaments. The levels and localization of vimentin, the principal constituent of the fibroblast IFs, did not vary in PD fibroblasts. Tubulin levels showed changes only in patients carrying parkin mutations, whereas MT organization did not appear to change in any of the experimental groups. It has been reported that parkin promotes α- and β-tubulin degradation and that its PD-linked mutations remove this ability [5]; thus, the enrichment of β-tubulin in patients with parkin mutation is not surprising. On the contrary, α-tubulin levels were unexpectedly unchanged, suggesting possible different regulatory mechanisms that need future and deeper investigations. Finally, we observed a dramatic increase in actin levels in patients with idiopathic PD; phalloidin staining revealed a higher amount of stress fibers that appeared to be randomly oriented whereas in the other experimental groups they were aligned with the major axis of the cells. Thus, these data demonstrate that alterations of the cytoskeleton occur in fibroblasts obtained from patients with parkin mutations and from idiopathic PD patients.

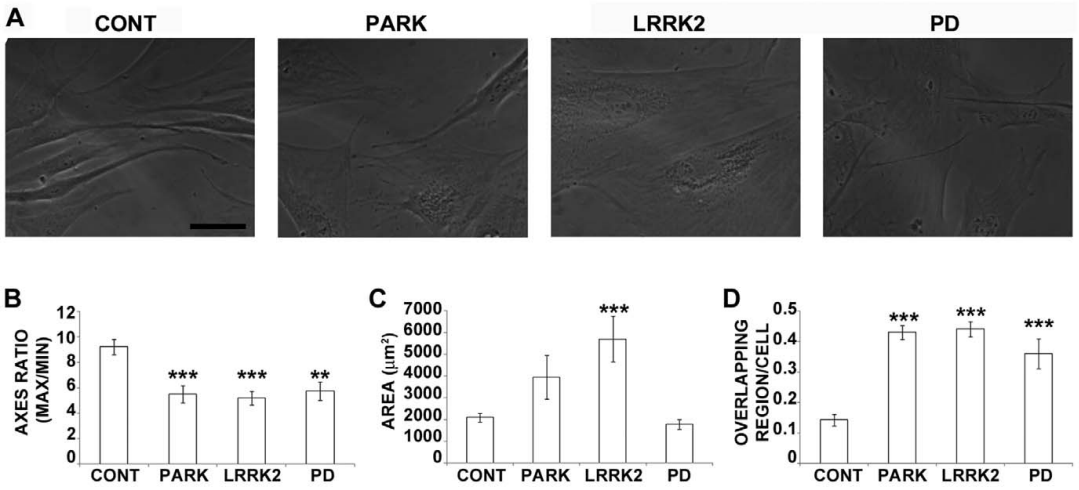


**Figure 1. Morphological alterations characterize PD fibroblasts.** (A) Representative phase contrast micrographs of cultured human fibroblasts of healthy and PD affected people. Scale bar: 25 μm. Morphometric analysis showed reduced ratio between maximum and minimum axes in parkinsonian fibroblast (B) and increased area in the presence of mutated parkin or LRRK2 (C). (D) Histogram showing the increased number of overlapping regions between cells in patient fibroblasts. *$p<0.05$ and ***$p<0.005$ vs control according to ANOVA, Tukey HSD *post hoc* test. All values are expressed as mean ± SEM. CONT = control (N = 10); PARK = patients with mutations of *parkin* (N = 6); LRRK2 = patients carrying mutations in *LRRK2* (N = 6); PD = idiopathic Parkinson's disease patients (N = 3).
doi:10.1371/journal.pone.0037467.g001

## Impairment of MT Stability is Shared by PD Fibroblasts

Since we have already reported that MT stability plays a crucial role in cultured PC12 cells exposed to $MPP^+$ [15], we undertook an in-depth analysis of α-tubulin PTMs and MT mass in human fibroblasts. Western blotting (Figure 3A–B) and immunofluorescence analyses (Figure S3) revealed severe alterations of tubulin PTMs in PD fibroblasts. Parkin mutations induced an increase in Tyr tubulin levels (Figure 3B, dark grey bars), meaning that in the presence of mutated parkin the MT system seemed to be more dynamic. On the other hand, LRRK2 mutation (Figure 3B, light grey bars) caused the enrichment of Ac tubulin, and fibroblasts from patients with idiopathic PD (Figure 3B, black bars) showed a significant increase in deTyr tubulin levels, suggesting that MT (over)stabilization has occurred. The LRRK2-mediated MT stabilization agrees with the results of Gillardon [10], showing that G2019S mutation, the same mutation carried by fibroblasts used here, promotes phosphorylation of β-tubulin and enhances MT stability. We looked further at the α-tubulin PTMs localization (Figure S3). Control cells showed an intense perinuclear Ac tubulin decoration, whereas Ac MTs filled the entire cell body of PD fibroblasts, suggesting that this particular subset of stable MTs had spread, interfering with cell morphology and behavior. Taken together, all these data point out that the alteration of MT stability seems to be a common feature of PD patient fibroblasts. As it has already been reported that PD-inducing neurotoxins affect the state of tubulin polymerization *in vitro* and in neuronal cells [12–15], we wondered whether the observed changes in MT stability were correlated with abnormal MT mass in patient fibroblasts. By Western blotting and densitometric analyses (Figure 3C–D) we evaluated the amount of α-tubulin associated with Triton-soluble, i.e. dimeric pool (Dim), and with Triton-insoluble fraction, polymerized MT fraction (MT). The ratio between free α-tubulin versus α-tubulin incorporated into MTs was significantly increased in PD fibroblasts in respect to control cells (Figure 3D), meaning that polymerized MTs were reduced. Thus, our work shows that MT depolymerization is shared by all patient fibroblasts here analyzed and obtained from idiopathic and genetic PD.

## GSK3β Phosphorylation is Reduced in PD Fibroblasts

Looking for a possible explanation for the observed MT destabilization in PD fibroblasts, it is reasonable that Parkin and LRRK2 mutations directly impact MT stability [9,10]. However, since MT depolymerization is observed also in idiopathic PD fibroblasts, we decided to evaluate the potential implication of signaling pathways converging on MT system. Therefore, in all the PD fibroblast groups, we investigated the level and the activity of glycogen synthase kinase 3 beta (GSK3β), p38 protein (p38) and extracellular signal-related kinases (Erk) that regulate MT stability through the phosphorylation of MT-associated proteins (MAPs). As shown in figure 4, the levels of total GSK3β were highly variable but they did not reach any statistical significance, whereas GSK3β phosphorylation was significantly reduced in all classes of PD fibroblasts (Figure 4C). Total p38 showed a significant reduction only in the presence of mutant LRRK2, whereas phospho-p38 was completely unchanged. On the other hand, LRRK2 induced also a slight decrease of Erk and the significant elevation of phospho-Erk; accordingly to Ren and colleagues [27], fibroblasts from patients with parkin mutation displayed an increase of Erk phosphorylation, although without statistical significance. Nevertheless, phosphorylated GSK3β is the inactive form and the phosphorylation of MAPs by GSK3β promotes their detachment from MT walls [28]. Therefore, showing the significant activation of GSK3β, our data offer a possible mechanistic explanation for the observed MT destabilization in idiopathic PD fibroblasts, but also in cells deriving from patients with genetic cases of the pathology.

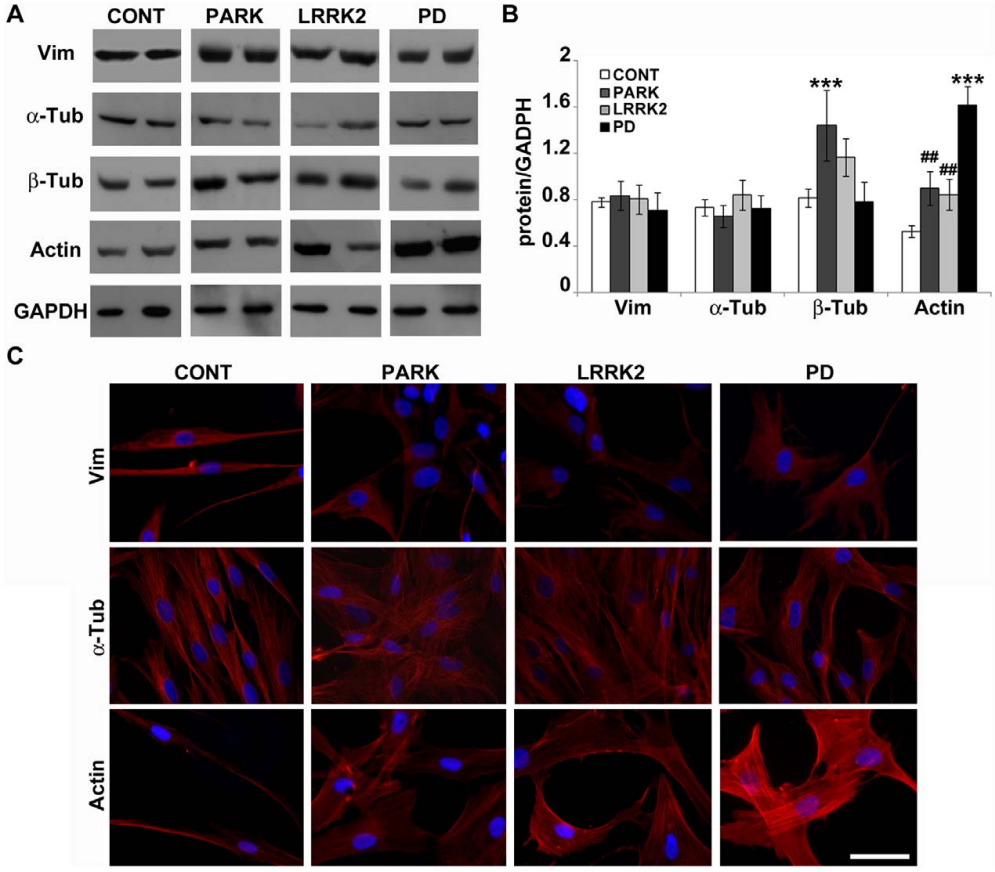


**Figure 2. PD fibroblasts show subtle cytoskeleton differences.** (A) Immunoblot and (B) densitometric analyses of vimentin (Vim), α-tubulin (α-Tub), β-tubulin (β-Tub) and actin (Actin) were performed in whole cell extracts from human fibroblasts deriving from control (CONT, white bars, N = 10), mutated *parkin* (PARK, dark grey bars, N = 6), mutated *LRRK2* (LRRK2, light grey bars, N = 6) and idiopathic PD (PD, black bars, N = 3). For the quantitation, values of each protein were normalized on the level of GAPDH of the relative sample. All values are expressed as mean ± SEM. *$p<0.05$ and ***$p<0.005$ vs control, ##$p<0.02$ vs PD, according to ANOVA, Tukey HSD *post hoc* test. (C) Cultured human fibroblasts were stained with anti-vimentin and anti-α-tubulin primary antibodies or with TRITC-conjugated phalloidin to reveal the organization of intermediate filaments (Vim, top), microtubules (α-Tub, middle) and actin fibers (Actin, bottom), respectively. Concurrent nuclear staining was made by using DAPI (Blue). Scale bar: 20 μm.
doi:10.1371/journal.pone.0037467.g002

## Stress-induced Pathways are not Activated in PD Fibroblasts

MT stability is crucial for the activation of apoptosis and autophagy [29,30], processes variously related to neurodegeneration in PD [31]. Thus, we decided to analyze the levels of caspase 3 (CASP 3), which is a terminal executioner of apoptosis, and heat shock protein 70 (HSP 70), which is a molecular chaperone with anti-apoptotic properties that prevents aggregation and misfolding of proteins [32]. First of all, the lack of the cleaved form of CASP 3 (Figure 5A) highlighted that there was no activation of the apoptotic programme; moreover, we observed the reduction in the inactive form of the enzyme in the presence of mutated parkin (Figure 5B, dark grey bars). On the other hand, mutant LRRK2 induced a significant reduction in HSP 70 (Figure 5B, light grey bars); interestingly, this finding could explain the higher sensitivity of LRRK2 mutant induced pluripotent stem cell (iPSC)-derived dopaminergic neurons to CASP 3 activation [33]. On the contrary, HSP 70 levels were hugely increased in fibroblasts from idiopathic PD patients (Figure 5B, dark bars). As it has already been reported that HSP 70 prevents MT assembly [34] and stabilizes actin filaments [35], these results, together with the reduction of GSK3β phosphorylation, could easily explain the above reported MT destabilization and the increase in actin filaments in idiopathic PD fibroblasts. Finally, we also looked at microtubule-associated protein 1 light chain 3 (LC3) I and II, well known markers of autophagy. The amount of LC3-II correlates with the extent of autophagosome formation and the conversion of LC3-I to LC3-II is a reliable indicator of autophagic activity [36]. Our results showed no significant changes in the levels of LC3-I and LC3-II (Figure 5), and therefore in PD fibroblasts the autophagic machinery is active at basal level. The levels of LC3-I

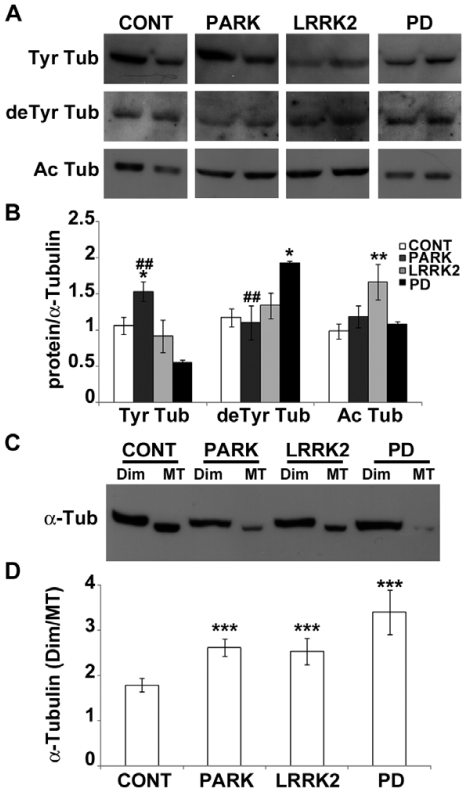


**Figure 3. Impairment of MT stability is shared by PD fibroblasts.** (A) Immunoblot and (B) densitometric analyses of Tyr, deTyr, and Ac tubulin, were performed in whole cell extracts from human fibroblasts deriving from control (white bars), mutated *parkin* (dark grey bars), mutated *LRRK2* (light grey bars) and idiopathic PD (black bars). For the quantitation, values of each α-tubulin PTM were normalized on the level of α-tubulin of the relative sample. Triton X-100-soluble (free α-tubulin, Dim) and -insoluble fraction (α-tubulin incorporated into MTs, MT) of human fibroblasts were analyzed by (C) immunoblot and (D) densitometric analyses and are shown as ratio. *$p<0.05$ and ***$p<0.005$ vs control, ##$p<0.02$ vs PD, according to ANOVA, Tukey HSD *post hoc* test. All values are expressed as mean ± SEM. CONT = control (N = 10); PARK = patients with mutations of *parkin* (N = 6); LRRK2 = patients carrying mutations in *LRRK2* (N = 6); PD = idiopathic Parkinson's disease patients (N = 3).
doi:10.1371/journal.pone.0037467.g003

and -II in LRRK2-linked PD differed from those already reported in knockout mice [37], suggesting that the lack or the mutation of LRRK2 may affect autophagy differently. These data highlight that there is no activation of stress-induced pathways in PD fibroblasts. However, these fibroblasts show MT system alterations that may eventually trigger neuronal death by other mechanisms.

## Pharmacological Stabilization of MTs Rescues Fibroblast Phenotype

To validate the idea that MTs and MT destabilization are crucial players in altering cell functions and behaviors in PD conditions, we decided to treat patient derived fibroblasts with taxol (Figure 6), a potent MT stabilizer that has proven to be neuroprotective in midbrain dopaminergic neurons in cultures [14]. After 2 h of treatment with 10 μM of Taxol, tubulin was completely shifted toward the Triton-insoluble fraction (Figure 6A), meaning that there was an increase in the MT pool in patients fibroblasts. The morphometric analyses (Figure 6B–D) showed that the increase in MTs correlated with a correction of cell morphology and behavior, pointed out by the increase of the ratio between maximum and minimum axis and by the reduction of overlapping regions. Furthermore, we treated control fibroblasts with colchicine or nocodazole, two well known MT destabilizing drugs. As expected, we observed almost all the tubulin associated to the unpolymerized pool (Figure 6E), the reduction of the axes ratio and the dramatic increase of overlapped cells (Figure 6F–H), showing that a direct interference with the MT system is sufficient to induce the same alterations we observed in PD fibroblasts (Figure 1). Taken together, these data demonstrate that impairment of MT stability in PD patient derived cells is directly correlated to changes in morphology and behavior, and strongly suggest that MT system may be a good "druggable" candidate for restoring the proper cell mechanics.

## Genetic Manipulation Restores MT Stability and Rescues Fibroblast Phenotype

To further consolidate our results, we decided to perform rescue experiments, by over-expressing the wild-type (WT) parkin or LRRK2 in the fibroblasts from patients bearing the mutations in parkin or LRRK2, respectively. Moreover, in order to validate the idea that genetic manipulations of these proteins directly influence MT system, and therefore cell architecture, we tried to affect control fibroblasts either by parkin silencing or by mutant LRRK2 expression. As reported in figure 7A, transfection of WT parkin increased polymerized MTs in patient fibroblasts, whereas parkin silencing reduced MT fraction in control cells. Consistent with our hypothesis, the analyses of cell morphology revealed that expression of WT parkin increased the axes ratio and reduced overlapping regions whereas its silencing exerted the opposite effects (Figure 7B–D), mimicking changes observed in patient fibroblasts. In the same way, over-expression of WT LRRK2 in patient fibroblasts increased MT fraction (Figure 7E), and induced a correction of cell morphology (Figure 7F–H), as highlighted by increased ratio between maximum and minimum axis. Similarly, the expression of mutant LRRK2 in control cells promoted MT destabilization, represented by the increase of free tubulin (Figure 7E), and worsened fibroblast morphology and behavior (Figure 7F–H), as showed by the reduced axes ratio and by the increased overlapping regions. Our data, not only demonstrate that alteration of cell morphology and behavior in genetic PD patient fibroblasts are dependent on impairment of MT stability, but, further, our results make light on the capacity of WT parkin or LRRK2 to correct cell defects by restoring MT stability. This point is further sharpened by the absence of significant differences between the morphology of patient fibroblasts transfected with WT parkin or LRRK2 and the cells from healthy subjects expressing control vectors, indicating that the correction of MT system is sufficient to rescue the cell architecture. Together with the pharmacological experiments, these data reinforce the idea of a pivotal role of MT destabilization, and make concrete the hypothesis of a possible MT-based PD therapy.

## Discussion

In this study, we demonstrate that MT stability is impaired in human fibroblasts derived from genetic PD patients and it is likely compromised in idiopathic PD patients, reporting the alterations

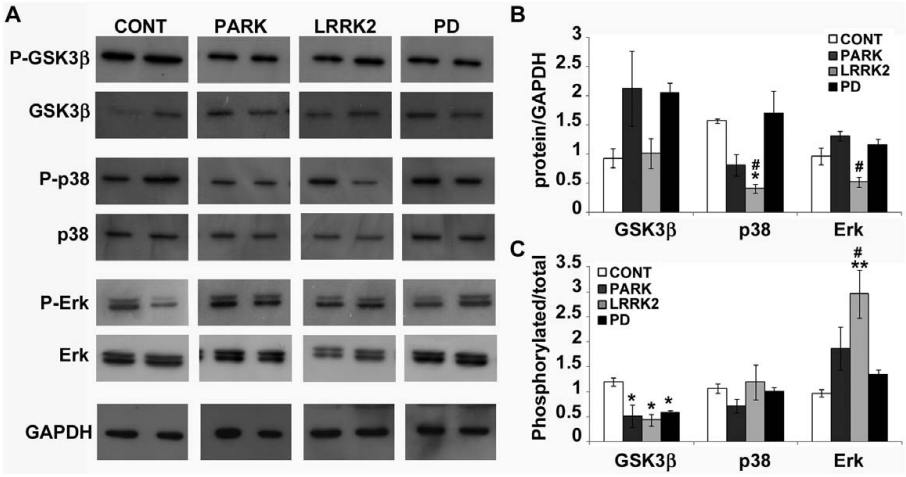


**Figure 4. GSK3β phosphorylation is reduced in PD fibroblasts.** (A) Immunoblot and densitometric analyses of (B) total and (C) phosphorylated glycogen synthase kinase 3 beta (GSK3β), p38 MAP Kinase (p38) and p44/42 MAPK (Erk) were performed in whole cell extracts from human fibroblasts deriving from control (CONT, white bars, N = 3), mutated *parkin* (PARK, dark grey bars, N = 3), mutated *LRRK2* (LRRK2, light grey bars, N = 3) and idiopathic PD (PD, black bars, N = 3). For the quantitation, values of total protein were normalized on the level of GAPDH of the relative sample, whereas the levels of phosphorylated form were normalized on the values of total protein. All values are expressed as mean ± SEM. *$p<0.05$ and **$p<0.02$ vs control, #$p<0.05$ vs PD according to ANOVA, Tukey HSD *post hoc* test.
doi:10.1371/journal.pone.0037467.g004

of α-tubulin PTMs and the significant MT depletion. It has been already shown that human fibroblasts carrying *parkin* with the deletion of the 4th exon, encoding the MT binding domains, show a higher degree of MT depolymerization when they challenged with a MT disruptor agent such as colchicine [27]. Here we report that MT depolymerization occurs in PD fibroblasts even without the addition of any stressor, and that MT destabilization seems to be a common feature shared by idiopathic and genetic parkinsonism. It is noteworthy, as we demonstrate here, that both pharmacological treatment and genetic approaches are able to restore the proper MT stability and, therefore, to rescue cell alterations deriving from MT destabilization. Thus, our work highlights, for the first time, that MT dysfunction is present in patients in baseline conditions and that correction of MT defects recovers cell phenotype, underlining the central role of MT system in PD.

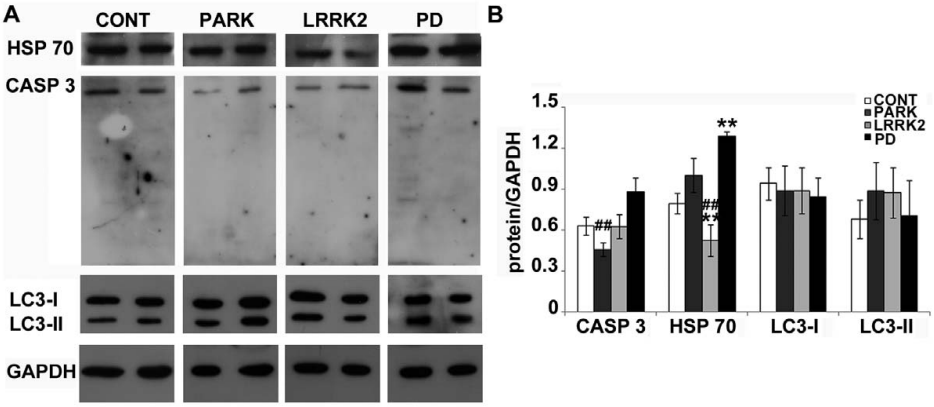


**Figure 5. Stress-induced pathways are not activated in PD fibroblasts.** (A) Immunoblot and (B) densitometric analyses of caspase 3 (CASP 3), heat shock protein 70 (HSP 70) and microtubule-associated protein 1 light chain 3 (LC3) I and II were performed in whole cell extracts from human fibroblasts deriving from control (CONT, white bars, N = 10), mutated *parkin* (PARK, dark grey bars, N = 6), mutated *LRRK2* (LRRK2, light grey bars, N = 6) and idiopathic PD (PD, black bars, N = 3). For the quantitation, values of each protein were normalized on the level of GAPDH of the relative sample. All values are expressed as mean ± SEM. *$p<0.05$ and ***$p<0.005$ vs control, ##$p<0.02$ vs PD according to ANOVA, Tukey HSD *post hoc* test.
doi:10.1371/journal.pone.0037467.g005

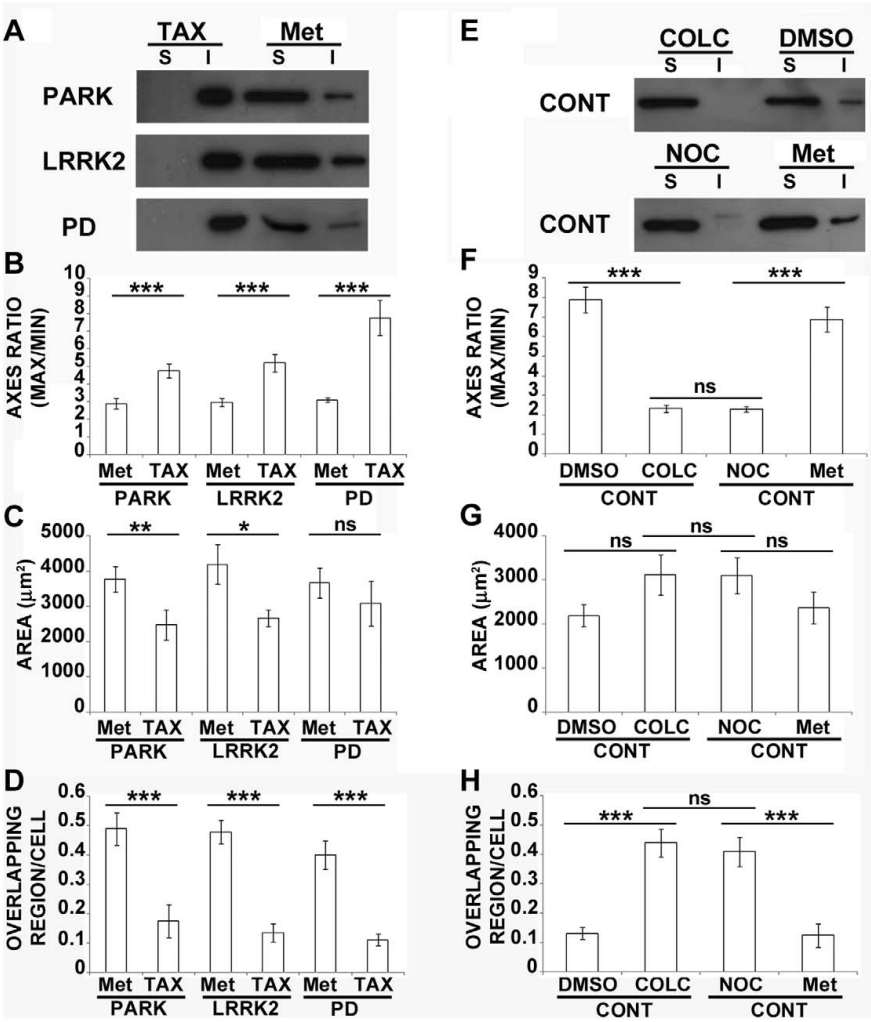


**Figure 6. Pharmacological MT stabilization rescues fibroblast phenotype.** (A) Representative immunoblot of Triton X-100-soluble (free α-tubulin, S) and -insoluble fraction (α-tubulin incorporated into MTs, I) of patients fibroblasts treated with paclitaxel (Tax) or solvent (Met). Morphometric analyses showing the ratio between maximum and minimum axes (B), the area (C) and the number of overlapping regions between cells (D) of paclitaxel (TAX) or solvent (Met)-treated patient fibroblasts. ns = not significant, $*p<0.05$, $**p<0.02$ and $***p<0.005$ according to ANOVA, Tukey HSD *post hoc* test. All values are expressed as mean ± SEM. PARK = patients with mutations of *parkin* (N = 4); LRRK2 = patients carrying mutations in *LRRK2* (N = 3); PD = idiopathic Parkinson's disease patients (N = 3). (E) Representative immunoblot of Triton X-100-soluble (free α-tubulin, S) and -insoluble fraction (α-tubulin incorporated into MTs, I) of control fibroblasts treated with colchicine (COLC), nocodazole (NOC) or solvents (DMSO or Met). Morphometric analyses showing the ratio between maximum and minimum axes (F), the area (G) and the number of overlapping regions between cells (H) of colchine (COLC, N = 5), nocodazole (NOC, N = 5) or solvent (DMSO or Met, N = 5 respectively)-treated control fibroblasts. ns = not significant and $***p<0.005$ according to ANOVA, Tukey HSD *post hoc* test. All values are expressed as mean ± SEM.
doi:10.1371/journal.pone.0037467.g006

Tubulin PTMs have recently been linked to neurodegenerative processes [38]. Our results, indeed, reveal the importance of α-tubulin PTM dysregulation in PD etiopathogenesis. Being Tyr tubulin the newly synthesized α-tubulin [8], the parkin-induced enrichment of Tyr tubulin can be viewed as an attempt to produce new MTs, as a consequence of the depolymerizaton of the older MTs. In addition, it is a clear sign of the increase of dynamic MTs. On the other hand, the enrichment of stable MTs, observed in idiopathic PD and in patients carrying mutations of LRRK2, could be the extreme effort of the cell to stabilize a collapsing system. In any case, both the hyper-dynamicity caused by mutant parkin and the over-stabilization associated with LRRK2, actually represent an imbalance of MT dynamics. Thus, the first outcome of our work is the suggestion

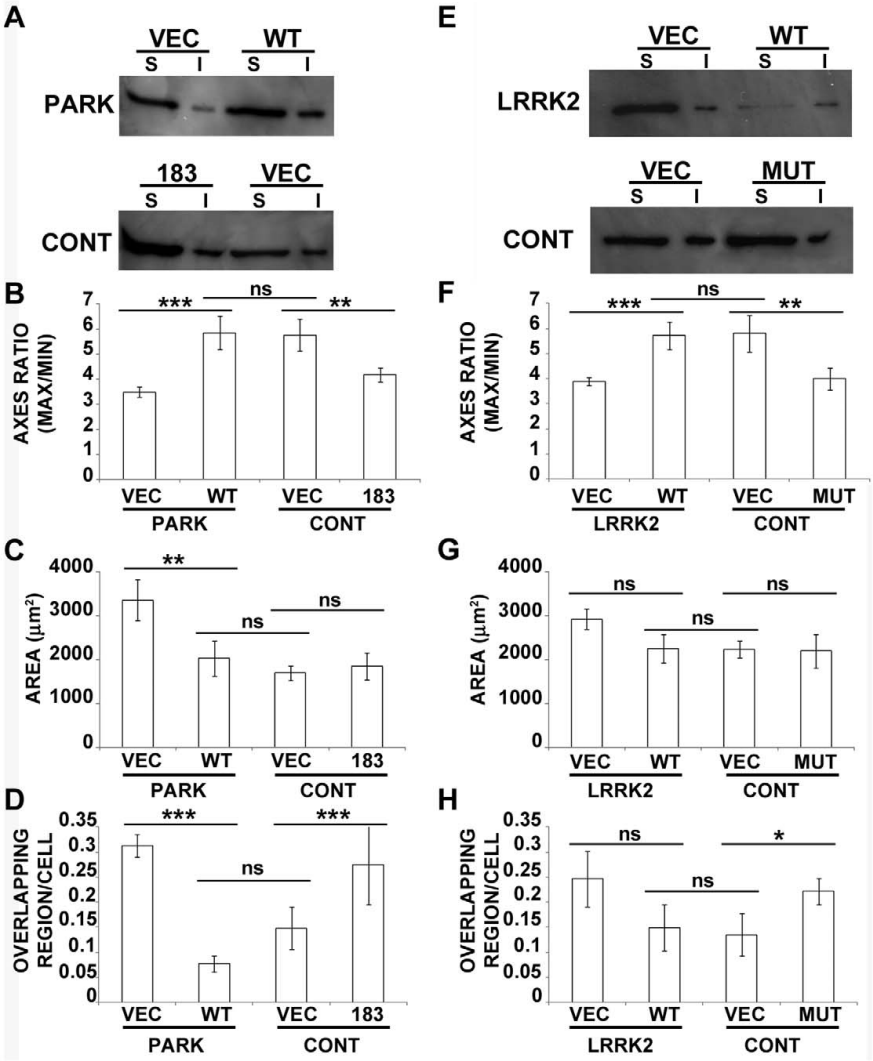


**Figure 7. Genetic manipulation restores MT stability and rescues fibroblast phenotype.** (A) Representative immunoblot of Triton X-100-soluble (free α-tubulin, S) and -insoluble fraction (α-tubulin incorporated into MTs, I) of fibroblasts collected from patients with parkin mutations (PARK) transfected with control plasmid (VEC) or WT parkin (WT), and of control fibroblasts (CONT) transfected with short hairpin RNA, sh-183 (183) or control shRNA (VEC). (B-D) Morphometric analyses of patients fibroblasts expressing control plasmid (PARK-VEC, N = 4) or WT parkin (PARK-WT, N = 4), and control fibroblasts transfected with control shRNA (CONT-VEC, N = 4) or silenced with sh-183 (CONT-183, N = 4), showing the ratio between maximum and minimum axes (B), the area (C) and the number of overlapping regions between cells (D). ns = not significant, $^{**}p<0.02$ and $^{***}p<0.005$ according to ANOVA, Tukey HSD *post hoc* test. All values are expressed as mean ± SEM. (E) Representative immunoblot of Triton X-100-soluble (free α-tubulin, S) and -insoluble fraction (α-tubulin incorporated into MTs, I) of fibroblasts collected from patients with LRRK2 mutations (LRRK2) transfected with control plasmid (VEC) or WT LRRK2 (WT), and of control fibroblasts (CONT) expressing control plasmid (VEC) or G2019S mutant LRRK2 (MUT). Morphometric analyses of patients fibroblasts expressing control plasmid (LRRK2-VEC, N = 3) or WT LRRK2 (LRRK2-WT, N = 3), or of control fibroblasts transfected with control plasmid (CONT-VEC, N = 3) or G2019S mutant LRRK2 (CONT-MUT, N = 3), showing the ratio between maximum and minimum axes (F), the area (G) and the number of overlapping regions between cells (H). ns = not significant, $^{*}p<0.05$, $^{**}p<0.02$ and $^{***}p<0.005$ according to ANOVA, Tukey HSD *post hoc* test. All values are expressed as mean ± SEM.
doi:10.1371/journal.pone.0037467.g007

of a new biological mechanism for LRRK2- and parkin-mediated regulation of MT stability, i.e. the modulation of α-tubulin PTMs.

Neurons are not-dividing cells with an extremely long life, and in their axons accumulate very stable MTs, that remain for much longer time than the usual MT half-life [39]. Thus, the

accumulation of aberrant tubulin dimers is likely to occur, especially if tubulin turnover is compromised. This is exactly the scenario we hypothesize for PD patients carrying parkin mutations on the basis that parkin promotes ubiquitination and degradation of tubulin [5] and that β-tubulin significantly increases in the presence of mutated parkin, as we reported in the present work. Moreover, a particularly long life of MTs could lead to an unconventional subset of tubulin PTMs, and the impairment of tubulin PMTs could have further impacts on neuronal functions, being crucial for the regulation of various MT-dependent functions. Through the modulation of binding and velocity of motor proteins, tubulin PTMs are supposed to be involved in the regulation of axonal transport [40] whose impairment has recently been suggested as a common and early event in neurodegeneration [41]. We have previously reported that imbalance of α-tubulin PTMs results in impairment of axonal transport and in mitochondrial damage in PC12 cells exposed to $MPP^+$ [15]. Here we show that parkin and LRRK2 modulate tubulin PTMs, offering alternative explanations for the reported capacity of parkin to arrest the movement of damaged mitochondria [42] and for the ability of LRRK2 to modulate trafficking and distribution of synaptic vesicles in cortical neurons [43]. Furthermore, we observe the significant activation of GSK3β in PD fibroblasts, that with its upstream and downstream regulators has key roles in many neuronal processes [28], as neurite outgrowth, neuronal polarization and, perhaps, axonal transport. Active GSK3β phosphorylates MAPs with the consequent MT depolymerization and the breakdown of the railways along which motor proteins move; therefore, an increase in GSK3β activation can likely affect axonal transport. Thus, having shown the ability of parkin and LRRK2 to modulate tubulin PTMs and MT-related signaling pathways, the present paper could be a good starting point to analyze the ability of parkin and LRRK2 to regulate axonal transport.

The proper regulation of MT dynamics is critical for the survival and for the establishment of cell-cell contacts in different cell types [44,45]. For example, when fibroblasts collide they undergo contact inhibition of locomotion that involves cell retraction and reversal of polarity, allowing cells to change the direction of migration and to move in a cell free environment. During aging, fibroblasts motility declines contributing to deficits in wound-healing, and this impaired behavior has been associated to disorganization of actin cytoskeleton [46]. Further data confirmed that mechanical properties are altered in consequence to the increased amount of polymerized actin in fibroblasts from old donors, whereas no significant changes in vimentin or MTs content are associated with aging process [47]. Very recently, Kadir and colleagues [45] have shown that this behavior resides on the fine tuning of MT dynamics and organization, especially at the sites of cell contact, where MT dynamics shall rise above a threshold to permits contact inhibition of locomotion; they also reported that Y24632-treated cells, which have hyper-stable MTs, are unable to re-orientate. Here, we demonstrate that PD patient fibroblasts have altered morphology and spatial organization that could be explained by the increased of stable MTs in LRRK2 and idiopathic PD, but also by the spreading of Ac MTs in all PD fibroblasts, that would locally interferes with the acceptable MT dynamics. Therefore, our data show that changes in MT stability are specifically associated to PD conditions and suggest that PD pathology could reside on compromised cell mechanics due to a failure of the MT system. This idea is strengthened by the fact that the administration of taxol, a MT stabilizing agent, or the expression of either WT parkin or WT LRRK2 in PD patient fibroblasts, provokes an increase in the polymerized MTs and a recovery of the cell morphology and behavior. Interestingly, the MT destabilization observed in patient fibroblasts unravels a possible intrinsic MT weakness in PD affected people that could be crucial for neuronal survival and especially for dopaminergic neurons, being shown to be particularly vulnerable to the colchicine-induced MT depolymerization [14,48].

Mitochondrial dysfunction has been related to the pathogenesis of PD for a long time, and recent papers show that both parkin [17] and LRRK2 [18] can be important for the regulation of mitochondria function and malfunction. In the last few years, tubulin has proved to be able to modulate mitochondrial respiration through its interaction with voltage-dependent anion channels, the most abundant protein in the mitochondrial outer membrane. In particular, it has been reported that tubulin decreases the respiration rate of isolated mitochondria [49] and that the increase in tubulin dimers induces mitochondrial depolarization in human cancer cells [50]. Under this light, the increased amount of free tubulin we observed in human PD fibroblasts could be responsible for the mitochondrial alterations in these cells, described elsewhere [17,18]. Thus, as we and others have already suggested [14,15,51], MTs and mitochondria collaborate in producing dopaminergic neuron death in PD.

Taken together, our results highlight, for the first time, that proteins associated with PD, such as parkin and LRRK2, have an impact on MT organization and stability in humans, and that idiopathic PD seems to display MT impairment as well. Furthermore, our analyses reveal that these MT alterations profoundly affects cells morphology and behavior, but also that MT stabilization, by taxol treatment or by expression of WT parkin or WT LRRK2, is sufficient to restore the correct cell mechanics. The groundbreaking technique of iPSC-derived dopaminergic neurons [52] offers the noteworthy advantage of recapitulating key molecular aspects in a human model of neurodegeneration, and, moreover, iPSCs enable the production of patient-specific cell lines, with the potential use for high-throughput drug screening and personalized therapies. We will move onto this exciting field soon to validate in human neurons the occurrence of MT dysfunction and to seek a possible MT-based therapy, trying to transfer to neurons our actual findings in human fibroblasts as well as to deeper investigate the biological relationship among parkin, LRRK2 and MTs. Thus, the present work can be the launch pad for the study of MT system in PD patients.

## Supporting Information

**Figure S1 Age distribution in the experimental groups.** Scatter plot representing the age distribution of the individuals in each experimental group. CONT = control (N = 10); PARK = patients with mutations of parkin (N = 6); LRRK2 = patients carrying mutations in *LRRK2* (N = 6); PD = idiopathic Parkinson's disease patients (N = 3). Statistical analyses did not reveal differences in age between control or patient groups ($p = 0.168$ according to ANOVA).
(TIF)

**Figure S2 Parkin over-expression and silencing.** (A) Representative micrographs of cultured fibroblasts deriving from PD affected patients bearing parkin mutation transfected with control plasmid (PARK+VEC) or WT parkin (PARK+WT). Scale bar: 20 μm. (B) Representative immunoblot of parkin performed on cultured fibroblasts deriving from healthy subjects transfected with control shRNA (CONT+VEC) or silenced with sh-183 (CONT+183).
(TIF)

**Figure S3 PD fibroblasts show altered α-tubulin PMT staining.** Human fibroblasts were immunostained for Tyr, deTyr and Ac tubulin, to investigate MT organization and stability. All cells were concurrently stained with DAPI (blue), to visualize the nucleus. Scale bar: 25 μm. CONT = control; PD = idiopathic Parkinson's disease; PARK = patients with mutations of *parkin*; LRRK2 = patients carrying mutations in *LRRK2*.
(TIF)

## Acknowledgments

The authors thank Dr. Jennifer S. Hartwig for reading and editing the manuscript, Dr Jenny Sassone (IRCCS Istituto Auxologico Italiano, Milano, Italy) and Dr Elisa Greggio (Department of Biology, University of Padova, Padova, Italy) for providing constructs. The samples were obtained from the "Cell Line and DNA Biobank from Patients affected by Genetic Diseases" (G. Gaslini Institute) and "Parkinson Institute Biobank" (Milan, http://www.parkinson.it/dnabank.html) of the Telethon Genetic Biobank Network (http://www.biobankbetwork.org) (project n. GTB07001).

## Author Contributions

Conceived and designed the experiments: DC GC. Performed the experiments: DC SG FC. Analyzed the data: DC FC SG GP GC. Contributed reagents/materials/analysis tools: SG GP. Wrote the paper: DC GC.

## References

1. Obeso JA, Rodriguez-Oroz MC, Goetz CG, Marin C, Kordower JH, et al. (2010) Missing pieces in the Parkinson's disease puzzle. Nat Med 16: 653–661.
2. Lesage S, Brice A (2009) Parkinson's disease: from monogenic forms to genetic susceptibility factors. Hum Mol Genet 18: R48–59.
3. Shimura H, Hattori N, Kubo S, Mizuno Y, Asakawa S, et al. (2000) Familial Parkinson's disease gene product parkin, is a ubiquitin-protein ligase. Nat Genet 2: 302–305.
4. MacLeod D, Dowman J, Hammond R, Leete T, Inoue K, et al. (2006) The familial Parkinsonism gene LRRK2 regulates neurite process morphology. Neuron 52: 587–593.
5. Ren Y, Zhao J, Feng J (2003) Parkin binds to α/β tubulin and increases their ubiquitination and degradation. J Neurosci 23: 3316–3324.
6. Gandhi PN, Wang X, Zhu X, Chen SG, et al. (2008) The Roc domain of leucine-rich repeat kinase 2 is sufficient for interaction with microtubules. J Neurosci Res 86: 1711–1720.
7. Mitchison T, Kirschener M (1984) Dynamic instability of microtubule growth. Nature 312: 237–242.
8. Werstermann S, Weber K (2003) Post-translational modifications regulate microtubule function. Nat Rev Mol Cell Biol 4: 938–947.
9. Yang F, Jiang Q, Zhao J, Ren Y, Sutton MD, et al. (2005) Parkin stabilizes microtubules through strong binding mediated by three independent domains. J Biol Chem 280: 17154–17162.
10. Gillardon F (2009) Leucine-rich repeat kinase 2 phosphorylates brain tubulin-β isoform and modulates microtubule stability: a point of convergence in parkinsonian neurodegeneration? J Neurochem 110: 1514–1522.
11. Alim MA, Ma QL, Takeda K, Aizawa T, Matsubara M, et al. (2004) Demonstration of a role for alpha-synuclein as a functional microtubule-associated protein. J Alzheimers Dis 6: 435–442.
12. Marshall LE, Himes RH (1978) Rotenone inhibition of tubulin self-assembly. Biochim Biophys Acta 543: 590–594.
13. Cappelletti G, Surrey T, Maci R (2005) The parkinsonism producing neurotoxin $MPP^+$ affects microtubule dynamics by acting as destabilising factor. FEBS Lett 579: 4781–4786.
14. Ren Y, Liu W, Jiang H, Jiang Q, Feng J (2005) Selective vulnerability of dopaminergic neurons to microtubule depolymerization. J Biol Chem 280: 34105–34112.
15. Cartelli D, Ronchi C, Maggioni MG, Rodighiero S, Giavini E, et al. (2010) Microtubule dysfunction precedes transport impairment and mitochondria damage in $MPP^+$-induced neurodegeneration. J Neurochem 115: 247–258.
16. Wu G, Wang X, Feng X, Zhang A, Li J, et al. (2011) Altered expression of autophagic genes in the peripheral leukocytes of patients with sporadic Parkinson's disease. Brain Res 1394: 105–111.
17. Rakovic A, Grünewald A, Seibler P, Ramirez A, Kock N, et al. (2010) Effect of endogenous mutant and wild-type PINK1 on Parkin in fibroblasts from Parkinson disease patients. Hum Mol Gen 19: 3124–3137.
18. Mortiboys H, Johansen KK, Aasly JO, Bandmann O (2010) Mitochondrial impairment in patients with Parkinson disease with the G2019S mutation in LRRK2. Neurology 75: 2017–2020.
19. Grünewald A, Voges L, Rakovic A, Kasten M, Vandebona H, et al. (2010) Mutant Parkin impairs mitochondrial function and morphology in human fibroblasts. PLoS ONE 5: e12962.
20. Auburger G, Klinkenberg M, Drost J, Marcus K, Morales-Gordo B, et al. (2012) Primary Skin Fibroblasts as a Model of Parkinson's Disease. Mol Neurobiol. [Epub ahead of print].
21. Hughes AJ, Ben-Shlomo Y, Daniel SE, Lees AJ (1992) What features improve the accuracy of clinical diagnosis in Parkinson's disease: a clinicopathologic study. Neurology 42: 1142–6. Erratum in: Neurology 42: 1436.
22. Hughes AJ, Ben-Shlomo Y, Daniel SE, Lees A (2001) What features improve the accuracy of clinical diagnosis in Parkinson's disease: a clinicopathologic study. 1992. Neurology 57: S34–38.
23. Goldwurm S, Zini M, Di Fonzo A, De Gaspari D, Siri C, et al. (2006) LRKK2 G2019S mutation and Parkinson's Disease: a clinical, neuropsychological and neuropsychiatric study in large Italian sample. Parkinsonism Relat Disord 12: 410–419.
24. Sironi F, Primignani P, Zini M, Tunesi S, Ruffmann C, et al. (2008) Parkin analysis in early Parkinson's disease. Parkinsonism Relat Disord 14: 326–333.
25. Kumar A, Greggio E, Beilina A, Kaganovich A, Chan D, et al. (2010) The Parkinson's disease associated LRRK2 exhibits weaker in vitro phosphorylation of 4E-BP compared to autophosphorylation. PLoS ONE 5: e8730.
26. Cappelletti G, Maggioni MG, Tedeschi G, Maci R (2003) Protein tyrosine nitration is triggered by nerve growth factor during neuronal differentiation of PC12 cells. Exp Cell Res 288: 9–20.
27. Ren Y, Jiang H, Yang F, Nakaso K, Feng J (2009) Parkin Protects Dopaminergic Neurons against Microtubule-depolymerizing Toxins by Attenuating Microtubule-associated Protein Kinase Activation. J Biol Chem 284: 4009–4017.
28. Hur EM, Zhou FQ (2010) GSK3 signalling in neural development. Nat. Rev. Neurosci. 11: 539–551.
29. Xiao D, Pinto JT, Soh JW, Deguchi A, Gundersen GG, et al. (2003) Induction of apoptosis by the garlic-derived compound S-allylmercaptocysteine (SAMC) is associated with microtubule depolymerization and c-Jun NH(2)-terminal kinase 1 activation. Cancer Res 63: 6825–6837.
30. Xie R, Nguyen S, McKeehan WL, Liu L (2010) Acetylated microtubules are required for fusion of autophagosomes with lysosomes. BMC Cell Biol 11: 89.
31. Levy OA, Malagelada C, Greene LA (2009) Cell death pathways in Parkinson's disease: proximal triggers, distal effectors, and final steps. Apoptosis 14: 478–500.
32. Witt SN (2010) Hsp70 molecular chaperones and Parkinson's disease. Biopolymers 93: 218–228.
33. Nguyen HN, Byers B, Cord B, Shcheglovitov A, Byrne J, et al. (2011) LRRK2 mutant iPSC-derived DA neurons demonstrate increased susceptibility to oxidative stress. Cell Stem Cell 8: 267–280.
34. Mitra G, Saha A, Gupta TD, Poddar A, Das KP, et al. (2007) Chaperone-mediated inhibition of tubulin self-assembly. Protein 67: 112–120.
35. Macejak DG, Luftig RB (1991) Stabilization of actin filaments at early times after adenovirus infection and in heat-shocked cells. Virus Res 19: 31–45.
36. Mizushima N, Yoshimori T, Levine B (2010) Methods in mammalian autophagy research. Cell 140: 313–326.
37. Tong Y, Yamaguchi H, Giaime E, Boyle S, Kopan R, et al. (2010) Loss of leucine-rich repeat kinase 2 causes impairment of protein degradation pathways, accumulation of alpha-synuclein, and apoptotic cell death in aged mice. Proc Natl Acad Sci USA 107: 9879–9884.
38. Rogowski K, van Dijk J, Magiera MM, Bosc C, Deloulme JC, et al. (2010) A Family of Protein-Deglutamylating Enzymes Associated with Neurodegeneration. Cell 143: 564–578.
39. Paturle-Lafanechere L, Manier M, Trigault N, Pirollet F, Mazarguil H, et al. (1994) Accumulation of delta 2-tubulin, a major tubulin variant that cannot be tyrosinated, in neuronal tissues and in stable microtubule assemblies. J Cell Sci 107: 1529–1543.
40. Janke C, Kneussel M (2010) Tubulin post-translational modifications: encoding functions on the neuronal microtubule cytoskeleton. Trends Neurosci 33: 362–372.
41. Morfini GA, Burns M, Binder LI, Kanaan NM, LaPointe N, et al. (2009) Axonal transport defects in neurodegenerative diseases. J Neurosci 29: 12776–12786.
42. Wang X, Winter D, Ashrafi G, Schlehe J, Wong YL, et al. (2011) PINK1 and Parkin target Miro for phosphorylation and degradation to arrest mitochondrial motility. Cell 147: 893–906.
43. Piccoli G, Condliffe SB, Bauer M, Giesert F, Boldt K, et al. (2011) LRRK2 controls synaptic vesicle storage and mobilization within the recycling pool. J Neurosci 31: 2225–2237.
44. Feinstein SC, Wilson L (2005) Inability of tau to properly regulate neuronal microtubule dynamics: a loss-of-function mechanism by which tau might mediate neuronal cell death. Biochim Biophys Acta 1739: 268–279.
45. Kadir S, Astin JW, Tahatamouni L, Martin P, Nobes CD (2011) Microtubule remodelling is required fro the front-rear polarity switch during contact inhibition of locomotion. J Cell Sci 124: 2642–2653.
46. Reed MJ, Ferara NS, Vernon RB (2001) Impaired migration, integrin function, and actin cytoskeletal organization in dermal fibroblasts from a subset of aged human donors. Mech. Ageing Dev. 122: 1203–1220.

47. Schulze C, Wetzel F, Kueper T, Malsen A, Muhr G, et al. (2010) Stiffening of human skin fibroblasts with age. Biophys. J. 99: 2434–2442.
48. Liang Y, Li S, Wen C, Zhang Y, Guo Q, et al. (2008) Intrastriatal injection of colchicine induces striatonigral degeneration in mice. J. Neurochem. 106: 1815–1827.
49. Rostovtseva TK, Sheldon KL, Hassanzadeh E, Monge C, Saks V, et al. (2008) Tubulin binding blocks mitochondrial voltage-dependent anion channel and regulates respiration. Proc Natl Acad Sci USA 105: 18746–18751.
50. Maldonado EN, Patnaik J, Mullins MR, Lemasters JJ (2010) Free tubulin modulates mitochondrial membrane potential in cancer cells. Cancer Res 70: 10192–10201.
51. Choi WS, Palmiter RD, Xia Z (2011) Loss of mitochondria complex I activity potentiates dopaminergic neuron death induced by microtubule dysfunction in a Parkinson's disease model. J Cell Biol 192: 873–882.
52. Caiazzo M, Dell'Anno MT, Dvoretskova E, Lazarevic D, Taverna S, et al. (2011) Direct generation of functional dopaminergic neurons from mouse and human fibroblasts. Nature 476: 224–227.

Cartelli et al., 2012

**SUPPLEMENTARY FIGURES**

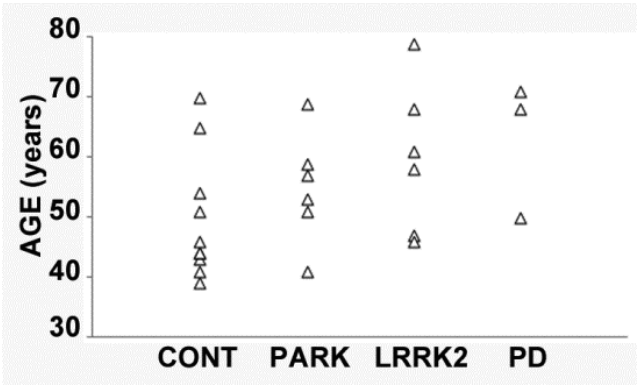


**Figure S1 Age distribution in the experimental groups.**
Scatter plot representing the age distribution of the individuals in each experimental group. CONT= control (N =10); PARK= patients with mutations of parkin (N = 6); LRRK2= patients carrying mutations in LRRK2 (N =6); PD= idiopathic Parkinson's disease patients (N =3). Statistical analyses did not reveal differences in age between control or patient groups (p= 0.168 according to ANOVA).

Cartelli et al., 2012

**SUPPLEMENTARY FIGURES**

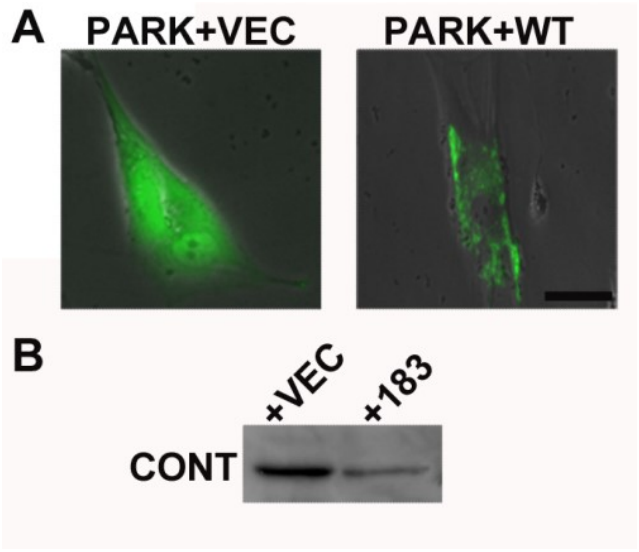


**Figure S2 Parkin over-expression and silencing.**
(A) Representative micrographs of cultured fibroblasts deriving from PD affected patients bearing parkin mutation transfected with control plasmid (PARK+VEC) or WT parkin (PARK+WT). Scale bar: 20 mm. (B) Representative immunoblot of parkin performed on cultured fibroblasts deriving from healthy subjects transfected with control shRNA (CONT+VEC) or silenced with sh-183 (CONT+183).

Cartelli et al., 2012

**SUPPLEMENTARY FIGURES**

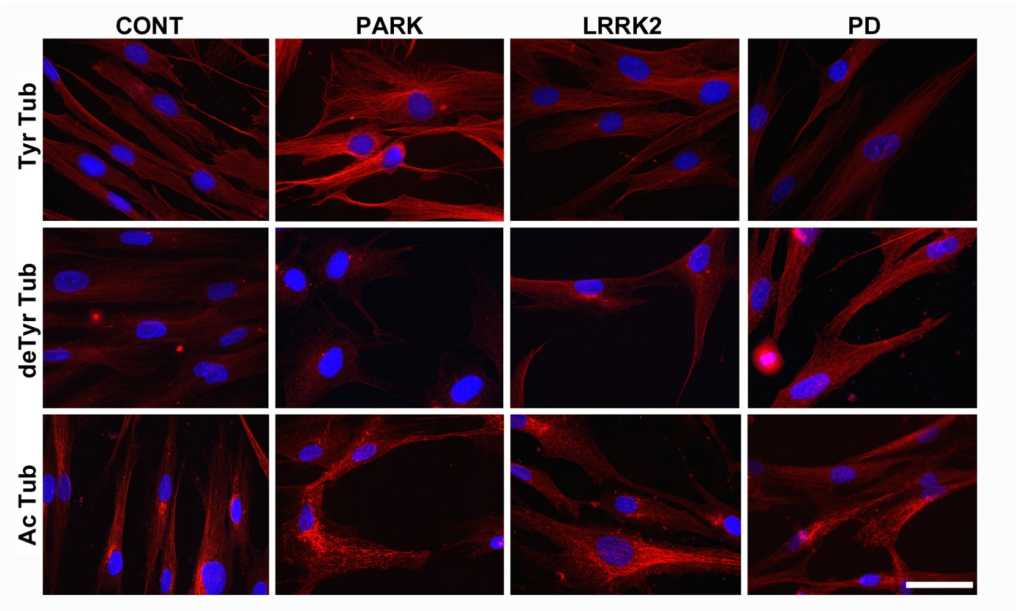


**Figure S3 PD fibroblasts show altered a-tubulin PMT staining.**
Human fibroblasts were immunostained for Tyr, deTyr and Ac tubulin, to investigate MT organization and stability. All cells were concurrently stained with DAPI (blue), to visualize the nucleus. Scale bar: 25 mm. CONT= control; PD = idiopathic Parkinson's disease; PARK =patients with mutations of parkin; LRRK2= patients carrying mutations in LRRK2.

Manuscript 1
Casagrande et al., *To be submitted*

# ROLE OF MICROTUBULE STABILITY IN 2,5-HEXANEDIONE-INDUCED NEURODEGENERATION

**Francesca Casagrande**[1], Daniele Cartelli[1], Kristyna Hanusova[1,§], Martina Ferrari[1], Alessandra M.E. Calogero[1], Carmelita De Gregorio[1], Jacopo Marangon[1], Stefano Goldwurm[2], Margherita Canesi[2], Gianni Pezzoli[2] and Graziella Cappelletti[1*]

[1]Department of Biosciences, University of Milan, Milan 20123, Italy;
[2]Parkinson Institute, I.C.P. Istituti Clinici di Perfezionamento, Milan 20126, Italy;
[§]Actually affiliated to San Raffaele Institute, Milan 20132, Italy.

***Corresponding Author:**
Graziella Cappelletti
Department of Biosciences
Università degli Studi di Milano,
Via Celoria 26,
20133 Milano
Italy.
Tel: 0039 02 50314752
Fax: 0039 02 50314801
E-mail: graziella.cappelletti@unimi.it

Running title: Microtubule dysfunction induced by 2,5-hexanedione
Keywords: Parkinson's disease, PC12 cells, microtubules, 2,5-hexanedione

**ABSTRACT**

Exposure to environmental toxins, including hydrocarbon solvents such as 2,5-hexanedione (2,5-HD) clearly increases the risk of developing Parkinson's disease (PD), whose pathogenesis is actually still unclear. Among the others, an emergent hypothesis is that microtubule dysfunction could be crucial in triggering neuronal degeneration in many diseases, including PD. Here, we used 2,5-HD to analyse the early effects of toxin-induced neurodegeneration on cytoskeleton, in NGF-differentiated PC12 cells as a model of dopaminergic neurons, the ones that are selectively lost during the disease. We found that 2,5-HD treatment affects all the cytoskeletal components, and moreover, we observed a very early specific alteration in microtubule distribution and stability, in addition to the unbalance of modified forms of α-tubulin. Interestingly, testing the effects of 2,5-HD on human skin fibroblasts obtained from healthy donors and patients affected by genetic PD, we found that microtubule system was also altered in these cells and that the genetic background may really make a difference in MT susceptibility to this environmental PD toxin. In conclusion, we suggest a key role of microtubules in 2,5-HD-induced damage.

## INTRODUCTION

Currently, there are just symptomatic treatments available for Parkinson's disease (PD), that is the second most common neurodegenerative disease after Alzheimer's disease, with an estimated 7 to 10 million people affected worldwide, and is predicted to increase in prevalence as the world population ages (Beitz 2014). Its central pathological features is the selective degeneration of dopaminergic neurons in the *substantia nigra* (SN) *pars compacta* projecting to the *corpus striatum* (CS), leading to a severe striatal dopamine (DA) deficiency resulting in the typical movement disorders of parkinsonism (Dauer and Przedborski 2003; Obeso et al. 2010). For the vast majority of PD cases, the etiology remains unknown even though both genetic and environmental factors are likely to be implicated (Sherer et al. 2012). It's well known indeed that parkinsonism can be induced by exposure to environmental toxins such as pesticides, chemical compounds and hydrocarbon solvents (Di Monte et al. 2002; Hatcher et al. 2008). The prolonged exposure to relatively high levels of certain aliphatic solvents (e.g. n-hexane) can cause a dose-dependent neurodegeneration that occurs clinically as a symmetrical peripheral neuropathy, with clear prevalence of the damage in the distal part of the nerve, known as dying-back neuropathy (Spencer et al. 2002). In particular, the γ-diketone 2,5-hexanedione (2,5-HD), the toxic metabolite of n-hexane, has been shown to induce parkinsonism both in humans and animals (Spencer et al. 1980; Pezzoli et al. 1990; Vanacore et al. 2000; Pezzoli et al. 2000) and to affect the cytoskeleton (Song et al. 2007; Wang et al. 2008; Zhang et al. 2010; Han et al. 2014). The 2,5-HD reacts with lysine amino groups of proteins forming pyrrole adducts, which probably undergo secondary oxidation, resulting in crosslinked proteins (Spencer et al. 1980; Graham et al. 1995; LoPachin and DeCaprio 2004). Neurofilament (NF) protein polymerization and crosslinking lead to giant neurofilamentous axonal swellings and eventual degeneration in central and peripheral nervous system, so they have been proposed as the cardinal lesion in aliphatic γ-diketone neuropathy (Graham et al. 1995; LoPachin and Gavin 2015). The accumulation of NFs, however, does not appear to explain the onset distal axonal degeneration, which is likely to be a consequence of axonal transport impairment (Stone et al. 1999). In addition, wild-type mice and transgenic mice not expressing NFs, revealed similar patterns of distal axonal degeneration in 2,5-HD neuropathy (Stone et al., 2001). Other potential targets of aliphatic and aromatic γ-diketones are microtubule (MT)-associated proteins (Han et al. 2014) and MTs themselves (Boekelheide 1987a; Boekelheide 1987b).

Interestingly, MTs have been found to interact with some of the proteins mutated in PD, such as α-synuclein, LRRK2 and parkin (Alim et al. 2002; Ren et al. 2003; Parisiadou and Cai 2010), and to be affected by the action of some PD toxins like $MPP^+$ and rotenone (Cappelletti et al. 2005; Ren et al. 2005). Moreover, due to their specific architecture, neuron functionality and survival are particularly dependent on intracellular transport, sustained by MTs, which impairment might result in accumulation of damaged proteins and organelles forming axonal swellings described in several neurodegenerative diseases (Millecamps and Julien 2013). MTs show a dynamic behaviour switching rapidly between growth and depolymerisation phases, but there is a limited range of acceptable MT dynamic behaviours in neurons, outside of which MTs cannot function normally and the cells cannot survive (Feinstein and Wilson 2005). Therefore, in the last years, the MT dysfunction has become an emerging hypothesis in neurodegenerative processes including PD (Feng 2006; De Vos et al. 2008; Cartelli et al. 2010).

In the attempt to highlight the crucial role of MTs in the molecular mechanisms underlying neurodegeneration in PD, here we investigate the changes in MT system induced by 2,5-HD in different cell lines, like nerve growth factor (NGF)-differentiated PC12 cell line as a model of dopaminergic neurons (Greene and Tischler 1976), and human skin fibroblasts obtained from healthy donors and PD patients.

## RESULTS

### 2,5-HD impacts cell viability and morphology in NGF-differentiated PC12 cells

We started our investigation about the effects of 2,5-HD on NGF-differentiated PC12 cells, as it is a well-characterized model of dopaminergic neurons in culture. In order to settle the PD toxin assays, the optimisation of the exposure time and concentration was performed (Fig. 1) by treating 5 days NGF-differentiated PC12 cells with different concentrations of 2,5-HD (0.2 mM, 2 mM and 20 mM) and performing the analyzes at 24, 48, and 72 h of treatment. Firstly, the toxin effect on cell viability was examined by MTT test, showing that the cell survival was significantly reduced only at the highest concentration (20 mM) of 2,5-HD after 48 ($p<0.001$) and 72 hours ($p<0.01$), but not after 24 hours (Fig. 1B). In parallel, the observation of living cells by phase-contrast microscope revealed several morphological alterations of the treated cells (Fig. 1A). In order to quantify these changes on cell morphology, morphometric analyses have been performed to evaluate the percentage of differentiated cells (Fig. 1C), the length of neurites of differentiated cells (Fig. 1D) and the percentage of neurites with small axonal swellings, called varicosities (Fig. 1E). According to these analyses, 2,5-HD induced shortening of the neurite length with consequent loss of the differentiated phenotype at higher concentrations following treatments of 48 and 72 h (Fig. 1C-D). On the other hand, it was also able to induce the formation of varicosities along neurites at higher concentrations already after 24 h of treatment (Fig. 1E). Based on these observations, we concluded that 2,5-HD affects cell morphology in NGF-differentiated PC12 cells at early time points leading to heavy alterations over time. Taking into account that the cell viability was not affected yet within 24 hours of treatment, ours could be applied as a good experimental paradigm to investigate the early events of neurodegeneration in the further experiments.

### Cytoskeletal proteins are affected by 2,5-HD treatment

In accordance with the published literature suggesting that 2,5-HD affects cytoskeletal components, in particular NFs that are the most studied cytoskeletal proteins in cellular and *in vivo* models of neuropathy (LoPachin and DeCaprio 2004), we hypothesized that the observed morphological changes could be probably caused by a dysfunction of the overall cytoskeleton. Thus the characterization of all its components (actin, NFs and MTs) after 2,5-HD treatment has been carried out with both biochemical and immunocytochemical approaches. The western blot and densitometric analysis (Fig. 2A-B) revealed a transient increase in actin level at 2 mM of 2,5-HD ($p<0.05$) and the significantly decrease at the

highest concentration for both NF-L and NF-M levels ($p<0.001$), while the overall content of α- and β-tubulin remains unchanged. In parallel, immunofluorescence staining has been performed to investigate in detail distribution and organization of the three cytoskeletal filaments (Fig. 1C). Actin accumulated at 2 mM of 2,5-HD and, in addition, showed a peculiar organization in bundle-like structures. Interestingly, this kind of rearrangement of microfilaments in ruffles has been seen also in epithelial cells after 6 mM 2,5-HD for 24 hours by Malorni and colleague (Malorni et al. 1989). On the other hand, NF-L, as well as NF-M (data not shown), accumulated in varicosities and in the perinuclear zone in a dose-dependent manner, as expected and already described in the literature in other neuron-like cellular models (Heijink et al. 1995; Hartley et al. 1997). The α-tubulin staining, instead, highlighted an evident fragmentation of the network in a dose-dependent manner and a perinuclear accumulation. These data revealed that 2,5-HD impacts on all cytoskeletal proteins in a model of dopaminergic neurons, NGF-differentiated PC12 cells, the cells that are selectively lost in PD neurodegeneration, respect to other type of neurons, astrocytes (Tuckwell et al. 1992) or glial cells (Boegner et al. 1992). More importantly, to our knowledge these results showed for the first time the loss of integrity of MTs in neuron-like cells following 2,5-HD treatment, likely leading to the impairment of axonal transport and so the consequent accumulation of NFs.

**2,5-HD is a strong microtubule-stabilizer agent**

The above results strongly suggest that the MT cytoskeleton could be a main target of 2,5-HD, having a key role in neurodegeneration processes. On this purpose, we focused on a deeper investigation of MTs through the analysis of different post-translational modifications (PTMs) of α-tubulin, that specifically correlate with subsets of MTs behaving differently (Janke 2014). Surprisingly, the analysis of PTMs showed significative changes in both level and distribution after 2,5-HD treatment (Fig. 3A-B-C), unlike the overall α- and β-tubulin content that was unchanged (Fig. 2A-B). The western blot analysis (Fig. 3A-B) and the immunofluorescence imaging (Fig. 3C) of the two PTMs of α-tubulin occurring specifically on stable MTs (acetylation and detyrosination) highlighted a significant increase in the level of stable MTs and their unusual perinuclear accumulation at the highest dose of 2,5-HD. Consistent with these results, the level of tyrosinated tubulin, marker of dynamic MTs, presented a decrease at the highest dose of 2,5-HD (Fig. 3A-B). The increased level of stable MTs and their subsequent accumulation in the cell body, like NFs (Fig. 2C) may likely be explained with alterations in the MT system that cause the impairment of axonal transport and

protein degradation by proteasome, leading to the observed accumulation in the perinuclear area. This could also explain the neurite retraction and the loss of neuronal phenotype caused by 2,5-HD in NGF-differentiated PC12 cells.

To further investigate the effect of the toxin on MT stability and dynamics, we have studied the state of tubulin polymerization *in cell* and the kinetics of tubulin assembly *in vitro* in the presence of 2,5-HD. In order to study the kinetics *in cell*, we analysed the free tubulin dimers fraction with respect to the tubulin in MT pool. The ratio revealed a shift of tubulin towards the polymerized pool caused by 2 mM 2,5-HD (Fig. 3D-E), indicating a strong MT stabilizing effect consistent with our data showing the significant increase levels and accumulation in the soma of stable MTs and with previous ones coming from different cell models (Markelewicz et al. 2004). On the other hand, we observed the shift back of the ratio towards free tubulin in cells exposed to 20 mM 2,5-HD (Fig. 3D-E), suggesting a depolymerization response of MT system at high toxin concentration. This compensative mechanism of the cell, due to a severe damage of MT system, could be probably dependent on the specific depolymerisation of dynamic MTs (tyrosinated ones), as shown by the ratio free/polymerized Tyr tubulin significantly shifted towards the free dimer pool at 20 mM of toxin (Fig. 3D-E).

Moving to *in vitro* assays, we checked for the direct effect of the toxin on MT system. We analysed the assembly kinetics of pure tubulin in the presence of increasing concentrations of 2,5-HD (Fig. 4A) and calculated the following parameters: *P* value for nucleation phase, the initial velocity (Vi) of polymerization and the final absorbance at 350 nm (Fig. 4B). No significant changes in the assembly curves and in the parameters defining their phases were observed in the presence of 2,5-HD. Probably a pre-incubation of 2,5-HD with tubulin is necessary to see the expected strong MT-stabilizing effect previously described by Boekelheide (Boekelheide 1987a; Boekelheide 1987b). Electron microscopy performed on this samples also revealed a conventional ultrastructure of MTs formed in the presence of 2,5-HD (Fig. 4C).

**Mitochondria are not an early target of 2,5-HD**

Since the most common PD toxins, such as $MPP^+$ or rotenone, are potent inhibitors of complex I of electron transport chain, mitochondrial dysfunction has been considered for long time one of the principal culprit of neuronal death in PD, together with oxidative stress and protein degradation inefficiency (Malkus et al. 2009). On this purpose, we have looked if 2,5-HD could induce oxidative stress and mitochondrial dynamics alteration, in the same condition in which we observed alterations of the cytoskeleton. In order to quantify the

reactive oxygen species (ROS) production as a sign of mitochondrial damage, the DCFA assay has been performed, revealing that a significant increase of ROS production was induced just at the highest concentration (20 mM) of treatment ($p<0.05$) (Fig. 5A). Interestingly, 2,5-HD strongly affects cytoskeleton in our cellular model both at 2 mM and 20 mM of treatment, allowing us to speculate that the increase in ROS formation could be not the first event in cell death, but a possible consequence of MT system impairment occurring earlier. Moreover, the levels of DRP1 and MFN2, two crucial proteins regulating mitochondrial fission and fusion, respectively, have been analysed by western blot. Both of them were decreased just at the 20 mM of toxin (for DRP1 $p<0.05$; for MFN2 $p<0.001$) (Fig. 5B-C). These data, together with those coming from MTT test (a cell viability test based on the activity of a crucial mitochondrial enzyme, the succinate dehydrogenase) (Fig. 1B) point out that the mitochondrial alteration do not occur in early phases of toxin action.

**2,5-HD alters microtubule system in human cells**

Having achieved a general picture of the impact of the 2,5-HD action on a neuron-like cellular model, we moved to human cells. We choose to use human skin fibroblasts, since they recently turned out to be an easy available and robust PD experimental model (Auburger et al. 2012), and because we could take advantage of the expertise already present in our lab on working with this kind of cell lines derived from patients with different type of PD (Cartelli et al. 2012). On this purpose, the effect of 2,5-HD has been tested on skin fibroblasts (Fig. 6A), obtained from healthy donors and patients carrying mutation in *PARK2*, a specific PD-related gene coding for an E3 ubiquitin ligase also able to bind and stabilize MTs. Since the majority of mutations in *PARK2* gene are supposed to cause a loss of function in the protein both in its E3 ligase activity and MT-binding ability, we wanted to evaluate if 2,5-HD could elicit peculiar effects in a baseline condition of MT destabilization. We applied the same experimental paradigm used for NGF-differentiated PC12 cells. The cell viability was not affected by 24 hours of treatment with the toxin (Fig. 6C), whereas the cell morphology between the two groups of fibroblasts appeared striking different. In fact, control fibroblasts were elongated, whereas fibroblasts from PD patients were wider and larger (Fig. 6B) at least in the presence of mutated parkin. Morphometric analyses confirmed that the PD fibroblasts presented a much higher cell area respect to control fibroblasts ($p<0.001$; Fig. 6D) with the consequent decrease of the ratio between maximum and minimum axis ($p<0.001$; Fig 6E), already reported by Cartelli and colleagues (Cartelli et al. 2012). It's noteworthy, the fact that 2,5-HD had no effects on control fibroblasts morphology for both cell area and axes ratio

(Fig. 6D-E), whereas PD fibroblasts showed a significant decrease in the cell area at the highest concentration of 2,5-HD ($p<0.05$; Fig.6D).

To assess the effect of 2,5-HD on the MT stability in human fibroblasts, the state of tubulin polymerization was analyzed as well. We firstly confirmed that MT dysfunction was present in patients already at baseline conditions without the addition of any stressor as previously reported (Cartelli et al. 2012), and then observed that 2,5-HD treatment was able to cause the stabilization of MTs in both PD patients and healthy controls (Fig 6F-G). Interestingly, MT stabilization occurred at the lowest dose of 2,5-HD in PD fibroblasts whereas healthy controls were affected just at 20 mM of toxin, suggesting a greater MT susceptibility in PD patients. These data show that 2,5-HD impacts MT system both in neuron-like cells and in human fibroblasts inducing MT stabilization, and, more interestingly, suggest that the genetic background may really make a difference in MT susceptibility to this environmental PD toxin.

## DISCUSSION

MT dysfunction has become an emerging hypothesis in PD pathogenesis (Ren et al. 2005; Cartelli et al. 2010). In this scenario, our goal was to deeply investigate the MT dysfunction induced by a toxin linked to PD using both NGF-differentiated PC12 cells, as a model of dopaminergic neurons, and skin fibroblasts, obtained from healthy donors and PD patients carrying mutations in *PARK2* gene, as human cellular model. We revealed a very early and specific alteration in microtubule distribution and stability other than the unbalance of modified forms of α-tubulin in PC12 cells treated with 2,5-HD. Testing the effects of the toxin on human skin fibroblasts, we found that microtubule system was targeted by and, interestingly, more susceptible to 2,5-HD in cells obtained from PD patients than from healthy donors. Taken together, our data strongly suggest a key role of microtubules in 2,5-HD-induced damage.

Dopaminergic neurons appears to be particularly sensitive to any insults that could damage the MT cytoskeleton because of their peculiar architecture, characterized by an extremely widespread arborization and particularly long axons, that made their function and survival strongly dependant by intracellular trafficking (Hunn et al. 2015). The dopaminergic cell line we used, NGF-differentiated PC12 cells, revealed morphological alterations following 2,5-HD treatment in a dose-dependent manner but the formation of small swellings along the neurites became evident very early and before any loss of cell viability (Fig. 1). Moreover, the immunocytochemical approach (Fig. 2) highlighted the presence of accumulations of NFs inside these axonal swellings, called varicosities, and in the perinuclear area as expected from data in other cellular models (Tuckwell et al. 1992; Heijink et al. 1995; Hartley et al. 1997) and in the clinical situation showing distal axonal accumulation of NFs (Herskowitz et al. 1971; Scelsi and Candura 2012). In addition, the level of both NF-L and NF-M was significantly decreased at the highest dose of 2,5-HD (Fig. 2A-B), in accordance with data coming from cultured rat dorsal root ganglia cells (Han et al. 2014) and *in vivo* studies (Zhang et al. 2005; Song et al. 2007; Wang et al. 2008). In these and other previous studies, the effects of 2,5-HD on intermediate filaments have been extensively described also in cultured fibroblasts, astrocytes, mouse neuroblastoma and melanoma, and epithelial cell lines (Durham 1988; Malorni et al. 1989; Sager 1989), but both microfilaments and MTs were poorly investigated. Here we show that actin seems to be just a few and transiently affected from 2,5-HD, showing an increased protein level and an altered distribution in bundles (Fig. 2C), also described in the literature (Malorni et al. 1989; Hall et al. 1992). At a glance, also MTs were

almost unaffected by the toxin treatment as the majority of the studies reported, since the tubulin levels were unchanged, but, interestingly, the fluorescent staining highlighted a partial fragmentation of the MT network and also a perinuclear accumulation like NFs at high doses (Fig. 2C). To our knowledge, this effect has been never seen before, nether in other neuron-like cell model nor primary neurons *in vitro* from human foetuses (Moretto et al. 1991). We think that this differences could be due to the cell type used because, as already explained above, the dopaminergic neurons are particularly sensitive for their peculiar structure so other kind of neurons could underestimate the effects of toxin on MTs. Under this light, it's possible to understand why the differentiated neuroblastoma cells were more sensitive compared to the undifferentiated ones or fibroblasts (Heijink et al. 1995; Hartley et al. 1997), because the neuronal-like structure is strictly dependent on cytoskeleton and, in particular, on MT functions. This different response of neuronal cells has been described for a much more percentage of cell survival, but presenting more morphological alterations, especially NF accumulations. Also, undifferentiated PC12 cells treated with comparable concentration of 2,5-HD for 24 hours, showed a significant cell mortality already at 5 mM (Qi et al. 2015), while we didn't observe any significant cell loss in 5-days NGF-differentiated PC12 cells. Moreover, Malorni and colleagues (Malorni et al. 1989) have already demonstrated that 2,5-HD interferes with the cell proliferation, reporting that the cells detached from the substrate when they were in the mitotic phase after treatment. From our point of view, this is an additional clue of the direct action of 2,5-HD on MTs, being them responsible of the mitotic spindle, cell shape and the attachment to the substrate, explaining even more clearly why the cell viability was not affected in non-dividing cell such as neurons.

Since MTs seemed playing a crucial role in 2,5-HD-induced neurodegeneration, we deeply evaluate in neuron-like cells the stability of MT system for the first time, through the analyses of different post-translational modified forms of α-tubulin and the state of tubulin polymerization *in cell* and *in vitro*. Surprisingly, although the overall tubulin content was unchanged, all the three PTMs analysed were significantly affected by 2,5-HD and changed in both levels and distributions (Fig. 3). Previous data reported that 2,5-HD is able to alter the tubulin assembly with a taxol-like effect (Boekelheide 1987a; Boekelheide 1987b), suggesting that it can likely affect the stability of MT cytoskeleton. Here we support this hypothesis showing that the expected MT stabilizing effect could be achieved specifically increasing the levels of acetylated and detyrosinated tubulin, associated to stable MTs, and consequently decreasing the levels of tyrosinated tubulin, marker of native and dynamic MT pool (Fig. 3A-B). Moreover, the localization of these stable MTs was unusual: they were

accumulated in the perinuclear area and partially fragmented (Fig. 3C) (meaning that these stable tubulins were in charge of the alterations previously observed for the distribution of total α-tubulin in figure 2C). Consistent with this, the analysis of tubulin polymerization *in cell* revealed a higher content of MT fraction respect to free tubulin pool caused by 2,5-HD (Fig. 3D-E). Indeed, this increase in MT mass represent a strong and direct proof that stabilization oh MTs occurs in treated cells. Unfortunately, we were not able to reproduce this MT stabilizing effect or any other differences respect to control with our *in vitro* data for kinetic parameters of polymerization curves neither to show any changes in MT ultrastructure (Fig. 4).

Interestingly, taking a look also to mitochondria, we found that in our experimental conditions the increase of ROS production (Fig. 5A) was induced later than the cytoskeletal modifications occurred (Fig. 2), especially MT stability alteration (Fig. 3). Qi and colleagues (Qi et al. 2015) have exhaustively analysed the effects of 2,5-HD in undifferentiated PC12 cells on mitochondria-related pathway, demonstrating that the toxin can induce apoptosis, down- and up-regulating the expression of the anti- and pro-apoptotic proteins Bcl-2 and Bax respectively, promoting the disruption of mitochondrial membrane potential, inducing the release of cytochrome c and finally increasing the activity of caspase-3. Unfortunately, the authors did not check for alterations in any components of the cytoskeleton in undifferentiated cells, so we can't really compare their results with ours and pinpoint the respective role of mitochondria- and MT-based effects in triggering cell death. We can speculate that, since differentiated cells are more comparable to mature neurons than undifferentiated ones, the cytoskeletal and MT alterations observed in NGF-differentiated PC12 cells may be more helpful in explaining the neurotoxic actions of 2,5-HD *in vivo* situations. In conclusion, our data show that MT system impairment is an early event in neurodegeneration of dopaminergic neurons in culture that could consequently cause all the other alterations described here and by other colleagues, supporting the hypothesis that MT dysfunction has a key role in the process leading neurons to death.

Finally, moving to the human cell model we have chosen the human fibroblasts since they are an easy available and robust PD experimental model as recently highlighted (Auburger et al. 2012). On this purpose, skin fibroblasts were obtained from healthy donors and PD patients, carrying mutations in *PARK2* gene, since *PARK2* gene encodes for an E3 ubiquitin ligase that is able to bind and stabilize MTs (Ren et al. 2003; Yang et al. 2005). This allowed us to study two different pathways, that triggered by 2,5-HD and that triggered by PARK2, both likely converging on MTs. We first confirmed that fibroblasts deriving from PD patients were

characterized by a wider cell area and a minor axes ratio at baseline conditions as we have previously described also for other type of PD patients (Cartelli et al. 2012). Interestingly, exposure to 2,5-HD could induce morphological changes just in PD fibroblasts, pushing the cell morphology back to the one of control fibroblasts, decreasing the cell area. It's noteworthy that healthy fibroblasts exposed to 2.8 mM 2,5-HD for many days underwent changes in their morphology already after 3 days of treatment, showing a large swollen cell body and thin elongated processes (Passarin et al. 1996), resembling our data obtained exposing PD fibroblasts to 20 mM 2,5-HD for 24 hours. Moreover, Passarin and colleagues found that exposed healthy fibroblasts presented a tubulin and tau immunostaining less intense and not uniform, while vimentin resulted normal, suggesting that the cytotoxicity of 2,5-HD is not restricted to intermediate filaments, but affects other cytoskeletal components, such as MTs, also emerging by the impairment of the cell cycle. Here, to assess the effect of 2,5-HD on the MT stability, we assessed the state of tubulin polymerization in fibroblasts. 2,5-HD treatment was able to cause the stabilization of MTs in both PD patients and healthy controls, but this occurred at the lowest dose of toxin just in PD fibroblasts (Fig. 6), suggesting a greater MT susceptibility, at least in these ones carrying mutations in *PARK2* gene. These data show that 2,5-HD impacts all the cytoskeletal components and in particular the MT system both in neuron-like cells and in human skin fibroblasts inducing MT stabilization and, more interestingly, suggest that the genetic background may really make a difference in MT susceptibility to this environmental PD toxin.

Nowadays no treatment exists that has been demonstrated to slow, delay or even reverse the disease progression. Consequently, PD will continue to be an important health issue and a strong economic drain due to its direct and indirect costs, moreover, the prevalence of the disease is expected to rise dramatically over the next 20 years as the population ages (Sherer et al. 2012). Unraveling the molecular mechanisms responsible for PD neurodegeneration represents the only way for developing new and more efficient therapy, in particular we suggest that MTs could be a good target for new neuroprotective drugs.

## MATERIALS AND METHODS

Maintenance and neural differentiation of PC12 cells

PC12 cells were maintained in RPMI 1640 (EuroClone, Pero, Italy) containing 10% horse serum and 5% fetal bovine serum (HyClone, Logan, UT, USA), supplemented with 2 mM L-glutamine (EuroClone), penicillin/streptomycin both 100 μg/ml (EuroClone), at 37°C in a humidified atmosphere, 5% $CO_2$. In routine condition, the medium has been changed every 3-4 days. Cells were plated at $1.5 \times 10^4/cm^2$ onto poly-L-lysine (Sigma Aldrich, St. Louis, MO)-coated cover glass in 35-mm petri dishes for immunofluorescence microscopy or directly onto poly-L-lysine-coated petri dishes for biochemical analysis. For neural differentiation, the cells were exposed to 50 ng/ml human β-NGF (PeproTeck, London, UK) in low serum medium (RPMI 1640 supplemented with 2% horse serum, 2 mM L-glutamine, penicillin/streptomycin). The differentiation medium is changed every 2-3 days with fresh one. The PC12 cells were exposed to 2,5-HD (Sigma-Aldrich) after 5 days of differentiation with human β-NGF and analysed at different time points.

Ethic statement, generation and maintenance of human fibroblast cell lines

Primary fibroblasts were obtained by skin biopsies from 6 individuals. They included 3 healthy subject as control group and 3 patients affected by PD, carrying mutation in *PARK2* gene, whose characteristics are summarized in the table of Figure 6A. All patients were examined by movement disorder neurologists and clinical diagnosis of PD was established according to the UK Parkinson Disease Society Brain Bank criteria (Hughes 1992). The mutations on the parkin (*PARK2*) gene were screened as previously described (Sironi et al. 2008). The study was approved by the local ethics committee (Istituti Clinici di Perfezionamento, July 13th 2010) and all participants gave written informed consent.

Human fibroblasts were cultured in RPMI 1640 (Hyclone) containing 15% foetal bovine serum (HyClone) supplemented with 2 mM L-glutamine, penicillin/streptomycin both 100 μg/ml (all from EuroClone) and 50 μM β-mercaptoethanol (Sigma-Aldrich), at 37°C in a humidified atmosphere, 5% $CO_2$. For 2,5-HD treatment, fibroblasts were plated at the density of $1.2 \times 10^4/cm^2$ on uncoated 35 mm petri dishes; the day after, the cells were incubated with different concentrations of 2,5-HD (Sigma-Aldrich), and then analysed. For the cell viability assay, the fibroblasts were grown with normal medium, and then maintained just before the experiments in medium with a lower fetal bovine serum concentration (only 7,5% instead of 15%) and without β-mercaptoethanol, that could both interfere with MTT test.

2,5-HD treatment

Five days NGF-differentiated PC12 cells were incubated for 24, 48 or 72 hours with the following concentrations of 2,5-HD: 0.2 mM, 2 mM and 20 mM. Human fibroblasts were exposed to the same concentration of 2,5-HD for 24 hours. The 2,5-HD was diluted in the fresh appropriate culture medium and filtered. Then, a change of medium with the one containing 2,5-HD was performed to start the treatment and the cells were incubated in standard conditions. When the incubations were finished, the living cells were viewed by phase contrast microscopy and random images were captured for morphometric analyses. Immediately after, the cells were fixed with 4% paraformaldehyde or cold methanol for immunofluorescence, lysed with cell lysis buffer for western blot analyses, or used for specific tests such as cell viability or reactive oxygen species production assays.

Morphometric analysis

The cell morphology of living cells at the end of treatment has been evaluated by phase contrast microscopy. Five random images at 20x magnification were captured per well per each condition using Axiovert S100 microscope (Zeiss, Oberkochen, Germany) equipped with AxiocamHR (Zeiss) and then analysed using digital image processing software (Interactive measurement module, Axiovision Release 4.8, Zeiss). All cells in each image were analysed. For PC12 cells were considered about 600 cells per condition, while for human fibroblasts were analysed about 80 cells per condition and at least 20 per individual. For PC12, three principal features of neuritogenesis were considered: the percentage of differentiated cells, the length of the longest neurite for each differentiated cell and the percentage of differentiated cells presenting varicosities on their longest neurite. A cell was considered differentiated when it had the longest neurite at least twice as long as the cell body diameter (Yamazaki et al. 2004). About human fibroblasts, the maximum and minimum axes and the cell area were measured. The ratio between the maximum and minimum axis has been calculated.

Cell viability assay

The MTT test has been used to assess the viability of cells in culture according to their mitochondria enzymatic activity. This colorimetric assay is based on the incubation of cells with the soluble yellowish MTT salt (3-(4,5-dimethylthiazol-2-yl)-2,5-diphenyltetrazolium bromide) (Sigma-Aldrich), as NADH dehydrogenase substrate. For NGF-differentiated PC12

cells the differentiation medium without NGF was used to dissolve the MTT salt, while for fibroblasts only RPMI was used. The filtered freshly prepared MTT solution (0.5 mg/ml) was added to culture medium of the cells previously plated in multi-well plates and treated with different concentrations of 2,5-HD. The cells were then incubated for three hours in the dark at 37°C. After incubation, a solution of 0.1 M HCl in isopropanol has been added to each well in equal volume to the one already present in the well pipetting vigorously, in order to lyse the cells and solubilize the insoluble purple crystals of formazan. The intensity of purple colour of each well has been measured through a plate-reader spectrophotometer (Infinite 200Pro, Tecan, Mannedorf, Switzerland) at wavelength of 570 nm.

DCFDA assay

Reactive oxygen species (ROS) production was detected using DCFDA Cellular ROS Detection Assay Kit (Abcam) according to manufacturer's instructions. Briefly, NGF-differentiated PC12 cells were grown in a black multiwell and after 5 days of differentiation were incubated for 45 min with 25 μM DCFDA at 37°C. After incubation, the cells were washed once with the kit buffer and then treated with 2,5-HD for 24 hours. The fluorescence intensity was measured through a plate-reader spectrophotometer (Infinite 200Pro, Tecan) using the excitation/emission wavelength 485 nm/535 nm.

Western blot analysis

Whole cell extracts, Triton X-100 (Sigma-Aldrich)-soluble and -insoluble fractions of PC12 cells and human fibroblasts were prepared as follows. For preparation of whole-cell extracts, cells were washed twice with phosphate-buffered saline (PBS) and scraped into sodium dodecyl sulfate polyacrylamide gel electrophoresis (SDS-PAGE) sample buffer (2% w/v SDS, 10% v/v glycerol, 5% v/v β-mercaptoethanol, 0.001% w/v bromophenol blue, and 62.5 mM Tris, pH 6.8; all from Sigma-Aldrich) containing protease inhibitor cocktail 1:1000 (Sigma-Aldrich). To determinate protein concentration of total lysates the bicinchoninic acid reagent assay (Micro BCA, Pierce, Rockford, IL, USA) was used and compared to a bovine serum albumin standard curve. To separate cytosolic tubulin dimers from the ones polymerized into MTs, cells were washed twice in PEM buffer (88 mM Pipes, pH 6.94, 10 mM EGTA, 1 mM $MgCl_2$, 2 M glycerol, protease inhibitor cocktail; all from Sigma-Aldrich), incubated for 10 min at room temperature with PEM buffer containing 0.1% v/v Triton X-100 to collect the soluble cytoplasmic proteins extracted with the Triton-containing PEM buffer, and rinsed once again briefly with PEM buffer, adding also this one to the previous collected

fraction. The obtained Triton X-100-soluble fractions were diluted 3:1 with 4X SDS-PAGE sample buffer. The insoluble material remaining attached to the dish was scraped into SDS-PAGE sample buffer. Equal proportions of each fraction or protein samples from whole cell extracts (25 µg per lane) were then boiled for 3 min, subjected to 7,5% SDS-PAGE and western-blotted onto PDVF Immobilon™-P membranes (Millipore, Billerica, MA). Blocking was performed by incubating the membranes in 5% w/v nonfat dry milk in 10 mM Tris, pH 7.4, 150 mM NaCl (TBS) with 0.05% v/v Tween 20 for 1 hour at room temperature. Primary antibody incubations were performed overnight at 4°C. Membranes were washed for 30 min with 3 changes and incubated with horseradish peroxidase-linked antibody for 1 hour at room temperature. After washing the reaction was developed using enhanced chemioluminescence (SuperSignal West Pico Chemiluminescent, Pierce). Membranes were probed with the following primary antibodies: actin mouse IgM (N350, Amersham, Little Chalfont, UK) 1:4000; NF-L rabbit IgG (AB-10685, Immunological Sciences, Rome, Italy) 1:40000, NF-M mouse IgG (MAB-10338, Immunological Sciences) 1:40000, α-tubulin mouse IgG (clone B-5-1-2, T6074, Sigma-Aldrich) 1:1000; β-tubulin mouse IgG (clone Tub 2.1, T4026, Sigma-Aldrich) 1:4000; deTyr tubulin rabbit IgG (ab 48389, Abcam) 1:1000; Tyr tubulin mouse IgG (clone TUB-1A2, Sigma-Aldrich) 1:1000; Ac tubulin mouse IgG (clone 6-11B-1, T7451, Sigma-Aldrich) 1:2000; DRP1 rabbit IgG (clone D6C7, #8570, Cell Signaling, Danvers, MA, USA) 1:1000; Mitofusin-2 rabbit IgG (clone D2D10, #9482, Cell Signaling) 1:1000; VDAC1 rabbit IgG (ab15895, Abcam) 1:500. As secondary antibodies were used: HRP goat anti-mouse IgG (31430, Pierce) 1:20000; HRP goat anti-rabbit IgG (31460, Pierce) 1:40000; HRP goat anti-mouse IgM (ab5930, Abcam) 1:5000. To ensure equal protein loading for the whole protein lysates (not for Triton-soluble/insoluble fractions), protein samples were assayed by densitometry of Coomassie blue-stained PVDF membranes and adjusted for blotting. Immunoblots were scanned with Epson WP-4525 color image scanner (Seiko Epson Corporation, Suwa, Japan) and analyzed by ImageJ software (National Institute of Health).

Immunofluorescence and labeling

Cells were fixed with methanol at -20°C or 4% paraformaldehyde for 10 min and incubated with the following primary antibodies and probes: Atto 565 Phalloidin (94072, Sigma-Aldrich) 1:100; NF-L rabbit IgG (AB-10685, Immunological Sciences) 1:1000, NF-M mouse IgG (MAB-10338, Immunological Sciences) 1:500; α-tubulin mouse IgG (clone B-5-1-2, T6074, Sigma-Aldrich) 1:500; Tyr tubulin mouse IgG (clone TUB-1A2, Sigma-Aldrich) 1:100; deTyr tubulin rabbit IgG (ab48389, Abcam) 1:100; Ac tubulin mouse IgG (clone 6-

11B-1, Sigma-Aldrich) 1:100; and 49,6-Diamidino-2-phenylindole dihydrochloride DAPI (D-8417, Sigma-Aldrich) 1:40000. As secondary antibodies we used: Alexa Fluor™ 568 goat anti-mouse (A11004, Life Tecnologies, Carlsbad, CA, USA) 1:1000; Alexa Fluor™ 488 goat anti-rabbit (ab150077, Abcam) 1:1000. The coverslips were mounted in Mowiol® (Calbiochem, San Diego, CA)–DABCO (Sigma-Aldrich) and samples were examined with the Axiovert 200M microscope (Zeiss) or with a confocal laser scan microscope imaging system (TCS SP5, Leica Microsystem, Heidelberg, Germany).

Tubulin purification

Tubulin was purified from fresh bovine brain conserved in ice-cold PBS (20 mM Na-phosphate, 150 mM NaCl, pH 7.2). Pure tubulin was obtained by two cycles of polymerization–depolymerization in a high-molarity buffer (Castoldi and Popov 2003) resuspended in BRB80 (80 mM K-Pipes pH 6.9, 2 mM EGTA, 1 mM $MgCl_2$; all from Sigma-Aldrich), snap-frozen in liquid nitrogen, and stored in small aliquots at -80 °C.

Tubulin assembly *in vitro*

The kinetics of tubulin polymerization was studied using a standard protocol (Contini et al. 2012) in the absence or presence of different concentration of 2,5-HD without preincubation. Reactions were followed turbidimetrically at 350 nm for 90 min at 37°C in a multimode plate reader (Infinite 200Pro, Tecan) equipped with a temperature controller. Pure bovine brain purified tubulin was diluted in assembly buffer (80 mM K-Pipes, pH 6.9, 2 mM EGTA, 1 mM $MgCl_2$, 10% glycerol, and 1 mM GTP) to the working concentration of 30 μM, previously degassed, and kept on ice; the reaction was started by warming the solution at 37°C.

Polymerization time-course was dissected in order to calculate the kinetic parameters describing the different phases of the process. The number of successive steps in the nucleation (P) was determined by plotting $\log(A(t)/A\infty)$ against $\log(t)$. The maximal velocity of polymerization (Vi) was calculated as the variation of mass versus time ($\delta A/\delta t$) at the very initial elongation phase, whereas total extent of MT assembly was deduced from the total absorbance variation ($\Delta A$) achieved as the steady-state was established. The tubulin critical concentration, namely the lowest tubulin concentration allowing MT formation, was extrapolated as the x-intercept of the linear dependence of $\Delta A$ from the initial tubulin concentration.

Electron microscopy

Negative staining of pure tubulin was prepared by leaving a drop of assembled MTs, previously fixed with 1% (v/v) glutaraldehyde, on Formvar Carbon Film-coated 200 square mesh Nickel grids (FCF200-Ni-50, Electron Microscopy Sciences, Hatfield, PA, USA) for 30 min at 25°C. The grids were first washed three times for 1 min with 5 mM EGTA, then dipped rapidly two times in 1% uranyl acetate for 5 sec and, finally, let dry on filter paper at room temperature protected from dust. The samples were viewed with Philips CM10 transmission electron microscope at 80 kV; images were acquired using a Morada Olympus digital camera with different magnifications (46000x, 92000x, 130000x).

Statistical analysis

Statistical analysis was performed using STATISTICA (StatSoft Inc., Tulsa, OK), and significant differences of 2,5-HD treated versus control cells were assessed by one-way ANOVA with Tukey HSD, Fisher LSD or Dunnett 2-sided as *post hoc* test; $\chi^2$ test was used to analyze qualitative variables. Data are expressed as means ± SEM. All experiments were repeated at least three times.

**Acknowledgements**

Human fibroblast cell lines were obtained from the "Cell Line and DNA Biobank from Patients affected by Genetic Diseases" (Istituto G. Gaslini) and the "Parkinson Institute Biobank" (Milano), members of the Telethon Network of Genetic Biobanks (project no. GTB12001), funded by Telethon Italy. The authors are thankful to Dr. Francolini (Department of Medical Biotechnology and Translational Medicine, Università degli Studi Di Milano, Milano, Italy) for the use of transmission electron microscope, technical advices and helpful discussion. The authors apologize for each possible involuntary paper omission. This work was supported by Fondazione Grigioni per il Morbo di Parkinson, Milan, Italy (to G.C.).

**Conflict of Interests**

The authors declare having no conflict of interest

**REFERENCES**


Alim MA, Hossain MS, Arima K, et al (2002) Tubulin seeds alpha-synuclein fibril formation. J Biol Chem 277:2112–7. doi: 10.1074/jbc.M102981200

Auburger G, Klinkenberg M, Drost J, et al (2012) Primary skin fibroblasts as a model of Parkinson's disease. Mol Neurobiol 46:20–7. doi: 10.1007/s12035-012-8245-1

Beitz JM (2014) Parkinson's disease: a review. Front Biosci 65–74.

Boegner F, Grüning W, Stoltenburg-Didinger G, et al (1992) 2 , 5-Hexanedione is a potent gliatoxin in in-vitro cell cultures of the nervous system . Neurotoxicology 13:151–154.

Boekelheide K (1987a) 2,5-Hexanedione alters microtubule assembly I. Toxicol Appl Pharmacol 88:370–382.

Boekelheide K (1987b) 2,5-Hexanedione alters microtubule assembly II. Toxicol Appl Pharmacol 88:383 – 396.

Cappelletti G, Surrey T, Maci R (2005) The parkinsonism producing neurotoxin MPP+ affects microtubule dynamics by acting as a destabilising factor. FEBS Lett 579:4781–6. doi: 10.1016/j.febslet.2005.07.058

Cartelli D, Goldwurm S, Casagrande F, et al (2012) Microtubule destabilization is shared by genetic and idiopathic Parkinson's disease patient fibroblasts. PLoS One 7:e37467. doi: 10.1371/journal.pone.0037467

Cartelli D, Ronchi C, Maggioni MG, et al (2010) Microtubule dysfunction precedes transport impairment and mitochondria damage in MPP+ -induced neurodegeneration. J Neurochem 115:247–58. doi: 10.1111/j.1471-4159.2010.06924.x

Castoldi M, Popov A V. (2003) Purification of brain tubulin through two cycles of polymerization- depolymerization in a high-molarity buffer. Protein Expr Purif 32:83–88. doi: 10.1016/S1046-5928(03)00218-3

Contini A, Cappelletti G, Cartelli D, et al (2012) Molecular dynamics and tubulin polymerization kinetics study on 1,14-heterofused taxanes: evidence of stabilization of the tubulin head-to-tail dimer–dimer interaction. Mol Biosyst 8:3254. doi: 10.1039/c2mb25326g

Dauer W, Przedborski S (2003) Parkinson ' s Disease : Mechanisms and Models. Neuron 39:889–909.

De Vos KJ, Grierson AJ, Ackerley S, Miller CCJ (2008) Role of axonal transport in neurodegenerative diseases. Annu Rev Neurosci 31:151–73. doi: 10.1146/annurev.neuro.31.061307.090711

Di Monte DA, Lavasani M, Manning-bog AB (2002) Environmental Factors in Parkinson ' s Disease. 23:487–502.

Durham H (1988) Aggregation of intermediate filaments by 2 , 5-hexanedione : comparison of effects on neurofilaments , GFAP-filaments and vimentin-filaments in dissociated cultures of mouse spinal cord- dorsal root ganglia. J Neuropathol Exp Neurol 47:432–42.

Feinstein SC, Wilson L (2005) Inability of tau to properly regulate neuronal microtubule dynamics: a loss-of-function mechanism by which tau might mediate neuronal cell death. Biochim Biophys Acta 1739:268–79. doi: 10.1016/j.bbadis.2004.07.002

Feng J (2006) Microtubule: a common target for parkin and Parkinson's disease toxins. Neuroscientist 12:469–76. doi: 10.1177/1073858406293853

Graham DG, Amarnath V, Valentine WM, et al (1995) Pathogenetic studies of hexane and carbon disulfide neurotoxicity. Crit Rev Toxicol 25:91–112. doi: 10.3109/10408449509021609

Greene L a, Tischler a S (1976) Establishment of a noradrenergic clonal line of rat adrenal pheochromocytoma cells which respond to nerve growth factor. Proc Natl Acad Sci U S A 73:2424–8.

Hall ES, Hall SJ, Boekelheide K (1992) Sertoli cells isolated from adult 2,5-hexanedione-exposed rats exhibit atypical morphology and actin distribution. Toxicol Appl Pharmacol 117:9–18.

Han X-Y, Cheng D, Song F-Y, et al (2014) Decelerated transport and its mechanism of 2,5-hexanedione on middle-molecular-weight neurofilament in rat dorsal root ganglia cells. Neuroscience 269:192–198. doi: 10.1016/j.neuroscience.2014.03.044

Hartley CL, Anderson VE, Anderton BH, et al (1997) Acrylamide and 2,5-hexanedione induce collapse of neurofilaments in SH-SY5Y human neuroblastoma cells to form perikaryal inclusion bodies. Neuropathol Appl Neurobiol 23:364–72.

Hatcher JM, Pennell KD, Miller GW (2008) Parkinson's disease and pesticides: a toxicological perspective. Trends Pharmacol Sci 29:322–9. doi: 10.1016/j.tips.2008.03.007

Heijink E, Bolhuis P, De Wolff F (1995) Sensitivity to 2,5-hexanedione of neurofilaments in neuroblastoma cell line SK-N-SH increases during differentiation. J Neuropathol Exp Neurol 54:82 – 90.

Herskowitz A, Ishii N, Schaumburg H (1971) N-hexane neuropathy A syndrome occurring as a result of industrial exposure. N Engl J Med 285:82 – 85.

Hughes A (1992) What features improve the accuracy of clinical diagnosis in Parkinson's

disease. Neurology 42:1142 – 1146.

Hunn BHM, Cragg SJ, Bolam JP, et al (2015) Impaired intracellular trafficking defines early Parkinson's disease. Trends Neurosci 38:178–188. doi: 10.1016/j.tins.2014.12.009

Janke C (2014) The tubulin code: Molecular components, readout mechanisms, and functions. J Cell Biol 206:461–472. doi: 10.1083/jcb.201406055

LoPachin RM, DeCaprio AP (2004) gamma-Diketone neuropathy: axon atrophy and the role of cytoskeletal protein adduction. Toxicol Appl Pharmacol 199:20–34. doi: 10.1016/j.taap.2004.03.008

LoPachin RM, Gavin T (2015) Toxic neuropathies: Mechanistic insights based on a chemical perspective. Neurosci Lett 596:78–83. doi: 10.1016/j.neulet.2014.08.054

Malkus K a, Tsika E, Ischiropoulos H (2009) Oxidative modifications, mitochondrial dysfunction, and impaired protein degradation in Parkinson's disease: how neurons are lost in the Bermuda triangle. Mol Neurodegener 4:24. doi: 10.1186/1750-1326-4-24

Malorni W, Iosi F, Formisano G, Arancia G (1989) Cytoskeletal changes induced in vitro by 2,5-hexanedione: an immunocytochemicalstudy. Exp Mol Pathol 50:50 – 68.

Markelewicz RJ, Hall SJ, Boekelheide K (2004) 2,5-Hexanedione and Carbendazim Coexposure Synergistically Disrupts Rat Spermatogenesis Despite Opposing Molecular Effects on Microtubules. Toxicol Sci 80:92–100. doi: 10.1093/toxsci/kfh140

Millecamps S, Julien J-P (2013) Axonal transport deficits and neurodegenerative diseases. Nat Rev Neurosci 14:161–76. doi: 10.1038/nrn3380

Moretto G, Monaco S, Passarin M, et al (1991) Cytoskeletal chenges induces by 2,5-hexanedione on developing human neurons in vitro. Arch Toxicol 65:409 – 413.

Obeso J a, Rodriguez-Oroz MC, Goetz CG, et al (2010) Missing pieces in the Parkinson's disease puzzle. Nat Med 16:653–61. doi: 10.1038/nm.2165

Parisiadou L, Cai H (2010) LRRK2 function on actin and microtubule dynamics in Parkinson disease. Commun Integr Biol 3:396–400. doi: 10.4161/cib.3.5.12286

Passarin M, Monaco S, Ferrari S, et al (1996) Cytoskeletal changes in cultured human fibroblasts following exposure to 2,5-hexanedione. Neuropathol Appl Neurobiol 22:60–67. doi: 10.1074/mcp.M111.015974

Pezzoli G, Canesi M, Antonini a., et al (2000) Hydrocarbon exposure and Parkinson's disease. Neurology 55:667–673. doi: 10.1212/WNL.55.5.667

Pezzoli G, Ricciardi S, Masotto C, et al (1990) N-Hexane Induces Parkinsonism in Rodents. Brain Res 531:355–7.

Qi Y, Li S, Piao F, et al (2015) 2,5-Hexanedione induces apoptosis via a mitochondria-

mediated pathway in PC12 cells. Mol Cell Toxicol 11:79–87. doi: 10.1007/s13273-015-0010-x

Ren Y, Liu W, Jiang H, et al (2005) Selective vulnerability of dopaminergic neurons to microtubule depolymerization. J Biol Chem 280:34105–12. doi: 10.1074/jbc.M503483200

Ren Y, Zhao J, Feng J (2003) Parkin binds to alpha/beta tubulin and increases their ubiquitination and degradation. J Neurosci 23:3316–24.

Sager PR (1989) Cytoskeletal effects of acrylamide and 2,5-hexanedione: selective aggregation of vimentin filaments. Toxicol Appl Pharmacol 97:141–155. doi: 10.1016/0041-008X(89)90063-X

Scelsi R, Candura SM (2012) Neuropatie tossiche occupazionali: quadri morfologici in biopsie del nervo periferico. G Ital Med Lav 34:410–419.

Sherer TB, Chowdhury S, Peabody K, Brooks DW (2012) Overcoming obstacles in Parkinson's disease. Mov Disord 27:1606–11. doi: 10.1002/mds.25260

Sironi F, Primignani P, Zini M, et al (2008) Parkin analysis in early onset Parkinson's disease. Parkinsonism Relat Disord 14:326–333. doi: 10.1016/j.parkreldis.2007.10.003

Song F, Zhang C, Yu S, et al (2007) Time-dependent alteration of cytoskeletal proteins in cerebral cortex of rat during 2,5-hexanedione-induced neuropathy. Neurochem Res 32:1407–14. doi: 10.1007/s11064-007-9325-x

Spencer PS, Kim MS, Sabri MI (2002) Aromatic as well as aliphatic hydrocarbon solvent axonopathy. Int J Hyg Environ Health 205:131–6. doi: 10.1078/1438-4639-00138

Spencer PS, Schaumburg HH, Sabri MI, Veronesi B (1980) The enlarging view of hexacarbon neurotoxicity. Crit Rev Toxicol 7:279–356.

Stone JD, Peterson a P, Eyer J, et al (1999) Axonal neurofilaments are nonessential elements of toxicant-induced reductions in fast axonal transport: video-enhanced differential interference microscopy in peripheral nervous system axons. Toxicol Appl Pharmacol 161:50–58. doi: 10.1006/taap.1999.8780

Stone JD, Peterson a P, Eyer J, et al (2001) Neurofilaments are nonessential to the pathogenesis of toxicant-induced axonal degeneration. J Neurosci 21:2278–2287. doi: 21/7/2278 [pii]

Tuckwell D, Laszlo L, Mayer R (1992) 2,5-Hexanedione-induces intermediate filament aggregates contain ubiquitin-protein conjugate immunoreactivity and resemble Rosenthal fibres. Neuropathol Appl Neurobiol 18:593 – 609.

Vanacore N, Gasparini M, Brusa L, Meco G (2000) A possible association between exposure

to n-hexane and parkinsonism. Neurol Sci 21:49–52.

Wang Q-S, Hou L-Y, Zhang C-L, et al (2008) Changes of cytoskeletal proteins in nerve tissues and serum of rats treated with 2,5-hexanedione. Toxicology 244:166–78. doi: 10.1016/j.tox.2007.11.009

Yamazaki M, Chiba K, Mohri T, Hatanaka H (2004) Cyclic GMP-dependent neurite outgrowth by genipin and nerve growth factor in PC12h cells. Eur J Pharmacol 488:35–43. doi: 10.1016/j.ejphar.2004.02.009

Yang F, Jiang Q, Zhao J, et al (2005) Parkin stabilizes microtubules through strong binding mediated by three independent domains. J Biol Chem 280:17154–62. doi: 10.1074/jbc.M500843200

Zhang L, Gavin T, DeCaprio AP, LoPachin RM (2010) Gamma-diketone axonopathy: analyses of cytoskeletal motors and highways in CNS myelinated axons. Toxicol Sci 117:180–9. doi: 10.1093/toxsci/kfq176

Zhang T, Zhao X, Zhu Z, et al (2005) 2,5-Hexanedione Induced Decrease in Cytoskeletal Proteins of Rat Sciatic?tibial Nerve. Neurochem Res 30:177–183. doi: 10.1007/s11064-004-2439-5

**LEGENDS**

**Figure 1.**

**2,5-HD treatment induces morphological changes in NGF-differentiated PC12 cells.**

(A) Representative phase-contrast micrographs of 5-days NGF-differentiated PC12 cells treated with different concentration of 2,5-HD (0.2 mM, 2 mM and 20 mM) for 24, 48 and 72 hours. Scale bar: 50 μm. For all the histograms (B, C, E) the following color code has been used: control (CTRL, white bars), 0.2 mM 2,5-HD (light grey bars), 2 mM 2,5-HD (dark grey bars) and 20 mM 2,5-HD (black bars). (B) The cell viability, evaluated by MTT test, was not affected just at 20 mM for 48 and 72 hours of exposure. *$p<0.01$ and **$p<0.001$ vs CTRL according to ANOVA, Tukey HSD *post hoc* test. (C-E) Morphometric analysis showed morphological alterations induced by 2,5-HD in a dose-dependent manner. Three principal features of neuritogenesis were considered: the percentage of differentiated cells (histogram, C), the length of the longest neurite for each differentiated cell (box plot, D) and the percentage of differentiated cells presenting varicosities on their longest neurite (histogram, E). 2,5-HD treatment induced the shortening of the neurite length with consequent loss of the differentiated state of the cells and induced the formation of small axonal swelling. For the percentage of neuronal differentiation (C) and neurites with varicosities (E) *$p<0.05$ and **$p<0.001$ vs CTRL according to $\chi^2$ test. For the neurite length (D) *$p<0.05$ and **$p<0.001$ vs CTRL according to ANOVA, Tukey HSD *post hoc* test. All values are expressed as mean ± SEM.

**Figure 2.**

**2,5-HD impacts all the components of the cytoskeleton in NGF-differentiated PC12 cells.**

(A) Immunoblot and (B) densitometric analyses of actin (Actin), NFs (NF-L and NF-M), α-tubulin (α-Tub) and β-tubulin (β-Tub) were performed in whole cell extracts from 5-days NGF-differentiated PC12 cells treated for 24 hours with different concentration of 2,5-HD: control (CTRL, white bars), 0.2 mM (light grey bars), 2 mM (dark grey bars) and 20 mM (black bars). For the quantitation, values of each protein were normalized on the total amount of protein loaded per lane, through the Coomassie blue staining. All values are expressed as mean ± SEM. *$p<0.05$ and **$p<0.001$ vs CTRL according to ANOVA, Tukey HSD *post hoc* test. (C) NGF-differentiated PC12 cells were stained with Atto 565-conjugated phalloidin or with primary antibodies anti-NF-L and anti-α-tubulin to reveal the organization of actin fibers (Actin, top), NFs (NF-L, middle) and MTs (α-Tub, bottom), respectively. Scale bar: 20 μm.

**Figure 3.**

**2,5-HD alters MT stability in NGF-differentiated PC12 cells.**

(A) Immunoblot and (B) densitometric analyses of post-translational modified forms of α-tubulin (α-Tub): tyrosinated tubulin (Tyr Tub), detyrosinated tubulin (deTyr Tub) and acetylated tubulin (Ac Tub). The analyses were performed on whole cell extracts from 5-days NGF-differentiated PC12 cells treated for 24 hours with different concentration of 2,5-HD: control (CTRL, white bars), 0.2 mM (light grey bars), 2 mM (dark grey bars) and 20 mM (black bars). For the quantitation, values of each protein were normalized on the total amount of protein loaded per lane, through the Coomassie blue staining. All values are expressed as mean ± SEM. *p<0.01 and **p<0.001 vs CTRL according to ANOVA, Tukey HSD *post hoc* test; #p<0.01 vs CTRL according to ANOVA, Fisher LSD *post hoc* test. (C) 2,5-HD altered the distribution of stable MTs. NGF-differentiated PC12 cells were stained for tyrosinated (Tyr), detyrosinated (deTyr) and acetylated (Ac) tubulin to investigate MT organization and stability. All cells were concurrently stained with DAPI (blue), to visualize the nucleus. Scale bar: 20 μm. (D-E) Triton-X100-soluble (representing the free α-tubulin dimers, Dim) and –insoluble fraction (α-tubulin incorporated into MTs, MTs) of modified forms of α-tubulin in NGF-differentiated PC12 cells were analysed by (D) immunoblot and (E) densitometric analyses, shown as ratio. 2,5-HD influenced the tubulin distribution between the two fractions. As expected for a MT-stabilizing action, in fact, the ratio was shifted towards the MTs fraction even at low doses of toxin. *p<0.05 vs healthy CTRL according to ANOVA, Fisher HSD *post hoc* test; **p<0.001 vs CTRL of each group according to ANOVA, Tukey HSD *post hoc* test. All values are expressed as mean ± SEM.

**Figure 4.**

**Tubulin assembly *in vitro* and MT ultrastructure in the presence of 2,5-HD.**

(A) Kinetic curves of pure tubulin (30 μM), purified from bovine brain, polymerized in assembly buffer in the absence (CTRL) or presence of different concentration of 2,5-HD (0.2 mM, 2 mM and 20 mM) without any preincubation. Reactions were followed turbidimetrically at 350 nm for 90 min at 37°C. (B) Table reporting the kinetic parameters calculated from the polymerization curves: the number of successive steps in the nucleation phase (*P* value), the maximal velocity of polymerization at the very initial elongation phase (Vi, ΔA/min) and the total extent of MT assembly as the total absorbance variation (ΔA). All values are expressed as mean ± SEM. (C) Ultrastructure of the tubulin assembly products performed in the same conditions described above. Control and 20 mM 2,5-HD treated

tubulin were fixed with 0.5% glutaraldehyde prior to perform the negative staining with uranyl acetate. Scale bar: 100 nm.

**Figure 5.**

**Mitochondria seemed not to be an early target of 2,5-HD.**

(A) Reactive oxygen species (ROS) production was measured using DCFDA Cellular ROS Detection assay on 5-days NGF-differentiated PC12 cells treated for 24 hours with different concentration of 2,5-HD: control (CTRL, white bars), 0.2 mM (light grey bars), 2 mM (dark grey bars) and 20 mM (black bars). *$p<0.05$ vs CTRL according to ANOVA, Fisher LSD *post hoc* test. (B) Immunoblot and (C) densitometric analyses of dynamin-related protein 1 (DRP1) and mitofusin-2 (MFN2) were performed in whole cell extracts from 5-days NGF-differentiated PC12 cells treated for 24 hours with different concentration of 2,5-HD: control (CTRL, white bars), 0.2 mM (light grey bars), 2 mM (dark grey bars) and 20 mM (black bars). For the quantitation, values of each mitochondrial protein were normalized on the level of mitochondrial porin (VDAC) of the relative sample. *$p<0.05$ and **$p<0.001$ vs CTRL according to ANOVA, Tukey HSD *post hoc* test. All values are expressed as mean ± SEM.

**Figure 6.**

**2,5-HD alters morphology and MT stability in PD fibroblasts.**

(A) Table presenting the information of investigated individuals: the identification code; the genotype (just for PD patients); the sex; the age at time of skin biopsy and establishment of fibroblast cell line; the age at which the patient first noticed a PD-related symptom was considered the age of onset of the disease. (B) Representative phase-contrast micrographs of cultured human skin fibroblasts of healthy and PD affected people treated for 24 hours with different concentration of 2,5-HD. Scale bar: 50 μm. For all the graphics the following color code has been used: control (CTRL, white bars), 0.2 mM 2,5-HD (light grey bars), 2 mM 2,5-HD (dark grey bars) and 20 mM 2,5-HD (black bars). (C) The cell viability, evaluated by MTT test, was not affected in both groups by the toxin. (D-E) Morphometric analysis showed increased area in the presence of mutated parkin (D) and reduced ratio between maximum and minimum axes in parkinsonian fibroblasts (E). Moreover, just PD fibroblasts morphology was affected by 2,5-HD, at 20 mM after 24 hours of treatment the cell area was significantly reduced. **$p<0.001$ vs control group according to ANOVA, Dunnett *post hoc* test; #$p<0.05$ vs PD CTRL according to ANOVA, Fisher LSD *post hoc* test. (F-G) Triton-X100-soluble (representing the free α-tubulin dimers, Dim) and –insoluble fraction (α-tubulin incorporated

into MTs, MTs) of human skin fibroblasts were analysed by (F) immunoblot and (G) densitometric analyses, shown as ratio. The genetic background influenced the tubulin distribution between the two fractions already at the base line condition. The PD fibroblast resulted also much more susceptible to the MT-stabilizing action of 2,5-HD, in fact, the ratio was shifted towards the MTs fraction even at low doses of toxin. ##$p<0.001$ vs healthy CTRL according to ANOVA, Tukey HSD *post hoc* test; **$p<0.001$ vs CTRL of each group according to ANOVA, Tukey HSD *post hoc* test. All values are expressed as mean ± SEM. CTRL= control (N=3); PD (PARK2)= patients with mutations in *PARK2* gene (N=3).

**FIGURE 1**

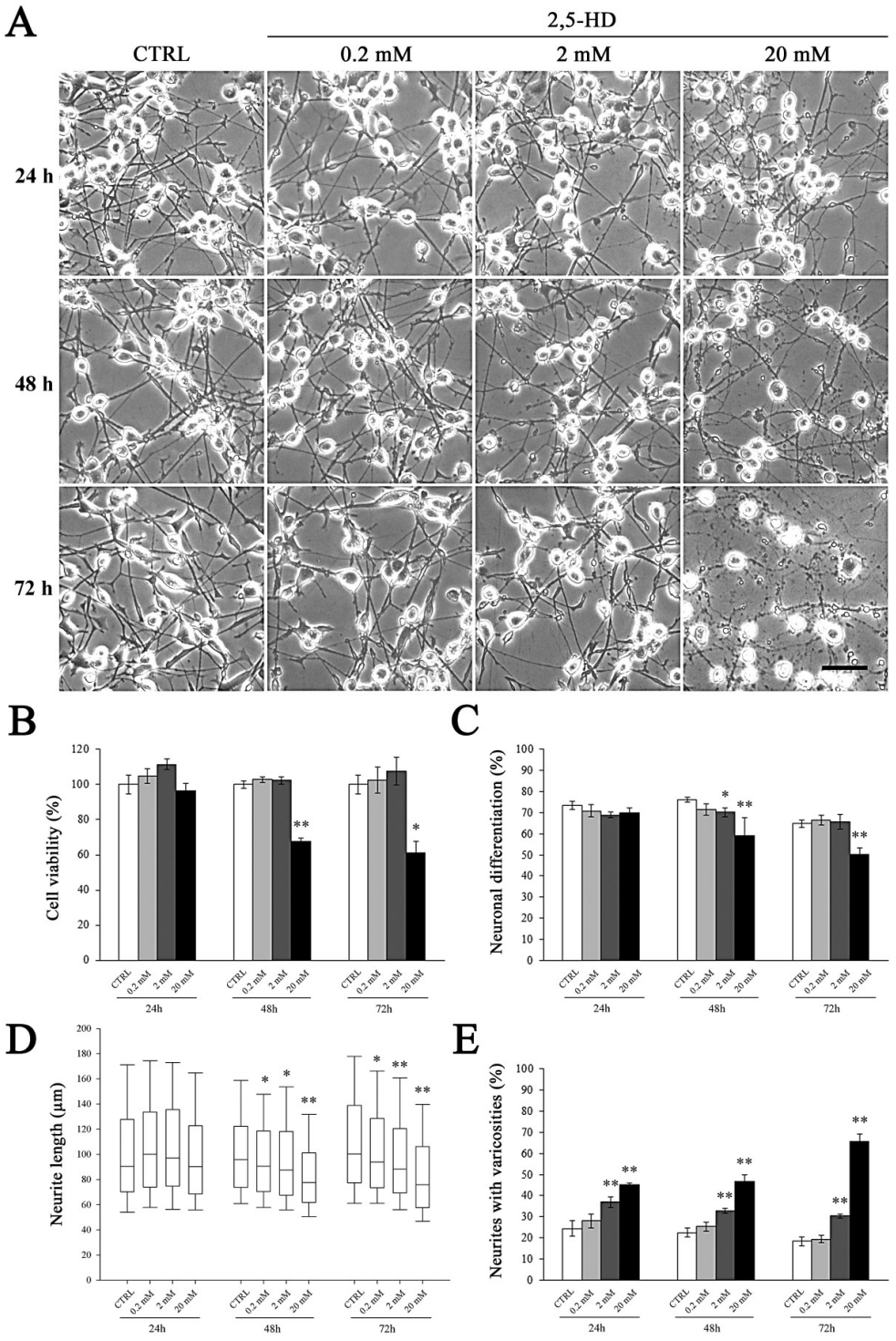
A
2,5-HD
CTRL
0.2 mM
2 mM
20 mM
24 h
48 h
72 h
B
Cell viability (%)
C
Neuronal differentiation (%)
D
Neurite length (µm)
E
Neurites with varicosities (%)
CTRL
0.2 mM
2 mM
20 mM
24h
48h
72h

**FIGURE 2**

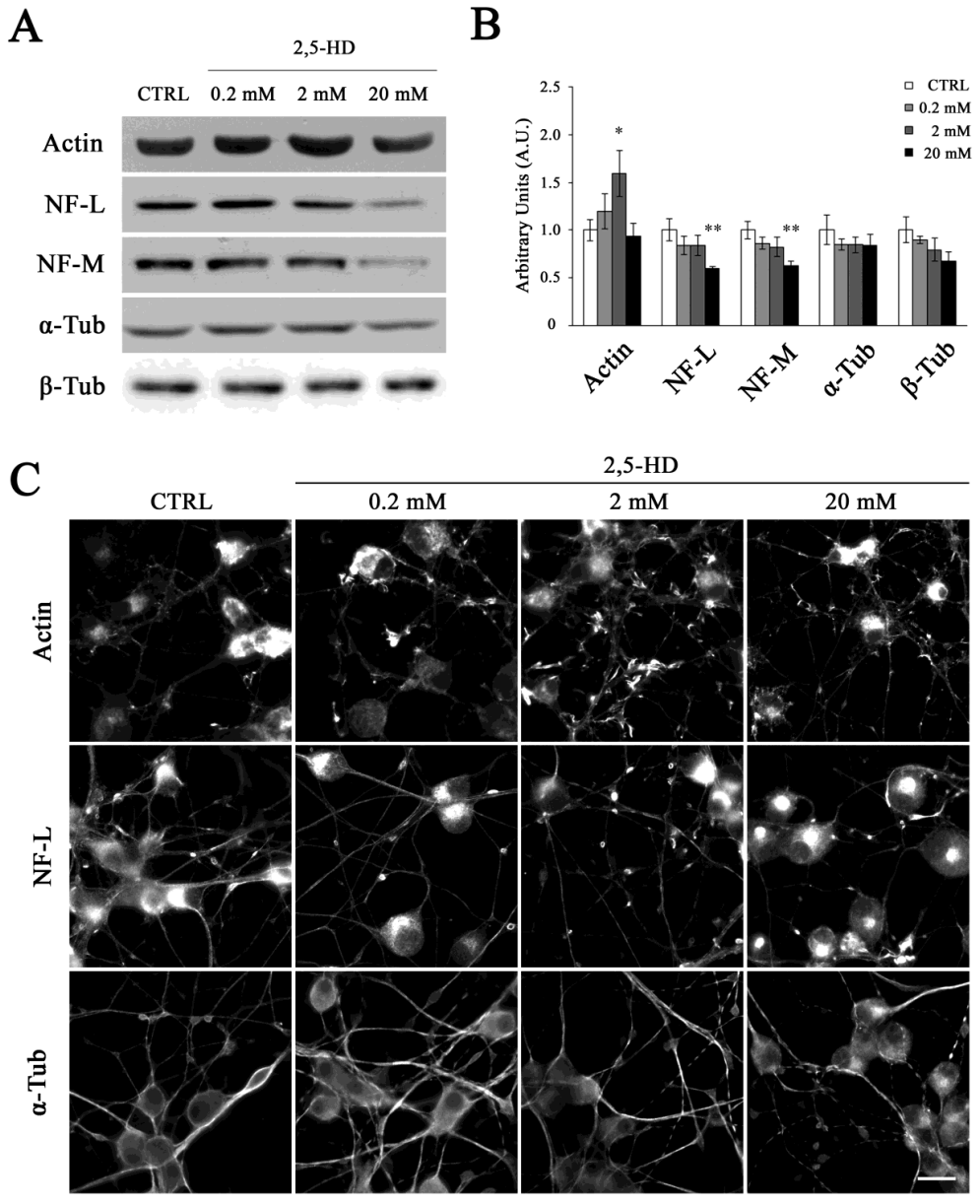
A
2,5-HD
CTRL
0.2 mM
2 mM
20 mM
Actin
NF-L
NF-M
α-Tub
β-Tub
B
Arbitrary Units (A.U.)
2.5
2.0
1.5
1.0
0.5
0
CTRL
0.2 mM
2 mM
20 mM
*
**
**
Actin
NF-L
NF-M
α-Tub
β-Tub
C
2,5-HD
CTRL
0.2 mM
2 mM
20 mM
Actin
NF-L
α-Tub

**FIGURE 3**

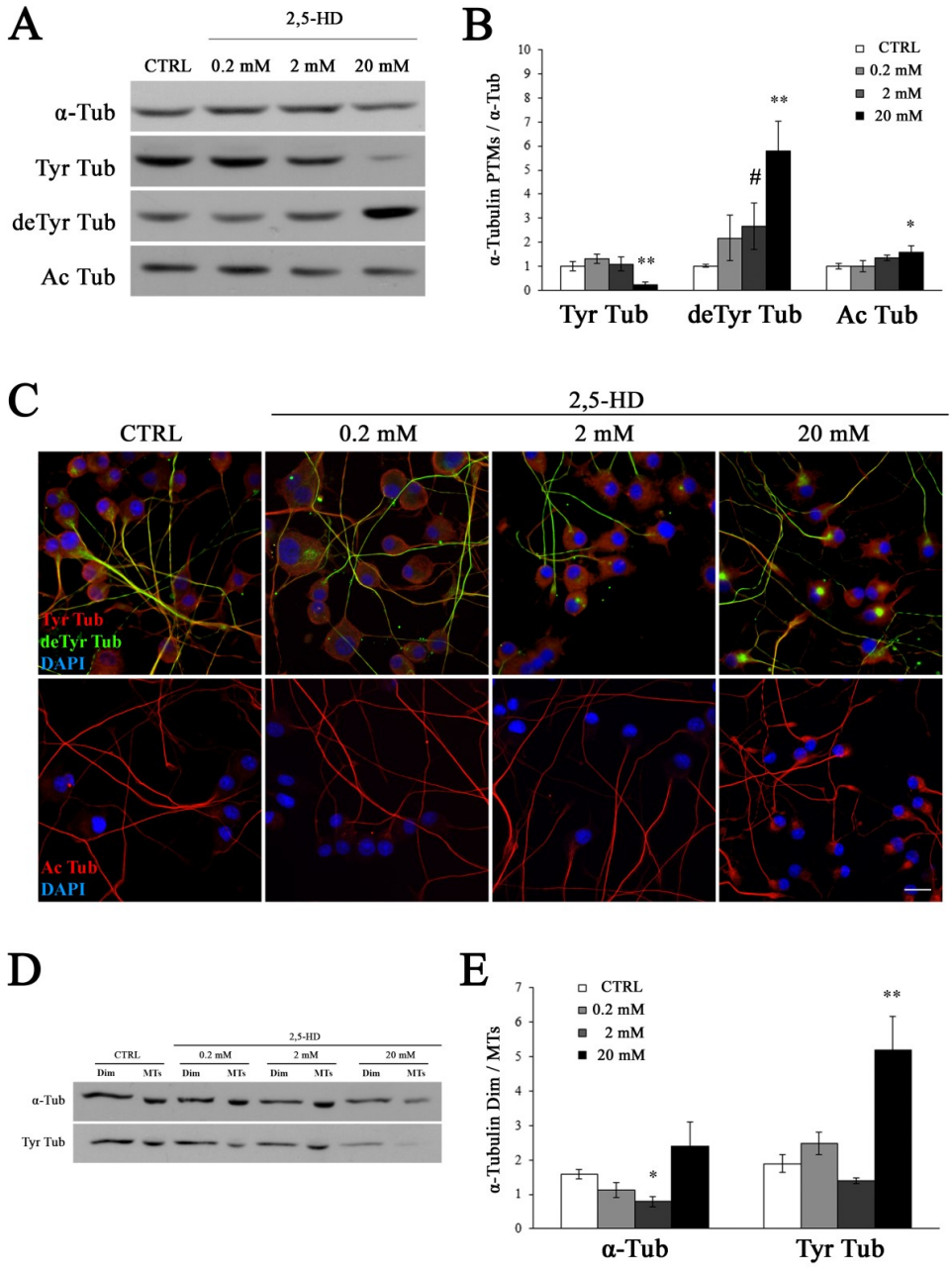
A
2,5-HD
CTRL
0.2 mM
2 mM
20 mM
α-Tub
Tyr Tub
deTyr Tub
Ac Tub
B
α-Tubulin PTMs / α-Tub
CTRL
0.2 mM
2 mM
20 mM
**
#
*
Tyr Tub
deTyr Tub
Ac Tub
C
2,5-HD
CTRL
0.2 mM
2 mM
20 mM
Tyr Tub
deTyr Tub
DAPI
Ac Tub
DAPI
D
2,5-HD
CTRL
0.2 mM
2 mM
20 mM
Dim
MTs
α-Tub
Tyr Tub
E
α-Tubulin Dim / MTs
CTRL
0.2 mM
2 mM
20 mM
*
**
α-Tub
Tyr Tub

**FIGURE 4**

A

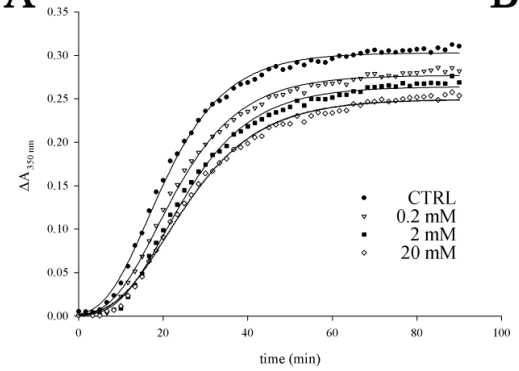


B

| Kinetic parameters | CTRL | 0.2 mM | 2 mM | 20 mM |
|---|---|---|---|---|
| *P* value | 4.00 ± 0.25 | 4.22 ± 0.23 | 4.91 ± 0.45 | 4.77 ± 0.79 |
| $V_i$ | 0.0067 ± 0.0017 | 0.0079 ± 0.0021 | 0.0057 ± 0.0037 | 0.0043 ± 0.0015 |
| ΔA | 0.221 ± 0.029 | 0.253 ± 0.036 | 0.196 ± 0.084 | 0.192 ± 0.035 |

C

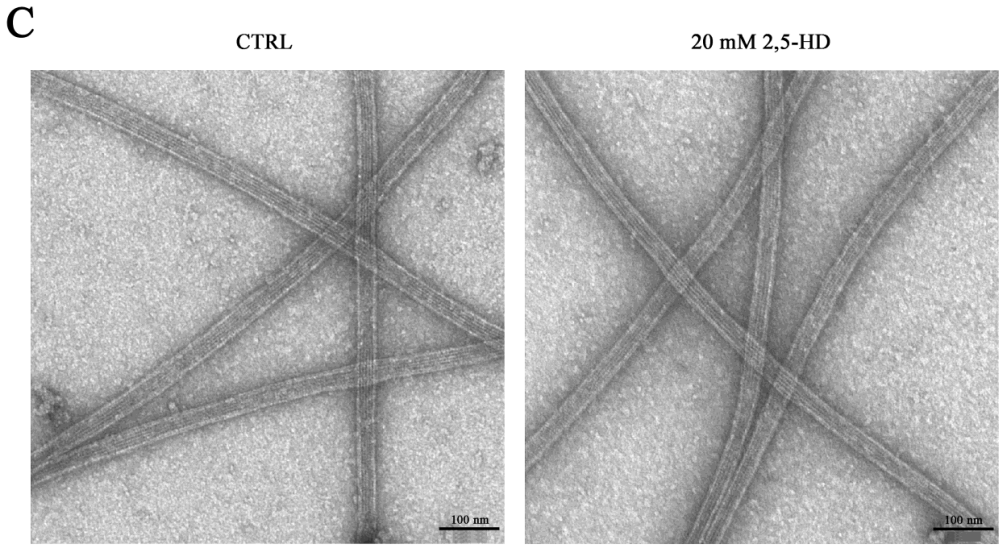

**FIGURE 5**

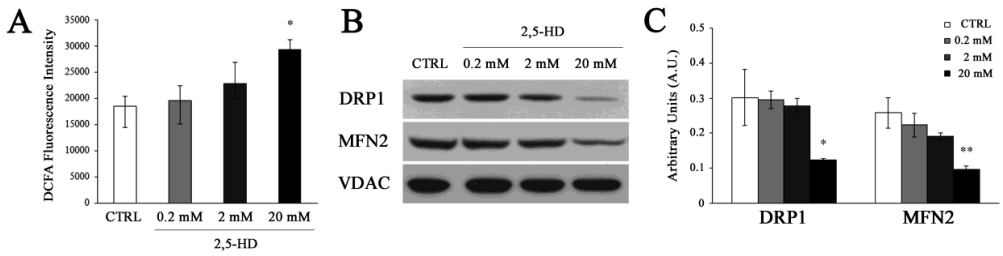
A
DCFA Fluorescence Intensity
35000
30000
25000
20000
15000
10000
5000
0
*
CTRL
0.2 mM
2 mM
20 mM
2,5-HD
B
2,5-HD
CTRL
0.2 mM
2 mM
20 mM
DRP1
MFN2
VDAC
C
Arbitrary Units (A.U.)
0.5
0.4
0.3
0.2
0.1
0
CTRL
0.2 mM
2 mM
20 mM
*
**
DRP1
MFN2

**FIGURE 6**

A

| | CODE | GENOTYPE | SEX | AGE OF BIOPSY | AGE OF ONSET |
|---|---|---|---|---|---|
| Healthy donors | FFF0422011 | | M | 69 | |
| | FFF0521978 | | M | 51 | |
| | FFF0531978 | | F | 44 | |
| PD patients (*PARK2* mutations) | FFF0142009 | c.C924T (p.R275W);exon 3 del. | F | 41 | 22 |
| | FFF0292009 | exon 3 del (homozygotes) | F | 69 | 39 |
| | FFF0902009 | c.del202_203AG (p.Q34/X43) (homozygotes) | M | 51 | 20 |

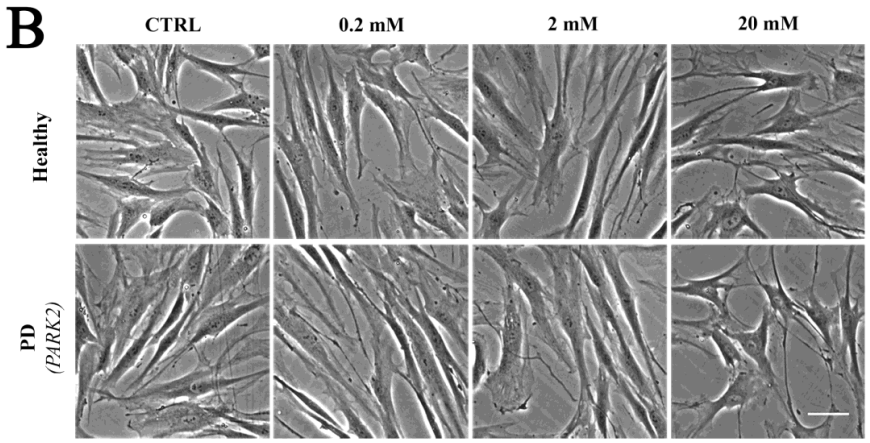


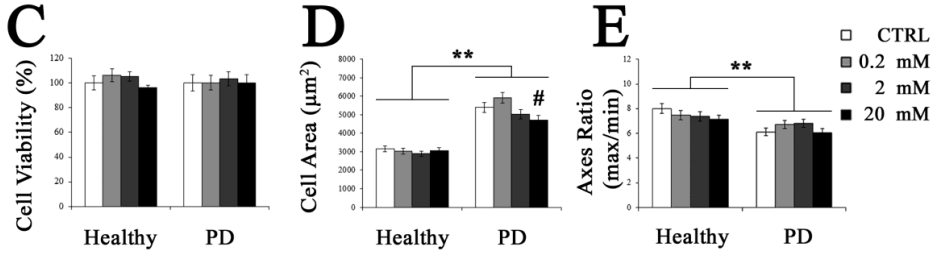


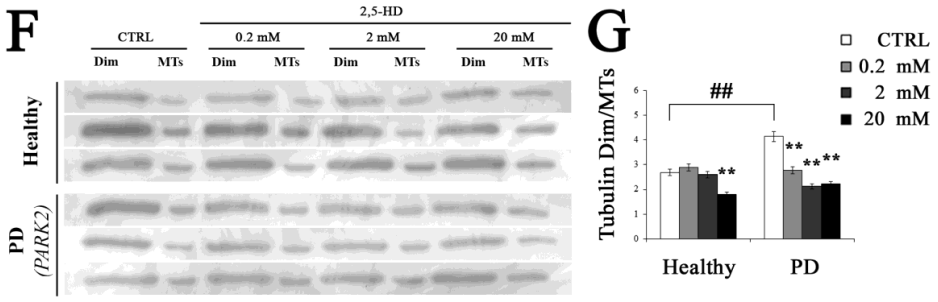

Manuscript 2
Cartelli et al., *To be submitted*

# PARKIN BALANCES TUBULIN POST-TRANSLATIONAL MODIFICATIONS AND MODULATES MICROTUBULE DYNAMICS

Cartelli D.*, Department of Biosciences, Università degli Studi di Milano, Milano, 20133, Italy;
Amadeo A.*, Department of Biosciences, Università degli Studi di Milano, Milano, 20133, Italy;
Casagrande F., Department of Biosciences, Università degli Studi di Milano, Milano, 20133, Italy;
De Gregorio C., Department of Biosciences, Università degli Studi di Milano, Milano, 20133, Italy;
Calogero A.M., Department of Biosciences, Università degli Studi di Milano, Milano, 20133, Italy;
Gioria M., Department of Biosciences, Università degli Studi di Milano, Milano, 20133, Italy;
Kuzumaki N. °, Department of Physiology, Keio University School of Medicine, Tokyo, 160-8582, Japan;
Costa I., Department of Biosciences, Università degli Studi di Milano, Milano, 20133, Italy;
Sassone J.#, Department of Neurology and Laboratory of Neuroscience, IRCCS Istituto Auxologico Italiano, Cusano Milanino (MI), 20095, Italy;
Ciammola A., Department of Neurology and Laboratory of Neuroscience, IRCCS Istituto Auxologico Italiano, Cusano Milanino (MI), 20095, Italy;
Hattori N., Department of Neurology, Juntendo University School of Medicine, Tokyo, 113-8421, Japan;
Okano H., Department of Physiology, Keio University School of Medicine, Tokyo, 160-8582, Japan;
Goldwurm S., Parkinson Institute, Istituti Clinici di Perfezionamento, Milano, 20126, Italy
Roybon L., Stem Cell laboratory for CNS Disease Modeling, Wallenberg Neuroscience Center, Department of Experimental Medical Science, Lund University, BMC A10, 22184, Lund, Sweden; Strategic Research Area MultiPark and Lund Stem Cell Center, Lund University, 22184, Lund, Sweden;
Pezzoli G., Parkinson Institute, Istituti Clinici di Perfezionamento, Milano, 20126, Italy
Cappelletti G. §, Department of Biosciences, Università degli Studi di Milano, Milano, 20133, Italy;

° present address: Department of Pharmacology, Hoshi University, Pharmacy and Pharmaceutical Sciences, Tokyo, 142-8501 Japan;
# present address: Neuroalgology and Headache Unit, IRCCS Foundation 'Carlo Besta' Neurological Institute, Milano, 20133, Italy.
* These authors contributed equally to the work
§ To whom correspondence should be addressed: Graziella Cappelletti, Department of Biosciences, Università degli Studi di Milano, Via Celoria 26, Milano, 20133, Italy. Tel: +39 0250314752; Fax: +30 0250315044; Email: graziella.cappelletti@unimi.it

**ABSTRACT**

Mutations in the parkin gene (*PARK2*) are associated with neurodegeneration and lead to familial forms of Parkinson's disease. In addition to the well-known ligase activity of parkin, it seems to regulate other cellular functions including mitochondria homeostasis and microtubule stability, although the latter one has been largely neglected during the past years. To gain more insights into the intracellular roles of parkin, here we investigated its influence on microtubule behaviour in murine and human neurons. Live cell imaging reveals that parkin-silencing alters mitochondria movement in cultured neuronal cells through microtubule destabilization, since this defect is rescued by paclitaxel. The imbalance of post-translationally modified tubulins, that are associated with differences in microtubule stability, occurs in *PARK2* knockout mice and precedes the block of mitochondrial transport. Finally, moving to human tissues, we observe changes in tubulin post-translational modifications in the autoptic brain of *PARK2* patients, and the increase in the fragmentation of stable (i.e. Acetylated) microtubules in *PARK2* patient-derived neurons. Therefore, our work pinpoints parkin as a regulator of microtubule stability in neurons, which would work through the balancing of tubulin post-translational modifications, and reinforces the idea that microtubule dysfunction may be important in the pathogenesis of Parkinson's disease.

## INTRODUCTION

Mutations in the parkin gene (*PARK2*) are tightly associated with neurodegeneration and lead to familial forms of Parkinson's disease (PD) known as Autosomal Recessive Juvenile Parkinsonism (ARJP, OMIM #600116) (1). Parkin is an ubiquitin E3-ligase involved in the maintenance of cellular health (2): its enzymatic activity promotes the degradation of misfolded and damaged proteins through the ubiquitin-proteasome system (UPS). In addition to its ligase activity, parkin seems to participate in other cellular functions (3) and is able to interact with two targets involved in the pathogenesis of PD: mitochondria and microtubules (MTs).

The ability of parkin to regulate mitochondrial dynamics, through the modulation of fusion and fission processes (4), is largely accepted. The phosphatase and tensin homolog (PTEN)-induced putative kinase 1 (PINK1)/parkin pathway acts upstream of mitofusin inducing mitochondrial fusion. The same pathway regulates the transport of mitochondria, promoting the docking of damaged ones prior to their degradation (5). Nevertheless, the direct involvement of PINK1/parkin in the regulation of mitophagy is somewhat controversial. Supporting observations came mainly from cultured mammalian cells overexpressing parkin, but in induced-pluripotent stem cell (iPSC)-derived human neurons the endogenous parkin is not sufficient to initiate mitophagy (6). Therefore, it is unclear whether parkin involvement in this process really is relevant in neurons or during PD pathogenesis or not (7).

Notably, parkin not only interacts with tubulin, the building block of MTs, promoting its ubiquitination and degradation via UPS (8), but it is also able to directly bind and stabilize MTs (9). Therefore, it is not surprising that *PARK2* mutations or exons' deletion destabilize MTs and abolish the ability of parkin to counteract the MT depolymerization induced by rotenone and colchicine in both murine and human midbrain dopaminergic neurons (10, 11). This process seems to be mediated by the regulation of MAP kinase pathway (10) which, interestingly, is a direct regulator of MT stability via the modulation of tubulin post-translational modifications (PTMs). In agreement with these observations, we recently reported that PD-patient skin fibroblasts bearing *PARK2* mutations display altered tubulin PTM patterns and reduced MT mass, and either MT-targeted pharmacological treatment or the overexpression of wild-type (WT) parkin rescues control phenotype (12).

In order to clarify the effects of parkin on the MT system and MT-dependent functions in neurons, using live cell imaging, we first demonstrate that parkin-silencing accelerates MT growth and, consequently, impairs mitochondrial trafficking. Afterward, we look at *PARK2* knock out (KO) mice and show that in absence of parkin the equilibrium between stable and

dynamic MTs is altered. Finally, through analysis of PD brain tissue and PD iPSC-derived neurons, we show for the first time that parkin deletions/mutations affect MT stability in PD patients.

## RESULTS

*Parkin regulates mitochondrial trafficking through MT dynamics*

In order to verify the hypothesis that parkin modulates MT dynamics directly and to investigate the interplay between MT system and mitochondrial transport in depth, we carried out live cell imaging analysis. We used parkin-silenced NGF-differentiated PC12 cells (Figure S1) expressing either mCherry-EB3, a fluorescent protein that specifically binds growing MT plus-end (13), or Mito-DsRed, which enables us to follow mitochondrial movement (14). The kymographs depict the overall effects of parkin-silencing on MT dynamics and mitochondrial transport (Figure 1A). According to its proposed MT-stabilizing effect (9), we show that parkin absence significantly accelerates MT-growth (Figure 1B); furthermore, since it has no effects on the frequency of MT catastrophes (Figure 1C), parkin also increase the MT growing distance (Figure 1D). At the same time, parkin-silencing speeds up the anterograde velocity of mitochondrial transport (Figure 1E), with no effects on retrograde transport (Figure 1F); furthermore, silenced cells display a higher fraction of mitochondria moving towards the soma (Figure 1G), meaning that parkin absence causes a disorientated mitochondrial trafficking. Therefore, to ascertain whether the mitochondrial motility defects were strictly related to alterations in the MT system, we performed rescue experiments using the MT-stabilizing agent paclitaxel. As shown in Figure 1, paclitaxel restores the physiological MT-growth rate and, very interestingly, rescues mitochondria transport defects, reverting the direction of mitochondria movement and slowing down its velocity. Altogether, our data pinpoint that parkin directly regulates MT dynamics and, in turn modulates mitochondrial trafficking.

*Parkin absence affects MT stability in knock out mice*

The majority of pathological *PARK2* mutations are loss-of-function and result in the absence or, at least, in an inactive form of parkin. Although the *PARK2* KO mouse is not a suitable PD model to investigate nigro-striatal neuronal degeneration (15, 16), it can be useful and informative for studing parkin biology. Therefore, we decided to evaluate MT stability in *Corpus striatum* (Figure 2) and *Substantia nigra* (Figure 3) of WT and *PARK2* KO mice at different ages, ranging from young adult to old mice (2-24 months). Biochemical analyses of α tubulin PTMs, which are markers of MTs with different stability (17), showed the enrichment of Tyrosinated (Tyr) tubulin, the most dynamic MT pool, in the *Corpus striatum* of *PARK2* KO mice (Figures 2A and 2B). The increase of Tyr tubulin is detectable already at

2 months of age but it vanishes over time. Furthermore, we observed a mild but significant increase in the level of Acetylated (Ac) tubulin in 7 months old *PARK2* KO mice (Figures 2A and 2B). To uncover whether the observed changes of tubulin PTMs in the *Corpus striatum* can be attributed to dopaminergic terminals, we used confocal microscopy and the analysis of Manders' parameters (18). Dopaminergic terminals showed a specific trend of tubulin PTM changing that somehow differs from the whole region (Figures 2C and 2D). Indeed, co-localization between stable MTs, i.e. Ac and deTyrosinated (deTyr) tubulin, and tyrosine hydroxylase (TH) staining increases, whereas loss of Tyr tubulin staining is detectable in young mice and exacerbated in old ones. This is intriguing as it suggests that the MT cytoskeleton inside dopaminergic terminals of *PARK2* KO mice specifically loses its dynamic component and accumulates stable MTs making terminals less prone to rapidly reorganize.
Western blotting analysis performed on *ventral mesencephalon* lysates (Figures 3A and 3B), revealed a significant increase of Tyr tubulin in young adult *PARK2* KO mice followed by a non significant decrease in older ones. Our analyses also revealed the reduction of Ac tubulin in 2-year old *PARK2* KO mice. Confocal analyses, and the quantification of fluorescence intensity inside dopaminergic neurons, showed that the early accumulation of Tyr tubulin and its later decrease occurred specifically in dopaminergic neurons (Figures 3C and 3D). Since fluorescence quantification revealed an enrichment of Ac MTs in dopaminergic neurons (Figures 3C and 3D), the slight reduction in Ac tubulin levels observed by Western blotting is probably due to an alteration occurring in other cell types, such as glia or non-dopaminergic neurons. Taken together, our data uncover the ability of parkin to modulate α tubulin PTMs *in vivo* and well agree with its capability in regulating MT dynamics directly.

*Parkin absence impacts mitochondrial transport*

Axonal transport is a process that is strictly dependent on the MT system. It has been shown that the PINK1/parkin pathway arrests mitochondrial movement to quarantine damaged mitochondria in hippocampal neurons (5). Thus, we analysed mitochondrial transport in *PARK2* KO mice, evaluating the distribution of mitochondria inside dopaminergic fibres, as previously described (19). We observed dopaminergic fibres with a homogeneous distribution of mitochondria as well as fibres showing mitochondria that are sparse or clustered into varicosities (Figure 4A), a typical sign of axonal transport impairment (20). We quantified the different types of fibres (Figure 4B) and found no differences in mitochondria distribution in 2-month old mice, whereas fibres with mitochondria clustering significantly increased in *PARK2* KO mice, starting from 7 months of age. We also performed qualitative ultrastructural

analysis of TH-positive fibres by pre-embedding immunocytochemistry, which enabled us to identify these two types of fibres (Figure 4C), as showed by the axons with one mitochondrion (arrowheads) and by the dopaminergic axons engulfed by several clustered mitochondria (arrows). In agreement with previous evidence (21), these mitochondria display a normal gross morphology (Figure 4C). Moreover, a rough estimation of the mitochondrial profile inside dopaminergic axons xxx mExxx (data not shown) reveals that the percentage of fibres with 3 or more clustered mitochondria is in agreement with the percentage of fibres with a "clustered" mitochondria distribution as evaluated by confocal microscopy, and indicate that in these fibers mitochondria cover a higher surface of the axon, easily leading to block of intracellular transport. Thus, our data show clustered mitochondria revealing transport failure in old mice. According to the chain of events we depicted in parkin-silenced cells, the evidences we thus far accumulated led us to hypothesize that the mitochondria accumulation observed in *PARK2* KO mice may be directly caused by the imbalance in post-translational regulation of tubulin, which is already noticeable in 2-month old *PARK2* KO mice.

*PARK2 mutations reduce MT stability in PD patients*

Thus far, our data strongly indicate that parkin modulates MT stability in rodent experimental models; yet, their relevance had to be validated in human cells, since MT stability in human brains in *PARK2*-linked pathological states is still elusive. Because of the unavailability of nigral tissue from *PARK2*-linked PD patients, we analysed the brain cortex obtained by autopsy of *PARK2*-related PD patients (Figure 5A). Looking at the levels of α tubulin PTMs, we found an unbalance of MT stability. Albeit non significant, an overall enrichment of Tyr tubulin, the most dynamic MT pool, and a mild increase in Ac tubulin occur in tissues from PD patients compared to controls (Figure 5B and 5C). These data are in agreement with our observations on the mouse nigro-striatal system (Figure 2 and 3) and suggest, for the first time, that *PARK2*-linked PD patient brains show MT stability defects. In order to refine our analyses, and especially to look at midbrain neurons, we took advantage of cellular reprogramming technologies to access dopaminergic neurons from iPSCs generated from *PARK2*-linked PD patients and evaluate any possible MT-linked phenotype reminiscent of alterations (deletions or mutations) in the *PARK2* gene (Figure 5D and Figure S2). Our observations unexpectedly revealed that patient-derived cultures show axons with specific disruption of stable MTs, as pointed out by the continuous Tyr Tubulin staining (Figure S2) and the fragmented Ac tubulin one (Figure 5). The z-projection (Figure 5E) and the 3D

reconstruction (supplementary video 1 and 2) demonstrate that this discontinuous staining is not a problem of focal plane but a real fragmentation of stable MTs. A carefull quantification of the axons with continuos or interrupted Ac staining highlighted the significantly higher percentage of fragmented MTs in PD patient-derived cultures (Figure 5F). This result highlights an intrinsic weakness of patient MTs, confirming the already reported MT destabilization in human cells (11, 12).

Overall, our data identify parkin as a modulator of MT stability in neurons. Hence, MT destabilization may play an important role in PD pathogenesis and is a relevant therapeutic target in PD.

## DISCUSSION

As for other PD-related proteins, the functional role of parkin is somewhat controversial. It is clearly related to the protein degradation system, via its ubiquitin-ligase activity (2), and to mitochondrial homeostasis (4). On the other hand, although the ability of parkin to modulate the MT system was proposed many years ago (22), it remained largely neglected. Here, we have demonstrated the direct involvement of parkin in the regulation of tubulin PTMs and MT dynamics in neurons, both in rodent experimental models and human systems. Furthermore, our data indicate that the impact of parkin on MT cytoskeleton likely leads to the impairment of mitochondrial transport.

We have shown that in absence of parkin the equilibrium between stable and dynamic MTs is altered and, hence, that parkin modulates MT growth directly. In accordance with the proposed MT-stabilizing effect of parkin (9), its absence results in a faster MT growing rate (Figure 1). This is consistent with the enrichment of the most dynamic MT pool, i.e. Tyr-MTs, both in human fibroblasts (12) and in human cortex (Figure 5). To our knowledge, this is the first suggestion of MT alterations in human *PARK2* PD brains. The very recent demonstration of MT destabilization induced by parkin mutations in iPSC-derived neurons (11) well matches with our observation of stable MT fragmentation in PD patient-derived neurons (Figure 5), regardless of whether they originate form patients with *PARK2* exon deletions (PA9 and PB2 lines) or a point mutation (CSC-7A). As a whole, these data strongly indicate that parkin may be a MT stability modulator in humans, both in physiological and in PD contexts. Moreover, in *PARK2* KO mice we observed early increase in dynamic MTs followed by the accumulation of stable MT pools, which are consistent with the fine tuning of MT dynamics and tubulin PTMs associated with neuronal development and brain aging (23). Therefore, our data unmask parkin as a novel regulator of MT stability/dynamics, via the modulation of tubulin PTMs.

An expected consequence of the alteration of MT stability is the dysregulation of axonal transport. Indeed, proteins and organelles run along MT tracks and we have already reported that mitochondrial transport block can be the result of MT destabilization in toxin-induced parkinsonism (14, 19). Our work adds on to the previous accrued evidence on the role of parkin, and reveals that parkin, a PD-related protein, physiologically modulates mitochondrial trafficking in a MT-dependent manner. Indeed, the analyses performed on brain slices and live cell imaging experiments on cultured cells revealed that the transport defects observed in the absence of parkin are dependent on MT dynamics, as they are rescued by MT stabilization. It has been already reported that parkin regulates the trafficking of mitochondria

in hippocampal neurons, especially of those that are damaged and have to be degraded, and that this process is dependent on Miro phosphorylation (5). In the present work, we provide further detail on this physiological event showing that parkin is able to regulate mitochondrial mobility *in vivo* (Figure 4) through the regulation of MT system. Nevertheless, our results are not necessarily in contrast with those of Wang and colleagues; indeed, Schwarz's lab had already demonstrated that the Miro/Milton complex acts as an adaptor recruiting the heavy chain of conventional kinesin-1 (24). Kinesin-1, which is highly expressed in neuronal cells, is sensitive to tubulin PTMs, which modulate its axonal recruitment (25), its preferential binding to specific MT subsets (26) and the velocity of its movement (27). Furthermore, MT acetylation rescues axonal transport and locomotor deficits caused by mutations of Leucine-Rich Repeat Kinase 2 (28), a common genetic cause of PD. Hence, the changes in tubulin PTMs and MT dynamics reported here could be an attempt designed to restore the correct mitochondrial trafficking in the absence of parkin.

Another aspect to be considered is the regulation of mitochondrial homeostasis. The direct involvement of parkin in mitophagy is debated (6, 7), although the PINK1/parkin pathway has been very recently implicated in the initiation of local mitophagy in the distal axon (29). Nevertheless, parkin is crucial for the maintenance of mitochondrial dynamics (4). It has also been reported that MTs participate in the regulation of this process (30), which is essential in the modulation of mitochondrial function and movement. In concordance with the evidence that *PARK2* KO mice do not accumulate mitochondria with an abnormal morphology (21), our qualitative ultrastructural analysis showed mitochondria with a conventional gross morphology (Figure 4C). Nevertheless, this mouse strain shows early respiratory defects in striatal mitochondria (21, 31) and MT alterations (present data). The fact that these problems do not worsen with time can be explained in two ways. First, there are many pathways converging on the regulation of either mitochondria or MTs; therefore the early defects, due to parkin absence, can likely be buffered over time. Second, mouse models have a shorter lifespans than humans and this does not allow the full unmasking of this particular phenotype and the accumulation of sufficient defects overcoming a hypothetical pathological threshold. The difficulties in developing animal models that exhibit all the key features of human PD are further exacerbated by the different scales of human and rodent nigral dopaminergic neurons, whose axons reach an average arborization of 460 and 46 cm, respectively (32, 33). This particular morphology gives rise to the selective vulnerability of these neuronal subtypes, and the different time- and space-scale could explain why in many animal models those neurons do not degenerate. Nevertheless, since MT destabilization and energy failure are associated

with the latency period of axonal degeneration (34), all data emerging from *PARK2* KO mice, as the ones presented here, can be used for the analyses of earlier events occurring in degenerating dopaminergic neurons, eventually leading to PD.

Altogether, our data indicate that parkin should be considered as a novel controller of MTs which, through the regulation of tubulin PTMs, balances stable and dynamic MTs in rodent and human experimental models as well as in human PD brain. When this equilibrium deviates from physiological conditions, as we have demonstrated here in the absence of parkin, it results in the alteration of mitochondrial transport and, likely, in mitochondrial damage and axonal degeneration, mirroring the pathological chain of events we reported in toxin-induced parkinsonism (19).

## MATERIALS & METHODS

*Animals*

Wild type and *PARK2* knock out (15) C57 Black mice (male and female) were purchased from Charles River (Calco, Italy) and used for all experiments. Mice were kept under environmentally controlled conditions (ambient temperature = 22°C, humidity = 40%) on a 12-h light/dark cycle with food and water *ad libitum*. Mice were kept in pathogen-free conditions and all procedures complied with Italian law (D. Lgs n° 2014/26, implementation of the 2010/63/EU) and were approved by the University of Milan Animal Welfare Body and by the Italian Minister of Health. All efforts were made to minimize suffering. Mice were killed by decapitation or by transcardiac perfusion to perform biochemical or immunohistochemical analysis respectively.

*Human brain samples*

Fresh frozen specimens of human prefrontal cortex were obtained from the Department of Neurology, Juntendo University School of Medicine, Japan. The samples were obtained from four patients with Autosomal Recessive Juvenile Parkinsonism and three control subjects, whose phenotype and genotype are summarized in Figure 5A. The diagnosis was confirmed by neuropathological examination of the brain tissues as PD, and neurodegenerative disorders were excluded in control subjects. Gene analyses of parkin and sample preparation were performed as previously reported (35). The study protocol was approved by the Human Ethics Review Committee of Juntendo.

*Western blot analysis*

Western blot analysis was performed on protein extracts obtained from human (35) or mouse brain regions, as follows. *Corpus striatum* and *ventral mesencephalon* were immediately dissected out on ice, mechanically homogenized and sonicated in SDS-PAGE sample buffer. Western blots were made as previously described (19) using the following antibodies: α tubulin mouse IgG (clone B-5-1-2, Sigma-Aldrich, Saint Louis, MO); deTyr tubulin rabbit IgG (Chemicon, Temecula, CA); Tyr tubulin rat IgG (clone YL 1/2, Abcam, Cambridge, UK); Ac tubulin mouse IgG (clone 6-11B-1, Sigma-Aldrich); parkin rabbit IgG (Abcam). Membranes were washed for 30 min and incubated for 1 h at room temperature with HRP donkey anti-mouse IgG (Pierce, Rockford, IL), HRP goat anti-rat IgG (Sigma-Aldrich), or HRP goat anti-rabbit IgG (Pierce). Immunostaining was revealed by enhanced

chemiluminescence (Super-Signal West Pico Chemiluminescent, Pierce). Acquisition and quantification were performed by ChemiDoc and Image Lab software (Bio-Rad, Hercules, CA).

*Confocal analysis*

Mice were anesthetized with chloralium hydrate (320 mg/kg, i.p.) and transcardially perfused with 4% paraformaldehyde (PFA) in 0.1 M phosphate buffer (PB), pH 7.4. Brains were removed, post-fixed 3 h in 4% PFA. Sagittal sections (50 µm thick) were cut with a Vibratome (VT1000S, Leica Microsystems, Heidelberg, Germany), and part of them were cryoprotected for long-term conservation at -20°C. Sections were stained with the following antibodies previously used for immunoblotting: deTyr tubulin rabbit IgG; Tyr tubulin rat IgG; Ac tubulin mouse IgG and with VDAC1/porin rabbit IgG (Abcam). To identify dopaminergic neurons and fibres, each section was concurrently stained with anti-TH antibody, made in mice (clone LCN1, Millipore, Darmstadt, Germany) or rabbits (Millipore) as appropriate. As secondary antibodies we used Alexa Fluor™ 568 donkey anti-mouse IgG, Alexa Fluor™ 488 goat anti-rabbit IgG and Alexa Fluor™ 568 donkey anti-rat IgG (Invitrogen). Samples were examined with a confocal laser scan microscope imaging system (TCS SP2 AOBS, Leica Microsystems) equipped with an Ar/Ar-Kr 488 nm, 561 nm and 405 nm diode lasers. Photomultiplier gain for each channel was adjusted to minimize background noise and saturated pixels and, once defined for control conditions, parameters were kept constant for all acquisitions. To estimate the overlapping area between red and green signals, analyses were carried out on single-plane raw images and Manders' coefficients were calculated applying the JACoP plug-in (developed and reviewed by 18) for ImageJ software. Quantification of the fluorescence inside dopaminergic neurons was performed using the appropriate module of the NIH ImageJ software. As previously described (19), to evaluate the mitochondria distribution, the porin signal was superimposed on dopaminergic fibres, using the Mask tool of the Leica Confocal Software (Leica); mitochondria accumulations were identified as white pixel-containing areas, as thick as long, clearly separated from other white pixels. A TH-positive signal longer than 5 µm was considered as dopaminergic fibre, and signals separated by more than 10 µm were counted as two distinct fibres.

*Immuno-electron microscopy*

Mice were perfused with 4% PFA and 0,5% glutaraldehyde in PB 0,1 M as described for confocal analysis. Vibratome sagittal sections were incubated sequentially with anti-TH rabbit IgG (Millipore), biotinylated goat anti-rabbit IgG (Vector Laboratories, Burlingame, CA) and with avidin biotinylated peroxidase complex (ABC method, Vector Laboratories). After completion of the immunoenzymatic procedure and visualization of reaction with DAB, sections were washed in PB, osmicated, dehydrated and flat embedded in Epon-Spurr between acetate foils (Aclar, Ted Pella, Reddin, CA). Selected areas of the embedded sections were then cut with a razor blade and glued to blank blocks of resin for further sectioning. Thin sections (70 nm) were obtained with an ultramicrotome (Reichert Ultracut E, Leica Microsystems, Heerbrugg, Switzerland) and were observed with a Philips CM10 transmission electron microscope at 80 kv; images were acquired using a Morada Olympus digital camera.

*Live cell imaging*

PC12 cells were maintained in cultures and differentiated for 3 days with NGF, as previously described (Cartelli et al., 2010). PC12 cells were transiently transfected using Lipofectamine 2000 (Invitrogen) (1:3 DNA to Lipofectamine ratio), with the shRNA previously reported (36, 37) and together with EB3-mCherry construct (13) or Mito-dsRed (14). 3 days after transfection, cultures were transferred to a live cell imaging workstation composed of an inverted microscope (Axiovert 200M, Zeiss), a heated (37°C) chamber (Okolab, Naple, Italy), and a Plan neofluar 63x/1.25 numerical aperture oil-immersion objective (Zeiss). Images were collected with a cooled camera (Axiocam HRM Rev. 2; Zeiss, Oberkochen, Germany), every 6 s for the analyses of MT growth and every 10-15 s for mitochondrial trafficking; single movie duration was set at 1-3 min and the total recording time did not exceed 60 min for each dish. For rescue experiments, cells were incubated for 2 h with 1 μM paclitaxel (Sigma-Aldrich) dissolved in methanol. MT growth dynamics were analyzed from EB3 time-lapse movies using plusTipTracker software (38), and the reported catastrophe frequency is calculated as the inverse of the average growth time; mitochondrial movement was analyzed by the Imaris software, kindly provided by Immagini & Computer (Bareggio, Italy). Kymographs were constructed using the MetaMorph Software.

*Generation and differentiation of human iPSCs*

The generation of iPSC lines B7, WD, PA7 and PB2 was reported elsewhere (39). Fibroblasts used to generate the lines CSC-9A (healthy control) and CSC-7A (PD patient carrying the

mutation C253Y located in exon 7 of *PARK2* gene in homozygosity) were obtained from the Parkinson Institute Biobank (Milano, Italy). Fibroblasts were reprogrammed according to previous published protocol (40). Randomly selected colonies (2-4 per line) were validated for pluripotency markers expression (by both immunocytochemistry and RT-qPCR for SOX2, NANOG, SSEA4, TRA1-80), alkaline phosphatase activity (86R-1KT, Sigma Aldrich), generation of cell types ($SMA^+$, $AFP^+$ and B-III-tubulin$^+$) reminiscent of the 3 embryonic germ layers following spontaneous differentiation of putative iPSC lines grown as embryoid bodies, when exposed to DMEM medium + 10% FBS, and telomerase activity (S7700, Millipore). Genetic analysis and karyotyping was outsourced to the Department of Genetics, at the hospital of Lund, Sweden (Medicinsk service/Labmedicin, Klinisk genetik och biobank) and showed no karyotype abnormalities for the 2 lines selected. Mutation in *PARK2* in line CSC-7A was confirmed by sequencing, using the primers AGGATTACAGAAATTGGTCT (forward) and TCTGTTCTTCATTAGCATTAGA (reverse). The differentiation of the iPSC lines B7, WD, PA7 and PB2 was carried out as previously reported (39). The differentiation of the lines CSC-7A and CSC-9A was carried out using a modified protocol (see 41), where LDN-193189 (100 nM, Stemgent) was employed instead of Noggin, and CHIR was kept in differentiation medium, together with neurotrophic factors. At 30 DIV, EBs were seeded on adherent coated surfaces for final differentiation for 7 additional days. Differentiated cells were stained with Ac tubulin mouse IgG (Sigma-Aldrich) and with anti-TH rabbit IgG (Millipore). As secondary antibodies we used Alexa Fluor™ 568 donkey anti-mouse IgG, and Alexa Fluor™ 488 goat anti-rabbit IgG (Invitrogen). Samples were examined with a confocal laser scan microscope imaging system (TCS SP5, Leica Microsystem, Heidelberg, Germany) and axonal fragmentation were analysed with ImageJ software. Thus, we used two sets of iPSC lines, generated in 2 different laboratories using two different protocols and bearing different parkin mutations as exon deletions (PA7: exon 2-4 homozygous deletion of *PARK2* gene, and PB2: exon 6,7 homozygous deletion of *PARK2* gene, from the Okano's Laboratory in Japan) or a point mutation (CSC-7A: C253Y located in exon 7 of *PARK2* gene, from the Roybon's Laboratory in Sweden).

*Statistical analysis and data management*

The statistical significance of genetic background or treatment was assessed by Student's t-test, one-way ANOVA with Fischer LSD *post-hoc* testing or $\chi^2$ test when appropriate. Analyses were performed using STATISTICA software (StatSoft Inc., Tulsa, OK).

**Funding**

This work was supported by Fondazione Grigioni per il Morbo di Parkinson, Milan, Italy [to G.C.]; ''Dote ricerca'', FSE, Regione Lombardia [to D.C.]; and the Program for Intractable Disease Research Utilizing Disease-specific iPS cells funded by the Japan Science and Technology Agency [JST, to H.O.].

**Aknowledgements**

Human fibroblast cell lines were obtained from the "Cell Line and DNA Biobank from Patients affected by Genetic Diseases" (Istituto G. Gaslini) and the "Parkinson Institute Biobank" (Milano), members of the Telethon Network of Genetic Biobanks (project no. GTB12001), funded by Telethon Italy. The authors are thankful to Dr. Francolini (Department of Medical Biotechnology and Translational Medicine, Università Degli Studi Di Milano, Milano, Italy) for the use of transmission electron microscope, technical advices and helpful discussion. The authors are grateful to Dr. Jennifer S. Hartwig for reading and editing the manuscript and apologize for each possible involuntary paper omission.

**Conflict of Interests**

H.O. is a paid scientific consultant to San Bio Co., Ltd.

**REFERENCES**


1. Lesage, S. and Brice, A. (2009) Parkinson's disease: from monogenic forms to genetic susceptibility factors. *Hum. Mol. Genet*., **18**, R48-59.
2. Shimura, H., Hattori, N., Kubo, S., Mizuno, Y., Asakawa, S., Minoshima, S., Shimizu, N., Iwai, K., Chiba, T., Tanaka, K., et al. (2000) Familial Parkinson disease gene product, parkin, is a ubiquitin-protein ligase. *Nat. Genet*., **25**, 302-305.
3. Alves da Costa, C. and Checler, F. (2012) Parkin: much more than a simple ubiquitin ligase. *Neurodegener. Dis*., **10**, 49-51.
4. Scarffe, L.A., Stevens, D.A., Dawson, V.L. and Dawson, T.M. (2014) Parkin and PINK1: much more than mitophagy. *Trends Neurosci*., **37**, 315-324.
5. Wang, X., Winter, D., Ashrafi, G., Schlehe, J., Wong, Y.L., Selkoe, D., Rice, S., Steen, J., LaVoie, M.J. and Schwarz, T.L. (2011) PINK1 and Parkin target Miro for phosphorylation and degradation to arrest mitochondrial motility. *Cell*, **147**, 893-906.
6. Rakovic, A., Shurkewitsch, K., Seibler, P., Grünewald, A., Zanon, A., Hagenah, J., Krainc, D. and Klein, C. (2013) Phosphatase and tensin homolog (PTEN)-induced putative kinase 1 (PINK1)-dependent ubiquitination of endogenous Parkin attenuates mitophagy: study in human primary fibroblasts and induced pluripotent stem cell-derived neurons. *J. Biol. Chem*., **288**, 2223-2237.
7. Grenier, K., McLelland, G.L. and Fon, E.A. (2013) Parkin- and PINK1-Dependent Mitophagy in Neurons: Will the Real Pathway Please Stand Up? *Front. Neurol*., **4**, 100.
8. Ren, Y., Zhao, J. and Feng, J. (2003) Parkin binds to alpha/beta tubulin and increases their ubiquitination and degradation. *J. Neurosci*., **23**, 3316-3324.
9. Yang, F., Jiang, Q., Zhao, J., Ren, Y., Sutton, M.D. and Feng, J. (2005) Parkin stabilizes microtubules through strong binding mediated by three independent domains. *J. Biol. Chem*., **280**, 17154-17162.
10. Ren, Y., Jiang, H., Yang, F., Nakaso, K. and Feng, J. (2009) Parkin protects dopaminergic neurons against microtubule-depolymerizing toxins by attenuating microtubule-associated protein kinase activation. *J. Biol. Chem*., **284**, 4009-4017.
11. Ren, Y., Jiang, H., Hu, Z., Fan, K., Wang, J., Janoschka, S., Wang, X., Ge, S. and Feng, J. (2015) Parkin Mutations Reduce the Complexity of Neuronal Processes in iPSC-derived Human Neurons. *Stem Cells*, **33**, 68-78.

12. Cartelli, D., Goldwurm, S., Casagrande, F., Pezzoli, G. and Cappelletti, G. (2012) Microtubule destabilization is shared by genetic and idiopathic Parkinson's disease patient fibroblasts. *PLoS ONE*, **7**, e37467.
13. Komarova, Y., De Groot, C.O., Grigoriev, I., Gouveia, S.M., Munteanu, E.L., Schober, J.M., Honnappa, S., Buey, R.M., Hoogenraad, C.C., Dogterom, M., et al. (2009) Mammalian end binding proteins control persistent microtubule growth. *J. Cell. Biol*., **184**, 691-706.
14. Cartelli, D., Ronchi, C., Maggioni, M.G., Rodighiero, S., Giavini, E. and Cappelletti, G. (2010) Microtubule dysfunction precedes transport impairment and mitochondria damage in $MPP^+$-induced neurodegeneration. *J Neurochem*., **115**, 247-258.
15. Goldberg, M.S., Fleming, S.M., Palacino, J.J., Cepeda, C., Lam, H.A., Bhatnagar, A., Meloni, E.G., Wu, N., Ackerson, L.C., Klapstein, G.J., et al. (2003) Parkin-deficient mice exhibit nigrostriatal deficits but not loss of dopaminergic neurons. *J. Biol. Chem*., **278**, 43628-43635.
16. Itier, J.M., Ibanez, P., Mena, M.A., Abbas, N., Cohen-Salmon, C., Bohme, G.A., Laville, M., Pratt, J., Corti, O., Pradeier, L., et al. (2003) Parkin gene inactivation alters behaviour and dopamine neurotransmission in the mouse. *Hum Mol Genet.,* **12**, 2277-2291.
17. Janke, C. (2014) The tubulin code: molecular components, readout mechanisms, and functions. *J. Cell. Biol*., **206**, 461-472.
18. Bolte, S. and Cordelières, F.P. (2006) A guided tour into subcellular colocalization analysis in light microscopy. *J. Microsc*., **224**, 213-232.
19. Cartelli, D., Casagrande, F., Busceti, C.L., Bucci, D., Molinaro, G., Traficante, A., Passarella, D., Giavini, E., Pezzoli, G., Battaglia, G., et al. (2013) Microtubule alterations occur early in experimental parkinsonism and the microtubule stabilizer Epothilone D is neuroprotective. *Sci. Rep.*, **3**, 1837.
20. De Vos, K.J., Grierson, A.J., Ackerley, S. and Miller, C.C. (2008) Role of axonal transport in neurodegenerative diseases. *Annu. Rev. Neurosci*., **31**, 151-173.
21. Palacino, J.J., Sagi, D., Goldberg, M.S., Krauss, S., Motz, C., Wacker, M., Klose, J. and Shen, J. (2004) Mitochondrial dysfunction and oxidative damage in parkin-deficient mice. *J. Biol. Chem*., **279**, 18614-18622.
22. Feng, J. (2006) Microtubule: a common target for Parkin and Parkinson's disease toxins. *Neuroscientist*, **12**, 469-476.

23. Janke, C. and Kneussel, M. (2010) Tubulin post-translational modifications: encoding functions on the neuronal microtubule cytoskeleton. *Trends Neurosci*., **33**, 362-372.
24. Glater, E.E., Megeath, L.J., Stowers, R.S. and Schwarz, T.L. (2006) Axonal transport of mitochondria requires milton to recruit kinesin heavy chain and is light chain independent. *J. Cell. Biol*., **173**, 545-557.
25. Konishi, Y. and Setou, M. (2009) Tubulin tyrosination navigates the kinesin-1 motor domain to axons. *Nat. Neurosci*., **12**, 559-567.
26. Dunn, S., Morrison, E.E., Liverpool, T.B., Molina-París, C., Cross, R.A., Alonso, M.C. and Peckham, M. (2008) Differential trafficking of Kif5c on tyrosinated and detyrosinated microtubules in live cells. *J. Cell. Sci*., **121**, 1085-1095.
27. Reed, N.A., Cai, D., Blasius, T.L., Jih, G.T., Meyhoferm, E., Gaertig, J. and Verhey, K.J. (2006) Microtubule acetylation promotes kinesin-1 binding and transport. *Curr. Biol*. **16**, 2166-2172.
28. Godena, V.K., Brookes-Hocking, N., Moller, A., Shaw, G., Oswald, M., Sancho, R.M., Miller, C.C., Whitworth, A.J. and De Vos, K.J. (2014) Increasing microtubule acetylation rescues axonal transport and locomotor deficits caused by LRRK2 Roc-COR domain mutations. *Nat. Commun*., **5**, 5245.
29. Ashrafi, G., Schlehe, J.S., LaVoie, M.J. and Schwarz, T.L. (2014) Mitophagy of damaged mitochondria occurs locally in distal neuronal axons and requires PINK1 and Parkin. *J. Cell. Biol*., **206**, 655-670.
30. Bowes, T. and Gupta, R.S. (2008) Novel mitochondrial extensions provide evidence for a link between microtubule-directed movement and mitochondrial fission. *Biochem. Biophys. Res. Commun*., **376**, 40-45.
31. Damiano, M., Gautier, C.A., Bulteau, A.L., Ferrando-Miguel, R., Gouarne, C., Paoli, M.G., Pruss, R., Auchère, F., L'Hermitte-Stead, C., Bouillaud, F., et al. (2014) Tissue- and cell-specific mitochondrial defect in Parkin-deficient mice. *PLoS ONE*, **9**, e99898.
32. Pissadaki, E.K. and Bolam, J.P. (2013) The energy cost of action potential propagation in dopamine neurons: clues to susceptibility in Parkinson's disease. *Front. Comput. Neurosci*., **7**, 13.
33. Matsuda, W., Furuta, T., Nakamura, K.C., Hioki, H., Fujiyama, F., Arai, R. and Kaneko, T. (2009) Single nigrostriatal dopaminergic neurons form widely spread and highly dense axonal arborizations in the neostriatum. *J. Neurosci*., **29**, 444-453.

34. Park, J.Y., Jang, S.Y., Shin, Y.K., Koh, H., Suh, D.J., Shinji, T., Araki, T. and Park, H.T. (2013) Mitochondrial swelling and microtubule depolymerization are associated with energy depletion in axon degeneration. *Neuroscience*, **238**, 258-269.
35. Fukae, J., Sato, S., Shiba, K., Sato, K., Mori, H., Sharp, P.A., Mizuno, Y. and Hattori, N. (2009) Programmed cell death-2 isoform1 is ubiquitinated by parkin and increased in the substantia nigra of patients with autosomal recessive Parkinson's disease. *FEBS Lett*., **583**, 521-525.
36. Helton, T.D., Otsuka, T., Lee, M.C., Mu, Y. and Ehlers, M.D. (2008) Pruning and loss of excitatory synapses by the parkin ubiquitin ligase. *Proc. Natl. Acad. Sci. USA*, **105**, 19492-19497.
37. Maraschi, A., Ciammola, A., Folci, A., Sassone, F., Ronzitti, G., Cappelletti, G., Silani, V., Sato, S., Hattori, N., Mazzanti, M., et al. (2014) Parkin regulates kainate receptors by interacting with the GluK2 subunit. *Nat. Commun*., **5**,5182.
38. Applegate, K.T., Besson, S., Matov, A., Bagonis, M.H., Jaqaman, K. and Danuser, G. (2011) plusTipTracker: Quantitative image analysis software for the measurement of microtubule dynamics. *J. Struct. Biol*., **176**, 168-184.
39. Imaizumi, Y., Okada, Y., Akamatsu, W., Koike, M., Kuzumaki, N., Hayakawa, H., Nihira, T., Kobayashi, T., Ohyama, M., Sato, S., et al. (2012) Mitochondrial dysfunction associated with increased oxidative stress and α-synuclein accumulation in PARK2 iPSC-derived neurons and postmortem brain tissue. *Mol. Brain*., **5**, 35.
40. Dimos, J.T., Rodolfa, K.T., Niaka, K.K., Weisenthal, L.M., Mitsumoto, H., Chung, W., Croft, G.F., Saphier, G., Leibel, R., Goland, R., et al. (2008) Induced pluripotent stem cells generated from patient with ALS can be differentiated into motor neurons. *Science*, **321**, 1218-1221.
41. Kirkeby, A., Nelander, J. and Parmar, M. (2013) Generating regionalized neuronal cells from pluripotency, a step-by-step protocol. *Front. Cell. Neurosci*., **6**, 64.

**LEGENDS**

**Figure 1.** Parkin modulates mitochondrial trafficking via the regulation of MT dynamics. ***A***, Representative kymographs (inverted contrast) of MT growth (EB3-mCherry) and mitochondrial movement (Mito-DsRed) in parkin-silenced (sh*PARK2*) and scramble-treated (shSCR) NGF-differentiated PC12 cells, in basal conditions (CONT) or after 2 h of treatment with 1 μM paclitaxel (PTX). ***B***, ***C*** and ***D,*** Box plots of the MT growth rate (***B***), histograms showing the catastrophe frequency ($f_{CAT}$, ***C***) and box plots of the MT growth displacement (***D***) in parkin-silenced (sh*PARK2*) and scramble-treated (shSCR) NGF-differentiated PC12 cells, in basal conditions (CONT) or after 2 h of treatment with 1 μM paclitaxel (PTX). n ≥ 1500 MTs deriving from at least 10-15 cells per experimental group. *p<0.05 vs shSCR/CONT, #p<0.05 vs sh*PARK2*/CONT according to ANOVA, Fischer LSD *post hoc* test. The actual statistical values correspond to: ***B***) F = 40.74, p = 0.00000001, and the indivual *p* value are shSCR/PTX vs shSCR/CONT = 0.000004, sh*PARK2*/CONT vs shSCR/CONT = 0.0000005 and sh*PARK2*/PTX vs sh*PARK2*/CONT = 0.000002; ***D***) F = 65.15, p = 0.00000001, and the indivual *p* value are shSCR/PTX vs shSCR/CONT = 0.008576, sh*PARK2*/CONT vs shSCR/CONT = 0.000008 and sh*PARK2*/PTX vs sh*PARK2*/CONT = 0.000008, sh*PARK2*/PTX vs shSCR/CONT = 0.008516. ***E*** and ***F,*** Box plots of anterograde velocity (***E***) and retrograde velocity (***F***) of mitochondrial transport in parkin-silenced (sh*PARK2*) and scramble-treated (shSCR) NGF-differentiated PC12 cells, in basal conditions (CONT) or after 2 h of treatment with 1 μM paclitaxel (PTX). n ≥ 200 mitochondria tracks per condition, deriving from at least 10-15 cells per experimental group. *p<0.05 vs shSCR/CONT, #p<0.05 vs sh*PARK2*/CONT according to ANOVA, Fischer LSD *post hoc* test. The actual statistical values correspond to: ***E***) F = 4.64, p = 0.00033, and the indivual *p* value are sh*PARK2*/CONT vs shSCR/CONT = 0.0014 and sh*PARK2*/PTX vs sh*PARK2*/CONT = 0.00018. ***G***, Histogram showing the percentage of immobile mitochondria (Stop, black), mitochondria forward (FWD, light grey) or backward (BWD, dark grey) moving and vibrating mitochondria (Vibr, white) in the same conditions reported in ***E*** and ***F***. *p<0.05 vs shSCR/CONT (*p* value = 0.00025), #p<0.05 vs sh*PARK2*/CONT (*p* value = 0.0013) according to $\chi^2$ test.

**Figure 2.** Parkin absence affects MT stability in the *Corpus striatum*. ***A*** and ***B***, Representative western blot (***A***) and densitometric analyses (***B***) of Tyrosinated (Tyr Tub), deTyrosinated (deTyr Tub) and Acetylated (Ac Tub) tubulin on lysates of *Corpus striatum* of wild type

(WT) and *PARK2* knockout (*PARK2*) mice of different ages (2, 7 and 24 months). The level of tubulin PTMs were normalized on the level of total α tubulin (α Tub) in the respective sample and are expressed as fold chance on wild type level (mean ± SEM, n = 3-5 individuals per group). *p<0.05 according to Student's t-Test, performed on the rough data. Actual *p* value are: Tyr Tub, 2 months = 0.035 and 7 months = 0.0099; Ac Tub, 7 months = 0.0124. ***C***, Confocal images of striatum of wild type (WT) and *PARK2* knockout (*PARK2*) mice of different ages (2, 7 and 24 months). Green represents TH staining and red signals tubulin PTMs. Scale bar, 50 µm. ***D***, Analysis of M1 parameter (Tubulins vs. TH) in striatal sections. Data are expressed as mean ± SEM, n = 2-3 sections for each mouse from 3-4 mice per group. *p<0.05 according to Student's t-Test. Actual *p* value are: Tyr Tub, 2 months = 0.017 and 24 months = 0.0047; deTyr Tub, 2 months = 0.034 and 7 months = 0.001; Ac Tub, 2 months = 0.021 and 7 months = 0.04.

**Figure 3.** Parkin absence affects MT stability in the dopaminergic neurons of *ventral mesencephalon*. ***A*** and ***B***, Representative western blot (***A***) and densitometric analyses (***B***) of Tyrosinated (Tyr Tub), deTyrosinated (deTyr Tub) and Acetylated (Ac Tub) tubulin on lysates of *ventral mesencephalon* of wild type (WT) and *PARK2* knockout (*PARK2*) mice of different ages (2, 7 and 24 months). The levels of tubulin PTMs were normalized on the level of total α tubulin (α Tub) in the respective sample and are expressed as fold chance on wild type level (mean ± SEM, n = 3-5 individuals per group). *p<0.05 according to Student's t-Test, performed on the rough data. Actual *p* value are: Tyr Tub, 2 months = 0.039; Ac Tub, 7 months = 0.02. ***C***, Confocal images of *Substantia nigra* of wild type (WT) and *PARK2* knock out (*PARK2*) mice of different ages (2, 7 and 24 months). Green represents TH staining and red signals tubulin PTMs. Scale bar, 50 µm. ***D***, Quantification of fluorescence of Tyrosinated (Tyr Tub), deTyrosinated (deTyr Tub) and Acetylated (Ac Tub) tubulin inside dopaminergic neurons in the *Substantia nigra*. Data are expressed as fold change on wild type level (mean ± SEM, n = 2-3 sections for each mouse from 3-4 mice per group). *p<0.05 according to Student's t-Test, performed on rough data. Actual *p* value are: Tyr Tub, 2 months = 0.000068 and 7 months = 0.000026; deTyr Tub, 2 months = 0.00000018, 7 months = 0.000055 and 24 months = 0.0001; Ac Tub, 2 months = 0.000024, 7 months = 0.000026 and 24 months = 0.00006.

**Figure 4.** Parkin absence impacts mitochondrial transport *in vivo*. ***A***, Representative confocal images showing the different distribution of mitochondria (Porin, red signal) inside

dopaminergic fibres (TH, green signal). Arrowhead indicates a fibre with an homogeneous distribution of mitochondria whereas arrow highlights a cluster. Scale bar, 20 μm. ***B***, Percentage of dopaminergic fibres displaying a homogeneous distribution of mitochondria (homogeneous, white) or mitochondria accumulation (clustered, black) in wild type (WT) and *PARK2* knockout (*PARK2*) mice of different ages (2, 7 and 24 months). n = 3 sections for each mouse from 3-4 mice per group. ns = not significant and *p<0.05 according to $\chi^2$ test. The actual *p* value are 7 months = 0.000005 and 24 months = 0.0000005. ***C***, Electron micrographs of TH-positive fibres. Arrowheads indicate fibres with an homogeneous distribution of mitochondria whereas arrows highlight mitochondrial clustering in both longitudinal (left) and trasversal (right) sectioned dopaminergic axons. Scale bar, 500 nm.

**Figure 5.** Parkin mutations reduce MT stability in PD patients. ***A***, Phenotype and genotype characterization of the investigated individuals. ***B*** and ***C***, Representative Western blot (***B***) and densitometry (***C***) of Acetylated (Ac Tub) and Tyrosinated (Tyr Tub) tubulin in extracts of human cerebral cortex deriving from healthy control (Healthy Control, white bars) or ARJP patients (*PARK2*, black bars). The levels of tubulin PTMs were normalized on the level of total α tubulin (α Tub) in the respective sample. ***D***, Confocal micrographs of control (Healthy Control) and patient (*PARK2*) iPSC-derived neurons, stained for Ac tubulin (Ac Tub, green) and tyrosine hydroxylase (TH, red). Scale bar, 20 μm. ***E***, Three dimensional reconstruction of the images showed in ***D***. Reconstructed orthogonal projections represented as viewed in the x-z (bottom) and y-z (right) planes. ***F***, Histogram showing the percentage of axons with continuous (CONT, white) or fragmented (FRAG, black) Ac tubulin staining in control (Healthy Control, iPSC-lines B7, WD, CSC-9A) and patient (*PARK2*, iPSC-lines PA9, PB2, CSC-7A) iPSC-derived neurons. *p<0.05 according to $\chi^2$ test (*p* value = 0.000026).

**Figure S1.** Representative western blot (A) and relative quantification of parkin (B), in parkin-silenced (sh*PARK2*) and scramble-treated (shSCR) NGF-differentiated PC12 cells. The level of parkin has been normalized on the total amount of loaded proteins (as revealed by Comassie Blue staining). *p<0.05 according to Student's t-Test (*p* value = 0.026).

**Figure S2.** Micrographs of control (Healthy Control) and patient (*PARK2*) iPSC-derived neurons, stained for Tyrosinated tubulin (Tyr Tub, green) and tyrosine hydroxylase (TH, red). DAPI signal is also shown (blue). Scale bar, 50 μm.

**Supplementary movie 1.** 3D reconstruction of the z-stack of the iPSC-derived neuronal culture obtained from Healthy Control. The movie refers to images shown in Figure 5D and 5E.

**Supplementary movie 2.** 3D reconstruction of the z-stack of the iPSC-derived neuronal culture obtaibed from *PARK2* patients. The movie refers to images shown in Figure 5D and 5E.

**FIGURE 1**

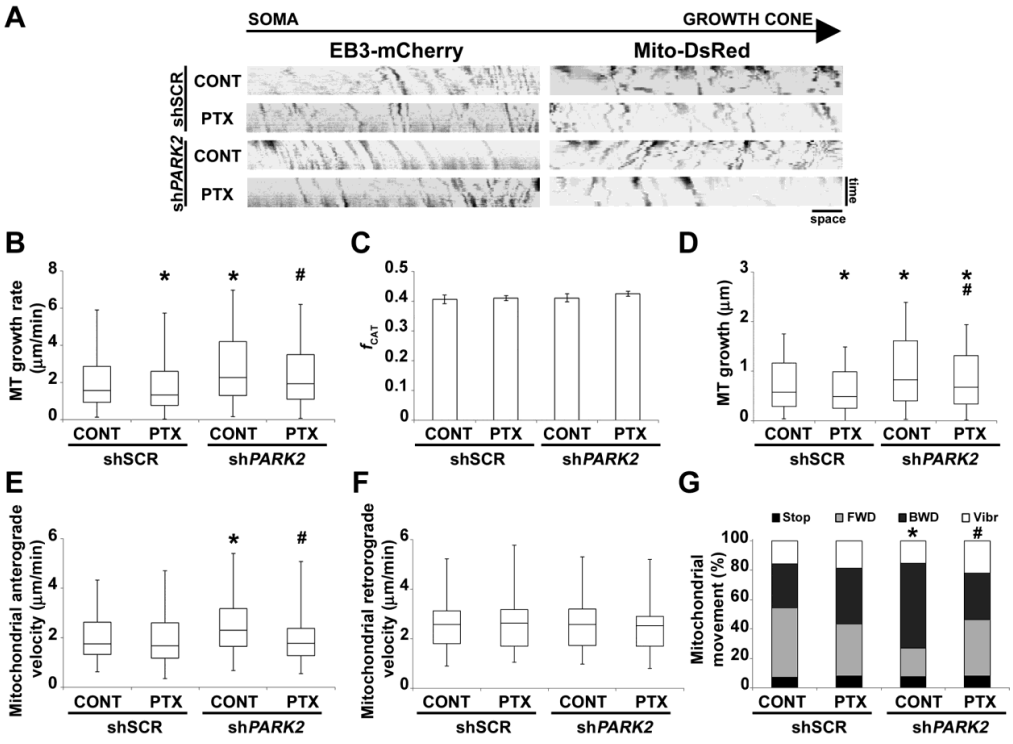
A
SOMA
GROWTH CONE
EB3-mCherry
Mito-DsRed
shSCR
CONT
PTX
shPARK2
CONT
PTX
time
space
B
MT growth rate (µm/min)
C
$f_{CAT}$
D
MT growth (µm)
E
Mitochondrial anterograde velocity (µm/min)
F
Mitochondrial retrograde velocity (µm/min)
G
Stop
FWD
BWD
Vibr
Mitochondrial movement (%)
CONT
PTX
shSCR
shPARK2

**FIGURE 2**

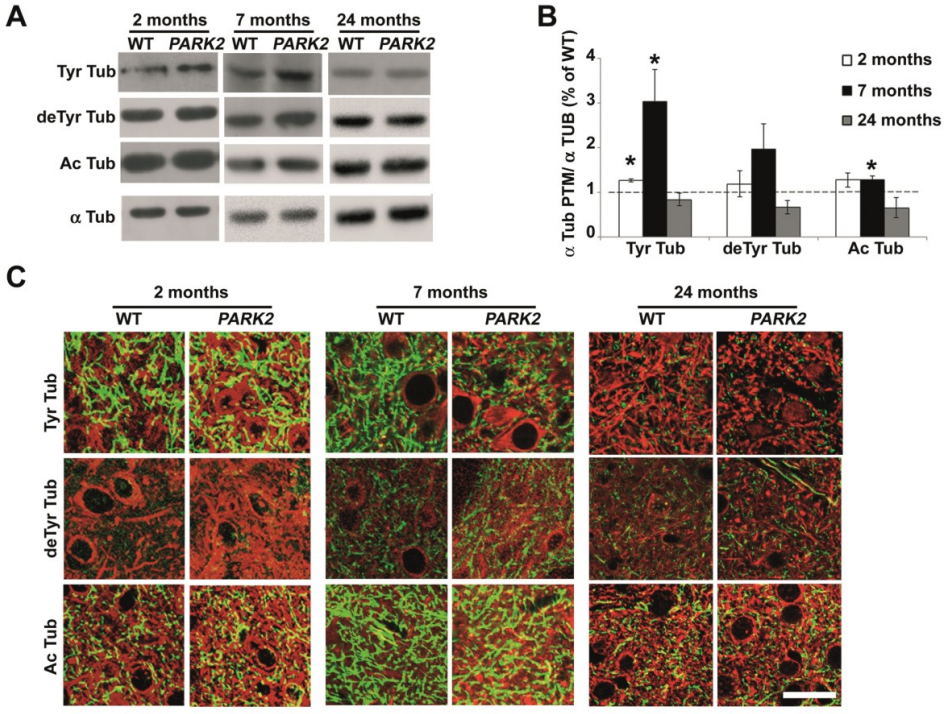


D

| | Tyr Tub | deTyr Tub | Ac Tub |
|---|---|---|---|
| WT, 2 months | 0.66±0.015 | 0.60±0.041 | 0.24±0.032 |
| *PARK2*, 2 months | 0.59±0.007 (*) | 0.84±0.075 (*) | 0.37±0.031 (*) |
| WT, 7 months | 0.61±0.178 | 0.30±0.047 | 0.38±0.049 |
| *PARK2*, 7 months | 0.63±0.171 | 0.65±0.111 (*) | 0.53±0.050 (*) |
| WT, 24 months | 0.39±0.046 | 0.40±0.032 | 0.49±0.041 |
| *PARK2*, 24 months | 0.18±0.014 (*) | 0.39±0.082 | 0.44±0.057 |

**FIGURE 3**

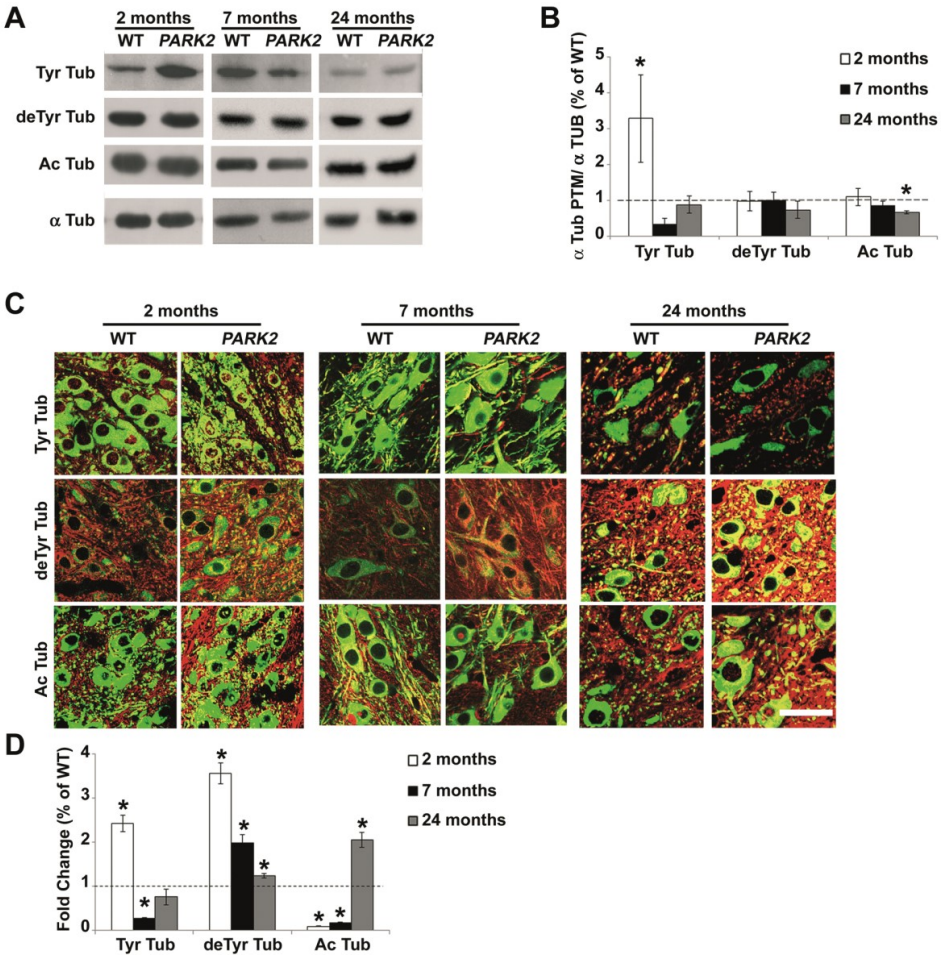
A
2 months
7 months
24 months
WT
PARK2
Tyr Tub
deTyr Tub
Ac Tub
α Tub
B
α Tub PTM/ α TUB (% of WT)
2 months
7 months
24 months
Tyr Tub
deTyr Tub
Ac Tub
C
D
Fold Change (% of WT)

**FIGURE 4**

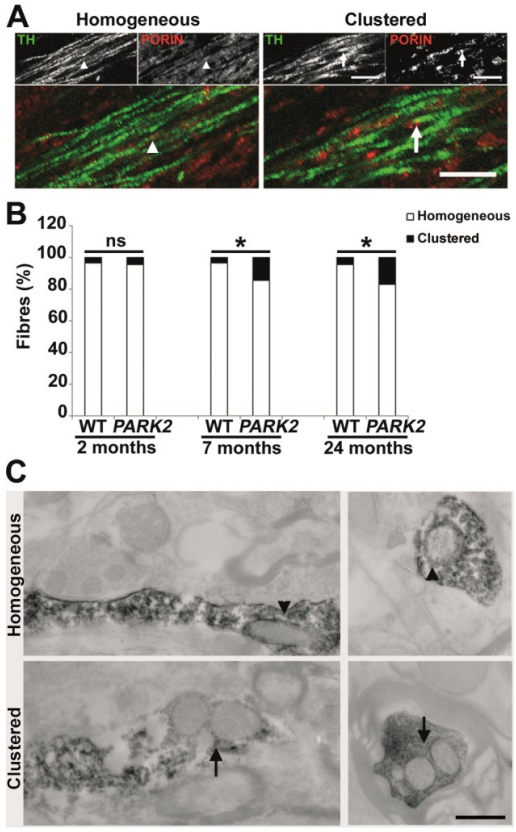
A
Homogeneous
Clustered
TH
PORIN
TH
PORIN
B
Homogeneous
Clustered
Fibres (%)
120
100
80
60
40
20
0
ns
*
*
WT PARK2
2 months
WT PARK2
7 months
WT PARK2
24 months
C
Homogeneous
Clustered

**FIGURE 5**

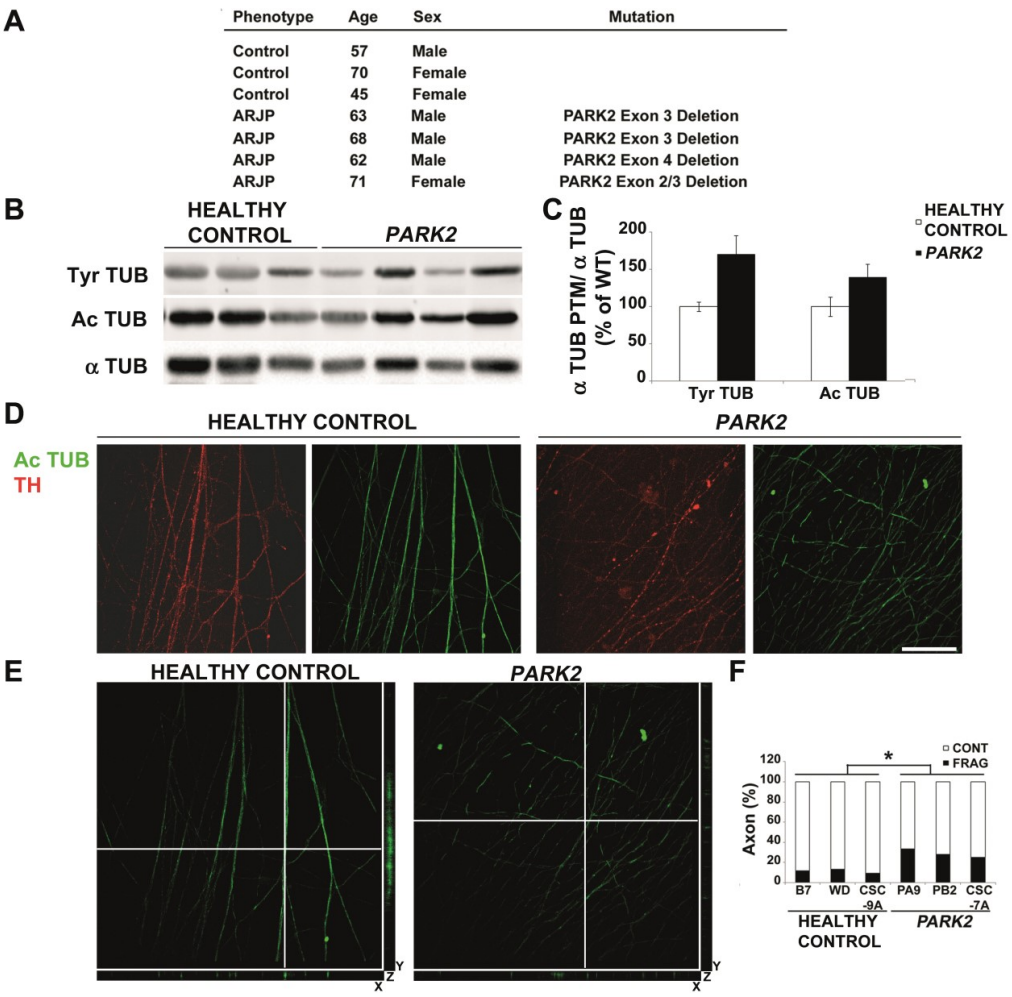
A
Phenotype Age Sex Mutation
Control 57 Male
Control 70 Female
Control 45 Female
ARJP 63 Male PARK2 Exon 3 Deletion
ARJP 68 Male PARK2 Exon 3 Deletion
ARJP 62 Male PARK2 Exon 4 Deletion
ARJP 71 Female PARK2 Exon 2/3 Deletion
B
HEALTHY CONTROL
PARK2
Tyr TUB
Ac TUB
α TUB
C
HEALTHY CONTROL
PARK2
α TUB PTM/ α TUB (% of WT)
200
150
100
50
0
Tyr TUB
Ac TUB
D
HEALTHY CONTROL
PARK2
Ac TUB
TH
E
HEALTHY CONTROL
PARK2
F
CONT
FRAG
Axon (%)
120
100
80
60
40
20
0
*
B7
WD
CSC -9A
PA9
PB2
CSC -7A
HEALTHY CONTROL
PARK2

**FIGURE S1**

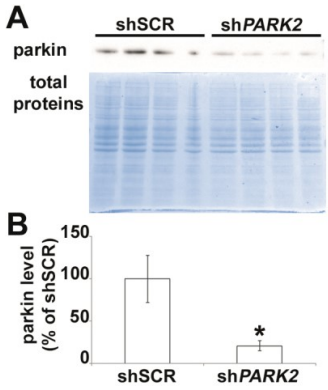
A
shSCR
shPARK2
parkin
total
proteins
B
parkin level
(% of shSCR)
150
100
50
0
*
shSCR
shPARK2

**FIGURE S2**

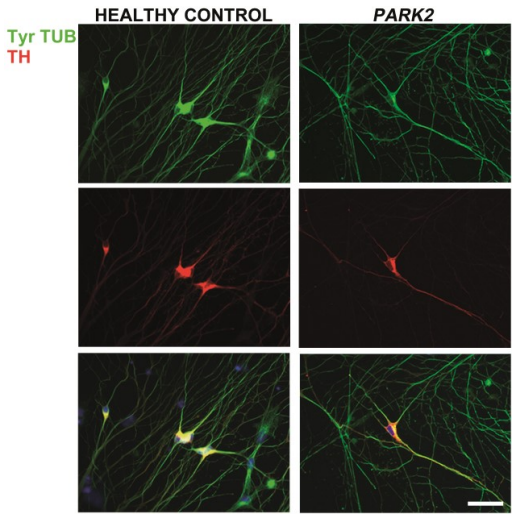

Published Review
Cappelletti et al., 2015

# Linking microtubules to Parkinson's disease: the case of parkin

**Graziella Cappelletti*[1], Francesca Casagrande*, Alessandra Calogero*, Carmelita De Gregorio*, Gianni Pezzoli† and Daniele Cartelli***

*Department of Biosciences, Università degli Studi di Milano, I-20133 Milano, Italy
†Parkinson Institute, Istituti Clinici di Perfezionamento, I-20125 Milano, Italy

## Abstract

**Microtubules (MTs) are dynamic polymers consisting of $\alpha/\beta$ tubulin dimers and playing a plethora of roles in eukaryotic cells. Looking at neurons, they are key determinants of neuronal polarity, axonal transport and synaptic plasticity. The concept that MT dysfunction can participate in, and perhaps lead to, Parkinson's disease (PD) progression has been suggested by studies using toxin-based and genetic experimental models of the disease. Here, we first learn lessons from MPTP and rotenone as well as from the PD related genes, including *SNCA* and *LRRK2*, and then look at old and new evidence regarding the interplay between parkin and MTs. Data from experimental models and human cells point out that parkin regulates MT stability and strengthen the link between MTs and PD paving the way to a viable strategy for the management of the disease.**

## Introduction

The molecular pathways implicated in neurodegenerative disorders are gradually being elucidated and several contributing factors have been identified. To date, aetiopathogenic mechanisms in Parkinson's disease (PD) converge on accumulation of aberrant or misfolded proteins, mitochondrial injury, and oxidative/nitrosative stress, making PD a multifactorial disease [1,2]. However, the primary degenerative events remain unclear, thus making it really hard to develop an efficient therapy for this devastating disorder.

PD is a progressive neurodegenerative disorder that is characterized by tremor, muscular rigidity and bradykinesia, with a prevalence of 2–5 % in the population aged 60 years, worldwide. PD can be defined in biochemical terms as a dopamine-deficiency state resulting from loss of dopamine neurons in the *substantia nigra pars compacta* accompanied by characteristic intraneuronal protein inclusions, termed Lewy bodies. On these grounds, starting in the 1950s, the strategy for treating PD has been to restore the dopamine concentrations in the brain by administering pharmacological treatment. However, thanks to a huge amount of clinical and basic research work, a redefinition of PD as a multiorgan disease has been proposed recently and novel therapeutic strategies are emerging [3].

In recent years, growing attention has been dedicated to neuronal cytoskeleton dysfunction and increasing evidence suggests a role for the microtubule (MT) system in the pathogenesis of neurodegenerative disorders. Mutations in tubulin, the major constituent of MTs, have been found to induce severe neurological disorders, such as peripheral neuropathy and loss of axons in many kinds of brain neurons [4] and, very recently, to be associated with familial amyotrophic lateral sclerosis [5]. Moreover, defects in the proper regulation of MT organization and stability are tightly linked to neuronal damages. Indeed, significant impairment in MT-associated proteins has been extensively reported in Alzheimer's disease, frontotemporal dementia and other tauopathies [6] and, notably, the failure in polyglutamilation of tubulin can dramatically lead to a rapid neuronal cell death in an ataxia mouse model [7]. Besides MT organization and stability, MT-dependent functions, such as overall axonal transport, are increasingly investigated in the field of neurodegeneration. The intracellular transport of organelles along an axon is a complex and crucial process for the maintenance and function of a neuron. Several different mechanisms including defects in the proper organization of MTs, mutations in MT-associated proteins and molecular motors, and activation of MT-targeting kinases act in concert and produce deficits in axonal transport underlying several neurodegenerative diseases, as extensively reviewed by Millecamps and Julien [8]. In addition, recent evidence suggests that axon degeneration underlying PD could depend mainly on the failure of axonal transport [9].

The question arises as to whether we can reasonably include MT dysfunction among the culprits triggering neurodegeneration in PD or not. Here, we bear in mind such a key question and move from a brief insight into the basis of MT functions in neurons to the evidence that MT dysfunction occurs in experimental parkinsonism and, finally, to the critical discussion on the interplay between parkin and MT system in cellular and animal models and in human tissues.

**Key words:** microtubules, microtubule stability, microtubule-dependent functions, neurodegeneration, parkin, Parkinson's disease.

**Abbreviations:** iPSC, induced-pluripotent stem cells; $MPP^+$, 1-methyl-4-phenylpyridinium; MPTP, *N*-methyl-4-phenyl-1,2,3,6-tetrahydropyridine; MT, microtubule; PD, Parkinson's disease.

[1]To whom correspondence should be addressed (email graziella.cappelletti@unimi.it).

## Microtubules and microtubule-dependent functions in neurons

MTs are non-covalent cytoskeletal filaments, which occur in all eukaryotic cell types from fungi to mammals. They consist of $\alpha/\beta$ tubulin heterodimers that assemble in a head-to-tail fashion into linear protofilaments whose lateral association forms polarized 25 nm wide hollow cylindrical polymers. MTs are heterogeneous in length and highly dynamic *in vivo* and *in vitro*, undergoing cycles of polymerization and rapid depolymerization. This 'dynamic instability' property was first described in 1984 [10] as a feature that is crucial to many MT functions. The tight regulation of their organization and dynamics depends on the incorporation of alternative tubulin isotypes, a highly complex and diverse set of MT-interacting proteins, and posttranslational modifications occurring on MTs [11].

MTs play several essential roles in cell shape acquisition and in the performance of many intracellular processes. Neurons are a striking example of cells in which MTs are essential to achieve a high degree of morphological and functional complexity. Neuronal MTs display different orientation and dynamics in axons and dendrites, and interact with specific associated proteins [12]. In addition, the incorporation of tubulin isotypes and posttranslational modifications of tubulin are selectively combined and distributed among different subcellular compartments, thus generating a tubulin code, that might regulate basic as well as higher-order neuronal functions. Highly dynamic MTs are enriched in tyrosinated tubulin and accumulate a set of factors known as MT plus-end tracking proteins; they are essential for rapid remodelling and reorganization in the growth cone underlying axonal elongation during neuronal differentiation [12] and synaptic plasticity in mature neurons [13]. On the contrary, a high stability is favoured for MT functions in the shaft of axons and for the preferential binding of MT-based motors transporting membrane-bound organelles and regulatory macromolecular complexes [12]. Neuronal MT stability is related to the accumulation of several posttranslational modifications of tubulin including acetylation, detyrosination, Δ2-tubulin, polyglutamylation and the very recently described polyamination [14], and to spatial gradient of tau [15].

Beyond their known conventional roles for supporting neuronal architecture, organelle transport and synaptic plasticity, a novel function as 'information carriers' has been attributed to neuronal MTs [16]. This amazing theory posits that both the short, stable and mobile MTs and the highly dynamic ends of longer MTs can act as information carriers in the neuron thanks to their ability to interact with a vast array of proteins. Short MTs, which appear to be unusually stable, move rapidly along axons and presumably in dendrites as well. It is reasonable to assume that they may convey information and signalling molecules with them. In addition, highly dynamic regions would act as scaffolds concentrating MT plus end tracking proteins, which, in turn, interact with many other proteins and structures contributing to the plasticity of the neuron, including kinases and small G proteins that impact the actin cytoskeleton and proteins that reside at the cell cortex [17].

## Microtubule dysfunction in experimental models of Parkinson's disease

The concept that MT dysfunctions can participate in, and perhaps lead to, PD progression has been suggested by studies on toxin-based and genetic experimental models of the disease.

Within the context of studies on PD-inducing neurotoxins, intriguing results have been reported with *N*-methyl-4-phenyl-1,2,3,6-tetrahydropyridine (MPTP), a neurotoxin widely used as a tool for studies on sporadic PD [1], and the herbicide rotenone. We showed that 1-methyl-4-phenylpyridinium ($MPP^+$), the toxic metabolite of MPTP, reduces MT polymerization and interferes with dynamic instability of MTs *in vitro* acting as a destabilizing factor [18]. Then, we confirmed and extended these results reporting that $MPP^+$ leads to MT alteration in neuronal cell and, in turn, to mitochondrial trafficking impairment [19]. Finally, we showed that systemic injection of MPTP to mice induces MT dysfunction that occurs very early, before axonal transport deficit, depletion of tyrosine hydroxylase and, ultimately, dopaminergic neuron degeneration [20]. Moving to the herbicide rotenone, old studies demonstrated its ability to induce MT depolymerization *in vitro* [21], whereas more recent data suggest that MT disruption may be an alternative mechanism underlying rotenone-induced dopamine neuron death in cellular models [22,23].

We can find further signs of MT involvement in PD looking at PD-linked genes. Interestingly, several independent GWAS and meta-analysis studies have shown a genome-wide significant association of single nucleotide polymorphisms in the gene coding for α-synuclein (*SNCA*) and the MT-associated protein tau [24]. α-Synuclein, the first protein associated to familial form of PD [25], interacts with tubulin with crucial consequences: the promotion of its aggregation in fibrils [26], the interference with tubulin assembly [27] and the recycling of monoamine transporter [28]. More recently, MT disruption has been reported in cells overexpressing α-synuclein [29] or following incubation with extracellular α-synuclein [30]. In addition, the kinase LRRK2 has been shown to interact with and to phosphorylate β-tubulin [31,32] and tubulin-associated tau, whereas a novel role of DJ-1 in the regulation of MT dynamics has been proposed [33].

Although these studies provide evidences that the MT cytoskeleton could be involved in neuronal damage caused by PD-related proteins or toxins, very little is known about MT dysfunction in patients. Using cybrid cell lines generated from idiopathic PD patients, Esteves et al. [34] showed significant alterations in MT integrity as compared with healthy subjects. Notably, we have recently analysed primary fibroblasts deriving from patients with idiopathic or genetic

PD and disclosed reduction in MT mass and significant changes in signalling pathways related to MT stability [35].

We believe that it is not a coincidence that tubulin and MTs represent a point of convergence in so many different PD experimental models, thus making the study of MT dysfunction a challenge leading to a better comprehension of PD pathogenesis.

## The interplay between parkin and microtubules

Exonic deletions in the *Parkin* gene were first reported in Japanese families with autosomal recessive juvenile-onset parkinsonism with onset frequently occurring before the age of 20 [36]. The *Parkin* gene encodes for a member of the E3 ligase family that catalyses the addition of ubiquitin to numerous target proteins [37]. The molecular understanding of the regulation of parkin E3 ligase activity is emerging [38]. However, it has been suggested that parkin, in addition to its ligase activity, has a number of other roles including the regulation of mitochondria dynamics and quality control designed to preserve mitochondria integrity [39]. Most of the supporting observations derive from mammalian cell lines overexpressing parkin, but endogenous parkin does not induce mitophagy in induced-pluripotent stem cell (iPSC)-derived human neurons [40]. This raises the issue of whether parkin involvement in this process is actually relevant in neurons or in PD pathogenesis [41]. Very recently, it has also been reported that parkin interacts with the kainate receptor GluK2 subunit and regulates the receptor function *in vitro* and *in vivo* [42].

Parkin interaction with tubulin and MTs has been proposed many years ago and remained largely neglected for a long time. Interestingly, parkin binds and increases the ubiquitination and degradation of both $\alpha$- and $\beta$-tubulin [43], whose complex folding reactions are prone to produce misfolded intermediates. In addition to its E3 ligase activity on tubulin, however, Yang et al. [44] proposed that parkin strongly binds tubulin/MTs through three redundant interaction domains resulting in MT stabilization. At the moment, we can simply speculate that the anchorage of parkin to MTs could provide an important environment for its E3 ligase activity on misfolded substrates that are usually transported on MTs themselves. Further work demonstrates that parkin protects midbrain dopaminergic neurons against PD-causing substances, as rotenone and colchicine, by stabilizing MTs [45]. This process seems to be mediated by the regulation of the MAP kinase pathway, which, interestingly, is a direct regulator of MT stability via the modulation of tubulin posttranslational modifications.

Bringing into focus the impact of parkin on MT-dependent functions, a reliable consequence of the alteration of MT stability could be the dysregulation of axonal transport. Indeed, previously, parkin has proved to regulate the trafficking of mitochondria in hippocampal neurons, especially when they are damaged and have to be degraded. This process was found to be dependent on the Miro phosphorylation [46].

Striking data coming from human cells have recently contributed to our understanding of the interplay between parkin and MTs strengthening interest in this aspect. We reported that PD-patient skin fibroblasts bearing *Parkin* mutations display reduced MT mass and imbalance in the pattern of tubulin posttranslational modifications, and that MT pharmacological stabilization or the overexpression of wild-type parkin rescue control phenotype [39]. This is not restricted to skin cells from patients but, interestingly, has been confirmed in iPSC-derived neurons. Ren et al. [47] found that the complexity of neuronal processes was greatly reduced in both dopaminergic and non-dopaminergic neurons from PD patients with parkin mutations and that MT stability was significantly decreased as demonstrated by the reduction in MT mass. Overexpression of parkin, but not its PD-linked mutants, restored the complexity of neuronal processes and MT mass. Notably, the MT depolymerizing agent colchicine mirrored the effect of parkin mutations by decreasing neurite complexity in control neurons while the MT stabilizing drug taxol mimicked the effect of parkin overexpression. These results strongly support the concept that the interaction of parkin with MTs in neurons may have an important physiological role. Thus, although the hypothesis of the interaction of parkin with MTs is supported mainly by studies in cellular models, it seems to be a promising theory, which provides a mechanistic explanation for the multiple intracellular functions and, possibly, dysfunctions of parkin. Indeed, we are currently undergoing the analyses of brain samples from *Parkin* knockout mice; our preliminary results have shown an early alteration of MT stability, thus confirming and expanding the importance of parkin in modulating the MT system.

## Concluding remarks

A growing body of evidence from experimental models and human cells indicates that parkin regulates MT stability and strengthens the link between MTs and PD. Indeed, the MT cytoskeleton represents a point of convergence in the action of various proteins mutated in PD and of PD-inducing neurotoxins, suggesting that it has a major role in the onset of the disease and providing the rationale for novel therapeutic interventions. Thus, MT stabilizing strategies may offer an opportunity for treating neurodegenerative diseases [48–50]. Importantly, we have recently demonstrated that this may be true also in PD showing that Epothilone D, a MT stabilizer drug, exerts neuroprotective effects in a toxin-based murine model of PD [20].

## Funding

This work was supported by the Fondazione Grigioni per il Morbo di Parkinson, Milan, Italy (2011–2015 grants to G.C.) and the 'Dote ricerca', FSE, Regione Lombardia (to D.C.).

## References


1 Dauer, W. and Przedborski, S. (2003) Parkinson's disease: mechanisms and models. Neuron **39**, 889–909 CrossRef PubMed
2 Obeso, J.A., Rodriguez-Oroz, M.C., Goetz, C.G., Marin, C., Kordower, J.H., Rodriguez, M., Hirsch, E.C., Farrer, M., Schapira, A.H.V. and Halliday, G. (2010) Missing pieces in the Parkinson's disease puzzle. Nat. Med. **16**, 653–661 CrossRef PubMed
3 Shapira, A.H.V., Olanow, C.W., Greenamyer, J.T. and Bezard, E. (2014) Slowing of neurodegeneration in Parkinson's disease and Huntington's disease: future therapeutic perspectives. Lancet **384**, 545–555 CrossRef PubMed
4 Tischfield, M.A., Baris, H.N., Wu, C., Rudolph, G., Van Maldergem, L., He, W., Chan, W.M., Andrews, C., Demer, J.L., Robertson, R.L. et al. (2010) Human TUBB3 mutations perturb microtubule dynamics, kinesin interactions, and axon guidance. Cell **140**, 74–87 CrossRef PubMed
5 Smith, B.N., Ticozzi, N., Fallini, C., Gkazi, A.S., Topp, S., Kenna, K.P., Scotter, E.L., Kost, J., Keagle, P., Miller, J.W. et al. (2014) Exome-wide rare variant analysis identifies TUBA4A mutations associated with familial ALS. Neuron **84**, 324–331 CrossRef PubMed
6 Spillantini, M.G. and Goedert, M. (2013) Tau pathology and neurodegeneration. Lancet Neurol **12**, 609–622 CrossRef PubMed
7 Rogowski, K., Van Dijk, J., Magiera, M.M., Bosc, C., Deloulme, J.C., Bosson, A., Peris, L., Gold, N.D., Lacroix, B., Bosch Grau, M. et al. (2010) A family of protein-deglutamylating enzymes associated with neurodegeneration. Cell **143**, 564–578 CrossRef PubMed
8 Millecamps, S. and Julien, J-P. (2013) Axonal transport deficits and neurodegenerative diseases. Nat. Rev. Neurosci. **14**, 161–176 CrossRef PubMed
9 Burke, R.E. and O'Malley, K. (2013) Axon degeneration in Parkinson's disease. Exp. Neurol. **246**, 72–83 CrossRef PubMed
10 Mitchison, T. and Kirschner, M. (1984) Dynamic instability of microtubules growth. Nature **312**, 237–242 CrossRef PubMed
11 Janke, C. and Bulinski, J.C. (2011) Post-translational regulation of the microtubule cytoskeleton: mechanisms and functions. Nat. Rev. Mol. Cell Biol. **12**, 773–786 CrossRef PubMed
12 Conde, C. and Cáceres, A. (2009) Microtubule assembly, organization and dynamics in axons and dendrites. Nat. Rev. Neurosci. **10**, 319–332 CrossRef PubMed
13 Jaworski, J., Kapitein, L.C., Montenegro Gouveia, S., Dortland, B.R., Wulf, P.S., Grigoriev, I., Camera, P., Spangler, S.A., Di Stefano, P., Demmers, J. et al. (2009) Dynamic microtubules regulate dendritic spine morphology and synaptic plasticity. Neuron **61**, 85–100 CrossRef PubMed
14 Song, Y., Kirkpastrick, L.L., Schilling, A.B., Helseth, D.L., Chabot, N., Keillor, J.W., Johnson, G.V.W. and Brady, S.T. (2013) Transglutaminase and polyamination of tubulin: posttranslational modification for stabilizing axonal microtubules. Neuron **78**, 109–123 CrossRef PubMed
15 Scholz, T. and Mandelkow, E. (2014) Transport and diffusion of Tau protein in neurons. Cell Mol. Life Sci. **71**, 3139–3159 CrossRef PubMed
16 Dent, E.W. and Baas, P.W. (2014) Microtubules in neurons as information carriers. J. Neurochem. **129**, 235–239 CrossRef PubMed
17 Akhmanova, A., Stehbens, S.J. and Yap, A.S. (2009) Touch, grasp, deliver and control: functional cross-talk between microtubules and cell adhesions. Traffic (Copenhagen, Denmark) **10**, 268–274 CrossRef PubMed
18 Cappelletti, G., Surrey, T. and Maci, R. (2005) The parkinsonism producing neurotoxin MPP+ affects microtubule dynamics by acting as a destabilising factor. FEBS Lett. **579**, 4781–4786 CrossRef PubMed
19 Cartelli, D., Ronchi, C., Maggioni, M.G., Rodighiero, S., Giavini, E. and Cappelletti, G. (2010) Microtubule dysfunction precedes transport impairment and mitochondria damage in $MPP^+$-induced neurodegeneration. J. Neurochem. **115**, 247–258 CrossRef PubMed
20 Cartelli, D., Casagrande, F., Busceti, C.L., Bucci, D., Molinaro, G., Traficante, A., Passarella, D., Giavini, E., Pezzoli, G., Battaglia, G. and Cappelletti, G. (2013) Microtubule alterations occur early in experimental parkinsonism and the microtubule stabilizer epothilone D is neuroprotective. Sci. Rep. **3**, 1837 CrossRef PubMed
21 Marshall, L.E. and Himes, R.H. (1978) Rotenone inhibition of tubulin self-assembly. Biochim. Biophys. Acta **543**, 590–594 CrossRef PubMed
22 Ren, Y., Liu, W., Jiang, Q. and Feng, J. (2005) Selectively vulnerability of dopaminergic neurons to microtubule depolymerization. J. Biol. Chem. **280**, 34105–34112 CrossRef PubMed
23 Choi, W.S., Palmiter, R.D. and Xia, Z. (2011) Loss of mitochondrial complex I activity potentiates dopamine neuron death induced by microtubule dysfunction in a Parkinson's disease model. J. Cell Biol. **192**, 873–882 CrossRef PubMed
24 Nalls, M.A., Plagnol, V., Hernandez, D.G., Sharma, M., Sheerin, U.M., Saad, M., Simon-Sanchez, J., Schulte, C., Lesage, S., Sveinbjornsdottir, S. et al. (2011) Imputation of sequence variants for identification of genetic risks for Parkinson's disease: a meta-analysis of genome-wide association studies. Lancet **377**, 641–649 CrossRef PubMed
25 Polymeropoulos, M.H., Lavedan, C., Leroy, E., Ide, S.E., Dehejia, A., Dutra, A., Pike, B., Root, H., Rubenstein, J., Boyer, R. et al. (1997) Mutation in the alpha-synuclein gene identified in families with Parkinson's disease. Science **276**, 2045–2047 CrossRef PubMed
26 Alim, M.A., Hossain, M.S., Arima, K., Takeda, K., Izumiyama, Y., Nakamura, M., Kaji, H., Shinoda, T., Hisanaga, S. and Ueda, K. (2002) Tubulin seeds alpha-synuclein fibril formation. J. Biol. Chem. **277**, 2112–2117 CrossRef PubMed
27 Alim, M.A., Ma, Q.L., Takeda, K., Aizawa, T., Matsubara, M., Nakamura, M., Asada, A., Saito, T., Kaji, H., Yoshii, M. et al. (2004) Demonstration of a role for alpha-synuclein as a functional microtubule-associated protein. J. Alzheimers Dis. **6**, 435–442 PubMed
28 Jeannotte, A.M. and Sidhu, A. (2007) Regulation of the norepinephrine transporter by alpha-synuclein-mediated interactions with microtubules. Eur. J. Neurosci. **26**, 1509–1520 CrossRef PubMed
29 Prots, I., Veber, V., Brey, S., Campioni, S., Buder, K., Riek, R., Bohm, K.J. and Winner, B. (2013) $\alpha$-Synuclein oligomers impair neuronal microtubule-kinesin interplay. J. Biol. Chem. **288**, 21742–21754 CrossRef PubMed
30 Gassowska, M., Czapski, G.A., Pajak, B., Cieślik, M., Lenkiewicz, A.M. and Adamczyk, A. (2014) Extracellular $\alpha$-synuclein leads to microtubule destabilization via GSK-3$\beta$-dependent Tau phosphorylation in PC12 cells. PLoS One **9**, e94259 CrossRef PubMed
31 Gillardon, F. (2009) Leucine-rich repeat kinase 2 phosphorylates brain tubulin-beta isoform and modulates microtubule stability: a point of convergence in parkinsonian neurodegeneration? J. Neurochem. **110**, 1514–1522 CrossRef PubMed
32 Law, B.M., Spain, V.A., Leinster, V.H., Chia, R., Beilina, A., Cho, H.J., Taymans, J.M., Urban, M.K., Sancho, R.M., Blanca Ramírez, M. et al. (2014) A direct interaction between leucine-rich repeat kinase 2 and specific $\beta$-tubulin isoforms regulates tubulin acetylation. J. Biol. Chem. **289**, 895–908 CrossRef PubMed
33 Sheng, C., Heng, X., Zhang, G., Xiong, R., Li, H., Zheng, S. and Chen, S. (2013) DJ-1 deficiency perturbs microtubule dynamics and impairs striatal neurite outgrowth. Neurobiol. Aging **34**, 489–498 CrossRef PubMed
34 Esteves, A.R., Arduino, D.M., Swerdlow, R.H., Oliveira, C.R. and Cardoso, S.M. (2010) Microtubule depolymerisation potentiates alpha-synuclein oligomerization. Front. Aging Neurosci. **1**, 5 CrossRef PubMed
35 Cartelli, D., Goldwurm, S., Casagrande, F., Pezzoli, G. and Cappelletti, G. (2012) Microtubule destabilization is shared by genetic and idiopathic Parkinson's disease patient fibroblasts. PLoS One **7**, e37467 CrossRef PubMed
36 Kitada, T., Asakawa, S., Hattori, N., Matsumine, H., Yamamura, Y., Minoshima, S., Yokochi, M., Mizuno, Y. and Shimizu, N. (1998) Mutations in the parkin gene cause autosomal recessive juvenile parkinsonism. Nature **392**, 605–608 CrossRef PubMed
37 Shimura, H., Hattori, N., Kubo, S., Mizuno, Y., Asakawa, S., Minoshima, S., Shimizu, N., Iwai, K., Chiba, T., Tanaka, K. and Suzuki, T. (2000) Familial Parkinson's disease gene product parkin, is a ubiquitin-protein ligase. Nat. Genet. **2**, 302–305
38 Walden, H. and Martinez-Torres, R.J. (2012) Regulation of Parkin E3 ligase activity. Cell. Mol. Life Sci. **69**, 3053–3067 CrossRef PubMed
39 Scarffe, L.A., Stevens, D.A., Dawson, V.L. and Dawson, T.M. (2014) Parkin and PINK1: much more than mitophagy. Trends Neurosci. **37**, 315–324 CrossRef PubMed
40 Rakovic, A., Shurkewitsch, K., Seibler, P., Grunewald, A., Zanon, A., Hagenah, J., Krainc, D. and Klein, C. (2013) PTEN-induced putative kinase 1 (PINK1)-dependent ubiquitination of endogenous Parkin attenuates mitophagy: study in human primary fibroblasts and induced pluripotent stem (iPS) cell-derived neurons. J. Biol. Chem. **288**, 2223–2237 CrossRef PubMed
41 Grenier, K., McLelland, G.L. and Fon, E.A. (2013) Parkin- and PINK1-dependent mitophagy in neurons: will the real pathway please stand up? Front. Neurol. **4**, 100 CrossRef PubMed
42 Maraschi, A.M., Ciammola, A., Folci, A., Sassone, F., Ronzitti, G., Cappelletti, G., Silani, V., Sato, S., Hattori, N., Mazzanti, M. et al. (2014) Parkin regulates kainate receptors by interacting with the GluK2 subunit. Nat. Commun. **5**, 5182 CrossRef PubMed
43 Ren, Y., Zhao, J. and Feng, J. (2003) Parkin binds to $\alpha/\beta$ tubulin and increases their ubiquitination and degradation. J. Neurosci. **23**, 3316–3324 PubMed

44 Yang, F., Jiang, Q., Zhao, J., Ren, Y., Sutton, M.D. and Feng, J. (2005) Parkin stabilizes microtubules through strong binding mediated by three independent domains. J. Biol. Chem. **280**, 17154–17162 CrossRef PubMed
45 Ren, Y., Jiang, H., Yang, F., Nakaso, K. and Feng, J. (2009) Parkin protects dopaminergic neurons against microtubule-depolymerizing toxins by attenuating microtubule-associated protein kinase activation. J. Biol. Chem. **284**, 4009–4017 CrossRef PubMed
46 Wang, X., Winter, D., Ashrafi, G., Schlehem, J., Wong, Y.L., Selkoe, D., Rice, S., Steen, J., LaVoie, M.J. and Schwarz, T.L. (2011) PINK1 and Parkin target Miro for phosphorylation and degradation to arrest mitochondrial motility. Cell **147**, 893–906 CrossRef PubMed
47 Ren, Y., Jiang, H., Hu, Z., Fan, K., Wan, J., Janoschka, S., Wang, X., Ge, S. and Feng, J. (2015) Parkin mutations reduce the complexity of neuronal processes in iPSC derived human neurons. Stem Cells **33**, 68–78 CrossRef PubMed
48 Gozes, I. (2011) Microtubules (tau) as an emerging therapeutic target: NAP (davunetide). Curr. Pharm. Des. **17**, 3413–3417 CrossRef PubMed
49 Baas, P.W. and Ahmad, F.J. (2013) Beyond taxol: microtubule-based treatment of disease and injury of the nervous system. Brain **136**, 2937–2951 CrossRef PubMed
50 Brunden, K.R., Trojanowski, J.Q., Smith, III, A.B., Lee, V.M.-Y. and Ballatore, C. (2014) Microtubule-stabilizing agents as potential therapeutics for neurodegenerative disease. Bioorg. Med. Chem. **22**, 5040–5049 CrossRef PubMed

Received 13 January 2015
doi:10.1042/BST20150007

# PART III

# *Contents*

Manuscript in preparation
Casagrande et al.

# *PARK2* HAPLOINSUFFICIENCY AFFECTS MICROTUBULE STABILITY IN MICE

Francesca Casagrande[1], Daniele Cartelli[1], Alida Amadeo[1], Alessandra M. Calogero[1], Carmelita De Gregorio[1], Debora Modena[1], Michela Signo[1], Gianni Pezzoli[2] and Graziella Cappelletti[1].

[1]Department of Biosciences, Università degli Studi di Milano, Milano, Italy
[2]Istituti Clinici di Perfezionamento, Parkinson Institute, Milano, Italy

## ABSTRACT

Currently, just symptomatic treatments are available for Parkinson's disease (PD), since the molecular mechanisms underlying the loss of dopaminergic cells in the *Substantia nigra* are not yet solved. Recently, the involvement of microtubule (MT) system has been clearly proved in many neurodegenerative diseases, so our goal is to understand if the MT dysfunction could be a primary cause in PD neurodegeneration. Mutations in a number of genes have been associated with familial PD and, among them, *PARK2* encodes for parkin, an E3 ubiquitin ligase that is also able to bind and stabilize MTs. Here, we investigate if *PARK2* haploinsufficiency could make aged mice differently susceptible to *Substantia nigra* damage and motor impairment and if this could be dependent on their MT system.

On this purpose, we have studied in deep the levels and the organization of cytoskeletal proteins in wt and *PARK2* heterozygous C57BL/6 sex-matched aged mice (15 months old). In particular, we focused on MT stability through the analysis of different post-translational modified forms of α-tubulin that are associated to MTs with different stability. The results highlighted a significant increase in the levels of dynamic pool of MTs in the two regions of interest, the *Substantia nigra* and *Corpus striatum*, in the heterozygous mice, with both immunoblotting and confocal microscopy approaches. Moreover, the stereological count of the number of dopaminergic neurons in the *Substantia nigra* and the quantification of dopaminergic terminals in the *Corpus striatum* have been performed. Finally, we have evaluated also the motor behaviour of these mice using a video-tracking system and, surprisingly, we found the heterozygous mice being significantly more active than wt ones.

Our data show that *PARK2* haploinsufficiency impacts MT system *in vivo* leading to a more dynamic MT cytoskeleton, and suggest a key role for MT stability in the dopaminergic neurons' survival and functionality.

**LEGENDS**

**Figure 1. 2,5-HD and *PARK2* haploinsufficiency do not impact level and distribution of cytoskeletal proteins in the *Corpus striatum*.** (A) Representative western blot and densitometric analysis of actin (42 kDa), NF-L (70 kDa), NF-M (160 kDa) and α-tubulin (α-Tub, 50 kDa) on striatal protein extracts of wt and *PARK2*$^{+/-}$ 15 months old mice treated with i.p. injection of 2,5-HD (8 mmol/kg) or saline for 19 days. The number of mice in the experimental groups was the following: wt saline (n = 3), wt 2,5-HD (n = 1), PARK2+/- saline (n = 7), PARK2+/- 2,5-HD (n = 5). All the values are expressed as mean ± SEM. No significative differences among the groups were observed. (B) Scheme of a sagittal section with the *Corpus striatum* shown in green. (C) Representative confocal images of dopaminergic fibers in sagittal sections of *Corpus striatum* of wt and *PARK2*$^{+/-}$ 15 months old mice treated with i.p. injection of 2,5-HD (8 mmol/kg) or saline for 19 days. Green represents tyrosine hydroxylase (TH) staining and red signals the NF proteins, in particular NF-L is shown. Scale bar, 20 μm.

**Figure 2. *PARK2* haploinsufficiency increases tyrosinated tubulin in the *Corpus striatum*.** (A) Representative western blot and densitometric analyses of tyrosinated (Tyr Tub), detyrosinated (deTyr Tub), acetylated (Ac Tub) and Δ2 (Δ2 Tub) tubulin on striatal protein extracts of wt and *PARK2*$^{+/-}$ 15 months old mice treated with i.p. injection of 2,5-HD (8 mmol/kg) or saline for 19 days. The number of mice in the experimental groups was the following: wt saline (n = 3), wt 2,5-HD (n = 1), *PARK2*$^{+/-}$ saline (n = 7), *PARK2*$^{+/-}$ 2,5-HD (n = 5). The level of tubulin PTMs were normalized on the level of total α-tubulin (α-Tub) in the respective sample and are expressed as the ratio α-tubulin PTM/α-tubulin (mean ± SEM). *$p<0.05$ vs wt saline group according to ANOVA, Fisher *post hoc* test; #$p<0.01$ vs *PARK2*$^{+/-}$ saline group according to ANOVA, Fisher *post hoc* test. (B) Scheme of a sagittal section with the *Corpus striatum* showed in green. (C) Representative confocal images of dopaminergic fibers in sagittal sections of *Corpus striatum* of wt and *PARK2*$^{+/-}$ 15 months old mice treated with i.p. injection of 2,5-HD (8 mmol/kg) or saline for 19 days. Green represents tyrosine hydroxylase (TH) staining and red signals the α-tubulin post-translational modifications (PTMs), in particular tyrosinated (Tyr Tub) and detyrosinated (deTyr Tub) are shown. Scale bar, 20 μm.

**Figure 3. 2,5-HD does not cause the loss of dopaminergic fibers in the *Corpus striatum*.** (A) Densitometric analyses of TH-positive fibers in total, dorsal and dorso-lateral *Corpus striatum* of wt and *PARK2*$^{+/-}$ 15 months old mice treated with i.p. injection of 2,5-HD (8 mmol/kg) or saline for 19 days, were performed with ImageJ software. The number of mice in the experimental groups was the following: wt saline (n = 6), wt 2,5-HD (n = 6), PARK2+/- saline (n = 7), PARK2+/- 2,5-HD (n = 4). All the values are expressed as mean ± SEM. No significative differences among the groups were observed. (B) Overview of representative micrographs of the *Corpus striatum* used for quantitative immunohistochemical analysis.

**Figure 4. 2,5-HD and *PARK2* haploinsufficiency do not impact level and distribution of cytoskeletal proteins in the dopaminergic neurons of ventral mesencephalon.** (A) Representative western blot and densitometric analysis of actin (42 kDa), NF-L (70 kDa), NF-M (160 kDa) and α-tubulin (α-Tub, 50 kDa) on ventral mesencephalon protein extracts of wt and *PARK2*$^{+/-}$ 15 months old mice treated with i.p. injection of 2,5-HD (8 mmol/kg) or saline for 19 days. The number of mice in the experimental groups was the following: wt saline (n = 3), wt 2,5-HD (n = 1), PARK2+/- saline (n = 7), PARK2+/- 2,5-HD (n = 5). All the values are expressed as mean ± SEM. No significative differences among the groups were observed. (B) Scheme of a sagittal section with the *Substantia nigra pars compacta* shown in green. (C) Representative confocal images of dopaminergic neurons in sagittal sections of *Substantia nigra* of wt and *PARK2*$^{+/-}$ 15 months old mice treated with i.p. injection of 2,5-HD (8 mmol/kg) or saline for 19 days. Green represents tyrosine hydroxylase (TH) staining and red signals the NF proteins, in particular NF-L is shown. Scale bar, 20 μm.

**Figure 5. Parkin haploinsufficiency affects tyrosinated tubulin levels in the dopaminergic neurons of ventral mesencephalon.** (A) Representative western blot and densitometric analyses of tyrosinated (Tyr Tub), detyrosinated (deTyr Tub), acetylated (Ac Tub) and Δ2 (Δ2 Tub) tubulin on ventral mesencephalon protein extracts of wt and *PARK2*$^{+/-}$ 15 months old mice treated with i.p. injection of 2,5-HD (8 mmol/kg) or saline for 19 days. The number of mice in the experimental groups was the following: wt saline (n = 3), wt 2,5-HD (n = 1), *PARK2*$^{+/-}$ saline (n = 7), *PARK2*$^{+/-}$ 2,5-HD (n = 5). The level of tubulin PTMs were normalized on the level of total α-tubulin (α-Tub) in the respective sample and are expressed as the ratio α-tubulin PTM/α-tubulin (mean ± SEM). *$p<0.05$ vs wt saline group according to ANOVA, Fisher *post hoc* test; #$p<0.05$ vs *PARK2*$^{+/-}$ saline group according to ANOVA, Fisher *post hoc* test. (B) Scheme of a sagittal section with the *Substantia nigra pars*

*compacta* shown in green. (C) Representative confocal images of dopaminergic neurons in sagittal sections of *Substantia nigra* of wt and *PARK2*$^{+/-}$ 15 months old mice treated with i.p. injection of 2,5-HD (8 mmol/kg) or saline for 19 days. Green represents tyrosine hydroxylase (TH) staining and red signals the α-tubulin post-translational modifications (PTMs), in particular tyrosinated (Tyr Tub) and detyrosinated (deTyr Tub) are shown. Scale bar, 20 μm.

**Figure 6. Heterozygous mice present an increased level of tyrosinated tubulin in sections of *Substantia nigra pars compacta*.** Quantification of fluorescence intensity with ImageJ software of tyrosinated (Tyr Tub) (A-B) and detyrosinated (deTyr Tub) (C-D) tubulin inside dopaminergic neurons in the *Substantia nigra pars compacta* in sagittal section of wt and *PARK2*$^{+/-}$ 15 months old mice treated with i.p. injection of 2,5-HD (8 mmol/kg) or saline for 19 days. The same sections stained for TH (green signal) and different forms of tubulin (red signal), shown in the figure 5C, were used for the analysis. Data are expressed as grey levels in box plot graphs (A-C, upper), while the tables (B-D, lower) report the number of animals, sections and cells counted during the analyses. ***$p<0.001$ vs wt saline or PARK2+/- saline group according to ANOVA, Tukey *post hoc* test.

**Figure 7. 2,5-HD does not induce the dopaminergic neuron death in the *Substantia nigra pars compacta*.** (A) Overviews of five caudo-rostral levels through the *Substantia nigra pars compacta* (SNpc) used for quantitative immunohistochemical analysis. Representative photomicrographs were taken under a 4x objective from the SNpc of wt (right) and *PARK2*$^{+/-}$ (left) mice treated with saline. (B) Stereological counts of TH-positive cells were performed with the StereoInvestigator software in the SNpc of wt and *PARK2*$^{+/-}$ 15 months old mice treated with i.p. injection of 2,5-HD (8 mmol/kg) or saline for 19 days. Values represent the mean ± SEM of seven sections per animal throughout the SNpc and are expressed as the total number of SN dopaminergic neurons in both hemispheres. The number of mice in the experimental groups was the following: wt saline (n = 8), wt 2,5-HD (n = 5), PARK2+/- saline (n = 8), PARK2+/- 2,5-HD (n = 6).

**Figure 8. Heterozygous mice are more active than wt ones and 2,5-HD causes motor impairment.** The motor behaviour of wt and *PARK2*$^{+/-}$ 15 months old mice, treated with i.p. injection of 2,5-HD (8 mmol/kg) or saline for 19 days, has been monitored with a video-tracking system once a week for 3 weeks. Each mouse was freely to move spontaneously for 1 hour within an open-field cage during the video-tracking sessions. The resulting movies

were analysed for (A) the total distance travelled, (B) the average speed and (C) the total time the mice were immobile in the cage. Data are expressed as mean ± SEM. The heterozygous group of mice resulted more active at each time point, nonetheless the 2,5-HD treatment that caused anyway a motor impairment in all the groups. Surprisingly, the wt mice resulted more susceptible to the toxin.

**FIGURE 1**

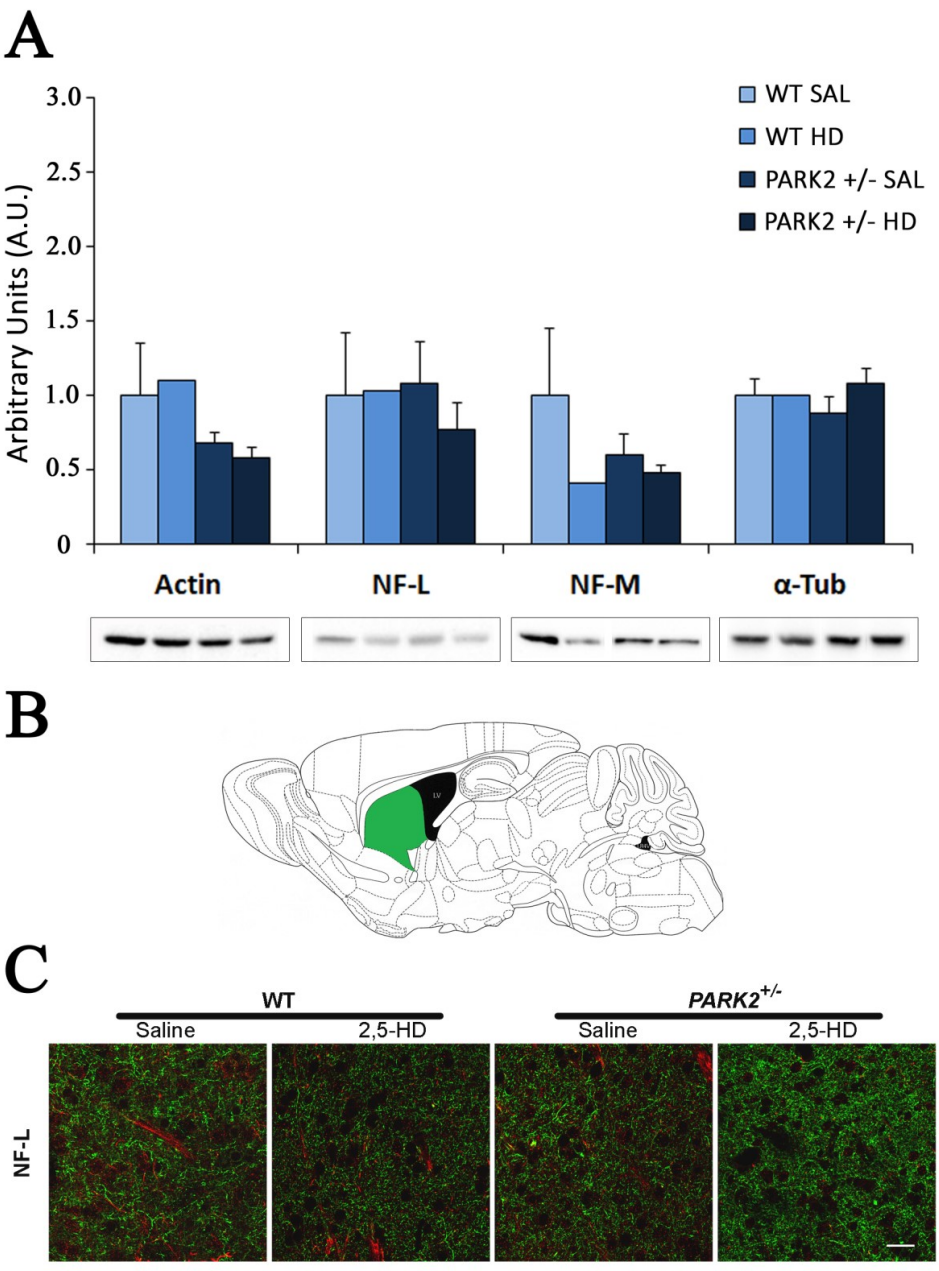
A
3.0
2.5
2.0
1.5
1.0
0.5
0
Arbitrary Units (A.U.)
WT SAL
WT HD
PARK2 +/- SAL
PARK2 +/- HD
Actin
NF-L
NF-M
α-Tub
B
C
WT
PARK2+/-
Saline
2,5-HD
Saline
2,5-HD
NF-L

**FIGURE 2**

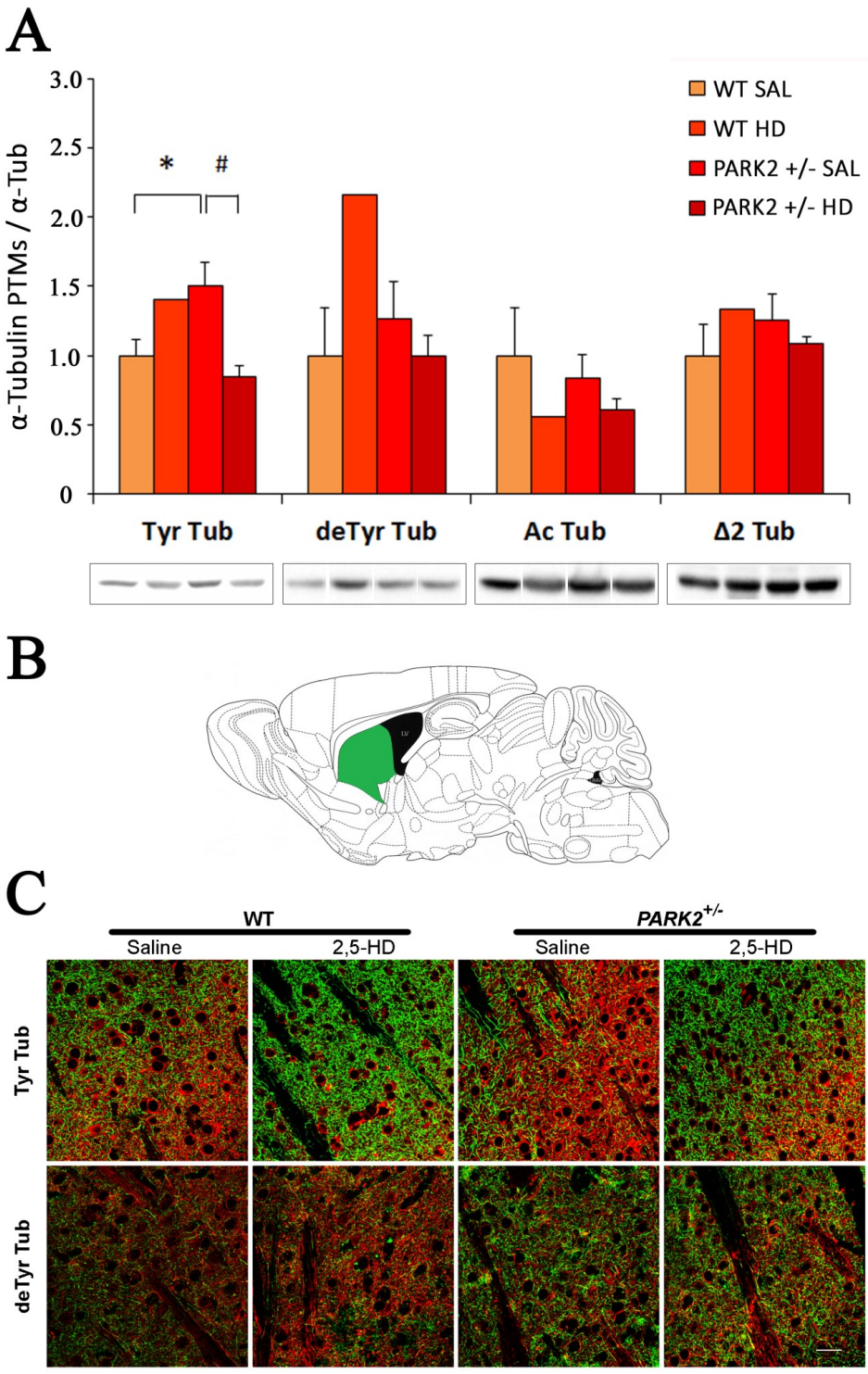
A
α-Tubulin PTMs / α-Tub
3.0
2.5
2.0
1.5
1.0
0.5
0
*
#
WT SAL
WT HD
PARK2 +/- SAL
PARK2 +/- HD
Tyr Tub
deTyr Tub
Ac Tub
Δ2 Tub
B
LV
C
WT
PARK2+/-
Saline
2,5-HD
Saline
2,5-HD
Tyr Tub
deTyr Tub

**FIGURE 3**

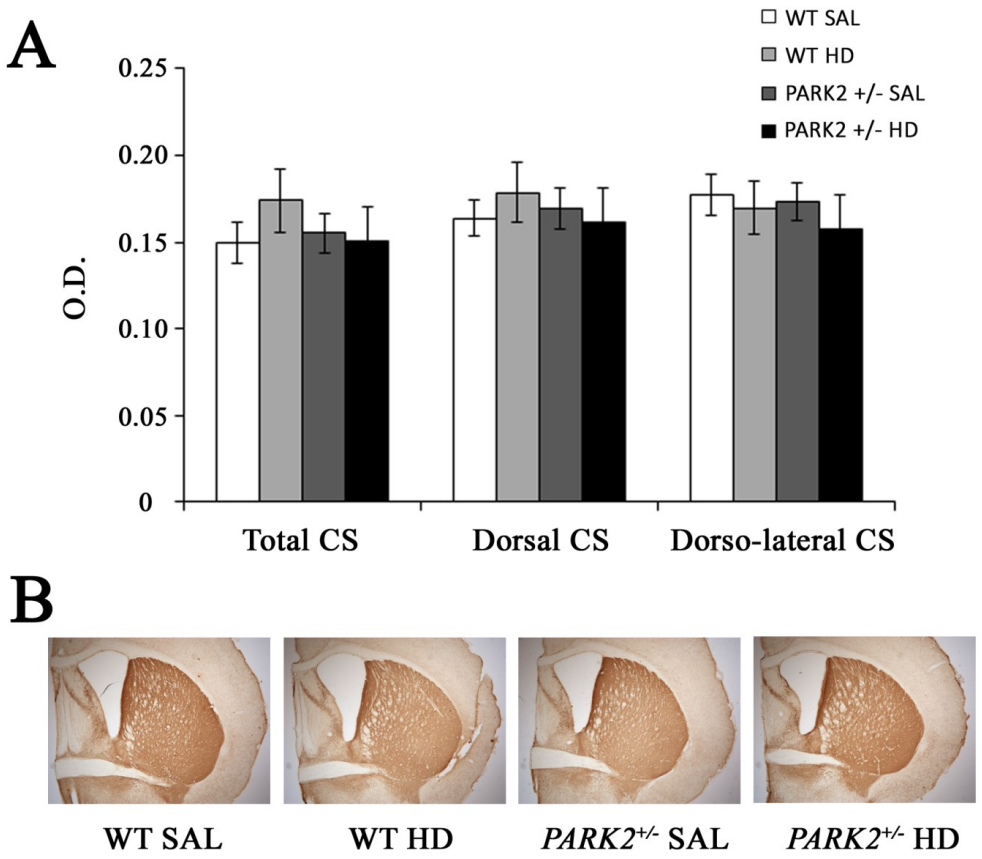
A
WT SAL
WT HD
PARK2 +/- SAL
PARK2 +/- HD
O.D.
0.25
0.20
0.15
0.10
0.05
0
Total CS
Dorsal CS
Dorso-lateral CS
B
WT SAL
WT HD
PARK2+/- SAL
PARK2+/- HD

**FIGURE 4**

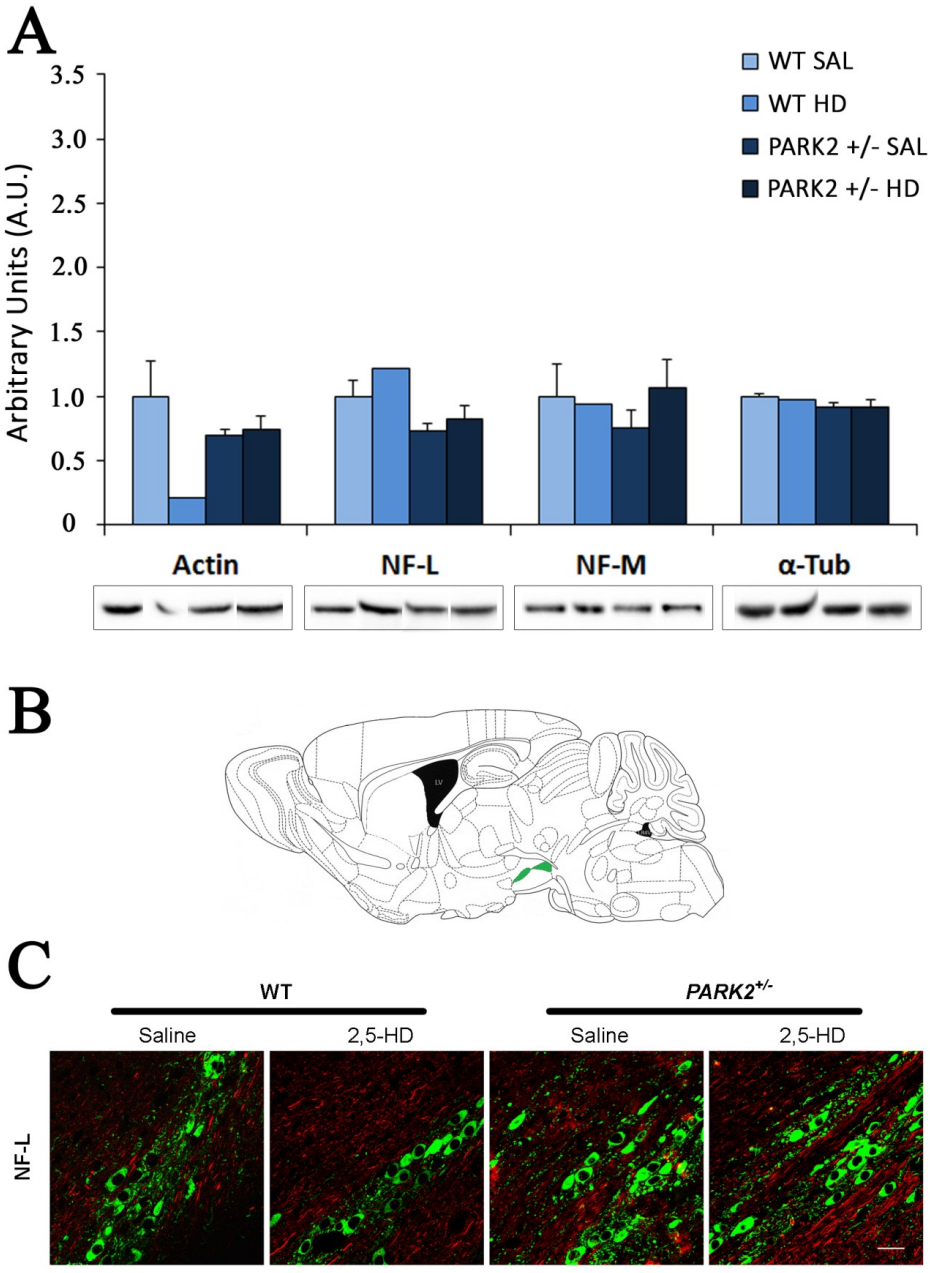
A
WT SAL
WT HD
PARK2 +/- SAL
PARK2 +/- HD
Arbitrary Units (A.U.)
3.5
3.0
2.5
2.0
1.5
1.0
0.5
0
Actin
NF-L
NF-M
α-Tub
B
LV
C
WT
PARK2+/-
Saline
2,5-HD
Saline
2,5-HD
NF-L

**FIGURE 5**

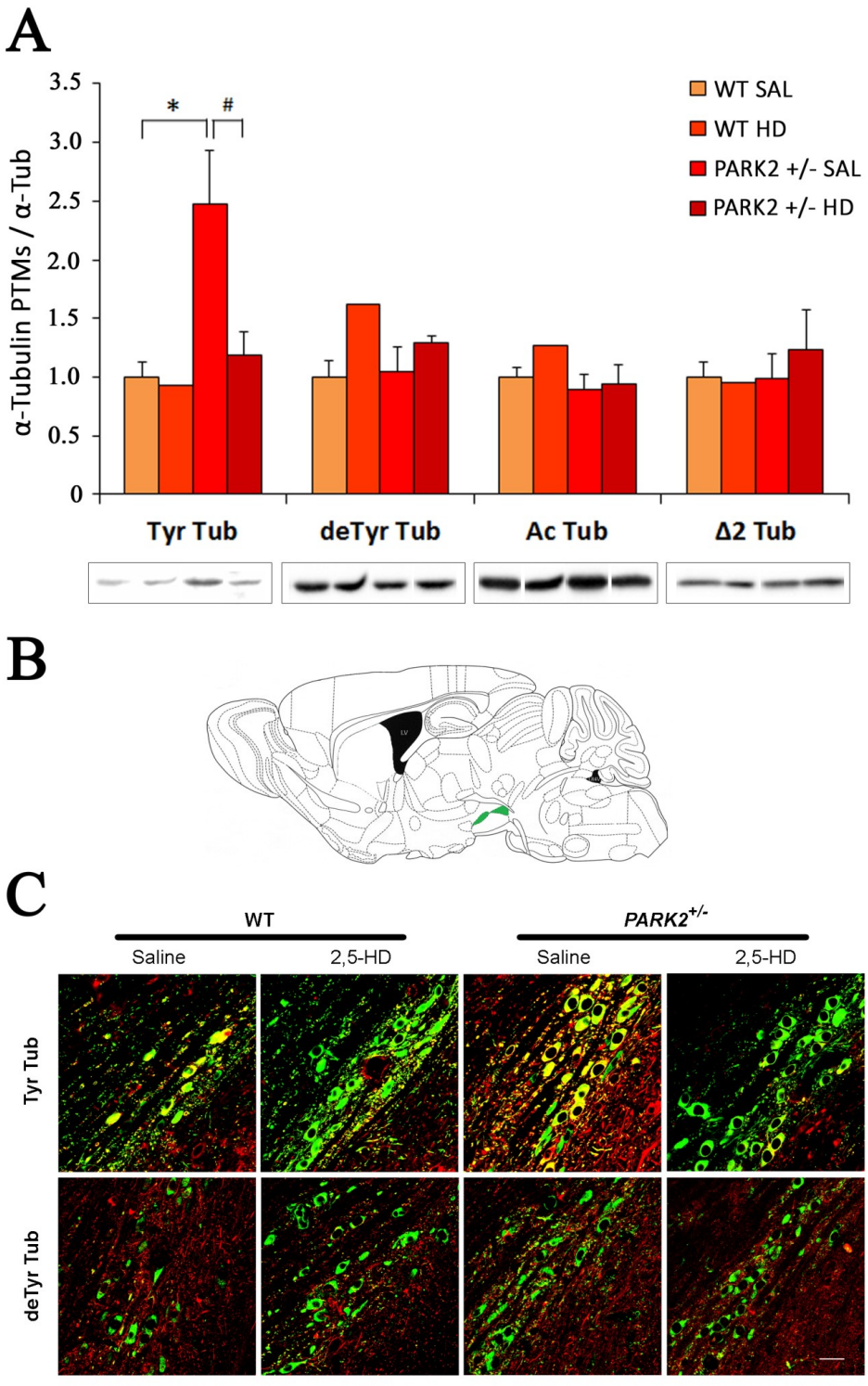
A
α-Tubulin PTMs / α-Tub
3.5
3.0
2.5
2.0
1.5
1.0
0.5
0
*
#
WT SAL
WT HD
PARK2 +/- SAL
PARK2 +/- HD
Tyr Tub
deTyr Tub
Ac Tub
Δ2 Tub
B
C
WT
PARK2+/-
Saline
2,5-HD
Saline
2,5-HD
Tyr Tub
deTyr Tub

**FIGURE 6**

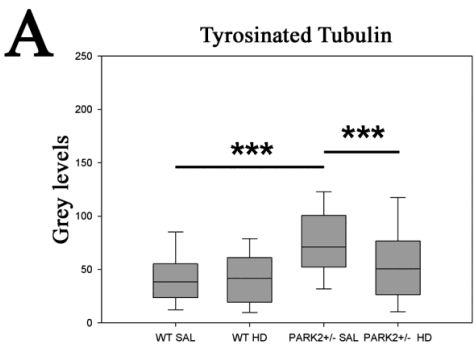


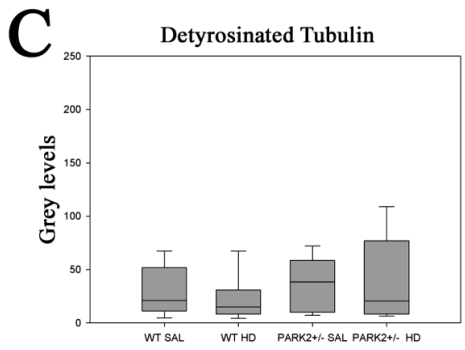


**B**

| | Tyr tub | | |
|---|---|---|---|
| | Number of animals | Number of sections | Number of cells |
| **WT SAL** | 8 | 15 | 127 |
| **WT HD** | 7 | 13 | 144 |
| ***PARK2*$^{+/-}$ SAL** | 9 | 15 | 154 |
| ***PARK2*$^{+/-}$ HD** | 6 | 12 | 149 |

**D**

| | deTyr tub | | |
|---|---|---|---|
| | Number of animals | Number of sections | Number of cells |
| **WT SAL** | 5 | 9 | 36 |
| **WT HD** | 2 | 3 | 26 |
| ***PARK2*$^{+/-}$ SAL** | 6 | 10 | 107 |
| ***PARK2*$^{+/-}$ HD** | 4 | 6 | 60 |

**FIGURE 7**

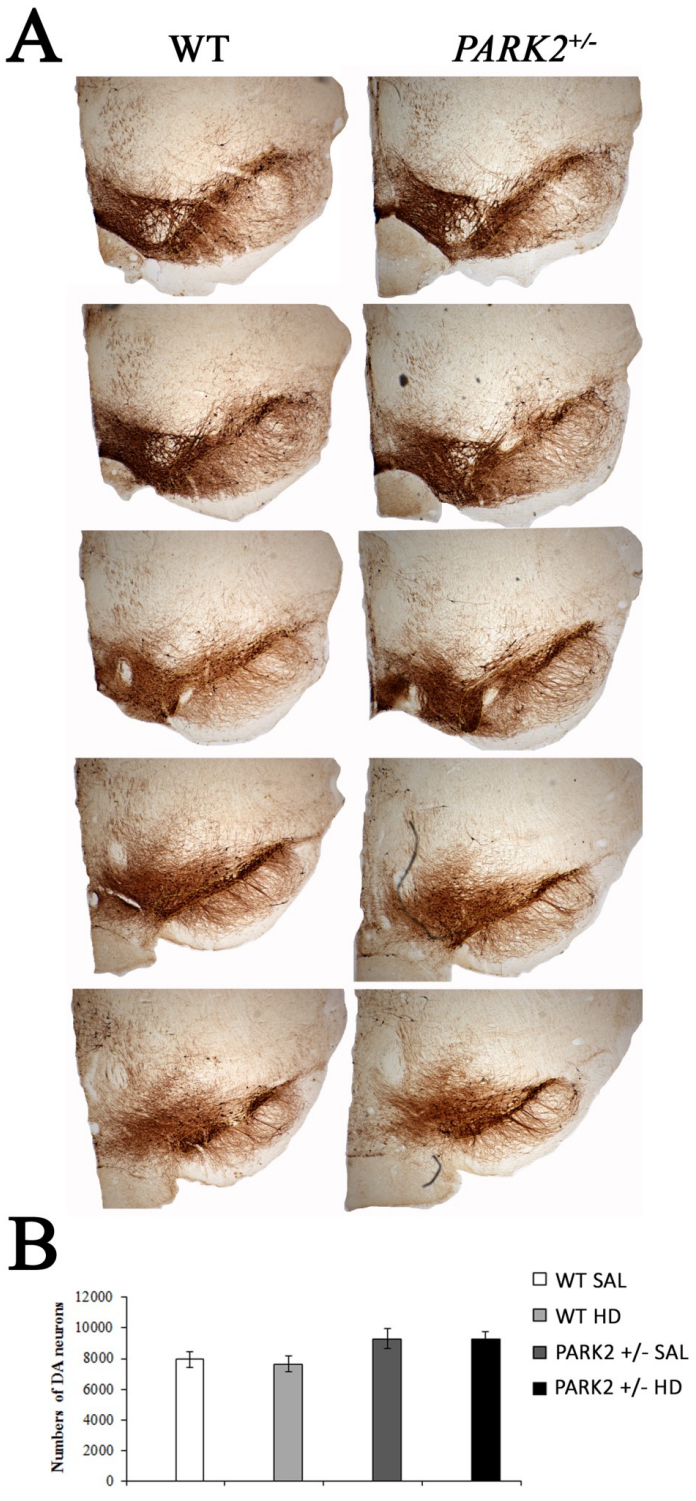
A
WT
PARK2+/-
B
Numbers of DA neurons
12000
10000
8000
6000
4000
2000
0
WT SAL
WT HD
PARK2 +/- SAL
PARK2 +/- HD

**FIGURE 8**

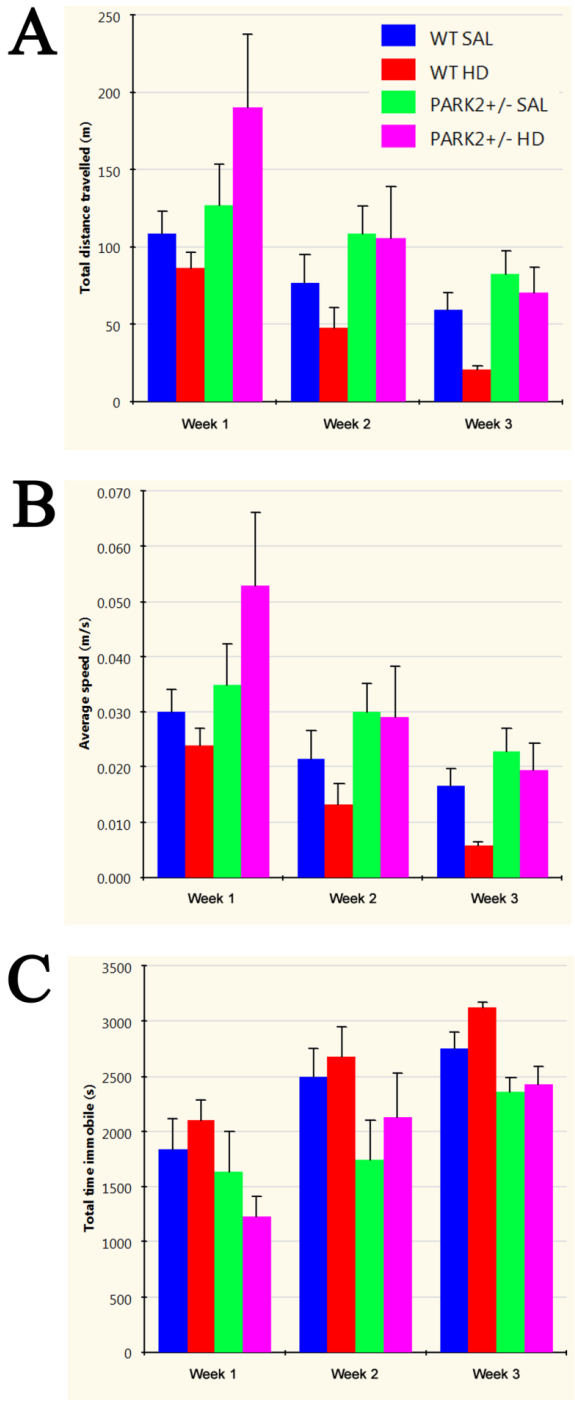
A
Total distance travelled (m)
250
200
150
100
50
0
WT SAL
WT HD
PARK2+/- SAL
PARK2+/- HD
Week 1
Week 2
Week 3
B
Average speed (m/s)
0.070
0.060
0.050
0.040
0.030
0.020
0.010
0.000
Week 1
Week 2
Week 3
C
Total time immobile (s)
3500
3000
2500
2000
1500
1000
500
0
Week 1
Week 2
Week 3

Published Paper 2
Cartelli et al., 2013

SCIENTIFIC REPORTS

OPEN

SUBJECT AREAS:
CELL DEATH IN THE NERVOUS SYSTEM
TARGET IDENTIFICATION
PARKINSON'S DISEASE
MICROTUBULES

Received
12 October 2012

Accepted
16 April 2013

Published
14 May 2013

Correspondence and requests for materials should be addressed to G.C. (graziella.cappelletti@unimi.it)

* These authors contributed equally to this work.

# Microtubule Alterations Occur Early in Experimental Parkinsonism and The Microtubule Stabilizer Epothilone D Is Neuroprotective

Daniele Cartelli[1], Francesca Casagrande[1], Carla Letizia Busceti[2], Domenico Bucci[2], Gemma Molinaro[2], Anna Traficante[2], Daniele Passarella[3], Erminio Giavini[1], Gianni Pezzoli[4], Giuseppe Battaglia[2]* & Graziella Cappelletti[1]*

[1]Department of Biosciences, Università degli Studi di Milano, Milan, Italy, [2]I.R.C.C.S. Neuromed, Pozzilli (IS), Italy, [3]Department of Chemistry, Università degli Studi di Milano, Milan, Italy, [4]Parkinson Institute, Istituti Clinici di Perfezionamento, Milan, Italy.

**The role of microtubule (MT) dysfunction in Parkinson's disease is emerging. It is still unknown whether it is a cause or a consequence of neurodegeneration. Our objective was to assess whether alterations of MT stability precede or follow axonal transport impairment and neurite degeneration in experimental parkinsonism induced by 1-methyl-4-phenyl-1,2,3,6-tetrahydropyridine (MPTP) in C57Bl mice. MPTP induced a time- and dose-dependent increase in fibres with altered mitochondria distribution, and early changes in cytoskeletal proteins and MT stability. Indeed, we observed significant increases in neuron-specific βIII tubulin and enrichment of deTyr tubulin in dopaminergic neurons. Finally, we showed that repeated daily administrations of the MT stabilizer Epothilone D rescued MT defects and attenuated nigrostriatal degeneration induced by MPTP. These data suggest that alteration of MTs is an early event specifically associated with dopaminergic neuron degeneration. Pharmacological stabilization of MTs may be a viable strategy for the management of parkinsonism.**

Axonogenesis and dendritogenesis, which are essential for the normal development of neurons, rely on the coordinated organization and dynamics of the actin and microtubule (MT) cytoskeleton. MTs are polymers built up by α/β tubulin heterodimers, characterized by an intrinsic resistance to bending and compression[1]. They are capable of switching between phases of slow growth and of rapid depolymerization[2], features implicated in generating pushing and pulling forces within cells[3]. During neuronal differentiation, MTs are highly dynamic and ensure outgrowth and branching[4]. In mature neurons, MT stability increases[5]. The proper control of MT dynamics is essential for many neuronal activities, such as synaptic remodelling[6], and both MT stability and neuronal functions are regulated through tubulin posttranslational modifications (PTMs)[7].

Axon degeneration is a hallmark of neurodegenerative disorders and often precedes the onset of symptoms. Axonal destruction is an active process rather than a passive event[8]. Although little is known about the mechanisms involved, a growing body of evidence suggests a primary role of the MT system. In fact, MT fragmentation is the first detectable event during Wallerian degeneration[9], and disorganized and bent MTs accompany the formation of retraction bulbs[10] and axonal retraction[11].

Parkinson's disease (PD) is the most common motor neurodegenerative disorder and each symptom depends on the reduction in dopamine (DA) levels in the striatum. Degeneration of nigrostriatal dopaminergic synaptic terminals precedes the death of dopaminergic neurons in the substantia nigra[12]. Many PD-linked proteins, such as α-synuclein[13], parkin[14], and leucine rich repeat kinase 2[15], modulate the stability of MTs, highlighting the crucial role of MTs during PD progression. Furthermore, PD is the only neurodegenerative disorder that is clearly related to environmental toxins, such as 1-methyl-4-phenylpiridinium ($MPP^+$) or rotenone[12], which both destabilize MTs[16,17]. Alterations in MT stability precede axonal transport impairment and neurite degeneration in $MPP^+$-exposed PC12 cells[18], suggesting that MT dysfunction plays an important role in mediating the toxicity of these compounds. It is noteworthy that both prophylactic and interventional treatments with the MT-stabilizer Epothilone D (EpoD), which is able to pass the blood-brain barrier, improve axonal MT density, reduce axonal

dystrophy and alleviate cognitive deficits in transgenic mouse models of tauopathies[19,20]. It has also been shown that the dynamicity of MTs is increased in tau transgenic mice and that treatment with EpoD restores MT dynamics to baseline levels and exerts beneficial effects on behavior, tau pathology and neurodegeneration[21].

We now show that C57Bl mice treated with 1-methyl-4-phenyl-1,2,3,6-tetrahydropyridine (MPTP) express early alterations of α-tubulin PTMs specifically in dopaminergic neurons, and that systemic injections of EpoD rescue MT defects and attenuate nigrostriatal degeneration in mice with parkinsonian symptoms produced by exposure to the toxin MPTP.

## Results

**Treatment paradigm underlines early alterations.** One single dose of MPTP (30 mg/kg, i.p.) induced about 50–60% reduction in striatal DA levels 7 days later in C57Bl mice, as expected[22]. To highlight very early alterations, mice were treated either with a single dose (30 mg/kg, i.p.) or with a cumulative dose (60 mg/kg) of MPTP, and sacrificed 12 or 72 h later. Biochemical analyses showed that MPTP induced a significant reduction in striatal DA and its metabolites, a sign of ongoing neurodegeneration (Fig. 1a). Western Blotting analysis showed that TH, the rate-limiting enzyme of DA biosynthesis, was decreased in the striatum and substantia nigra only with the highest dose of MPTP (Fig. 1b,c). Ara and colleagues[23] showed that MPTP induces early inactivation of the enzyme, followed by reduction in TH levels; therefore, mice treated with the low dose of MPTP (30 mg/kg), which do not show any changes in TH levels, can be considered to be in an early phase of neurodegeneration, and may be used to uncover very early alterations in experimental parkinsonism.

**MPTP causes axonal transport impairment in dopaminergic fibres.** Mitochondria, as well the other organelles, accumulate into varicosities when axonal transport is impaired[24], and there is evidence that $MPP^+$ interferes with this process[18,25,26]. Therefore, to assess the status of axonal transport in MPTP-treated mice, we evaluated mitochondria distribution within dopaminergic fibres by performing a double immunohistochemical analysis in sagittal sections of TH and voltage-dependent anion channel (VDAC)-porin, a structural protein of the mitochondrial pore. We observed dopaminergic fibres with a homogeneous distribution of mitochondria and fibres showing sparse or accumulated mitochondria (Fig. 2a, arrowheads). It is noteworthy that only mice treated with MPTP and killed 72 h later showed empty fibres (Fig. 2a, arrow), as the mitochondria had been kept out of neuronal processes. Quantification of the different types of fibres (Fig. 2b), showed a time- and dose-dependent increase in fibres with altered mitochondria distribution in treated mice. No significant differences were observed between control mice and mice treated for 12 h with 30 mg/kg MPTP. These data show that MPTP affects axonal transport *in vivo*.

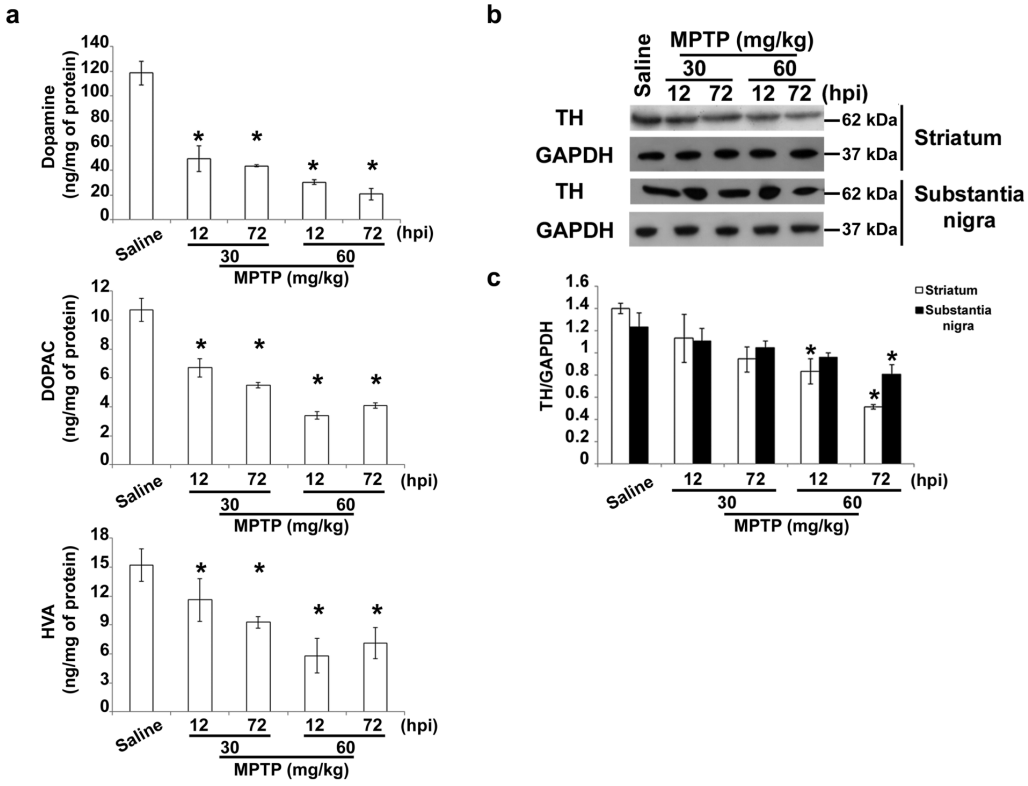


**Figure 1 | Treatment paradigm underlines early alterations.** (a) Biochemical analyses of striatal dopamine, DOPAC and HVA levels in C57Bl mice injected with saline or MPTP (30 mg/kg, i.p., single injection or 20 mg/kg, i.p., × 3, 2 h apart) and killed 12 or 72 hours later (mean ± S.E.M., n = 8–10 mice per group). *$P < 0.05$; one-way ANOVA, Dunnett *post hoc* versus saline-injected mice. (b) Immunoblot of TH levels in lysates of the corpus striatum and substantia nigra of mice injected with saline or MPTP as in a. (c) Densitometric analyses of immunoblot reported in b (mean ± S.E.M., n = 8–10 mice per group). *$P < 0.05$; one-way ANOVA, Dunnett *post hoc* test versus saline-injected mice. hpi = hours post last injection of MPTP.

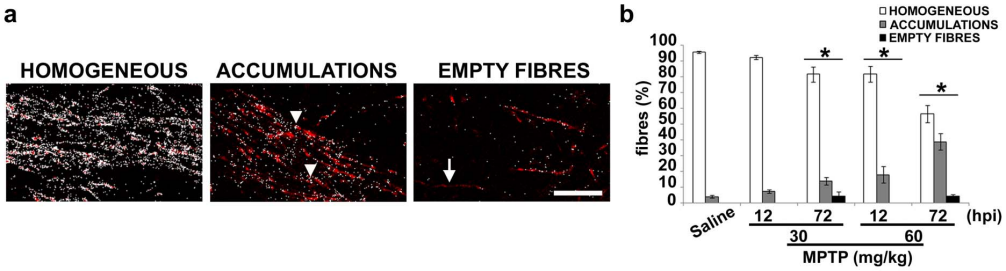


**Figure 2 | MPTP causes axonal transport impairment.** (a) Mask projections of sagittal sections of the nigrostriatal pathway in mice injected with saline or MPTP as in Fig. 1, showing the distribution of mitochondria (white spots) inside dopaminergic fibres (red). Arrowheads indicate mitochondria accumulations and arrow highlights an empty fibre. Scale bar = 20 μm. (b) Percentage of fibres displaying a homogeneous distribution of mitochondria, fibres showing dispersed or accumulated mitochondria or empty fibres. hpi = hours post last injection of MPTP (mean ± S.E.M., n = 9 sections from 3 different mice per group). $*P < 0.05$; $\chi^2$ test versus saline-injected mice.

**MPTP increases the neuron-specific βIII tubulin isotype.** Axonal transport defects could be related to alterations of cytoskeletal proteins and molecular motors. Thus, we evaluated levels of actin, α- and β-tubulin, and the neuron-specific βIII tubulin isotype. Western blotting and densitometric analyses showed that levels of actin and α/β tubulin were unchanged in the striatum (Fig. 3a,b) and substantia nigra (Fig. 3c,d) of MPTP-treated mice. β-tubulin was significantly reduced in the striatum of mice treated with MPTP (30 mg/kg) and killed 72 h later (Fig. 3a,b). The specific change in β-tubulin is not surprising, because Chung and colleagues[27] already showed differential variations in α- and β-tubulin monomers in a rat model of synucleinopathy, and we have recently found significant enrichment of β-tubulin in the fibroblasts of PD patients carrying parkin mutations[28]. On the other hand, the neuron-specific βIII tubulin isotype was significantly increased by MPTP treatment in both striatum and substantia nigra, although at different time points

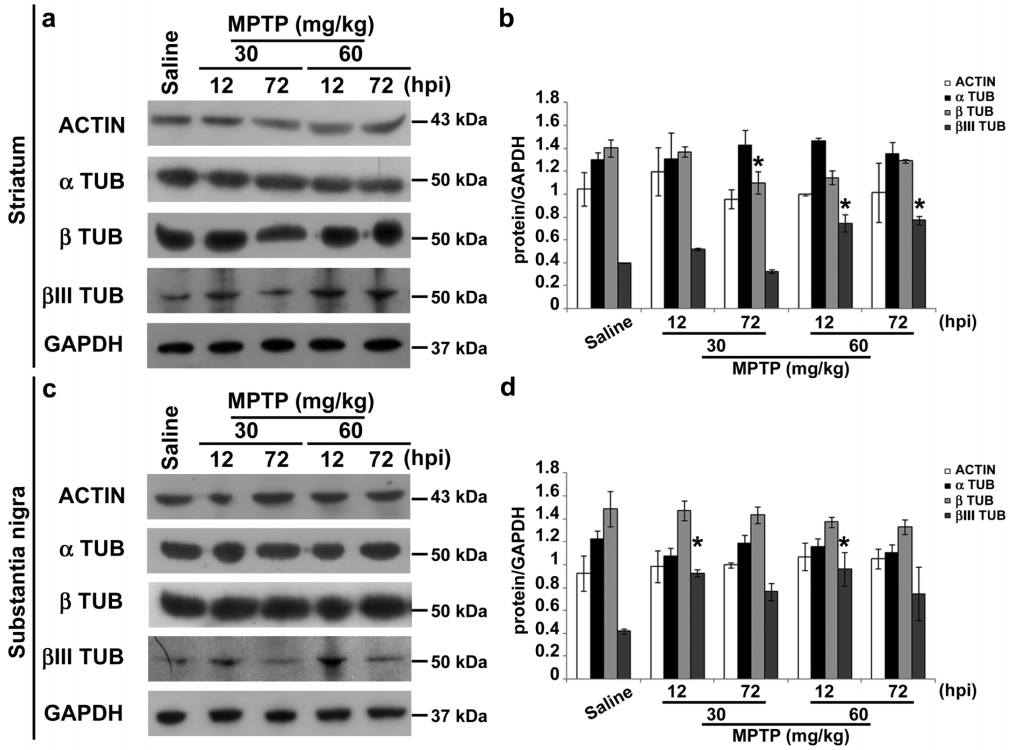


**Figure 3 | MPTP treatment increases the βIII tubulin isotype.** (a) Immunoblots of actin, α-tubulin, β-tubulin and βIII tubulin in lysates of striatum of mice treated as in Fig. 1. (b) Densitometric analyses of immunoblot reported in a (mean ± S.E.M., n = 4–6 individuals per group). $*P < 0.05$; one-way ANOVA, Dunnett *post hoc* test versus saline-injected mice. (c) Immunoblot of actin, α-tubulin, β-tubulin and βIII tubulin in lysates of substantia nigra of mice treated as in Fig. 1. (d) Densitometric analyses of immunoblot reported in c (mean ± S.E.M., n = 4–6 individuals per group). $*P < 0.05$; one-way ANOVA, Dunnett *post hoc* test versus saline-injected mice. hpi = hours post last injection of MPTP.

(Fig. 3). Levels of kinesin and dynein, responsible for MT-dependent anterograde and retrograde axonal transport, respectively[29], were not affected by MPTP treatment (Supplementary Fig. S1), suggesting that axonal transport defects may be due to alternative factors.

**MPTP specifically affects MT stability in dopaminergic neurons.** α-tubulin PTMs are usually used as markers of MTs with different stability, being tyrosinated (Tyr) MTs the most dynamic, and acetylated (Ac) or detyrosinated (deTyr) MTs the most stable pools[7]. Recently, it has been shown that α-tubulin PTMs are directly linked to neurodegeneration in mice[30] and $MPP^+$ affects α-tubulin PTMs in PC12 cells[18]. Therefore, we evaluated MT stability in the striatum (Fig. 4) and substantia nigra (Fig. 5) of MPTP-treated mice, as well as along their nigrostriatal pathway (Supplementary Fig. S2). Biochemical analyses showed the enrichment of deTyr tubulin in striatum (Fig. 4a,b), which was detectable already 12 h after the injection of the lowest dose of MPTP, and a later increase in both Tyr and Ac tubulins. Confocal analyses and the evaluation of Manders' coefficients (M1 and M2, reported in Table 1 and Supplementary Table S1, respectively), which are good indicators of relative signal distribution[31], showed that changes in the levels of tubulin PTMs were located in dopaminergic terminals. In fact, we observed an increased co-localization between deTyr or Ac Tub and TH signals (Fig. 4c) and significant elevation in M1 parameter (Table 1). On the other hand, the significant decrease in the M1 parameter (Table 1) demonstrated that the enrichment of Tyr tubulin was associated with neurons residing in the striatum.

Western blotting analysis performed on substantia nigra lysates (Fig. 5a, b), revealed a significant decrease in Tyr tubulin in MPTP-treated mice, suggesting that the dynamic MT pool was reduced, as we already showed in cultured cells[18]. On the other hand, MPTP induced a significant enrichment of deTyr tubulin in mice treated with MPTP (60 mg/kg) and killed 12 h later, suggesting an increase in stable MTs, which mirrors the changes observed in the striatum. Confocal analyses showed that α-tubulin PTM changes occurred in dopaminergic cell soma (Fig. 5c), and the quantification of fluorescence intensity within single cells (Supplementary Table S2) showed that alterations of MT stability are higher in dopaminergic neurons. Indeed, we observed a significant reduction in Tyr tubulin and an early increase in deTyr and Ac tubulins that resulted in the decrease of stable MTs.

Finally, as α-tubulin PTMs influence axonal transport[32,33], we evaluated potential changes within dopaminergic fibres by confocal microscopy (Supplementary Fig. S2). Besides the slight changes observed in Tyr and Ac tubulin content, the overall result we obtained is an early increase in deTyr tubulin, in line with the modifications of this subset of stable MTs in the striatum and substantia nigra of MPTP-treated mice, which could be responsible for the impairment of axonal transport, as already suggested[18]. Taken together, these results show that MPTP affects MT stability *in vivo*, and that the alteration of α-tubulin PTMs is an early event specifically associated with dopaminergic neurons.

**Stabilization of MT attenuates MPTP-induced neurodegeneration.** To test the hypothesis that stabilization of MT is able to exert a neuroprotective effect in experimental parkinsonism, we used the classical model induced by MPTP. C57 Black mice were challenged with a single dose of MPTP (30 mg/kg, i.p.), which led, 7 days later, to about 50% reduction in striatal DA levels. Similar reductions were found in the striatal levels of DOPAC and HVA, although changes in DOPAC and HVA levels were variable in different experiments (Fig. 6a). Reductions in DA were not affected in mice systemically injected with 1 or 3 mg/kg, i.p., of EpoD 30 min prior to MPTP (Fig. 6a). Repeated treatment with EpoD (1 mg/kg, i.p.), injected 30 min prior to MPTP and then for the following 4 days once a day, induced substantial attenuation of MPTP-induced striatal DA reduction (Fig. 6b). Note that, for unknown reasons, MPTP toxicity was greater in control animals injected with DMSO alone. Neuroprotection by repeated injections of EpoD was confirmed by stereological counts of TH-positive neurons in the pars compacta of substantia nigra (Fig. 6c,d). To assess the effects of EpoD on motor activity, mice were treated i.p. with EpoD alone (3 mg/kg, every day for four days) or 30 min prior MPTP and then every day for four days. EpoD did not affect the

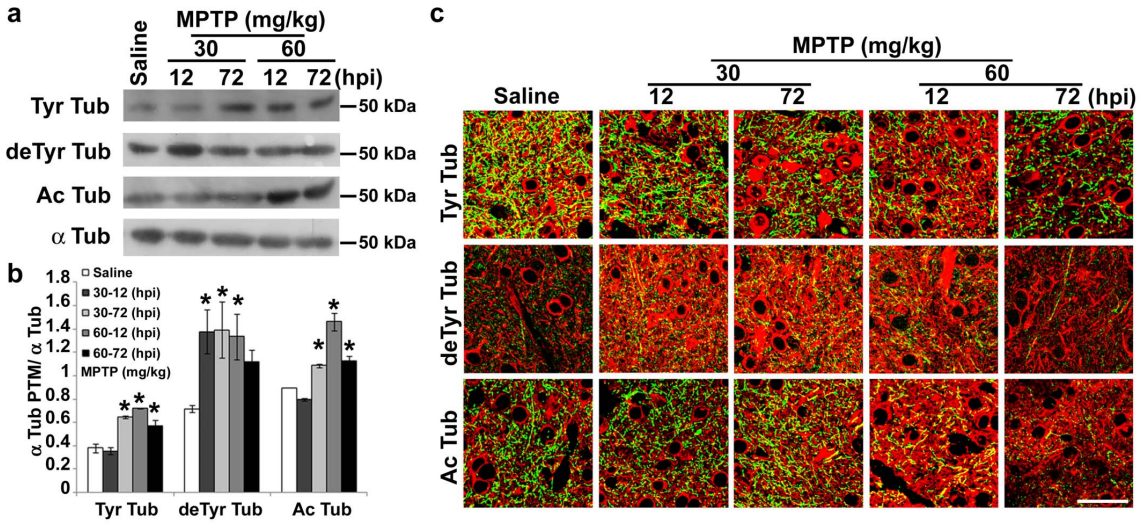


**Figure 4 | MPTP affects MT stability in dopaminergic terminals.** (a) Immunoblot of levels of tyrosinated tubulin (Tyr Tub), detyrosinated tubulin (deTyr Tub) and acetylated tubulin (Ac Tub) in lysates of striatum of mice treated as in Fig. 1. (b) Densitometric analyses of immunoblot reported in a (mean ± S.E.M., n = 4–6 mice per group). For the quantitation, values of each α-tubulin PTM were normalized on the level of α-tubulin (α Tub) of the relative sample. $*P < 0.05$; one-way ANOVA, Dunnett *post hoc* test versus saline-injected mice. (c) Confocal images of striatum of mice treated as in Fig. 1. Green represents TH staining and red signals the various tubulin PTMs. Scale bar = 50 μm. hpi = hours post last injection of MPTP.

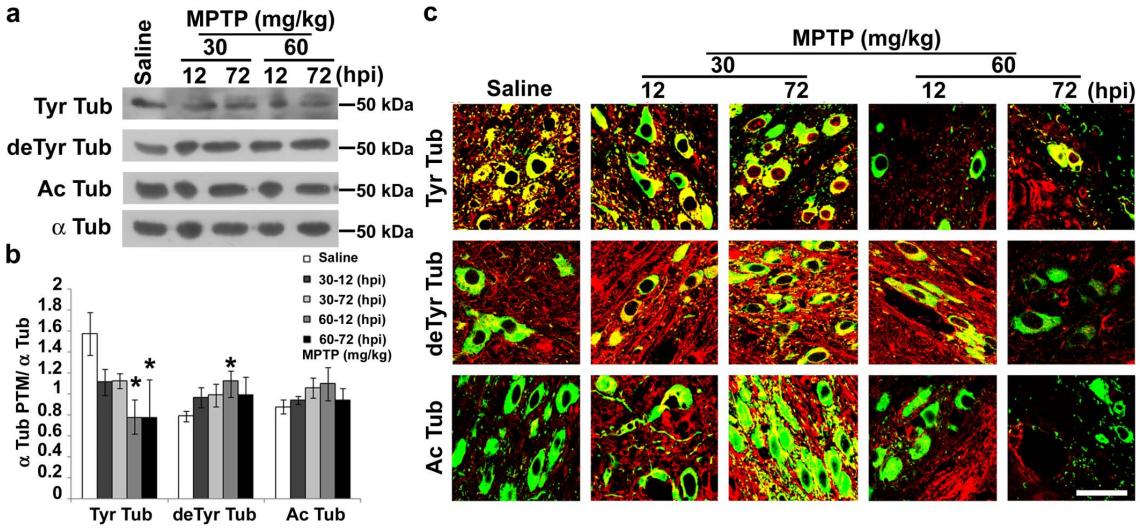


**Figure 5 | MPTP affects MT stability in dopaminergic neurons.** (a) Immunoblot of levels of tyrosinated tubulin (Tyr Tub), detyrosinated tubulin (deTyr Tub) and acetylated tubulin (Ac Tub) in lysates of substantia nigra of mice treated as in Fig. 1. (b) Densitometric analyses of immunoblot reported in a (mean ± S.E.M., n = 4–6 mice per group). For the quantitation, values of each α-tubulin PTM were normalized on the level of α-tubulin (α Tub) of the relative sample. $*P < 0.05$; one-way ANOVA, Dunnett *post hoc* test versus saline-injected mice. (c) confocal images of substantia nigra of mice treated as in Fig. 1. Green represents TH staining and red signals the various tubulin PTMs. Scale bar = 50 μm. hpi = hours post last injection of MPTP.

motor performance on the rotarod test by itself (not shown). At the doses of MPTP used, we did not observe any modification of motor performance and EpoD treatment did not modify the motor coordination at the rotarod test (not shown). We also monitored general health conditions of mice treated with EpoD and MPTP+EpoD. Both fur and body weight were not affected by EpoD or MPTP+EpoD treatments.

To verify that the neuprotective effect of EpoD was due to its action on MT system, we analyzed α-tubulin PTMs in the corpus striatum and substantia nigra of mice challenged with MPTP and chronically treated with EpoD. We observed significant increase of both Tyr and deTyr tubulin in the striatum of MPTP-treated mice (Fig. 7a,b), whereas only deTyr tubulin was increased by MPTP in the substantia nigra (Fig. 7c,d). Furthermore, our data show the ability of EpoD to restore deTyr tubulin baseline levels, both in striatum (Fig. 7a,b) and substantia nigra (Fig. 7c,d). The reduction in a marker of stable MTs, as deTyr tubulin is, induced by a stabilizer drug, as EpoD is, could seem surprising. However, this is perfectly consistent with the hypothesis that the increase of stable MTs in MPTP-treated mice may be an attempt to counteract the drug-induced MT destabilization[18]. $MPP^+$ is known to promote MT catastrophes[16] and, in respect to dynamic ones, deTyr MTs are more resistant to induced MT depolymerization; hence, tubulin detyrosination could reduce $MPP^+$-provoked MT catastrophes. On the other side, as many other MT-stabilizing agent, EpoD directly induces MT polymerization under conditions in which tubulin is not more able to assemble, shifting the equilibrium of tubulin toward the polymeric state. To verify our hypothesis, we measured the amount of tubulin associated to cytosolic dimers and to polymeric MTs (Fig. 7e,f), both in striatum and substantia nigra. Our data reveal, for the first time, that MPTP is able to specifically destabilize MTs in the substantia nigra of treated mice and that chronic treatment with EpoD prevents the MPTP-induced destabilization (Fig. 7e,f).

## Discussion

Cytoskeletal alterations have been described in many central nervous system disorders, but it is unclear whether they are a cause or simply a by-product of neurodegeneration. Here, we show that systemic injection of MPTP in mice induces MT dysfunction that occurs very early, before axonal transport impairment, TH depletion, and, ultimately, dopaminergic neuron degeneration. Noteworthy is that chronic administration of the MT stabilizer Epo D rescues MT defects and is neuroprotective, supplying reliable proof that MT dysfunction may contribute to actually cause neurodegeneration.

Axonal transport impairment in the MPTP model of PD was first suggested by Morfini et al. (2007), who proposed that it was an early event in neurodegeneration, based on the outcome of a study on giant squid axons. Here we demonstrate that axonal transport impairment occurs in MPTP-treated mice, showing changes in mitochondria distribution in dopaminergic fibres. In addition, the earlier decrease

Table 1 | Analysis of M1 parameter (Tubulins vs. TH) in striatal sections

| | Tyr Tubulin | deTyr Tubulin | Ac Tubulin |
|---|---|---|---|
| Saline | 0.41 ± 0.032 | 0.30 ± 0.025 | 0.16 ± 0.013 |
| MPTP, 30 mg/kg (12 h) | 0.27 ± 0.021 (*) | 0.39 ± 0.013 | 0.28 ± 0.028 (*) |
| MPTP, 30 mg/kg (72 h) | 0.27 ± 0.048 (*) | 0.51 ± 0.027 (*) | 0.33 ± 0.021 (*) |
| MPTP, 60 mg/kg (12 h) | 0.17 ± 0.029 (*) | 0.34 ± 0.034 | 0.36 ± 0.019 (*) |
| MPTP, 60 mg/kg (72 h) | 0.24 ± 0.043 (*) | 0.32 ± 0.030 | 0.16 ± 0.023 |

Data are expressed as mean ± S.E.M., n = 4 sections for each mouse from 4–6 mice per group. $*P < 0.05$; one-way ANOVA, Dunnett *post hoc*: *versus* saline-injected mice.

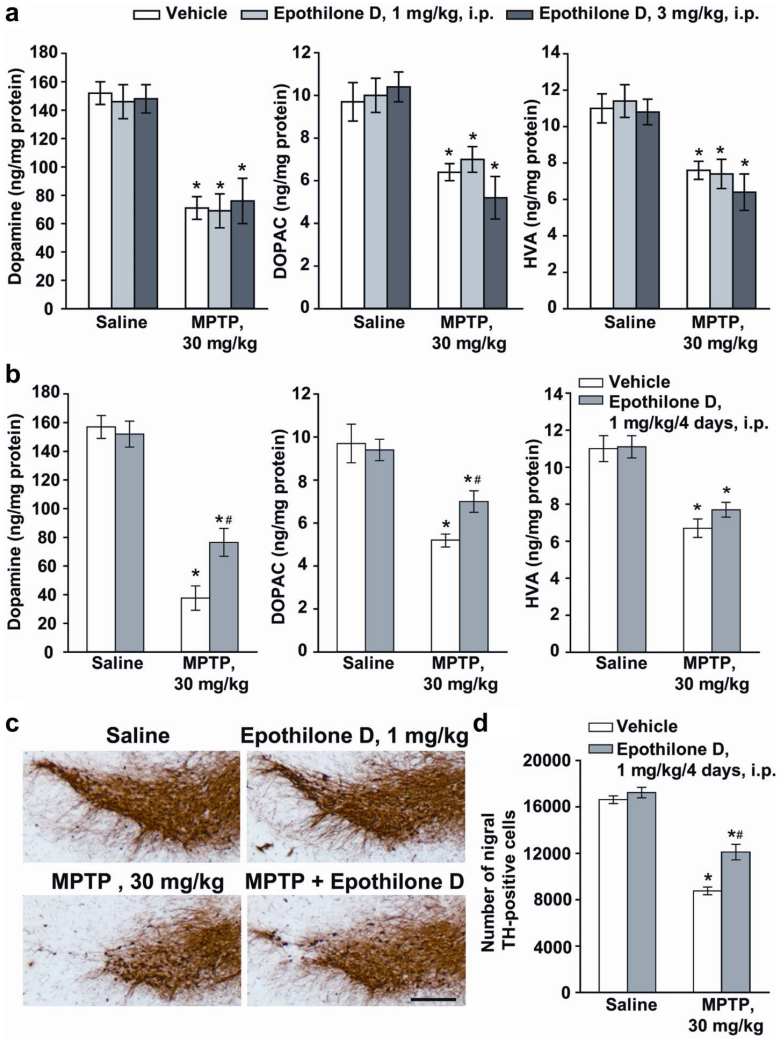


**Figure 6 | Repeated systemic injections of EpoD attenuate MPTP toxicity in mice.** (a) Biochemical analyses of striatal dopamine, DOPAC, and HVA levels in C57Bl mice injected with MPTP (30 mg/kg, i.p., single injection) alone or in combination with EpoD (1 or 3 mg/kg, i.p.) dissolved in DMSO and injected 30 min before MPTP. Mice were killed 7 days later (mean ± S.E.M., n = 8–10 mice per group). *$P < 0.05$; one-way ANOVA, Dunnett *post hoc* test versus saline-injected mice. (b) Biochemical analyses of striatal dopamine, DOPAC, and HVA levels in C57Bl mice injected with MPTP (30 mg/kg, i.p., single injection) alone or in combination with EpoD (1 mg/kg, i.p.) dissolved in DMSO and injected 30 min before MPTP and then for the following 4 days once a day. Mice were killed 7 days later (mean ± S.E.M., n = 8–10 mice per group). *, # $P < 0.05$; one-way ANOVA, Dunnett *post hoc* test versus saline-injected mice (*) or versus mice injected with MPTP alone (#). (c) Immunohistochemical analysis of TH in the pars compacta of substantia nigra of mice injected with a single i.p. injection of 30 mg/kg of MPTP, alone or combined with EpoD (1 mg/kg, i.p., 30 min prior to MPTP and then for the following 4 days, once a day). Scale bar = 250 μm. (d) Stereological counts of TH-positive cell in the substantia nigra pars compacta (mean ± S.E.M., n = 5 mice per group). *, # $P < 0.05$; one-way ANOVA, Dunnett *post hoc* test versus saline-injected mice (*) or versus mice injected with MPTP alone (#).

in TH in striatum, followed by TH depletion in substantia nigra, can easily be explained by impairment of axonal transport, other than by the dying back mechanism of degeneration, typical of PD[12] and mice exposed to MPTP[34]. Looking for the mechanisms underlying axonal transport impairment, we found that MPTP does not impact motor protein levels. However, it affects the levels of deTyr MTs, suggesting that altered MT stability is responsible for the alterations of axonal transport. Indeed, Kinesin 1, which is particularly abundant in neurons, is preferentially recruited, but moves slowly along highly modified MTs[33]. Furthermore, $MPP^+$ induces increases in deTyr tubulin content that precede and therefore may cause the reduction in mitochondrial transport in PC12 cells[18]. Consequently, we supposed that a similar scenario is likely to occur in MPTP-treated mice. Nevertheless, another paper by O'Malley's group[26] reported that $MPP^+$ specifically impairs mitochondria transport in dopaminergic neurons, an event that precedes autophagy and MT defects. However, they looked at gross, i.e. Ac-MT fragmentation and α-tubulin content reduction, rather than at subtle alterations of MTs, such as

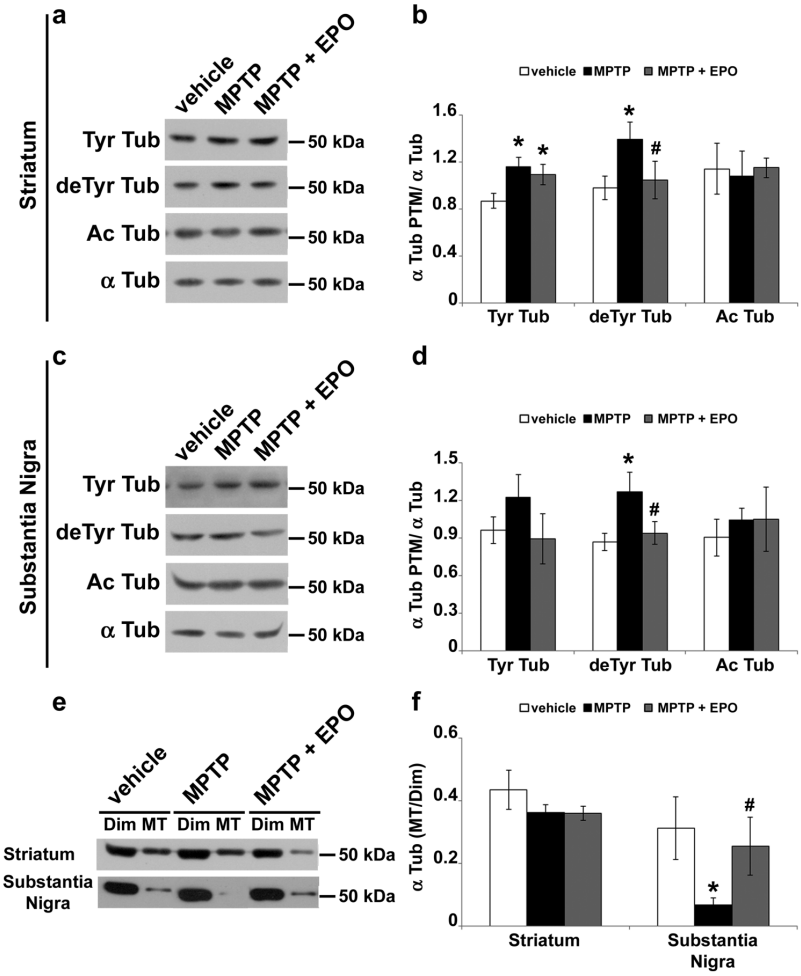


**Figure 7 | EpoD rescues MT system in MPTP-treated mice.** (a) Immunoblot of levels of tyrosinated tubulin (Tyr Tub), detyrosinated tubulin (deTyr Tub) and acetylated tubulin (Ac Tub) in lysates of striatum of mice treated as in Fig. 6. (b) Densitometric analyses of immunoblot reported in a (mean ± S.E.M., n = 5 mice per group). For the quantitation, values of each α-tubulin PTM were normalized on the level of α-tubulin (α Tub) of the relative sample. *, # $P < 0.05$; one-way ANOVA, Fischer LSD *post hoc* test versus saline-injected mice (*) or versus mice injected with MPTP alone (#). (c) Immunoblot of levels of tyrosinated tubulin (Tyr Tub), detyrosinated tubulin (deTyr Tub) and acetylated tubulin (Ac Tub) in lysates of substantia nigra of mice treated as in Fig. 6. (d) Densitometric analyses of immunoblot reported in c (mean ± S.E.M., n = 5 mice per group). For the quantitation, values of each α-tubulin PTM were normalized on the level of α-tubulin (α Tub) of the relative sample. *, # $P < 0.05$; one-way ANOVA, Fischer LSD *post hoc* test versus saline-injected mice (*) or versus mice injected with MPTP alone (#). Tubulin dimers (Dim) and MT polymers (MT) of corpus striatum and substantia nigra were analyzed by (e) immunoblot and (f) densitometric analyses and are shown as ratio (mean ± S.E.M., n = 3 mice per group). *, # $P < 0.05$; one-way ANOVA, Fischer LSD *post hoc* test versus saline-injected mice (*) or versus mice injected with MPTP alone (#).

changes in PTMs. A further possible cause of the axonal transport block is MT reorientation, which is induced either by $MPP^+$ [18] or by human mutant Tau expression[35] leading to traffic jams. Therefore, the observed impairment of axonal transport is likely mediated by alterations of MT stability and organization, which, in turn, lead to distal axon degeneration, as dying back is, and to the accumulation of DA loaded vesicles in cell soma. This could really be detrimental to the neurons since DA oxidation produces large quantities of reactive oxygen species (ROS) triggering dopaminergic neuron death[36].

The observation that levels of the neuron-specific βIII tubulin, which is the most dynamic among the β-tubulin isotypes[37], are increased points out the importance of MT dynamics and its tight regulation in MPTP-mediated neurodegeneration, as we have already shown[16,18]. βIII tubulin enrichment could be explained as an adaptive mechanism to counteract the MPTP-induced reduction in Tyr α−tubulin, usually associated with highly dynamic MTs. Moreover, βIII tubulin expression is primarily restricted to the nervous system[38], and it has been suggested that different β-tubulin isotypes could serve specific and unique roles[39], such as neuronal elongation and axon guidance. Banarjee and colleagues[40] showed that in the presence of Tau, a neuron-specific MT binding protein, βIII tubulin was more prone to polymerize than the other isotypes. Worthy of note is the recent suggestion that the Tau-MTs interaction may be important not only in the pathogenesis of Alzheimer's disease, but also of PD. Indeed, both MPTP and α-synuclein mutations promote Tau phosphorylation, causing MT instability, which leads

to loss of dopaminergic neurons in PD brain[41]. Nevertheless, trying to counteract the ongoing axonal destruction, the dopaminergic neurons could promote MT polymerization through increase in the βIII tubulin content or in MT stability, as suggested by the enrichment in deTyr and Ac α-tubulin.

Mitochondria are largely considered crucial players in the pathogenesis of PD. Indeed, both $MPP^+$ [42] and rotenone[43] inhibit mitochondrial complex I, reducing ATP synthesis and increasing ROS production. However, the lack of complex I does not protect dopaminergic neurons from toxin administration[44], suggesting the existence of alternative mechanisms of action. It is well known that tubulin interacts with VDAC, the most abundant protein in the mitochondrial outer membrane, and mitochondria-associated tubulin is enriched in βIII isotype[45]. Recently, it has been reported that tubulin decreases the respiration rate of isolated mitochondria[46] and that the increase in tubulin dimers induces mitochondrial depolarization in human cancer cells[47]. Furthermore, the administration of tubulin-targeted drugs induces mitochondrial depolarization and $Ca^{++}$ release[48]. This body of evidence clearly shows that interfering with MT system impairs mitochondria activity. Therefore, enrichment in free tubulin dimers in PC12 cells[18] and MPTP-induced increase in βIII tubulin (present data) could induce adverse effects, such as mitochondrial dysfunction. Being life a matter of balance, when the equilibrium shifts from a beneficial event, such as MT polymerization induced by βIII tubulin increases, toward a detrimental one, such as mitochondrial dysfunction caused by the same factor, dopaminergic neurons may die leading to PD. In this context, it is essential to consider parkin, an E3 ligase promoting degradation of tubulin and other proteins, known to interact with MTs and to play a central role in the regulation of mitophagy. Thanks to its particular position, parkin may quarantine damaged mitochondria, by severing their connection to the MT network, before promoting their clearance[49]. If MT-parkin interaction was impaired, as in the case of MT destabilization, proper regulation of mitophagy would fail, leading to dopaminergic neuron loss. Thus, tubulin partitioning between dimer and polymer pools regulates multiple steps in mitochondrial metabolism and, therefore, in the control of neuronal health and death.

A first step designed to block the progression of the disease would be the regeneration of collapsing axons. MT stabilization could be useful to physically counteract axon disruption, reinforcing the pillars that support the structures, and to prevent mitochondrial damage, reducing the level of free tubulin dimers. In fact, the activation of signal cascades that converge on MT stability modulation has trophic effects on axon formation *in vivo*[50,51]. It has already been shown that the MT-stabilizer Taxol protects cultured dopaminergic neurons against rotenone toxicity[17,52], reduces scarring formation and promotes regeneration of central nervous system axons[53,54]. Unfortunately, the blood-brain barrier penetration of Taxol is very poor[55]. EpoD, another MT-stabilizing compound, penetrates through the blood-brain barrier and has resulted to be neuroprotective in mouse models of schizophrenia[56] and tauopathy[19]. Moreover, it improves axonal MT density, reduces axonal dystrophy and alleviates cognitive deficits in transgenic mouse models of tauopathies[19,20]. What is more, the dynamicity of MTs is increased in tau transgenic mice and treatment with EpoD restored MT dynamics. MT stabilization had beneficial effects on behavior, tau pathology and neurodegeneration[21]. Here, we used the classical model of experimental parkinsonism induced by MPTP to test the hypothesis that MT stabilization is also able to counteract degeneration in another model of neurodegeneration. Acute injections of EpoD did not affect the toxic effect induced by MPTP, whereas repeated injections of EpoD restored tubulin PTMs and MT mass in the substantia nigra and exerted neuroprotective effects in the dopaminergic nigrostriatal system of MPTP-treated mice. Therefore, doses of EpoD, which were chosen according to Barten and colleagues[21], are also effective in the MPTP model of dopaminergic neurotoxicity. These data pinpoint that alterations of MTs are very early events, which specifically occur in dopaminergic neurons in experimental parkinsonism, and reinforce the idea that the cytoskeleton of dopaminergic neurons is particularly vulnerable but is also highly responsive to MT-targeting agents.

Taken together with our recent findings that MT stability is impaired in human fibroblasts deriving from PD patients and that MT stabilization rescues control phenotype[28], the present work suggests that MTs are a potential target for pharmacological therapy designed to block the axonal disruption leading to PD. Thus, chronic pharmacological stabilization of MT may be a viable strategy for the management of the disease.

## Methods

**Materials.** 1-Methyl-4-phenyl-1,2,3,6-tetrahydropyridine (MPTP) was purchased from Sigma (St. Louis, MO). Epothilone D was purchased from Acme Bioscience (Palo Alto, CA).

**Animals.** Male C57 Black mice (22–24 g, b.w., 8–9 week old) were purchased from Charles River (Calco, Italy) and used for all experiments. Mice were kept under environmentally controlled conditions (ambient temperature = 22°C, humidity = 40%) on a 12-h light/dark cycle with food and water *ad libitum*. The study was carried out in strict accordance with the recommendations in the Guide for the Care and Use of Laboratory Animals of the National Italian Institute of Health. The protocol was approved by the Committee on the Ethics of Animal Experiments of the I.R.C.C.S. Neuromed Institute. Permit Number 432007/A was issued by the Italian Ministry of Health. All efforts were made to minimize suffering.

**Treatments.** Mice were treated with one single i.p. injection of 36 mg/kg of MPTP (corresponding to 30 mg/kg of free MPTP) or with three doses of 24 mg/kg of MPTP hydrochloride (corresponding to 20 mg/kg of free MPTP), injected i.p. at 2 h intervals (cumulative dose = 60 mg/kg of free MPTP). Twelve or 72 h after last injection of MPTP, mice were killed by decapitation or by intracardiac perfusion, to perform biochemical or immunohistochemical analysis, respectively. One cerebral hemisphere of mice used for biochemical analysis, was used to evaluate levels of striatal DA and its metabolites, 3,5-dihydroxyphenylactic acid (DOPAC) and homovanillic acid (HVA). For EpoD experiments, mice were injected with a single i.p. dose of 36 mg/kg of MPTP and then acutely (1 or 3 mg/kg, i.p., 30 min prior to MPTP) or chronically treated (1 mg/kg, i.p., 30 min prior to MPTP and then every day for 4 days) with EpoD. Mice were killed 7 days later for biochemical analysis of MTs and biochemical and immunohistochemical assessment of nigro-striatal damage. EpoD was dissolved in DMSO and injected i.p. (in a volume of 50 µl/mouse). Control mice were injected with the vehicle alone.

**Motor activity assessment.** Motor coordination was assessed by the rotarod test. The rotarod apparatus consisted of a motor driver control unit (Ugo Basile, Varese, Italy) and a rotating horizontal cylinder (30 mm), divided into five separate rotating compartments and fully enclosed to ensure that the mice did not jump out of their area. Automatic timers recorded the time (in seconds) the mice remained on the rod, which was rotating at an accelerating speed from 5 to 15 rpm. Mice were tested for 10 min on the rotarod every day, starting 2 days after MPTP or EpoD injection (as above). General health conditions (fur, body weight and mortality) were also monitored by an experimenter unaware of treatments.

**Monoamine assay.** The corpus striatum was immediately dissected out homogenized by sonication in 0.6 ml of ice-cold 0.1 M PCA. Fifty µl of the homogenate were used for protein determination[57]. The remaining aliquot was centrifuged at 8,000 *g* for 10 min, and 20 µl of the supernatant was injected into an HPLC equipped with autosampler 507 (Beckman Instruments, Fullerton, CA), a programmable solvent module 126 (Beckman), an analytical C-18 reverse-phase column kept at 30°C (Ultrasphere ODS 5 µm, 80 Å pore, 250 × 4.6 mm (Beckman), and a Coulochem II electrochemical detector (ESA, Inc., Chelmsford, MA). The holding potentials were set at +350 and −350 mV for the detection of DA, DOPAC and HVA. The mobile phase consisted of 80 mM sodium phosphate, 40 mM citric acid, 0.4 mM EDTA, 3 mM 1-heptansulphonic acid and 8.5% methanol, brought to pH 2.75 with phosphoric acid (run under isocratic conditions, at 1 ml/min).

**Western blot analysis.** Western blot analysis was performed on protein extracts or cytoskeletal fractions obtained from mouse brain regions. To get total proteins, corpus striatum and substantia nigra were immediately dissected out on ice, mechanically homogenized and, subsequently, sonicated in SDS-PAGE sample buffer. Separation of cytosolic tubulin dimers from MT polymers was performed accordingly to Fanara and colleagues[58]. Briefly, corpus striatum and substantia nigra were gently homogenized in MT-stabilizing buffer and postnuclear supernatants were centrifuged at 200,000 *g* at 20°C for 20 min; the supernatant (containing the soluble dimeric tubulin) and the pellet (containing the MT fraction) were separated and stored at −20°C. Western blots were made as previously described[18] using the

following antibodies: α-tubulin mouse IgG (clone B-5-1-2, Sigma-Aldrich); deTyr tubulin rabbit IgG (Chemicon, Temecula, CA); Tyr tubulin mouse IgG (clone TUB-1A2, Sigma-Aldrich); Ac tubulin mouse IgG (clone 6-11B-1, Sigma-Aldrich); β-tubulin mouse IgG (clone Tub 2.1, Sigma-Aldrich); βIII tubulin mouse IgG (clone TU-20, kindly provided by Dr. Pavel Dràber, Prague, Czec Republic); actin mouse IgM (N350, Amersham, Little Chalfont, UK); tyrosine hydroxylase (TH) mouse IgG (clone 6dt, Abcam, Cambride, UK) 1 : 600; kinesin rabbit IgG (Abcam) 1 : 1000; Dynein mouse IgG (clone 74.1, Millipore) 1 : 500, GAPDH (Abcam). Membranes were washed for 30 min with 3 changes and incubated for 1 h at room temperature with HRP donkey anti-mouse IgG (Pierce), HRP goat anti-mouse IgM (Sigma-Aldrich), or HRP goat anti-rabbit IgG (Pierce). Immunostaining was revealed by enhanced chemiluminescence (Super-Signal West Pico Chemiluminescent, Pierce). Quantification was performed by ImageJ software (NIH, Bethesda, MD).

**Confocal analysis.** Mice were anesthetized with chloralium hydrate (320 mg/kg, i.p.) and transcardially perfused with 4% PFA in 0.1 M phosphate buffer, pH 7.4. Brains were removed, postfixed overnight in 4% PFA, and then transferred in 30% sucrose for cryoprotection. Sagittal sections (50 μm thick) were cut with a Vibratome (VT1000S, Leica). Sections were stained with porin rabbit IgG (VDAC1/porin, Abcam, Cambride, UK) and the following antibodies previously used for immmunoblotting: deTyr tubulin rabbit IgG; Tyr tubulin mouse IgG; Ac tubulin mouse IgG; porin rabbit IgG (VDAC1/porin, Abcam). To identify dopaminergic neurons and fibres, each section was concurrently stained with anti-TH antibody, made in mice (clone LCN1, Millipore) or rabbits (Millipore) as appropriate. As secondary antibodies we used Alexa Fluor™ 568 donkey anti-mouse IgG, and Alexa Fluor™ 488 goat anti-rabbit IgG (Invitrogen). Coverslips were mounted in PBS-glycerol and examined with a confocal laser scan microscope imaging system (TCS SP2 AOBS, Leica Microsystems, Heidelberg, Germany) equipped with an Ar/Ar-Kr 488 nm, 561 nm and 405 nm diode lasers. Photomultiplier gain for each channel was adjusted to minimize background noise and saturated pixels and, once defined for control conditions, parameters were kept constant for all acquisitions. To estimate the overlapping area between red and green signals, analyses were carried out on single-plane raw images and Manders' coefficients were calculated applying the JACoP plug-in (developed and reviewed by 31) for ImageJ software. To evaluate the mitochondria distribution, the porin signal was superimposed on dopaminergic fibres, using the Mask tool of the Leica Confocal Software (Leica); mitochondria accumulations were identified as white pixels-containing area, as thick as long, clearly separated from other white pixels. TH-positive signal longer than 5 μm was considered as dopaminergic fibre, and signals separated by more than 10 μm were counted as two distinct fibres.

**Immunohistochemical analysis of tyrosine hydroxylase.** Brains were removed, fixed in ethanol (60%), acetic acid (10%), and chloroform (30%), and included in paraffin. Tissue sections (30 μm) were incubated overnight with monoclonal mouse anti-TH (1 : 200; Sigma-Aldrich) and then for 1 h with secondary biotin-coupled anti-mouse antibodies (1 : 200; Vector Laboratories, Burlingame, CA). 3,3-Diaminobenzidine tetrachloride (Sigma) was used for detection.

**Stereological cell counting of tyrosine hydroxylase-positive cells in the substantia nigra pars compacta.** The number of TH-positive cells in the substantia nigra pars compacta was assessed by stereological technique and an optical fractionator using a Zeiss Axio Imager M1 microscope equipped with a motorized stage and focus control system (Zeta axis), and with a digital video camera. The software Image-Pro Plus 6.2 for Windows (Media Cybernetics, Inc., Bethesda, MD) equipped with a Macro was used for the analysis of digital images. The Macro was obtained by "Immagini e Computer" (Bareggio, Italy). The characteristics of this Macro are published[59]. The analysis was performed on 6 sections of 20 μm, sampled every 200 μm on the rostro-caudal extension, in which the substantia nigra was identified and outlined at 2.5× magnification. TH-positive cells were counted at 100× magnification as described[60]. For stereological analysis, we used a grid of disectors (counting frame of 100 × 100 μm; grid size 50 × 50 μm), with 1.3 as numerical aperture of the lens. The total number of TH-positive cells in the substantia nigra was computed from the formula: $N = \Sigma(n) \times 1/SSF \times 1/ASF \times 1/TSF$, where n is the total number of cells counted on each disector; SSF (fraction of sections sampled) the number of regularly spaced sections used for counts divided by the total number of sections across the substantia nigra pars compacta; ASF (area sampling frequency) the disector area divided by the area between disectors (7500 $\mu m^2$ × disector number/region area); and TSF (thickness sampling frequency) the disector thickness divided by the section thickness (20 μm).

**Statistical analysis and data managing.** The statistical significance of treatment was assessed by one-way ANOVA with Dunnett 2-sided or Fischer LSD post-hoc testing or $\chi^2$ test when appropriate. Analyses were performed using STATISTICA (StatSoft Inc., Tulsa, OK).


1. Sato, M., Schwart, W. H., Selden, S. C. & Pollard, T. D. Mechanical properties of brain tubulin and microtubules. *J. Cell. Biol.* **106**, 1205–1211 (1988).
2. Mitchison, T. & Kirschener, M. Dynamic instability of microtubule growth. *Nature* **312**, 237–242 (1984).
3. Inoué, S. & Salmon, E. D. Force generation by microtubule assembly/disassembly in mitosis and related movements. *Mol. Biol. Cell* **6**, 1619–1640 (1995).
4. Conde, C. & Caceres, A. Microtubule assembly, organization and dynamics in axons and dendrites. *Nat. Rev. Neurosci.* **10**, 319–332 (2009).
5. Baas, P. W. & Black, M. M. Individual microtubules in the axon consist of domain that differ both in composition and stability. *J. Cell Biol.* **111**, 495–509 (1990).
6. Trotta, N., Orso, G., Rosetto, M. G., Draga, A. & Broasle, K. The ereditary spastic paraplegia gene, spastin, regulates microtubule stability to modulate synaptic structure and function. *Neuron* **14**, 1135–1147 (2004).
7. Janke, C. & Kneussel, M. Tubulin post-translational modifications: encoding functions on the neuronal microtubule cytoskeleton. *Trends Neurosci.* **33**, 362–372 (2010).
8. Raff, M. C., Whitmore, A. V. & Finn, J. T. Axonal self-destruction and neurodegeneration. *Science* **296**, 868–871 (2002).
9. Zhai, Q. *et al.* Involvement of the ubiquitin-proteasome system in the early stages of wallerian degeneration. *Neuron* **39**, 217–225 (2003).
10. Ertürk, A., Hellal, F., Enes, J. & Bradke, F. Disorganized microtubules underlie the formation of retraction bulbs and the failure of axonal regeneration. *J. Neurosci.* **27**, 9169–9180 (2007).
11. He, Y., Yu, W. & Baas, P. W. Microtubule reconfiguration during axonal retraction induced by nitric oxide. *J. Neurosci.* **22**, 5982–5991 (2002).
12. Dauer, W. & Przedborski, S. Parkinson's disease: mechanisms and models. *Neuron* **39**, 889–909 (2003).
13. Alim, M. A. *et al.* Demonstration of a role for alpha-synuclein as a functional microtubule-associated protein. *J. Alzheimer's Dis.* **6**, 435–442 (2004).
14. Yang, F. *et al.* Parkin stabilizes microtubules through strong binding mediated by three independent domains. *J. Biol. Chem.* **280**, 17154–17162 (2005).
15. Gillardon, F. Leucine-rich repeat kinase 2 phosphorylates brain tubulin-β isoform and modulates microtubule stability: a point of convergence in parkinsonian neurodegeneration? *J. Neurochem.* **110**, 1514–1522 (2009).
16. Cappelletti, G., Surrey, T. & Maci, R. The parkinsonism producing neurotoxin $MPP^+$ affects microtubule dynamics by acting as destabilising factor. *FEBS Lett.* **579**, 4781–4786 (2005).
17. Ren, Y., Liu, W., Jiang, H., Jiang, Q. & Feng, J. Selective vulnerability of dopaminergic neurons to microtubule depolymerization. *J. Biol. Chem.* **280**, 34105–34112 (2005).
18. Cartelli, D. *et al.* Microtubule dysfunction precedes transport impairment and mitochondria damage in $MPP^+$-induced neurodegeneration. *J. Neurochem.* **115**, 247–258 (2010).
19. Brunden, K. R. *et al.* Epothilone D improves microtubule density, axonal integrity, and cognition in a transgenic mouse model of tauopathy. *J. Neurosci.* **30**, 13861–13866 (2010).
20. Zhang, B. *et al.* The microtubule-stabilizing agent, epothilone D, reduces axonal dysfunction, neurotoxicity, cognitive deficits, and Alzheimer-like pathology in an interventional study with aged tau transgenic mice. *J. Neurosci.* **32**, 3601–3611 (2012).
21. Barten, D. M. *et al.* Hyperdynamic microtubules, cognitive deficits, and pathology are improved in tau transgenic mice with low doses of the microtubule-stabilizing agent BMS-241027. *J. Neurosci.* **32**, 7137–7145 (2012).
22. Battaglia, G. *et al.* Pharmacological activation of mGlu4 metabotropic glutamate receptors reduces nigrostriatal degeneration in mice treated with 1-methyl-4-phenyl-1,2,3,6-tetrahydropyridine. *J. Neurosci.* **26**, 7222–7229 (2006).
23. Ara, J. *et al.* Inactivation of tyrosine hydroxylase by nitration following exposure to peroxynitrite and 1-methyl-4-phenyl-1,2,3,6-tetrahydropyridine (MPTP). *Proc. Natl. Acad. Sci. USA* **95**, 7659–7663 (1998).
24. De Vos, K. J., Grierson, A. J., Ackerley, S. & Miller, C. C. Role of axonal transport in neurodegenerative diseases. *Annu. Rev. Neurosci.* **31**, 151–173 (2008).
25. Morfini, G. *et al.* 1-methyl-4-phenylpyridinium affects fast axonal transport by activation of caspase and protein kinase C. *Proc. Natl. Acad. Sci. USA* **104**, 2442–2447 (2007).
26. Kin-Han, J. S., Antenor-Dorsey, J. A. & O'Malley, K. L. The parkinsonian mimetic, MPP+, specifically impairs mitochondrial transport in dopaminergic axons. *J. Neurosci.* **31**, 7212–7221 (2011).
27. Chung, C. Y., Koprich, J. B., Siddigi, H. & Isacson, O. Dynamic changes in presynaptic and axonal transport proteins combined with striatal neuroinflammation precedes dopaminergic neuronal loss in a rat model of AAV alpha-synucleinopathy. *J. Neurosci.* **29**, 3365–3373 (2009).
28. Cartelli, D., Goldwurm, S., Casagrande, F., Pezzoli, G. & Cappelletti, G. Microtubule destabilization is shared by genetic and idiopathic Parkinson's disease patients fibroblasts. *PLoS One* **7**, e37467 (2012).
29. Hirokawa, N., Niwa, S. & Tanaka, Y. Molecular motors in neurons: transport mechanisms and roles in brain function, development, and disease. *Neuron* **68**, 610–638 (2010).
30. Rogowski, K. *et al.* A Family of Protein-Deglutamylating Enzymes Associated with Neurodegeneration. *Cell* **143**, 564–578 (2010).
31. Bolte, S. & Cordelières, F. P. A guided tour into subcellular colocalization analysis in light microscopy. *J. Microsc.* **224**, 213–232 (2006).
32. Reed, N. A. *et al.* Microtubule acetylation promotes kinesin-1 binding and transport. *Curr. Biol.* **16**, 2166–2172 (2006).
33. Dunn, S. *et al.* Differential trafficking of Kif5c on tyrosinated and detyrosinated in live cells. *J. Cell. Sci.* **121**, 1085–1095 (2008).
34. Cochiolo, J. A., Ehsanian, R. & Bruck, D. K. Acute ultrastructural effect of MPTP on the nigrostriatal pathway of the C57Bl/6 adult mouse: evidence of

compensatory plasticity in nigrostriatal neurons. *J. Neurosci. Res.* **59**, 126–135 (2000).
35. Shemesh, O. A., Erez, H., Ginzburg, I. & Spira, M. E. Tau-induced traffic jams reflect organelles accumulation at points of microtubule polar mismatching. *Traffic* **9**, 458–471 (2008).
36. Hastings, T. G., Lewis, D. A. & Zigmond, M. J. Role of the oxidation in the neurotoxic effect of intrastriatal dopamine injections. *Proc. Natl. Acad. Sci. USA* **93**, 1956–1961 (1996).
37. Panda, D., Miller, H. P., Banerjee, A., Ludueña, R. F. & Wilson, L. Microtubule dynamics in vitro are regulated by the tubulin isotype composition. *Proc. Natl. Acad. Sci. USA* **91**, 11358–11362 (1994).
38. Katsetos, C. D., Herman, M. M. & Mörk, S. J. Class III beta-tubulin in human development and cancer. *Cell. Motil. Cytoskeleton* **55**, 77–96 (2003).
39. Ludueña, R. F. Are tubulin isotypes functionally significant. *Mol. Biol. Cell* **4**, 445–57 (1993).
40. Banerjee, A., Roach, M. C., Trcka, P. & Luduena, R. F. Preparation of a monoclonal antibody specific for the class IV isotype of beta-tubulin. Purification and assembly of alpha beta II, alpha beta III, and alpha beta IV tubulin dimers from bovine brain. *J. Biol. Chem.* **267**, 5625–5630 (1992).
41. Qureshi, H. Y. & Paudel, H. K. Parkinsonian neurotoxin 1-methyl-4-phenyl-1,2,3,6-tetrahydropyridine (MPTP) and alpha-synuclein mutations promote Tau protein phosphorylation at Ser262 and destabilize microtubule cytoskeleton in vitro. *J. Biol. Chem.* **286**, 5055–5068 (2011).
42. Nicklas, W. J., Vyas, I. & Hekkila, R. E. Inhibition of NADH-linked oxidation in brain mitochondria by $MPP^+$, a metabolite of the neurotoxin MPTP. *Life Sci.* **36**, 2503–2508 (1985).
43. Betabert, R. *et al.* Chronic systemic pesticide exposure reproduces features of Parkinson's disease. *Nat. Neurosci.* **3**, 1301–1306 (2000).
44. Choi, W. S., Kruse, S. E., Palmiter, R. D. & Xia, Z. Mitochondrial complex I inhibition is not required for dominergic neurons death induced by rotenone, $MPP^+$, or paraquat. *Proc. Natl. Acad. Sci. USA* **105**, 15136–15141 (2008).
45. Carré, M. *et al.* Tubulin is an inherent component of mitochondrial membranes that interacts with the voltage-dependent anion channel. *J. Biol. Chem.* **277**, 33664–33669 (2002).
46. Rostovtseva, T. K. *et al.* Tubulin binding blocks mitochondrial voltage-dependent anion channel and regulates respiration. *Proc. Natl. Acad. Sci. USA* **105**, 18746–18751 (2008).
47. Maldonado, E. N., Patnaik, J., Mullins, M. R. & Lemasters, J. J. Free tubulin modulates mitochondrial membrane potential in cancer cells. *Cancer Res.* **70**, 10192–10201 (2010).
48. Mironov, S. L., Ivannikov, M. V. & Johansson, M. $[Ca2+]_i$ signaling between mitochondria and endoplasmic reticulum in neurons is regulated by microtubules. From mitochondrial permeability transition pore to $Ca2^+$-induced $Ca2^+$ release. *J. Biol. Chem.* **280**, 715–721 (2005).
49. Wang, X. PINK1 and Parkin Target Miro for Phosphorylation and Degradation to Arrest Mitochondrial Motility. *Cell* **147**, 893–906 (2011).
50. Ries, V. *et al.* Oncoprotein Akt/PKB induces trophic effects in murine models of Parkinson's disease. *Proc. Natl. Acad. Sci. USA* **103**, 18757–18762 (2006).
51. Hirai, S., Banba, Y., Satake, T. & Ohno, S. Axon formation in neocortical neurons depends on stage-specific regulation of microtubule stability by the dual leucine zipper kinase-c-Jun N-terminal kinase pathway. *J. Neurosci.* **31**, 6468–6480 (2011).
52. Choi, W. S., Palmiter, R. D. & Xia, Z. Loss of mitochondrial complex I activity potentiates dopamine neuron death induced by microtubule dysfunction in a Parkinson's disease model. *J. Cell. Biol.* **192**, 873–882 (2011).
53. Hellal, F. *et al.* Microtubule stabilization reduces scarring and causes axon regeneration after spinal cord injury. *Science* **331**, 928–931 (2011).
54. Sengottuvel, V., Leibinger, M., Pfreimer, M., Andreadaki, A. & Fischer, D. Taxol facilitates axon regeneration in the mature CNS. *J. Neurosci.* **31**, 2688–2699 (2011).
55. Fellner, S. *et al.* Transport of paclitaxel (Taxol) across the blood-brain barrier in vitro and in vivo. *J. Clin. Invest.* **110**, 1309–1318 (2002).
56. Andrieux, A. *et al.* Microtubule stabilizer ameliorates synaptic function and behavior in a mouse model for schizophrenia. *Biol. Psychiatry* **60**, 1224–1230 (2006).
57. Lowry, O. H., Rosebrough, N. Y., Farr, A. L. & Randall, R. Y. Protein measurement with Folin phenol reagent. *J. Biol. Chem.* **193**, 265–275 (1951).
58. Fanara, P. *et al. In vivo* measurment of microtubule dynamics using stable isotyoe labeling with heavy water. *J. Biol. Chem.* **279**, 49940–49947 (2004).
59. King, M. A., Scotty, N., Klein, R. L. & Meyer, E. M. Particle detection, number estimation, and feature measurement in gene transfer studies: optical fractionator stereology integrated with digital image processing and analysis. *Methods* **28**, 293–299 (2002).
60. Gundersen, H. J. G. & Jensen, E. B. The efficiency of systematic sampling in stereology and its prediction. *J. Microsc.* **147**, 229–263 (1987).

## Acknowledgements

The authors are grateful to Dr. Alida Amadeo and Dr. Carmelita De Gregorio (Università degli Studi di Milano) for technical support and helpful discussions, and Dr. Jennifer S. Hartwig for reading and editing the manuscript. This work was supported by Fondazione Grigioni per il Morbo di Parkinson, Milan, Italy (to G.C.), and "Dote ricerca", FSE, Regione Lombardia (to D.C.).

## Author contributions

D.C. performed protein analysis by Western blotting and confocal microscopy analysis; F.C. performed immunohistochemistry; C.L.B. and G.M. performed in vivo experiments and prepared tissue for protein analysis; D.B. performed immunohistochemistry and stereological counts of tyrosine hydroxylase-positive cells; A.T. performed biochemical analysis of striatal dopamine and its metabolite levels; D.P. and E.G. designed experiments; D.C., G.P., G.B. and C.G. designed the experiments, analysed the data and wrote the paper.

## Additional information

**Supplementary information** accompanies this paper at http://www.nature.com/scientificreports

**Competing financial interests:** The authors declare no competing financial interests.



**How to cite this article:** Cartelli, D. *et al.* Microtubule Alterations Occur Early in Experimental Parkinsonism and The Microtubule Stabilizer Epothilone D Is Neuroprotective. *Sci. Rep.* **3**, 1837; DOI:10.1038/srep01837 (2013).

**MICROTUBULE ALTERATIONS OCCUR EARLY IN EXPERIMENTAL PARKINSONISM AND THE MICROTUBULE STABILIZER EPOTHILONE D IS NEUROPROTECTIVE**

Daniele Cartelli, Francesca Casagrande, Carla Letizia Busceti, Domenico Bucci, Gemma Molinaro, Anna Traficante, Daniele Passarella, Erminio Giavini, Gianni Pezzoli, Giuseppe Battaglia, Graziella Cappelletti[1]

**Supplementary Figure S1**. **MPTP does not affect the levels of motor proteins**.

**(a)** Immunoblot of levels of kinesin (Kin) and dynein (Dyn) in lysates of striatum and substantia nigra of mice treated as in Fig. 1. (**b**) Densitometric analyses of immunoblot reported in **d** (mean ± S.E.M., n = 4-6 mice per group). hpi = hours post last injection of MPTP.

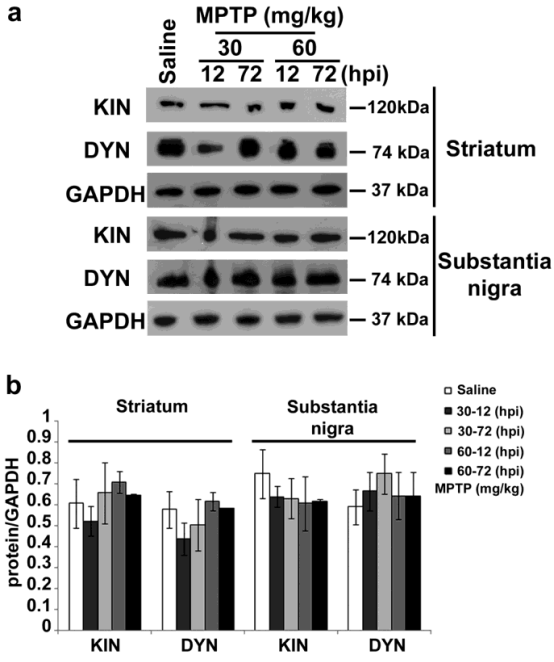

**Supplementary Figure S2**. **MPTP affects MT stability inside dopaminergic fibres.**

Confocal images of the nigrostriatal pathways of mice treated as in Fig. 1. Green represents TH staining and red signals the various tubulin PTMs. Scale bar = 50 μm. hpi = hours post last injection of MPTP.

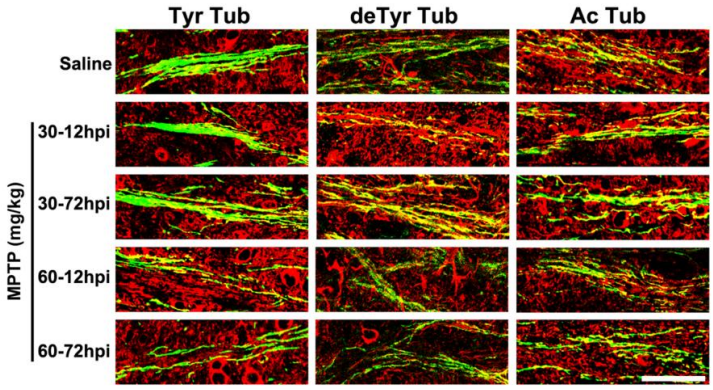

***Supplementary Table S1***

Analysis of M2 parameter (TH vs. tubulins) in striatal section.

| | Tyr Tubulin | deTyr Tubulin | Ac Tubulin |
|---|---|---|---|
| Saline | 0.79±0.019 | 0.77±0.049 | 0.88±0.040 |
| MPTP, 30 mg/kg (12 h) | 0.77±0.052 | 0.92±0.017 | 0.79±0.043 |
| MPTP, 30 mg/kg (72 h) | 0.75±0.043 | 0.90±0.041 | 0.86±0.026 |
| MPTP, 60 mg/kg (12 h) | 0.64±0.052 | 0.85±0.048 | 0.80±0.049 |
| MPTP, 60 mg/kg (72 h) | 0.67±0.083 | 0.94±0.081 | 0.94±0.011 |

Data are expressed as mean ± S.E.M., n=4 sections for each mouse from 4-6 mice per group.

***Supplementary Table S2***

Analysis of the Fluorescence Intensity (AU) inside dopaminergic neuron.

| | Tyr Tubulin | deTyr Tubulin | Ac Tubulin |
|---|---|---|---|
| Saline | 93.6 ± 3.6 | 32.9 ± 2.8 | 28.8 ± 3.1 |
| MPTP, 30 mg/kg (12 h) | 48.0 ± 4.9 (*) | 104 ± 6.5 (*) | 58.2 ± 6.5 (*) |
| MPTP, 30 mg/kg (72 h) | 77.5 ± 6.9 | 97.9 ± 5.6 (*) | 89.6 ± 5.3 (*) |
| MPTP, 60 mg/kg (12 h) | 22.8 ± 4.4 (*) | 106 ± 8 (*) | 25.2 ± 4.7 |
| MPTP, 60 mg/kg (72 h) | 53.6 ± 8.3 (*) | 20.6 ± 3.8 | 2.4 ± 1.3 (*) |

Data are expressed as mean ± S.E.M., n=4 sections for each mouse from 4-6 mice per group. *$P <$ 0.05; one-way ANOVA, Dunnett *post hoc*: *versus* saline-injected mice.

Manuscript 3
Cartelli et al., *Submitted*

# α-Synuclein is a Novel Microtubule Dynamase

**Daniele Cartelli**[1,§]
Email: daniele.cartelli@unimi.it
**Alessandro Aliverti**[1]
Email: alessandro.aliverti@unimi.it
**Alberto Barbiroli**[2]
Email: alberto.barbiroli@unimi.it
**Carlo Santambrogio** [3]
Email: carlo.santambrogio@unimib.it
**Enzio M. Ragg**[2]
Email: enzio.ragg@unimi.it
**Francesca Casagrande**[1]
Email: francesca.casagrande@unimi.it
**Carmelita De Gregorio**[1]
Email: carmelita.degregorio@unimi.it
**Vittorio Pandini**[1]
Email: vittorio.pandini@unimi.it
**Marco Emanuele**[4]
Email: marco.emanuele@iit.it
**Evelina Chieregatti** [4]
Email: Evelina.Chieregatti@iit.it
**Stefano Pieraccini**[5]
Email: stefano.pieraccini@unimi.it
**Staffan Holmqvist**[6,7]
Email: staffan.holmqvist@med.lu.se
**Laurent Roybon**[6,7]
Email: laurent.roybon@med.lu.se
**Gianni Pezzoli**[8]
Email: pezzoli@fondazioneparkinson.com
**Rita Grandori**[3]
Email: rita.grandori@unimib.it
**Isabelle Arnal**[9]
Email: isabelle.arnal@ujf-grenoble.fr
**Graziella Cappelletti**[1,*]
Email: graziella.cappelletti@unimi.it

[1]Dept. Biosciences, Università degli Studi di Milano, Milano (Italy);
[2]Dept. of Food, Environmental and Nutritional Sciences, Università degli Studi di Milano, Milano (Italy);
[3]Dept. Biotecnology and Biosciences, Università degli Studi di Milano-Bicocca, Milano (Italy);
[4]Dept. Neuroscience and Brain Technologies, Istituto Italiano di Tecnologia, Genova (Italy);
[5]Dept. Chemistry, Università degli Studi di Milano, Milano (Italy);
[6] Stem Cell laboratory for CNS Disease Modeling, Wallenberg Neuroscience Center, Department of Experimental Medical Science, Lund University, Lund, Sweden;
[7] Strategic Research Area MultiPark and Lund Stem Cell Center, Lund University, Lund, Sweden
[8]Parkinson Institute, Istituti Clinici di Perfezionamento, Milano (Italy);
[9]Grenoble Institut des Neurosciences, Grenoble (France).

[*]Corresponding author to whom correspondence and proofs are to be sent:
Graziella Cappelletti, Università degli Studi di Milano, Dept. Biosciences, Via Celoria 26, 20133 Milano, Italy, Tel.: 0039 02 50314752; E-mail: graziella.cappelletti@unimi.it

[§]Co-corresponding author:
Daniele Cartelli, Università degli Studi di Milano, Dept. Biosciences, Via Celoria 26, 20133 Milano, Italy, Tel.: 0039 02 50314748; E-mail: daniele.cartelli@unimi.it

**ABSTRACT**

**Background:** α-Synuclein is a presynaptic unfolded protein associated to Parkinson's disease. After decades of intense studies, α-Synuclein physiology is still difficult to clear up due to its interaction with multiple partners and its involvement in a *pletora* of neuronal functions. Here, we looked at the remarkably neglected interplay between α-Synuclein and microtubules, which potentially has a profound impact on synaptic functionality.

**Results:** We first show that human α-Synuclein is able to set microtubule mass at the presynapse by inducing microtubule nucleation and by modulating their dynamics in a rat neuronal cell line. Confocal analyses indicated that these are direct effects, since transfected human α-Synuclein show a significant higher degree of co-localization with the most dynamic microtubule pool. As well, endogenous α-Synuclein co-localizes with polymerization prone subsets of microtubules in both murine primary neuronal cultures and human neurons. In order to identify the mechanisms underlying these actions, we investigated the interaction between purified α-Synuclein and tubulin. We demonstrated that α-Synuclein binds to microtubules and the tubulin $\alpha_2\beta_2$ tetramer; the latter interaction induces the formation of helical segment(s) in the α-Synuclein polypeptide. This structural change enables α-Synuclein to promote microtubule nucleation and to enhance both microtubule growth rate and catastrophe frequency. Finally, we showed that α-Synuclein variants that are linked to Parkinson's disease do not undergo tubulin-induced folding and cause tubulin aggregation rather than polymerization, *in vitro* as well as in neuronal cells.

**Conclusions:** Our data enable us to propose α-Synuclein as a novel, foldable, microtubule-dynamase, which organizes the microtubular cytoskeleton at the presynapse, through its binding to tubulin and its regulation of microtubule nucleation and dynamics, and lend support to the concept that the α-Synuclein/microtubule interaction plays a pivotal role in modulating synaptic physiology and in causing neuronal dysfunction.

**Keywords**

α-Synuclein, tubulin, microtubules, protein folding, Parkinson's disease

## BACKGROUND

Microtubules (MTs) are dynamic polymers consisting of αβ tubulin dimers that play an essential role in cell shape acquisition and in the performance of many intracellular processes [1]. In large cells, such as neurons, little is known about how MTs nucleate far away from the cell body and the MT-organizing center, i.e. in the axonal compartment, and about the regulation of the MT dynamics underlying synaptic functions. Many MT-interacting proteins are believed to regulate these phenomena; for example, dispersed γ tubulin complexes are reliable nucleating structures in the axon [2].

Nowadays, there is increasing evidence for a direct interplay between MTs and α-Synuclein (Syn), a presynaptic protein widely expressed in brain tissues. Despite the controversial issues on its physiology, Syn has been clearly associated with neurodegeneration, since its overproduction due to multiplications of the *SNCA* locus encoding for Syn and point mutations in the gene itself cause familial forms of Parkinson's disease (PD) [3]. The underlying pathogenic mechanism is still unclear. Cytotoxicity is currently attributed to Syn oligomers [4], whose overexpression induces MT disruption in cells [5]. MT disruption is also achieved by incubating cells with extracellular Syn [6, 7]. Furthermore, tubulin is known to promote Syn fibrillation *in vitro* [8]. However, it is not clear whether destabilization of the MT cytoskeleton potentiates [9] or prevents [10] Syn aggregation *in vivo*.

Although many efforts have been devoted to the identification of a link between tubulin and Syn in pathological contexts, their physiological interaction has been largely ignored. Alim and colleagues [11] have revealed that wild type (WT) Syn promotes MT assembly, whereas Chen and colleagues have claimed that neither monomeric nor oligomeric Syn influences MT polymerization *in vitro* [12]. Here we point out the physiological relevance of the interaction between Syn and MTs, showing that Syn organizes the MT cytoskeleton at the presynapse, through its binding to tubulin and its regulation of MT nucleation and dynamics.

## RESULTS

### Syn induces MT nucleation and increases MT dynamics in neuronal cells

To define the effects of Syn on MT system, we looked at two essential steps in the MT assembly process, i.e. the regulation of MT nucleation and MT dynamics. Up to now, it has been reported that the only nucleating structures in the axon are the plus ends of pre-existing MTs [13] or the dispersed γ tubulin complexes [2]. Syn is a presynaptic protein [3] and could likely interact with MTs in axon terminals. Thus, we assessed its ability in nucleating MTs in distal neurites using differentiated rat PC12 cells, a long-standing model of sympathetic neuronal differentiation. PC12 cells naturally express rat Syn starting from 7$^{th}$ day of NGF treatment [14], therefore we decided to perform experiments at 5$^{th}$ day of NGF-induced differentiation when parental PC12 cells lack of endogenous Syn whereas transfected ones display expression of either WT or mutant human Syn (Figure S1). Thereby, we analysed the distal neurite of differentiated PC12 cells expressing either WT GFP-Syn or GFP alone under basal conditions (cells kept at 37 °C), after MT-destabilizing cold-treatment (30 min at 4 °C), and during MT (re)nucleation (15 and 60 min at 37 °C); α tubulin staining shows the presence of MTs in cells overexpressing WT Syn after 15 min of re-warming unlike control cells and MTs are more abundant in transfected than in control cells after 60 min of rewarming (Figure 1A). This suggests that the recovery of MT network is more favoured in the presence than in the absence of WT Syn. In order to substantiate our observations, we next removed the pool of unassembled tubulin and measured the fluorescence of total α tubulin (Figure 1B), which is proportional to MT mass, and of tyrosinated (Tyr) tubulin (Fig. 1C), which is associated with dynamic and neo-synthetized MTs [15]. The quantification was performed in the distal part of the neurite taking into account total fluorescence intensities that were measured in comparable areas, as shown in Figure S2. Our analysis reveals that, after 15 min of re-warming, the presence of Syn significantly increases α tubulin fluorescence and, notably, enhances Tyr MTs, highlighting that Syn favours MT (re)nucleation. In parallel, we performed biochemical analyses on cytoskeletal fractions obtained from cells following destabilization and (re)nucleation of MTs as described above. We measured the amount of α tubulin and Tyr tubulin associated to cytosolic dimers and to polymeric MTs under basal conditions, after MT-destabilizing cold-treatment, and during MT (re)nucleation (Figure 1D-E). Our results show, a significant Syn-dependent increase of α tubulin and Tyr tubulin incorporated into MTs. Collectively, our results indicate, for the first time, that WT Syn promotes MT nucleation in neuronal cells.

We next used end-binding protein 3 (EB3)-mCherry [16], a fluorescent protein which specifically binds growing MT plus-ends, and live cell imaging to visualize MT dynamics under basal conditions or during the MT recovering phase following cold-treatment (Figure 2). This approach reveals that Syn increases the number of detectable growing MTs per cell (Figure 2C), even though the analysed surfaces do not change (Figure S3), and thus confirms that Syn favours MT nucleation. Moreover, Syn accelerates MT growth (Figure 2B-D) and reduces MT lifetime (Figure 2E), the latter observation being consistent with an enhancement of the catastrophe frequency.

To elucidate whether Syn acts as a simple catalyst or, in addition, steadily interacts with MTs, we examined the interplay between Syn and MTs in PC12 cells and primary cultures from mouse ventral mesencephalon. Confocal analyses show that both transfected human Syn in PC12 cells and endogenous mouse Syn in primary mesencephalic neurons decorates MTs at growth cone and distal neurite (Figure S4). We performed the analyses of co-localization parameters [17] that allow to correlate the distribution of Syn with different MT subpopulations. As pointed out in Table 1, Syn preferentially co-localizes with the most dynamic MT subset, i.e. the Tyr and βIII MTs, as revealed by the higher value of superimposition between the Syn and tubulin(s) signals. These latter data are consistent with the already reported interaction of Syn with tubulin βIII isotype [10]. To confirm the relevance of our observations, we assessed endogenous human Syn localisation in midbrain neurons derived from human embryonic stem cells and showing dopaminergic phenotype (Figure 3). Our confocal analyses confirm that Syn decorates polymerization-prone MTs, with a mild preference for Tyr MTs in respect to βIII MTs as revealed by Manders' coefficients, 0.57±0.08 and 0.46±0.06, respectively. Our analyses therefore suggest that Syn promotes MT dynamics at neuronal growth cone via its preferential association with Tyr-enriched MTs. Moreover, these data are a clear and convincing indication of an interaction between Syn and tubulin in human samples.

**Syn binds to MTs and folds upon interaction with the tubulin $\alpha_2\beta_2$ tetramer**

In order to further investigate the mechanism by which Syn regulates MTs and to exclude that the above results were mediated by the action of a third player, we studied the interaction between purified Syn and tubulin. First of all, differential interference contrast (DIC) and fluorescence microscopy analyses confirmed that WT Syn co-polymerizes with MTs (Figure S5). Co-sedimentation assay, an approach which allows investigating the capability of a protein to bind polymerized and stabilized MTs, revealed that Syn also interacts with

preformed MTs (Figure 4A-B) and enabled us to calculate an apparent $K_d$ of 7.48 ± 1.38 μM, which is indicative of loose binding between Syn and MTs. These data confirm our results obtained in cells (see Figure 3 and Figure S4) and the already reported binding of Syn to MTs [11]. Previously reported co-immunoprecipitation and affinity chromatography offer additional evidence that Syn interacts with free tubulin [18], although it is still unclear whether it forms a complex with tubulin dimers or with higher-order assemblies. This issue has been addressed by native mass spectrometry (MS) and nano-electrospray ionization (nano-ESI). The spectra of 14 μM tubulin and a mixture of 14 μM tubulin and 14 μM Syn (Figure 4C-F) show that Syn forms a specific complex with the tubulin $\alpha_2\beta_2$ tetramer. The measured mass of the complex (217.8 kDa) was in agreement with the calculated one and its average charge (34.5+) is close to the expected value for a globular protein of the same mass (36.1+) [19], suggesting that the complex has a compact conformation. Therefore, Syn seems to acquire an ordered structure upon binding. However, bound Syn does not necessarily have a globular conformation; it cannot be ruled out that the protein wraps around the tubulin tetramer in an ordered, but extended conformation. Structural changes resulting from the tubulin/Syn interaction were studied by far UV circular dichroism (CD). These studies confirmed that Syn is unfolded in the absence of the ligand, whereas an equimolar Syn/tubulin mixture gives an overall secondary structure CD signal, which is more intense than the sum of the signals of the two individual proteins (Figure 5A). Moreover, the CD signal originating in the mixture shows a minimum at 220 nm, which is typical of α-helix structures. Considering that (i) the interaction of tubulin with ligands is widely studied and an increase in its α-helix content has never been observed, and (ii) Syn is a soluble, intrinsically unfolded protein [20, 21] able to adopt α-helix structure in adequate conditions [22], we hypothesize that Syn folds into a structure of high α-helix content upon its interaction with tubulin. This resembles the behavior (in terms of complex stoichiometry and secondary structure transition) of the complex formation between tubulin and RB3-SLD (Figure 5B). The latter protein belongs to the stathmin-like family of proteins, which share several structural features with Syn, as discussed below. According to this hypothesis, the CD spectra of Syn in a complex with tubulin has been extrapolated (Figure 5A, differential spectrum) and the related α-helix content estimated as 35%. It is worth remembering that such helical content does not reflect the amount of α-helix in a single folded molecule, but rather the average content of α-helix in the whole sample, taking into account the Syn folded molecules that interact with tubulin and the unfolded ones that remain free in solution. Evidence for the formation in solution, at neutral pH, of a Syn/tubulin complex came from $^1$H-NMR diffusion

measurements (Figure 5C). Tubulin had a diffusion coefficient (D= $0.37x10^{-10}$ $m^2sec^{-1}$) consistent with the presence of αβ dimers in solution, whereas Syn showed a D value (D= $0.83x10^{-10}$ $m^2sec^{-1}$) smaller than expected for a globular ~14 kDa protein and consistent with the presence of unfolded species [23]. In the presence of tubulin, the diffusion coefficient measured for Syn significantly decreased from $0.83x10^{-10}$ $m^2sec^{-1}$ to $0.59x10^{-10}m^2sec^{-1}$. This clearly indicates complex formation; however, as the measured value is actually less than that one expected for a stable 1:1 complex, it should be concluded that in our conditions a certain fraction of Syn still remains in its free state in solution and that the Syn molecules exchange between the free and bound states at a rate which is fast compared to both the NMR chemical shift and diffusion measurement time scales (fast exchange limit, $k_{ex} < 100$ $sec^{-1}$). The fraction of free Syn has been estimated within the 45-55% range, leading to a corresponding estimate of the Syn/tubulin dissociation constant between 10 and 20 μM.

Altogether, our data provide a relatively detailed insight into the binding of Syn to tubulin and MTs, demonstrating, for the first time, the formation of a complex between Syn and the tubulin $\alpha_2\beta_2$ tetramer, which enables us to posit a Syn folding step.

**Folded Syn promotes MT nucleation and increases MT dynamics**

Until now, the effects of Syn on MT polymerization have been studied without a preincubation [11, 12] that is to say without previous induction of Syn folding. Here, we decided to incubate Syn for 10 min at 20 °C with tubulin in order to allow Syn conformational rearrangement (as demonstrated in Figure 5) and, then, we carefully analysed the tubulin assembly kinetics (Figure 6A-B), finding that only pre-folded Syn impacts MT assembly, as revealed by the impacts on initial velocity of polymerization (Vi) and MT assembly at plateau (ΔA). By plotting log(A(t)/A∞) against log(t) we extrapolated the parameter *P*, which is indicative of the successive steps during the nucleation phase [24]; the significant reduction of *P* (Figure 6B) and of tubulin critical concentration (Figure 6C), underscored the ability of structured Syn to nucleate MTs, in agreement with the above reported effects in neuronal cells (Figure 1). Electron microscopy analyses revealed the conventional ultrastructure of MTs assembled in the presence of folded Syn (Figure 6D). Furthermore, we estimated the length and the number of assembled MTs in the presence of folded Syn (Figure 6 E-G), during the early phase and at the steady state of the polymerization process, by using optical microscopy and fluorescent tubulin (Figure S6), which allow the analyses of higher amount of MTs. Our analyses revealed that Syn leads to formation of shorter and more abundant MTs. Thus, besides stimulating MT nucleation, Syn might reduce MT elongation, either by slowing down

MT growth rate or increasing catastrophe frequency, as strongly suggested by the reduction in (initial velocity of polymerization *in vitro*) and the reduction of MT growth lifetime in cells. Notably, this would explain the decrease in total polymer mass (ΔA in Figure 6A-B).

Thus, we used video-enhanced differential interference contrast (VE-DIC) light microscopy to analyse Syn effects on MT dynamics directly (Table 2). Tubulin (10 and 15 μM) was assembled from purified axonemes, in the absence or in the presence of increasing concentrations of Syn (0-15 μM). These protein to protein ratios are comparable to those observed *in vivo,* since the actual cellular concentration of tubulin is up to 40 μM [25] and the estimated presynaptic Syn concentration varies between 30 and 60 μM in neurons [26]. At low tubulin concentrations (10 μM), Syn dramatically increased catastrophe frequency, up to 6.5-fold in comparison to the control, an effect that was mitigated at the highest tubulin concentration (15 μM). With the two highest Syn concentrations (10 and 15 μM), we also noticed a significant increase in the MT growth rate in the presence of 15 μM tubulin. These results indicate that Syn increases MT dynamics by speeding up the growth rate and promoting catastrophe events. Altogether, our data demonstrate that, upon interaction with the tubulin $\alpha_2\beta_2$ tetramer, Syn acquires helical structure and becomes able to govern multiple steps of MT assembly and dynamics, such as nucleation, growth rate and catastrophe frequencies, both in purified systems and in neuronal cells.

**Syn displays sequence similarity to stathmin**

Syn displays striking structural and functional similarities with the tubulin-interacting protein stathmin. Both of them are about 14-15 kDa, intrinsically disordered proteins, capable of adopting α-helix conformation upon interaction with binding partners [28, 29]. It is noteworthy that Syn, like stathmin and RB3-SLD, interacts with the tubulin $\alpha_2\beta_2$ tetramer and promotes MT catastrophes. Thus, we explored sequence similarities between Syn and the members of the stathmin family. Pairwise alignment of WT Syn to stathmin showed about 20% identical residues and over 50% conservative substitutions. Interestingly, the 21-residue fragment centred around Syn residue 53, in which four of the five PD-linked point mutations are clustered [30], aligned to a functionally relevant region of the stathmin family (Figure 7, blue lines), namely one of the tubulin-binding domains [31]. This region displays multiple invariant residues (Figure 7, asterisks), including the sites of the Syn pathological mutations A53T and E46K (Figure 7, red arrows), besides several other conservative or semi-conservative substitutions (Figure 7, colons and dots, respectively). Therefore, the pathological point mutations likely compromise Syn/tubulin interaction. These data

demonstrate that Syn and stathmin share physico-chemical and functional properties. Furthermore, the good alignment with functionally relevant regions of stathmin strongly indicates that Syn and proteins belonging to the stathmin-family may be involved in the same biological processes, namely the regulation of MT cytoskeleton.

**Pathological Syn mutations corrupt Syn/tubulin interaction**

Having shown that four out of five PD-linked mutations map to the putative tubulin-binding domain of Syn (Figure 7), these substitutions are expected to have a profound effect on protein-protein interactions and, therefore, on Syn induced folding. Indeed, CD analyses revealed that the A53T variant is much less sensitive than WT Syn to the structuring effect of tubulin (Figure 8A). Although the pathological A30P mutation mapped far away from the tubulin-interacting domain (Figure 7), this amino acid substitution has the potential to interfere with tubulin-induced folding of Syn, as confirmed by CD analyses (Figure 8A). As a consequence, MTs assembled following preincubation with A30P and A53T mutants are conventional but flanked and surrounded by abundant tubulin aggregated *in vitro*, as revealed by both optical (Figure S5) and electron microscopy (Figure 8B). NGF-differentiated PC12 cells expressing mutant GFP-Syn showed a lower extent of individual MTs (Figure 8C) in respect to control cultures (as shown in Figure S4); furthermore, MTs seem to be confined into the most proximal part of the growth cone (Figure 8C). Noteworthy, during the recovery after cold-induced depolymerization, the presence of mutant Syns causes MT bundling and aggregation (Figure 8D) instead of proper regrowth as we observed with WT Syn (Figure 1A). Co-localization analysis reveals a slight, but significant, reduction in Syn/tubulin overlapping (Table 1), which we hypothetically attribute to the aberrant conformation of the mutated Syn. Furthermore, these analyses revealed a decrease in the co-localization between mutated Syn and Ac tubulin and no change in the supposed interaction with deTyr MTs. The impaired binding can likely result from conformational changes due to aminoacidic substitutions in mutants Syn. Indeed, our data revealed that mutant Syn forms do not undergo tubulin-induced folding and promote tubulin aggregation rather than polymerization *in vitro*, as well as in neuronal cells. Therefore, mutant Syn forms impair the correct organization of the MT system and, consequently, could have a profound impact on neuronal processes in which Syn is implicated, as for example neuronal differentiation [32, 33]. Indeed, our analyses (Figure S7) show that mutant Syns reduce morphological differentiation of PC12 cells, whereas the WT one slightly favours this process, in agreement with the effects on MT nucleation and dynamics we undisclosed.

## DISCUSSION

As stated by Feng and Walsh [34] a decade ago: "Protein-protein interactions are a little like human relationships. Some are dedicated, faithful and lifelong, while other relationships are brief flings with a promiscuous variety of partners that may leave no lasting trace or may induce profound changes". Here we show that the interplay between Syn and tubulin is a multifaceted protein-protein interaction. Indeed, their encounter triggers the structural rearrangement of Syn which, in turn, regulates the birth, the growth and the lifespan of individual MTs. Therefore, we set forth the hypothesis that Syn is a MT "dynamase", a term introduced by Erent and colleagues [35] for Kinesin-8, which is able to regulate both MT nucleation and catastrophes in *S. pombe*, exactly as Syn does in neuronal cells, setting MT mass at the neuronal growth cone.

MTs exhibit non-equilibrium dynamics that depend on free-tubulin concentration. In cell systems, a constant free tubulin concentration, and the presence of a multitude of MT-interacting proteins, likely buffers and mitigates perturbations in MT dynamics, conferring a degree of robustness and homeostasis to the MT cytoskeleton [36]. Such a mechanism could explain why we did not observe large differences in tubulin partitioning between polymerized and free tubulin in the presence of Syn under basal conditions, differences that, in contrast, are magnified under stress conditions, such as cold treatment, in which the free tubulin content changes considerably. When tubulin concentration is high, the initial response of a MT-associated protein will be potent and would induce MT assembly, as we observe at the beginning of assembly kinetics in the presence of Syn or in VE-DIC experiments performed at high tubulin concentrations. In the mechanistic model we propose, the ability of Syn to interact with the tubulin $\alpha_2\beta_2$ tetramer enables Syn to fold (Figure 9, STEP 1) and, possibly, to act as a tubulin carrier by delivering small tubulin oligomers ($\alpha_2\beta_2$ tetramers), which have recently been recognized as the species that usually occurs in MT nuclei and is added during MT elongation [37]. This is a very controversial issue. Indeed, while a previous paper stated that MT assembly occurs almost exclusively via single-subunit addition [38], a concomitant study proposed that +TIPs proteins share the ability of multimerizing tubulin, thus acting as polymerization chaperones that aid in subunit addition to the MT plus ends [39]. Thus, Syn could either crosslink tubulin heterodimers, inducing nucleation (Figure 9, STEP 2-high $[Tub]_{free}$), and/or stabilize them in a favourable orientation promoting the supramolecular interactions involved in MT formation. As net polymerization is promoted, the free tubulin concentration drops down, mitigating the assembly-inducing activity of Syn, as observed at

the steady state of assembly kinetics or with low tubulin concentrations in VE-DIC experiments, when catastrophe stimulation prevails. How are these catastrophe events induced? If we consider stathmin, the destabilization of MT is supposed to rely on two possible mechanisms [40]: (i) the sequestering of soluble tubulin into an assembly-incompetent tubulin/stathmin complex, which has the same stoichiometry of the Syn/tubulin complex observed here, or (ii) the direct binding to MT ends, which would increase the frequency of switching from growth to shortening. The mechanism by which Syn promotes MT catastrophes is not known. It is unlikely that it acts by sequestering tubulin dimers, since such a phenomenon would reduce MT growth rate in contrast to our observations. We hypothesize that, once bound to the MT lattice, Syn affects the whole stability of the polymer, inducing a change in the intra- or inter-dimer angle that amplifies the intrinsic tendency of MTs to undergo catastrophes (Figure 9, STEP 2-low $[Tub]_{free}$). Nevertheless, further studies are needed to definitively solve the mechanism by which Syn promotes MT catastrophes.

Besides a similar effect on MT catastrophes and similar binding to tubulin tetramer, we also show that the primary structure of Syn and stathmin is very similar. Considering that both Syn knock-out [41] and stathmin knock-out [42] mice develop normally and show neuronal defects only with aging, we propose the existence of some functional redundancies. Indeed, both stathmin [43] and Syn, as we demonstrated here, are involved in the regulation of neuronal process outgrowth. Our data confirm the recent evidence that WT Syn promotes neuronal differentiation [33] and, notably, provide a possible mechanistic explanation, showing that Syn enhances both MT dynamics and stability, which are crucial aspects of axon specification [44] and elongation [2]. Also the effects of Syn on MT dynamics support our hypothesis of a possible biological redundancy between Syn and the proteins belonging to the stathmin family, especially under forcing circumstances. Indeed, the mean MT growth rate in basal condition is mildly affected by the presence of Syn (p value = 0.02) but it is more significantly speeded up under stressful condition, i.e. recovery after cold treatment (p value = 0.007). These data are clearly supported by the analyses on pure protein; hence, we can imagine a realistic biological significance for the Syn-mediated regulation of MT dynamics especially under limiting conditions, and this can give reason why the alteration of Syn (i.e. mutations) takes time to become detrimental (i.e. during aging processes). Furthermore, our co-localization analyses, performed on rat PC12 cell line as well as on murine and human neurons, showed that Syn displays some specificity toward MT subtypes, preferentially interacting with the most polymerization-prone MTs, which allows Syn to be in the right place at the right time. Indeed, the ability of Syn to interact with many fundamental synaptic

elements makes it the master of control at the synapse. Syn interacts with synaptic vesicles [45] and its chemistry enables it to work as a membrane-curvature sensor mediating selective lipid binding [46]. Furthermore, Syn regulates the polymerization of both actin [47] and MT cytoskeleton and, in addition, interacts with Tau [48], a neuronal MT associated protein that bundles MTs and modulates the interplay with actin microfilaments [49]. As a whole, this body of evidence indicates that Syn is a central player in coordination the interactions between membrane phospholipids and cytoskeletal proteins, which are necessary to govern force at cell cortex and synapses, to organize membrane subdomains and, in turn, to modulate axon advancement.

Here, we demonstrate that PD-linked Syn variants do not exhibit binding-induced folding in the presence of tubulin and induce tubulin aggregation instead of proper MT assembly. A30P mutation is located on the short helix of the lipid-folded Syn [30], and the fact that the polypeptide region that includes this mutation is not part of the putative tubulin-interacting domain could explain why it is the most "benign" PD point mutation [50]. Conversely, the other 4 described point mutations of Syn (E46K, H50Q, G51D and A53T) fall inside a region corresponding to the tubulin-interacting domain of proteins belonging to the stathmin family, providing a stimulating mechanistic insight into the molecular pathology of PD. Indeed, as we and others [11] have demonstrated, Syn mutations induce tubulin aggregation, and both Syn [52] and tubulin [52] occur in Lewy bodies, the pathological hallmark of PD. Furthermore, Lewy bodies and, more specifically, excessive MT bundles engulf axons [53]. It has been reported that mutant Syn is defectively transported [54] and induces alterations of cytoskeletal and motor proteins [55]. Therefore, axonal transport disruption could be the missing link between Syn/tubulin interaction and PD. In accordance, a very recent paper showed that Syn oligomers, the most toxic Syn species, reduce MT stability, kinesin/MTs interplay and neuritic kinesin-dependent cargoes, promoting early neurite pathology [5]. Although alteration of axonal transport is considered one of the earliest events in neurodegeneration [56], we showed that it follows MT dysfunction in the 1-methyl-4-phenyl-1,2,3,6-tetrahydropiridine-induced model of PD [57, 58]. Hence, MT dysfunction may trigger the chain of events leading to PD. Indeed, MT-targeted molecules have beneficial effects in both 1-methyl-4-phenyl-1,2,3,6-tetrahydropiridine-treated [58] and Syn-overexpressing [59] mice and the correction of MT defects rescues control phenotype and cell homeostasis in PD patient derived cell lines [60-62]. Therefore, providing insights into the interaction between Syn and MT, our data would clear up some essential steps in neuronal function and degeneration.

## CONCLUSIONS

Many controversial issues remain to be clarified, such as solving the puzzle of the actual naïve state of Syn: is it a folded tetramer [63] or a labile unstructured monomer [21]? Nevertheless, here we have demonstrated that monomeric Syn forms a specific complex with the tubulin $\alpha_2\beta_2$ tetramer, acquiring a defined secondary structure. We could speculate that local accumulation of free tubulin dimers would change the equilibrium between unfolded and tetrameric Syn, which may have evolved to act as a sensor for the state of MT cytoskeleton. In addition, we have clearly shown the co-localization between Syn and the different MT subpopulations, with a preference for polymerization prone subtypes, in various models of neuronal cells, ranging from differentiated rat PC12 cells to murine and human mesencephalic neurons. Last, but not least, we have unmasked a new physiological role for Syn, namely that it locally regulates both MT nucleation and dynamics. Therefore, we propose that Syn can be considered a neuronal MT dynamase, which sets MT mass at the presynapse.

## METHODS

### Protein purification

Tubulin was purified by two cycles of polymerization/depolymerization in high molar Pipes buffer [64], suspended in BRB buffer (80 mM K-Pipes, pH 6.9, 2 mM EGTA, 1 mM $MgCl_2$), snap-frozen in liquid nitrogen, and stored in small aliquots at -80 °C.

Recombinant Syn was overproduced in *Escherichia coli* using the plasmid constructs and culturing conditions reported by Martinez et al. [65]. Recombinant RB3-SLD (kindly gifted by prof. Patrick A. Curmi, Evry University, France) was produced and purified according to Charbaut et al. [66]. For the isolation of both proteins, bacterial pellets were lysed by sonication and followed by incubation at 90 °C for 5 min. After removal of cell debris and denatured proteins by centrifugation, supernatants were subjected to ion exchange chromatography on a Q Sepharose HP column (GE Healthcare, Uppsala, Sweden). Aliquots of Syn (in 20 mM Hepes, pH 7.4, 100 mM KCl) and RB3-SLD (in 10 mM Hepes, pH 7.2,150 mM NaCl) were snap-frozen in liquid nitrogen and kept at -80 °C until needed. Each aliquot was clarified by ultracentrifugation (230000×*g* at 4 °C for 30 min) immediately before use.

### MT self-assembly

The kinetics of tubulin polymerization was studied using a standard protocol [67] or after preincubation with Syn. Reactions were followed turbidimetrically at 350 nm in a multimode plate reader (Infinite 200Pro, Tecan, Mannedorf, Switzerland) equipped with a temperature controller. Tubulin was diluted to different concentrations in assembly buffer (80 mM K-Pipes, pH 6.9, 2 mM EGTA, 1 mM $MgCl_2$, 10% glycerol, and 1 mM GTP), previously degassed, and kept on ice; as WT or mutated Syns were added, the reaction was started by warming the solution at 37 °C. For the preincubation, two solutions were prepared: T1 (80 mM K-Pipes, pH 6.9, 2 mM EGTA, 1 mM $MgCl_2$, 20% glycerol, and 2 mM GTP) and T2 (80 mM K-Pipes, pH 6.9, 2 mM EGTA, 1 mM $MgCl_2$, and double of the final protein concentration); T2 was incubated 10 min at 20 °C, allowing Syn folding, but preventing tubulin polymerization; the reaction was started mixing T1 and T2 1:1 and raising the temperature at 37 °C.

Polymerization time-course was dissected in order to calculate the kinetic parameters describing the different phases of the process [24]. The number of successive steps in the nucleation (*P*) was determined by plotting $\log(A(t)/A\infty)$ against $\log(t)$ and extrapolated as the pendency of the linear part of the resulting plot [24]. The maximal velocity of polymerization

(Vi) was calculated as the variation of mass *versus* time (δA/δt) at the very initial elongation phase, whereas total extent of MT assembly was deduced from the total absorbance variation (ΔA) achieved as the steady-state was established. The tubulin critical concentration, namely the lowest tubulin concentration allowing MT formation, was extrapolated as the x-intercept of the linear dependence of ΔA from the initial tubulin concentration.

To assess the ultrastructure of assembled MTs, at the end of polymerization, samples were fixed with 0.5% glutaraldehyde and then placed on Formvar-coated nickel grids. MTs were negative stained with uranyl acetate and observed with a Philips CM10 transmission electron microscope at 80 kV; images were acquired using a Morada Olympus digital camera. To verify the capability of Syn to co-polymerize with MTs, the sedimentable fraction obtained by centrifugation of tubulin polymerized in the presence of Syn was gently resuspended in BRB buffer, laid on poly-L-lysine coated coverslips, and immunostained with anti-Syn rabbit IgG (Sigma-Aldrich, St. Louis, MO) and Alexa Fluor™ 488-labeled goat anti-rabbit IgG (Invitrogen, Carlsbad, CA,) antibodies. The coverslips were mounted in Mowiol® (Calbiochem, San Diego, CA)–DABCO (Sigma-Aldrich) and examined with an Axiovert 200M microscope (Carl Zeiss, Oberkochen, Germany), using differential interference contrast (DIC) optics to observe MTs and fluorescence to visualize Syn staining.

To evaluate MT length and number, 2.7 μM rhodamine-labelled tubulin (Cytoskeleton, Denver, CO) was included in the polymerization solutions before starting assembly. Reaction was stopped at different times by addition of 0.5% glutaraldehyde. MTs were laid on slides and images acquired with the Axiovert 200M microscope. Length was measured using a digital image processing software (Axiovision, Zeiss).

**Co-sedimentation assay**

MTs were polymerized 20 min at 37 °C, stabilized 10 min with equimolar paclitaxel and then diluted to 4 μM (calculated on the tubulin concentration). Syn at different concentrations (0.5-32 μM) was incubated 20 min at 37 °C in the absence or in the presence of MTs and then centrifuged at 70000x*g* for 15 min at 25 °C. Supernatant and pellet were loaded on SDS-PAGE. According to Ackmann et al. [68], $[Syn]_{bound}$ was plotted *versus* $[Syn]_{free}$ and the data fitted by nonlinear regression to a standard binding equation (Equation 1) using SigmaPlot (Jandel, CA):

$$[Syn]_{bound} = \frac{B_{max}\ [Syn]_{free}}{K_d + [Syn]_{free}} \qquad (1)$$

**Mass spectrometry**

Nano-ESI-MS was performed on a hybrid quadrupole-time-of-flight instrument (QSTAR Elite, Applied Biosystems, Foster City, CA) with minor modifications to previously reported conditions [69]. Purified proteins were thawed and buffer exchanged by two cycles of desalting on Micro Bio-Spin™ P-6 Gel columns (Bio-Rad laboratories, Hercules, CA), immediately before use. All spectra were acquired in 10 mM ammonium acetate after incubation at room temperature for at least 10 min and no longer than 1h.

**Circular dichroism**

Circular dichroism spectra were acquired using a Jasco J810 spectropolarimeter. Secondary structure of Syn (0.2 mg/ml) and RB3-SLD (0.1 mg/ml), either alone or in the presence of tubulin (1.4 mg/ml), was investigated by recording far-UV circular dichroism spectra in 0.1 cm quartz cuvettes. All proteins were dissolved in BRB buffer. Spectra of pure Syn and RB3-SLD were baseline-corrected by subtracting a buffer spectrum, while difference spectra of the Syn/tubulin and RB3-SLD/tubulin mixtures were "tubulin-corrected" by subtracting the spectrum of the pure tubulin from those of the mixtures. Syn spectra were normalized in terms of mean residual ellipticity by using a mean residue weight of 103 Da. Since BRB buffer does not allow to record spectra below 215 nm, the α-helical content was estimated from the mean residual ellipticity at 222 nm according to Chen and Yang [70].

**NMR spectroscopy**

The NMR spectra were recorded at 25 °C on a Bruker AV600 spectrometer (Bruker Spectrospin AG, Rheinstetten, Germany), operating at 600.10 MHz for the $^{1}H$ nucleus and equipped with a standard triple-resonance probe with z-axis gradients. Temperature control was achieved through the spectrometer BVT3000 temperature control unit, using nitrogen gas (flow 270 l/h) pre-cooled with a Bruker BCU20 refrigeration unit. $^{1}H$-NMR chemical shifts (δ) were measured in ppm, using as reference external sodium 4,4-dimethyl-2-silapentane-1-sulfonate (DSS) set at 0.00 ppm. DOSY (Diffusion Oriented Spectroscopy) measurements were performed at 25 °C on a freshly prepared 27 μM solution of tubulin, dissolved in 0.6ml $H_2O$:$D_2O$ 9:1 (v/v), pH 6.8 50 mM phosphate buffer, in the presence of various amounts of Syn (Syn/tubulin molar ratios were between 0 and 10) after at least 0.5 h incubation. DSS, deuterium oxide (99.8% purity) and 5 mm O.D. NMR tubes (Wilmad 535-PP type) were purchased from Sigma-Aldrich. Solvent suppression was achieved by including in the DOSY pulse-sequence a WATERGATE pulse-scheme [71]. A gradient-based stimulated echo

bipolar pulse sequence was utilized [72], with a 0.3 s diffusion delay ("big delta") and a 1.5 ms gradient pulse length ("little delta"). 32 one-dimensional spectra were collected with a gradient strength varying between 0.67 and 33.4 Gauss/cm. Values for "little delta" and "big delta" parameters were chosen by taking also into account the expected short transverse relaxation rates due to the formation of high molecular weight aggregates. Other relevant acquisition parameters: time-domain: 2 K; number of scans: 196; relaxation delay: 2 s. Raw data were Fourier-transformed after apodization with a 90 °-shifted sine-bell-squared function and baseline corrected. Log(D) values were derived by a two-components non-linear fitting and displayed as pseudo-2D spectra.

Limiting values for the molar fraction of free Syn (α) were estimated from the experimental diffusion coefficients (D, Equation 2) as:

$$\frac{(D_{exp}-D_{tub:syn})}{(D_{syn}-D_{tub:syn})} < a < \frac{(D_{exp}-D_{tub2:syn})}{(D_{syn}-D_{tub2:syn})} \qquad (2)$$

where $D_{syn}$ is the experimental value determined for free Syn. $D_{tub:syn}$ and $D_{tub2:syn}$ are the D values expected for complexes formed by Syn with αβ tubulin dimer and $\alpha_2\beta_2$ tubulin tetramer, respectively. These last values were estimated by applying the following correction factors to $D_{tub}$:

$$\log\left(D_{tub:syn}\right) = \log\left(D_{tub}\right) - \frac{1}{3}\log\left(\frac{MW_{tub:syn}}{MW_{tub}}\right) = -10.44 \qquad (3)$$

$$\log\left(D_{tub_2:syn}\right) = \log\left(D_{tub}\right) - \frac{1}{3}\log\left(\frac{MW_{tub_2:syn}}{MW_{tub}}\right) = -10.54 \qquad (4)$$

The dissociation constant $K_d$ of Syn-tubulin complex was derived by applying the following equation 5 [74]:

$$K_d = [TUB]_0 \frac{D_{bound} - D_{exp}}{D_{exp} - D_{syn}} + [Syn]_0 \frac{D_{exp} - D_{bound}}{D_{bound} - D_{syn}} \qquad (5)$$

where $D_{bound}$ can be either $D_{tub:syn}$ or $D_{tub2:syn}$ as derived from equation 3 and 4.

**Video-microscopy and data analysis**

MTs were assembled from purified axonemes with tubulin (10-15 μM) and increasing concentrations of preincubated Syn (5-15 μM). Samples were prepared in perfusion chambers, previously saturated with 50 μM Syn, and observed at 37 °C with an Olympus BX-51

microscope equipped with DIC prisms and a video camera coupled to an Argus 20 image processor (Hamamatsu, Hamamatsu City, Japan), as previously described [73]. Images were recorded every 2 s over periods of 5 min. The total recording time did not exceed 60 min for each chamber. Measurements of MT dynamics and data analysis were carried out using Image J (NIH, Bethesda, MD) and Kaleidagraph (Synergy Software Systems, Dubai, UAE), as previously described [73].

**Cell cultures and transfection**

PC12 cells were maintained in cultures and differentiated as previously described [57]. PC12 cells were transiently transfected using Lipofectamine 2000 (Invitrogen) (1:3 DNA to Lipofectamine ratio), with GFP-fused WT or mutated Syns or with GFP-containing control vector; the quantity of DNA was chosen according to previously reported data, as the Syn expression level was low (see Figure 1D) and comparable to the average physiological levels of the protein in the brain [47]. For live cell imaging experiments, GFP-WT Syn and GFP-containing vectors were co-transfected with EB3-mCherry construct [16]) (kindly provided by Dr Galjart, Medical Genetic Center, Erasmus University, Rotterdam, The Netherlands).

For morphometric analyses, living cells were observed by phase contrast microscopy (Axiovert 200M) with 10 random images captured per plate, and measurements were made using the Axiovision software. Cells were considered to be differentiated when the longest neurite became twice as long as the cell diameter [74]. All cells in each image were analyzed and only the longest neurite was measured.

**Primary mesencephalic cultures**

According to a described protocol [75], ventral mesencephalons were taken from E12.5 C57Bl mouse embryos, dissected in ice-cold PBS with 1% of penicillin-streptomycin, 1% of gentamicin and 1 μg/ml amphotericin B (EuroClone, Pero, Italy) and then transferred to PBS containing 0,6% glucose. Tissues were incubated in Accumax™ (Merk Millipore, Darmstadt, Germany) at room temperature for 30 min and then mechanically dissociated. The cells were resuspended in MACS Neuro Medium (Miltenyi Biotech, Italy), containing 1% L-glutamine, 1% penicillin-streptomycin and 2% of MACS NeuroBrew-21 and were seeded in one drop ($5x10^4$ cells/ml) on 0.1 mg/ml poly-D-lysine (Millipore) – 0.01 mg/ml laminin (Sigma Aldrich) pre-coated coverslip. Cells were kept at 37 °C in a humidified 5% CO2 incubator and half volume of the medium was changed every two days. Cells were fixed in cold methanol (6 min at -20 °C) at the $6^{th}$ day *in vitro* (DIV).

**Differentiation of human embryonic stem cells into midbrain neurons**

The differentiation of the human embryonic stem cells (line HuES13= H13) toward mesencephalic neurons was performed according to previous published protocol [76] with the following modifications: LDN-193189 (100 nM, Stemgent) was employed instead of Noggin, and CHIR was kept in differentiation medium together with neurotrophic factors until embryoid bodies were dissociated and seeded onto coated surfaces, at 30DIV. Three days later cultures were fixed in cold methanol (6 min at -20 °C) and processed for immunocytochemistry.

**Western blotting**

Whole cell extracts, Triton X-100 soluble and insoluble fractions of PC12 cells were made as previously reported [57]. After SDS-PAGE, proteins were transferred onto polyvinylidene difluoride membranes and immunostained with the following antibodies: anti-α tubulin mouse IgG (clone B-5-1-2, Sigma-Aldrich); anti-tyrosinated tubulin mouse IgG (clone TUB-1A2, Sigma-Aldrich); anti-Syn rabbit IgG (Sigma-Aldrich); anti-actin mouse IgM (N350, Amersham, Little Chalfont, UK). Membranes were washed for 30 min with 3 changes and incubated for 1 h at room temperature with HRP donkey anti-mouse IgG (Pierce, Waltham, MA), HRP goat anti-rabbit IgG (Sigma-Aldrich) or HRP goat anti-mouse IgM (Sigma-Aldrich). Immunostaining was revealed by enhanced chemiluminescence (Super-Signal West Pico Chemiluminescent, Pierce). Quantification was performed by Image J software (NIH) and subtracting the background around bands.

**Live cell imaging**

Cultures were transferred to a live cell imaging workstation composed of an inverted microscope (Axiovert 200M), a heated (37 °C) chamber (Okolab, Naples, Italy), and a Plan neofluar 63x/1.25 numerical aperture oil-immersion objective (Zeiss). Images were collected every 6 s with a cooled camera (Axiocam HRM Rev. 2; Zeiss) for periods of 3-4 min, and the total recording time did not exceed 60 min for each dish. MT growth dynamics were automatically analysed from EB3 time-lapse movies using plusTipTracker software [77]. In order to get a representative image, kymographs were constructed using the Multiple Kymograph plug-in for Image J [78]. The area of the analysed neurites was estimated by ImageJ software, just to ascertain that no differences were present in the surface extension (Figure S3).

**Immunofluorescence**

Transfected PC12 cells were fixed with cold methanol (6 min at -20°C); to remove unassembled tubulin, before fixation, some slides were extracted in PEM buffer (80 mM K-Pipes, 5 mM EGTA, 1 mM $MgCl_2$, pH 6.8, containing protease inhibitors) with 0.5% Triton X-100, 0.2 M NaCl and 10 µM Paclitaxel (Sigma-Aldrich). PC12 cells, murine and human neurons were saturated 15 min with 5% BSA and stained with anti-α tubulin mouse IgG, anti-tyrosinated tubulin mouse IgG, anti-detyrosinated tubulin rabbit IgG, anti-acetylated tubulin mouse IgG, anti-βIII tubulin mouse IgG, anti-Syn rabbit IgG or anti-Syn mouse IgG (clone 4D6, abcam) for 1h at 37 °C. After washing in PBS, samples were stained with Alexa Fluor™ 568 goat anti-mouse, Alexa Fluor™ 488 donkey anti-rabbit, Alexa Fluor™ 568 donkey anti-rabbit or Alexa Fluor™ 488 goat anti-mouse IgG (Invitrogen). Coverslips were mounted in Mowiol®-DABCO and examined either with epifluorescence microscope (Axiovert 200M) or with a confocal laser scan microscope imaging system (TCS SP5 AOBS, Leica Microsystems, Heidelberg, Germany) equipped with Ar/Ar-Kr 488 nm, 561 nm and 405 nm diode lasers. For co-localization analyses photomultiplier gain for each channel was adjusted to minimize background noise and saturated pixels and parameters were kept constant for all the acquisitions. To estimate the co-localization area between red and green signals, analyses were carried out on single-plane raw images and Manders' coefficients were calculated using the JACoP plug-in for Image J software [17], and using a threshold-based approach to exclude background noise.

By using Image J software, total fluorescence intensity was measured on the growth cone area. The region of interest was manually drowned, and the analyses of the surface extension revealed that there were no significant differences between control cultures and WT-expressing PC12 cells (Figure S2).

**Protein alignment**

Pairwise alignments between Syn and stathmin sequences were made using Pam250 or Bl50 matrix, whereas multiple protein alignment was performed with ClustalW software.

**Statistical analyses**

For multiple comparisons, the statistical significance of treatment was assessed by one-way ANOVA with Dunnett 2-sided or Fischer LSD *post-hoc* testing, whereas differences between WT Syn and controls were assessed using Student's t-test. For the analyses of qualitative

variables, $\chi^2$ test was used. All analyses were performed using STATISTICA (StatSoft Inc., Tulsa, OK).

**Abbreviations**

Ac, acetylated; CD, circular dichroism; ΔA, absorbance variation; deTyr, detyrosinated; DIC, differential interference contrast; EB3, end-binding protein 3; MT, microtubule; PD, Parkinson's disease; Syn, α-Synuclein; Tyr, tyrosinated; VE-DIC, video-enhanced differential interference contrast; WT, wild type

**Competing Interests**

The authors declare that they have no competing interests.

**Authors' Contributions**

DC and GC conceived of the study and partecipated in its design and coordination. DC, AA, VP and AB carried out protein purification and circular dichroism assays. EMR carried out NMR spectrometry. CS and RG performed mass spectrometry analysis. DC performed *in vitro* assays and electron microscopy analyses. DC and IA performed video microscopy assays. DC, CDG, ME, and EC set up primary cell cultures and performed immunofluorescence analyses. DC performed western blotting and live cell imaging studies. FC, SH and LR carried out analyses on human embryonic stem cells. SP participated in the sequence alignment. DC, GP and GC designed the analysis based on experimental data. DC, IA and GC wrote the article. All authors read and approved the final manuscript.

**Acknowledgements**

The authors are grateful to Dr. Croci (Università degli Studi di Milano) for support with bioinformatics tools and to Dr. Pavesi (Universita`degli Studi di Milano) for helpful discussion on bioinformatics data. We thank Dr. Galjart (Erasmus University) for the pEB3-mCherry. The authors are thankful to Dr. Francolini (Department of Medical Biotechnology and Translational Medicine, Università degli Studi di Milano, Milano, Italy) for the use of electron microscope. The authors are also grateful to Dr. Bonomi (Università degli Studi di Milano) for critical reading of the manuscript and Dr. Jennifer S. Hartwig for reading and editing the manuscript. Finally, the authors thank Dr. M. Gritti, Dr. M. Magri and the present members of the lab who contributed to the preparation of the manuscript and whose names

are not included in the authors list, and we apologize for each possible involuntary paper omission. This work was supported by Fondazione Grigioni per il Morbo di Parkinson, Milan, Italy (to G.C.), and ‘‘Dote ricerca’’, FSE, Regione Lombardia (to D.C.).

**REFERENCES**


1. Conde C, Cáceres A. Microtubule assembly, organization and dynamics in axons and dendrites. Nat. Rev. Neurosci. 2009;10:319-332.
2. Stiess M, Maghelli N, Kapitein LC, Gomis-Ruth S, Wilsch-Brauninger M, Hoogenraad CC, et al. Axon extension occurs independently of centrosomal microtubule nucleation. Science. 2010;327: 704-707.
3. Lashuel HA, Overk CR, Oueslati A, Masliah E. The many faces of α-synuclein: from structure and toxicity to therapeutic target. Nat. Rev. Neurosci. 2013;14:38-48.
4. Winner B, Jappelli R, Maji SK, Desplats PA, Boyer L, Aigner S, et al. In vivo demonstration that alpha-synuclein oligomers are toxic. Proc. Natl. Acad. Sci. U.S.A. 2001;108:4194-4199.
5. Prots I, Veber V, Brey S, Campioni S, Buder K, Riek R, et al. α-Synuclein oligomers impair neuronal microtubule-kinesin interplay. J. Biol. Chem. 2013;288:21742-21754.
6. Zhou RM, Huang YX, Li XL, Chen C, Shi Q, Wang GR, et al. Molecular interaction of α-synuclein with tubulin influences on the polymerization of microtubule in vitro and structure of microtubule in cells. Mol. Biol. Rep. 2010;37:3183-3192.
7. Gąssowska M, Czapski GA, Pająk B, Cieślik M, Lenkiewicz AM, Adamczyk A. Extracellular α-Synuclein Leads to Microtubule Destabilization via GSK-3β-Dependent Tau Phosphorylation in PC12 Cells. PLoS One. 2014;9: e94259.
8. Alim MA, Hossain MS, Arima K, Takeda K, Izumiyama Y, Nakamura M, Tubulin seeds alpha-synuclein fibril formation. J. Biol. Chem. 2002;277:2112-2117.
9. Esteves AR, Arduíno DM, Swerdlow RH, Oliveira CR, Cardoso SM. Microtubule depolymerization potentiates alpha-synuclein oligomerization. Front. Aging Neurosci. 2010;1:5.
10. Nakayama K, Suzuki Y, Yazawa I. Microtubule depolymerization suppresses alpha-synuclein accumulation in a mouse model of multiple system atrophy. Am. J. Pathol. 2009;174:1471-1480.
11. Alim MA, Ma QL, Takeda K, Aizawa T, Matsubara M, Nakamura M, et al. Demonstration of a role for alpha-synuclein as a functional microtubule-associated protein. J. Alzheimers Dis. 2004;6:435-442.
12. Chen L, Jin J, Davis J, Zhou Y, Wang Y, Liu J, et al. Oligomeric alpha-synuclein inhibits tubulin polymerization. Biochem. Biophys. Res. Commun. 2007;356:548-553.

13. Baas PW, Ahmad FJ. The plus ends of stable microtubules are the exclusive nucleating structures for microtubules in the axon. J. Cell Biol. 1992;116:1231-1241.
14. Stefanis L, Kholodilov N, Rideout HJ, Burke RE, Greene LA. Synuclein-1 is selectively up-regulated in response to nerve growth factor treatment in PC12 cells. J. Neurochem. 2001;76:1165-1176.
15. Janke C, Bulinski JC. Post-translational regulation of the microtubule cytoskeleton: mechanisms and functions. Nat. Rev. Mol. Cell Biol. 2011;12:773-786.
16. Komarova Y, De Groot CO, Grigoriev I, Gouveia SM, Munteanu EL, Schober JM, et al. Mammalian end binding proteins control persistent microtubule growth. J. Cell Biol. 2009;184:691-706.
17. Bolte S, Cordelières FP. A guided tour into subcellular colocalization analysis in light microscopy. J. Microsc. 2006;224:213-232.
18. Payton JE, Perrin RJ, Clayton DF, George JM. Protein-protein interactions of alpha-synuclein in brain homogenates and transfected cells. Brain Res. Mol. Brain Res. 2001;95:138-145.
19. Testa L, Brocca S, Samalikova M, Santambrogio C, Alberghina L, Grandori R. Electrospray ionization-mass spectrometry conformational analysis of isolated domains of an intrinsically disordered protein. Biotechnol. J. 2011;6:96-100.
20. Weinreb PH, Zhen W, Poon AW, Conway KA, Lansbury PT Jr. NACP, a protein implicated in Alzheimer's disease and learning, is natively unfolded. Biochemistry. 1995;35:13709-13715
21. Burré J, Vivona S, Diao J, Sharma M, Brunger AT, Südhof TC. Properties of native brain α-synuclein. Nature. 2013;498:E4-6.
22. Eliezer D, Kutluay E, Bussell R Jr, Browne G. Conformational properties of alpha-synuclein in its free and lipid-associated states. J. Mol. Biol. 2001;307:1061-1073.
23. Uversky VN, Li J, Fink AL. Evidence for Partially Folded Intermediate in α-Synuclein Fibril Formation. J. Biol. Chem. 2001;276:10737-10744.
24. Bonfils C, Bec N, Lacroix B, Harricane MC, Larroque C. Kinetic analysis of tubulin assembly in the presence of the microtubule-associated protein TOGp. J. Biol. Chem. 2007;282:5570-5581.
25. Hiller G, Weber K. Radioimmunoassay for tubulin: a quantitative comparison of the tubulin content of different established tissue culture cells and tissues. Cell. 1978;14:795-804.

26. Kamp F, Exner N, Lutz AK, Wender N, Hegermann J, Brunner B, et al. Inhibition of mitochondrial fusion by α-synuclein is rescued by PINK1, Parkin and DJ-1. EMBO J. 2010;29:3571-3589.
27. Walker RA, O'Brien ET, Pryer NK, Soboeiro MF, Voter WA, Erickson HP, Salmon ED Dynamic instability of individual microtubules analysed by video light microscopy: rate constants and transition frequencies. J. Cell Biol. 1988;107:1437-1448.
28. Uversky VN. Neuropathology, biochemistry, and biophysics of alpha-synuclein aggregation. J. Neurochem. 2007;103:17-37.
29. Steinmetz MO. Structure and thermodynamics of the tubulin-stathmin interaction. J. Struct. Biol. 2007;158:137-147.
30. Kara E, Lewis PA, Ling H, Proukakis C, Houlden H, Hardy J. α-Synuclein mutations cluster around a putative protein loop. Neurosci. Lett. 2013;546:67-70.
31. Honnappa S, Cutting B, Jahnke W, Seelig J, Steinmetz MO. Thermodynamics of Op18/stathmin-tubulin interaction. J. Biol. Chem. 2003;278:38926-38934.
32. Takenouchi T, Hashimoto M, Hsu LJ, Mackowski B, Rockenstein E, Mallory M, et al. Reduced neuritic outgrowth and cell adhesion in neuronal cells transfected with human alpha-synuclein. Mol. Cell Neurosci. 2001;17:141-150.
33. Liu G, Wang P, Li X, Li Y, Xu S, Ueda K, et al. Alpha-synuclein promotes early neurite outgrowth in cultured primary neurons. J. Neural Transm. 2013;120:1331-1343.
34. Feng Y, Walsh CA. Protein-protein interactions, cytoskeletal regulation and neuronal migration. Nat. Rev. Neurosci. 2001:2:408-416.
35. Erent M, Drummond DR, Cross RA. S. pombe kinesins-8 promote both nucleation and catastrophe of microtubules. PLoS One. 2008;7:e30738.
36. Gardner MK, Zanic M, Gell C, Bormuth V, Howard J. Depolymerizing kinesins Kip3 and MCAK shape cellular microtubule architecture by differential control of catastrophe. Cell. 2011;147:1092-1103.
37. Mozziconacci J, Sandblad L, Wachsmuth M, Brunner D, Karsenti E. Tubulin dimers oligomerize before their incorporation into microtubules. PLoS One. 2008;3:e3821.
38. Schek HT 3rd, Gardner MK, Cheng J, Odde DJ, Hunt AJ. Microtubule assembly dynamics at the nanoscale. Curr. Biol. 2007;17:1445-1455.
39. Slep KC, Vale RD. Structural basis of microtubule plus end tracking by XMAP215, CLIP-170, and EB1. Mol. Cell. 2007;27:976-991.

40. Manna T, Thrower DA, Honnappa S, Steinmetz MO, Wilson L. Regulation of microtubule dynamic instability in vitro by differentially phosphorylated stathmin. J. Biol. Chem. 2009;284:15640-15649.
41. Abeliovich A, Schmitz Y, Fariñas I, Choi-Lundberg D, Ho WH, Castillo PE, et al. Mice lacking alpha-synuclein display functional deficits in the nigrostriatal dopamine system. Neuron. 2000;25:239-252.
42. Liedtke W, Leman EE, Fyffe RE, Raine CS, Schubart UK. Stathmin-deficient mice develop an age-dependent axonopathy of the central and peripheral nervous systems. Am. J. Pathol. 2002;160:469-468.
43. Di Paolo G, Pellier V, Catsicas M, Antonsson B, Catsicas S, Grenningloh G. The phosphoprotein stathmin is essential for nerve growth factor-stimulated differentiation. J. Cell Biol. 1996;133:1383-1390.
44. Witte H, Neukirchen D, Bradke F. Microtubule stabilization specifies initial neuronal polarization. J. Cell Biol. 2008;180:619-632.
45. Larsen KE, Schmitz Y, Troye MD, Mosharov E, Dietrich P, Quazi AZ. Alpha-synuclein overexpression in PC12 and chromaffin cells impairs catecholamine release by interfering with a late step in exocytosis. J. Neurosci. 2006;26:11915-11922.
46. Pranke IM, Morello V, Bigay J, Gibson K, Verbavatz JM, Antonny B, et al. α-Synuclein and ALPS motifs are membrane curvature sensors whose contrasting chemistry mediates selective vesicle binding. J. Cell Biol. 2011;194:89-103.
47. Sousa VL, Bellani S, Giannandrea M, Yousuf M, Valtorta F, Meldolesi J, et al. {alpha}-synuclein and its A30P mutant affect actin cytoskeletal structure and dynamics. Mol. Biol. Cell. 2009;20:3725-3739.
48. Esposito A, Dohm CP, Kermer P, Bähr M, Wouters FS. alpha-Synuclein and its disease-related mutants interact differentially with the microtubule protein tau and associate with the actin cytoskeleton. Neurobiol. Dis. 2006;26:521-531.
49. Farias GA, Muñoz JP, Garrido J, Maccioni RB. Tubulin, actin, and tau protein interactions and the study of their macromolecular assemblies. J. Cell. Biochem. 2002;85:315-324.
50. Gasser T, Hardy J, Mizuno Y. Milestones in PD genetics. Mov. Disord. 2011;26:1042-1048.
51. Spillantini MG, Schmidt ML, Lee VM, Trojanowski JQ, Jakes R, Goedert M. Alpha-synuclein in Lewy bodies. Nature. 1997;388:839-840.

52. Galloway PG, Grundke-Iqbal I, Iqbal K, Perry G. Lewy bodies contain epitopes both shared and distinct from Alzheimer neurofibrillary tangles. J. Neuropathol. Exp. Neurol. 1988;47:654-663.
53. Salinas S, Carazo-Salas RE, Proukakis C, Schiavo G, Warner TT. Spastin and microtubules: Functions in health and disease. J. Neurosci. Res. 2007;85:2778-2782.
54. Saha AR, Hill J, Utton MA, Asuni AA, Ackerley S, Grierson AJ, et al. Parkinson's disease alpha-synuclein mutations exhibit defective axonal transport in cultured neurons. J. Cell Sci. 2004;117:1017-1024.
55. Chung CY, Koprich JB, Siddiqi H, Isacson O Dynamic changes in presynaptic and axonal transport proteins combined with striatal neuroinflammation precede dopaminergic neuronal loss in a rat model of AAV alpha-synucleinopathy. J. Neurosci. 2009;29:3365-3373.
56. Morfini GA, Burns M, Binder LI, Kanaan NM, LaPointe N, Bosco DA, et al. Axonal transport defects in neurodegenerative diseases. J. Neurosci. 2009;29:12776-12786.
57. Cartelli D, Ronchi C, Maggioni MG, Rodighiero S, Giavini E, Cappelletti G. Microtubule dysfunction precedes transport impairment and mitochondria damage in MPP+-induced neurodegeneration. J. Neurochem. 2010;115:247-258.
58. Cartelli D, Casagrande F, Busceti CL, Bucci D, Molinaro G, Traficante A, et al. Microtubule alterations occur early in experimental parkinsonism and the microtubule stabilizer epothilone D is neuroprotective. Sci. Rep. 2013;3:1837.
59. Fleming SM, Mulligan CK, Richter F, Mortazavi F, Lemesre V, Frias C, et al. A pilot trial of the microtubule-interacting peptide (NAP) in mice overexpressing alpha-synuclein shows improvement in motor function and reduction of alpha-synuclein inclusions. Mol. Cell. Neurosci. 2011;46:597-606.
60. Cartelli D, Goldwurm S, Casagrande F, Pezzoli G, Cappelletti G. Microtubule destabilization is shared by genetic and idiopathic Parkinson's disease patient fibroblasts. PLoS One. 2012;7:e37467.
61. Esteves AR, Gozes I, Cardoso SM. The rescue of microtubule-dependent traffic recovers mitochondrial function in Parkinson's disease. Biochim. Biophys. Acta 2014;1842:7-21.
62. Ren Y, Jiang H, Hu Z, Fan K, Wang J, Janoschka S, et al. Parkin Mutations Reduce the Complexity of Neuronal Processes in iPSC-derived Human Neurons. Stem Cells. 2015;33:68-78.

63. Bartels T, Choi JG, Selkoe DJ. α-Synuclein occurs physiologically as a helically folded tetramer that resists aggregation. Nature. 2011;477:107-110.
64. Castoldi M, Popov AV. Purification of brain tubulin through two cycles of polymerization-depolymerization in a high-molarity buffer. Protein Expr. Purif. 2003;32:83-88.
65. Martinez J, Moeller I, Erdjument-Bromage H, Tempst P, Lauring B. Parkinson's disease-associated alpha-synuclein is a calmodulin substrate. J. Biol. Chem. 2003;278:17379-17387.
66. Charbaut E, Curmi PA, Ozon , Lacjhkar S, Redeker V, Sobel A. Stathmin family proteins dispay specific molecular and tubulin binding properties. J. Biol. Chem. 2001;276:16146-16154.
67. Contini A, Cappelletti G, Cartelli D, Fontana G, Gelmi GL. Molecular dynamics and tubulin polymerization kinetics study on 1,14-heterofused taxanes: evidence of stabilization of the tubulin head-to-tail dimer-dimer interaction. Mol Biosyst. 2012;8:3254-3261.
68. Ackmann M, Wiech H, Mandelkow E. Nonsaturable Binding Indicates Clustering of Tau on the Microtubule Surface in a Paired Helical Filament-like Conformation. J. Biol. Chem. 2000;275:30335-30343.
69. Santambrogio C, Ricagno S, Colombo M, Barbiroli A, Bonomi F, Bellotti V, et al. DE-loop mutations affect beta2 microglobulin stability, oligomerization, and the low-pH unfolded form. Protein Sci. 2010;19:1386-1397.
70. Chen YH, Yang JT. A new approach to the calculation of secondary structures of globular proteins by optical rotatory dispersion and circular dichroism. Biochem. Biophys. Res. Commun. 1971;44:1285-1291.
71. Piotto M, Saudek V, Sklenar V. Gradient-tailored excitatiojn for single-quantum NMR spectroscopy of aqueous solutions. J. Biomol. NMR 1992;2:661-665.
72. Wu D, Chen A, Johnson CS Jr. An Improved Diffusion-Ordered Spectroscopy Experiment Incorporating Bipolar-Gradient Pulses. J. Magn. Reson. Series A. 1995;108:255-258.
73. Vitre B, Coquelle FM, Heichette C, Garnier C, Chrétien D, Arnal I. EB1 regulates microtubule dynamics and tubulin sheet closure in vitro. Nat. Cell Biol. 2008;10:415-421.
74. Peunova N, Enikolopov G. Nitric oxide triggers a switch to growth arrest during differentiation of neuronal cells. Nature. 1995;375:68-73.

75. Studer L. Culture of substantia nigra neurons. Curr. Protoc. Neurosci. 2001;Chapter 3.
76. Kirkeby A, Nelander J, Palmar M. Generating regionalized neuronal cells from pluripotency, a step-by-step protocol. Front. Cell Neurosci. 2013;6:64.
77. Applegate KT, Besson S, Matov A, Bagonis MH, Jaqaman K, Danuser G. plusTipTracker: Quantitative image analysis software for the measurement of microtubule dynamics. J. Struct. Biol. 2011;176:168-184.
78. Gumy LF, Chew DJ, Tortosa E, Katrukha EA, Kapitein LC, Tolkovsky AM, et al. The kinesin-2 family member KIF3C regulates microtubule dynamics and is required for axon growth and regeneration. J. Neurosci. 2013;33:11329-11345.

**LEGENDS**

**FIGURE 1. WT Syn promotes MT nucleation in differentiated PC12 cells.** A. Fluorescence microscopy micrographs of PC12 cells differentiated 5 days with NGF expressing GFP-Syn chimera (Syn) or GFP control vector (GFP), fixed before (BASAL), immediately after the MT destabilizing cold-treatment, 30 min at 4 °C (0), or at various times after rewarming (15 and 60 min at 37 °C) and stained for α tubulin (α TUB). Insets represent the GFP channel, and the yellow boxes the magnified areas shown on the right (GFP channel in green and α tubulin in red). Scale bar, 10 μm. Quantification of total fluorescence of α tubulin (α TUB, B) and tyrosinated tubulin (Tyr TUB, C) in PC12 cells expressing GFP-Syn chimera (Syn) or GFP (GFP), extracted and fixed after the treatment described in A. Values are expressed as mean ± SEM, and the cells analysed are at least 12 for each experimental condition. *$p<0.05$ vs CONT, according to Student's t-test. ROI's area is reported in Figure S2. Western blotting (D) and densitometric analyses (E) of α tubulin (α TUB) and tyrosinated tubulin (Tyr TUB) associated to tubulin dimers (Dim) or to MTs (MT) in PC12 cells expressing GFP-Syn chimera (Syn) or GFP (GFP), treated as described in A. In E, values (mean ± SEM) represent ratio between MTs and dimers of α tubulin (α TUB, white bars) and tyrosinated tubulin (Tyr TUB, black bars) of Syn-transfected PC12 cells, and are expressed as control percentage (GFP-expressing PC12 cells). Data are obtained from at least three independent experiments. *$p<0.05$, according to Student's t-test, performed on the rough data.

**FIGURE 2. WT Syn increases MT dynamics in differentiated PC12 cells.** A. Representative kymographs illustrating the growth of EB3-mCherry-decorated MT tips in GFP-expressing (GFP) or GFP-Syn (Syn) transfected PC12 cells. Box plots of the number (B), speed (C) and lifetime (D) of MT growths, in each experimental condition. BASAL indicates cell cultures maintained at 37 °C whereas RECOVERY indicates registration during the rewarming phase after 30 min at 4 °C. At least 30 cells per condition were analysed, for a total number of 2200 tracks, or more. *$p<0.05$ vs GFP, according to Student's t-test. The analysis of the relative neurite's area is reported in Figure S3.

**FIGURE 3. Syn interacts with MTs in human mesencephalic neurons.** A. Human embryonic stem cell-derived mesencephalic neurons co-express otx2 and TH. B. Confocal micrographs of human mesencephalic neurons stained for endogenous Syn (Syn, green) and

tyrosinated tubulin (Tyr TUB, red), or βIII tubulin (βIII TUB, red). The co-localizing pixels are shown (Coloc). Scale bar, 5 µm.

**FIGURE 4. WT Syn interacts with preformed MTs and tubulin $\alpha_2\beta_2$ tetramer**. A-B. Co-sedimentation assay. Representative Western blotting (A) of Syn recovered in the supernatant (S) or pellet (P) fraction without (Syn) or after (Syn+MTs) incubation with preformed MTs (Tub) at constant total MT concentration (4 µM tubulin dimers). B. Bound Syn plotted versus free Syn ($r^2$ = 0.94). C-F. Mass spectrometry analyses. Nano-ESI-MS spectra of 14 µM tubulin: the peak distributions relative to the tubulin dimer and the $\alpha_2\beta_2$ tetramer are grouped by brackets, with the indication of the measured mass (C). Overlay of spectra of 14 µM tubulin (black), and a mixture of 14 µM tubulin and 14 µM Syn (red), in the *m/z* range 4000-5200 (D, αβ dimer) or in the *m/z* range 5600-7000 (E, $\alpha_2\beta_2$ tetramer). The peaks corresponding to the $\alpha_2\beta_2$/Syn complex are labelled by asterisks. F. Magnification of panel E, in the *m/z* range 6100-6500. The arrows point to the peaks of the $\alpha_2\beta_2$/Syn complex, labelled by the corresponding charge state. The measured mass of the complex is also indicated. In each panel, the most intense peak of each distribution is labelled by the corresponding charge state.

**FIGURE 5. WT Syn interacts with tubulin and acquires secondary structure**. A. Far UV CD spectra of isolated WT Syn (dashed line, Syn Alone) and differential spectra of 14 µM WT Syn in the presence of equimolar tubulin (solid line, differential spectrum). B. Far UV CD spectra of isolated RB3-SLD (dashed line, RB3 alone) and differential spectra of 7 µM RB3-SLD in the presence of 14 µM tubulin (solid line, differential spectrum). C. $^1$H-NMR diffusion coefficient measurements at 25 °C from 2D-DOSY projections of 27 µM Syn (Syn), Syn/tubulin equimolar mixture ([Syn]/[TUB]=1) and 27 µM tubulin (TUB).

**FIGURE 6. Folded Syn promotes MT nucleation *in vitro*.** A. Tubulin assembly was recorded as a function of time by measuring the increase in absorbance (ΔA) at 350 nm. Tubulin (40 µM) was polymerized in the absence (CONT) and in the presence of 5 µM of naïve (Syn w/o pre-incubation) or preincubated (Syn with preincubation) WT Syn. B. Parameters describing nucleation (*P*), elongation (Vi) and steady state (ΔA), were calculated from the analysis of the sigmoid kinetics of polymerization of tubulin (40 µM) in the absence (CONT) and in the presence of 5 µM of naïve (Syn w/o pre-incubation) or preincubated (Syn with preincubation) WT Syn. Values are expressed as mean ± SEM of at least five

independent experiments. *p<0.05vs CONT and #p<0.05 vs Syn w/o pre-incubation, according to ANOVA, Fisher LSD *post hoc* test. C. Final ΔA obtained with different initial concentrations of tubulin were plotted against tubulin concentration, and the x-intercept of fitting lines, representing the tubulin critical concentration (arrows), was calculated for polymerization in the absence (CONT, black line) and in the presence of 5 μM of WT Syn (Syn, blue line). Plotted values are mean ± SEM of at least three independent experiments. D. Electron microscope images of MTs assembled *in vitro* in the absence (CONT) or in the presence of WT Syn (Syn). Micrographs were taken at two different magnifications: 46000x (left column, scale bar, 200 nm) and 130000x (right column, scale bar, 100 nm). MT length measured during the initial phase (E) and at steady state (F) of tubulin polymerization (40 μM) in the absence (CONT) and in the presence of 5 μM of WT Syn (Syn). The number of measured MTs is at least 600 for each experimental condition, obtained from two independent experiments. *p<0.05 vs CONT, according to Student's t-test. G. Quantification of MT number over time assembled in the presence of WT Syn (Syn, blue points). Values (mean ± SEM) are expressed as control percentage, and the number of analysed fields is at least 15 for each experimental condition, obtained from two independent experiments. *p<0.05 vs CONT, according to Student's t-test, performed on the raw data. MT length and number were obtained from fluorescent microscopy images of MTs assembled in the presence of rhodamine-labelled tubulin (see Figure S6).

**FIGURE 7. Syn displays sequence similarities with stathmin.** Multiple alignment of Syn with four members of stathmin family was performed by ClustalW. Blue lines delimitate the domains of stathmin family involved in tubulin binding. Arrows mark the sites of Syn pathological mutations: Ala30 (green arrow), the conserved Glu46 and Ala53 (red arrows), His50 and Gly51 (blue arrows). Asterisks mark invariant positions, while dots and colons highlight semi-conservative and conservative substitutions, respectively.

**FIGURE 8. Pathological Syn mutations corrupt Syn/tubulin interaction**. A. Far UV CD spectra of mutated Syns, obtained with naïve proteins (A30P w/o pre-incubation or A53T w/o pre-incubation) or after pre-incubation (A30P with pre-incubation or A53T with pre-incubation) with equimolar tubulin, performed at 20 °C for 10 min in the presence of 14 μM tubulin. B. Electron microscope images of MTs assembled *in vitro* in the presence of mutated (A30P and A53T) Syns. Micrographs were taken at two different magnifications: 46000x (left column; scale bar, 200 nm) and 130000x (right column; scale bar, 100 nm). C. Confocal

micrographs of PC12 cells differentiated 5 days with NGF expressing A30P (A30P) or A53T (A53T) GFP-Syn chimeras (green) and stained for α tubulin (red). By side merge images, are shown the Syn channel (I), the tubulin channel (II) and the co-localizing pixels (III). Scale bar, 10 μm. D. Fluorescent microscopy photographs of PC12 cells differentiated 5 days with NGF expressing mutated (A30P and A53T) GFP-Syn chimeras, fixed before (BASAL), immediately after the MT destabilizing cold-treatment, 30 min at 4 °C (0), or at 15 min after rewarming (37 °C), and stained for α tubulin. Insets show the GFP channel and the yellow boxes the magnified areas. Scale bar, 10 μm.

**FIGURE 9. Model for Syn/MTs interaction.** Syn senses and binds free tubulin dimers forming a specific complex with tubulin $\alpha_2\beta_2$ tetramer and acquiring α-helix conformation (STEP 1). Afterwards, Syn behaves like a tubulin deliverer promoting MT nucleation (STEP 2-High $[Tub]_{free}$). When entrapped in the MT wall, Syn promotes MT catastrophes probably inducing changes in intra- or inter-dimer angles (STEP 2-Low $[Tub]_{free}$).

**FIGURE S1. Expression of human Syn.** Western blot showing the level of expression of human Syn (Syn) in 5 days NGF-differentiated control (CONT) and transfected PC12 cells. The staining was performed using an antibody (cod. S3062, Sigma-Aldrich) that recognizes both human and rat Syn. Actin is used as loading reference.

**FIGURE S2. Measurement of growth cone area.** Histogram representing the area of the growth cone (region of interest, ROI) of Syn-expressing PC12 cells, differentiated 5 days with NGF, used to evaluate α tubulin (α *TUB*) and Tyr tubulin (Tyr TUB) fluorescence, before (BASAL), immediately after the MT destabilizing cold-treatment (30 min at 4°C) or at various times after rewarming (15 and 60 min at 37°C). Values (mean ± SEM) are expressed as percentage of the area of growth cone of GFP-expressing cells. The statistical analyses (Student's t-test, performed on the rough data) reveal that there are no significant differences among the groups. The analyses refer to Figure 1.

**FIGURE S3. Measurement of neurite area.** Histogram representing the area of the neurite of PC12 cells expressing GFP (GFP) or GFP-Syn (Syn), differentiated 5 days with NGF, and used to evaluate MT growth by the analyses of EB3 movies in basal conditions (BASAL, cell maintained at 37 °C) and during the rewarming phase (RECOVERY) after 30 min at 4 °C. The analyses refer to Figure 2.

**FIGURE S4. WT Syn co-localizes with MTs in murine neurons**. Confocal micrographs of rat PC12 cells (PC12) differentiated 5 days with NGF expressing human WT GFP-Syn chimeras (green) and of ventral mesencephalon neurons (ventral mesencephalon) from mouse stained for endogenous Syn (green). Both cell types were stained for α tubulin (α TUB, red), tyrosinated tubulin (Tyr TUB, red), detyrosinated tubulin (deTyr TUB, red), acetylated tubulin (Ac TUB, red) and βIII tubulin (βIII TUB, red). Under the merge images, for each group of images are shown the Syn channel (I), the tubulin channel (II) and the co-localizing pixels (III). Scale bar, 5 μm.

**FIGURE S5. Syn co-polymerizes with MTs.** MTs assembled *in vitro* in the presence of WT (WT) or mutated (A30P and A53T) Syn are observed by DIC microscopy, and stained with anti-Syn (Syn) antibody (green). Scale bar, 2 μm.

**FIGURE S6. Rhodamine-labelled MTs.** Images of MTs assembled using rhodamine-labelled tubulin were captured after 2 and 45 min of polymerization by fluorescent microscope and showed in inverted contrast. The images obtained in the absence (CONT) or in the presence of WT Syn (WT) were analysed to measure the MT length and number (as reported in Figure 6). Scale bar, 2 μm.

**Figure S7. WT Syn promotes neuronal differentiation.** A. Phase contrast micrographs of PC12 cells differentiated 5 days with NGF, naïve (CONT) or expressing wild type (WT) or mutated (A30P and A53T) Syns (Syn). Scale bar, 50 μm. B-C. Morphometric analyses of differentiated cells. B. Histogram representing the percentage of differentiated cells (i.e. cells with a neurite's length equal to double of the cell body, according to Peunova and Enikolopov [74]). Values are expressed as mean ± SEM of at least three independent experiments (around 800 cells analysed per experimental condition). *$p<0.05$ vs CONT and $^{\#}p<0.05$ vs WT, according to $\chi^2$ test. C. Box plot of the neurite length. Measured neurites were at least 200 per experimental condition. *$p<0.05$ vs CONT and $^{\#}p<0.05$ vs WT, according to ANOVA, Fischer LSD *post hoc* test.

**FIGURE 1**

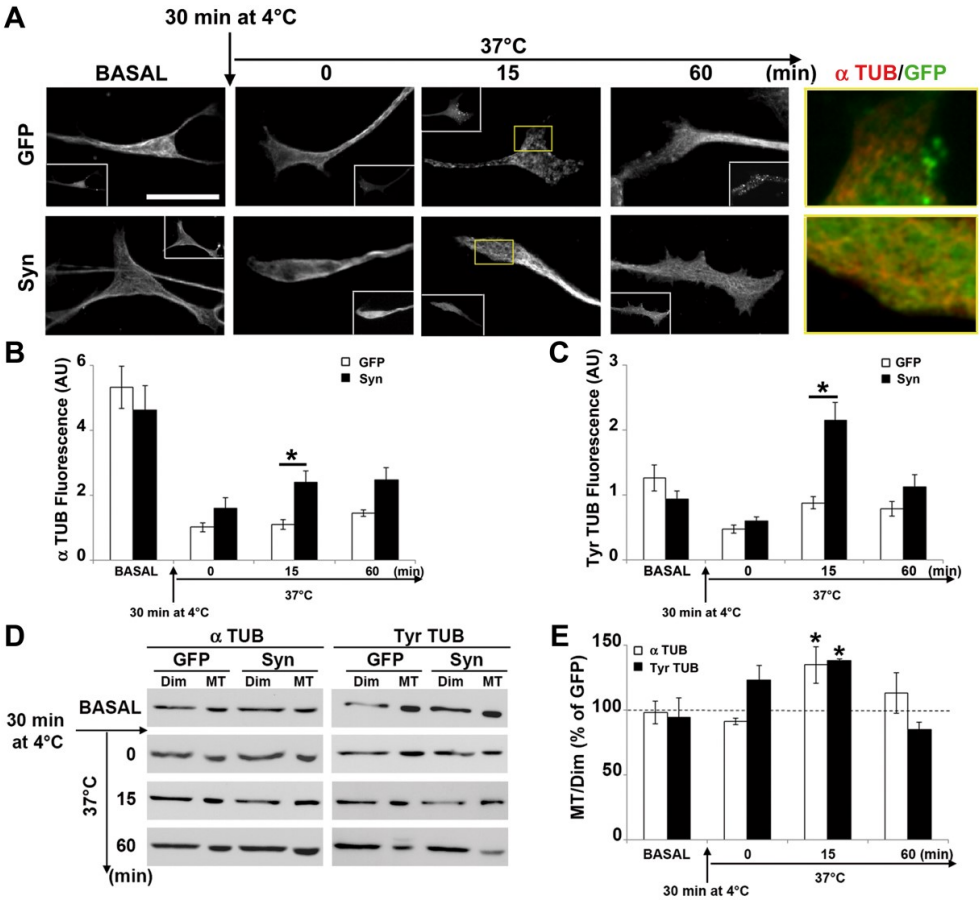
A
30 min at 4°C
37°C
BASAL
0
15
60
(min)
α TUB/GFP
GFP
Syn
B
α TUB Fluorescence (AU)
GFP
Syn
BASAL
0
15
60 (min)
37°C
30 min at 4°C
C
Tyr TUB Fluorescence (AU)
GFP
Syn
BASAL
0
15
60 (min)
37°C
30 min at 4°C
D
α TUB
Tyr TUB
GFP
Syn
Dim
MT
30 min at 4°C
BASAL
0
15
60
37°C
(min)
E
α TUB
Tyr TUB
MT/Dim (% of GFP)
BASAL
0
15
60 (min)
37°C
30 min at 4°C

**FIGURE 2**

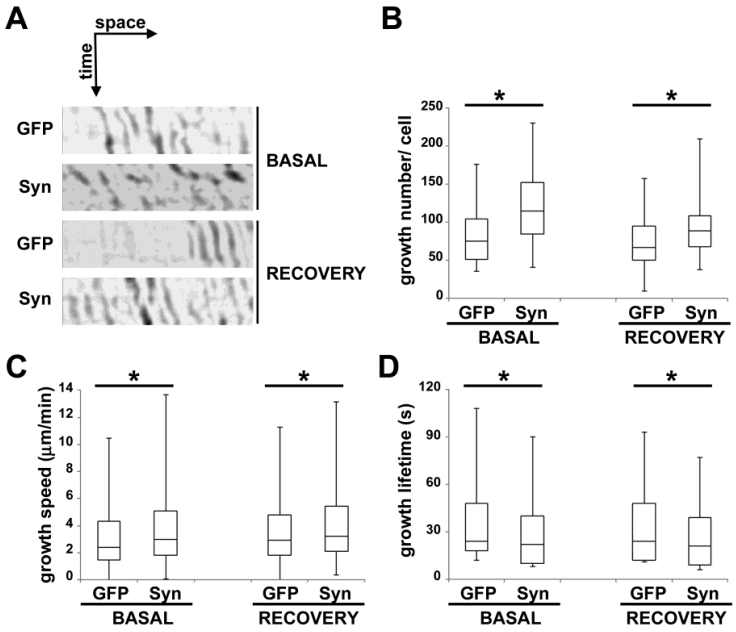
A
space
time
GFP
Syn
BASAL
GFP
Syn
RECOVERY
B
growth number/ cell
250
200
150
100
50
0
*
*
GFP Syn
BASAL
GFP Syn
RECOVERY
C
growth speed (µm/min)
14
12
10
8
6
4
2
0
*
*
GFP Syn
BASAL
GFP Syn
RECOVERY
D
growth lifetime (s)
120
90
60
30
0
*
*
GFP Syn
BASAL
GFP Syn
RECOVERY

**FIGURE 3**

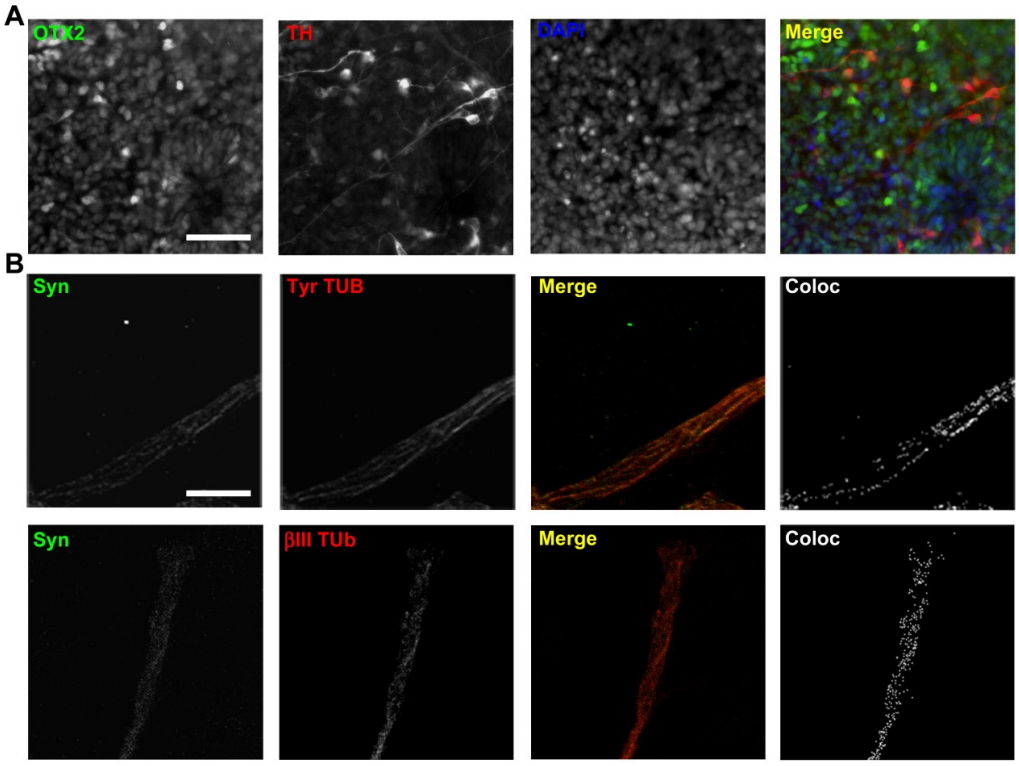
A
OTX2
TH
DAPI
Merge
B
Syn
Tyr TUB
Merge
Coloc
Syn
βIII TUb
Merge
Coloc

**FIGURE 4**

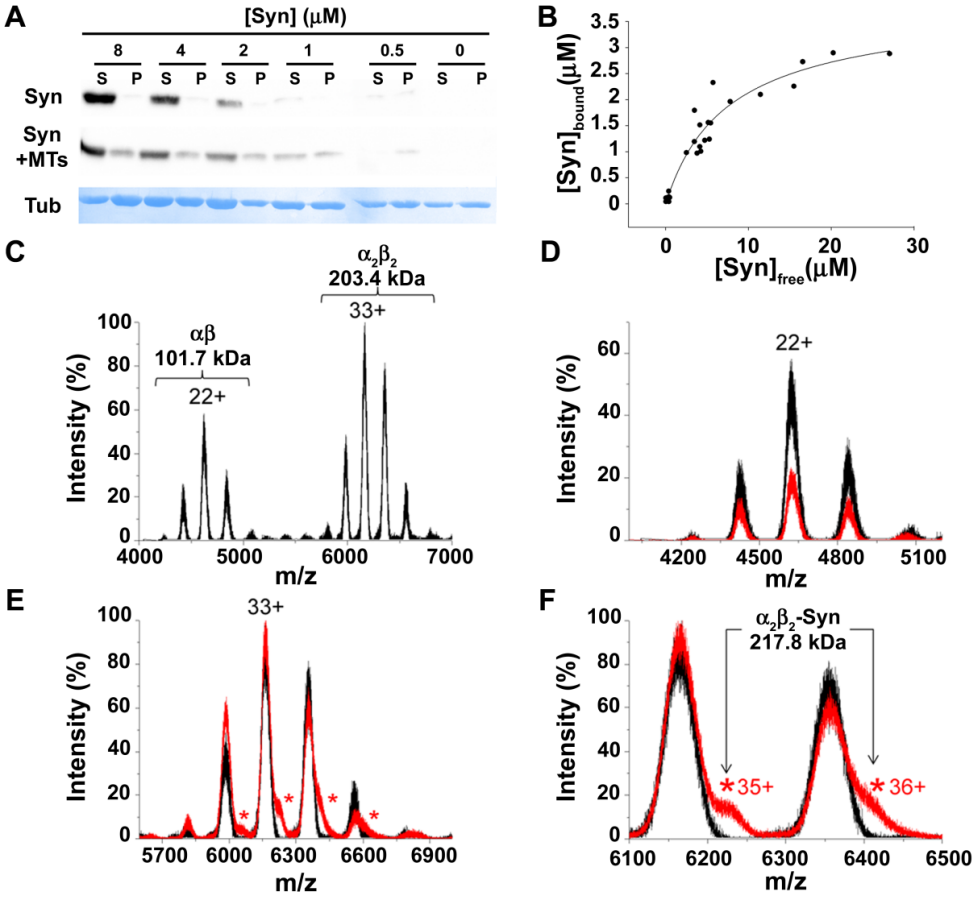
A
[Syn] (μM)
8
4
2
1
0.5
0
S P S P S P S P S P S P
Syn
Syn +MTs
Tub
B
[Syn]bound(μM)
[Syn]free(μM)
C
α2β2 203.4 kDa
33+
αβ 101.7 kDa
22+
Intensity (%)
m/z
D
22+
Intensity (%)
m/z
E
33+
Intensity (%)
m/z
F
α2β2-Syn 217.8 kDa
35+
36+
Intensity (%)
m/z

**FIGURE 5**

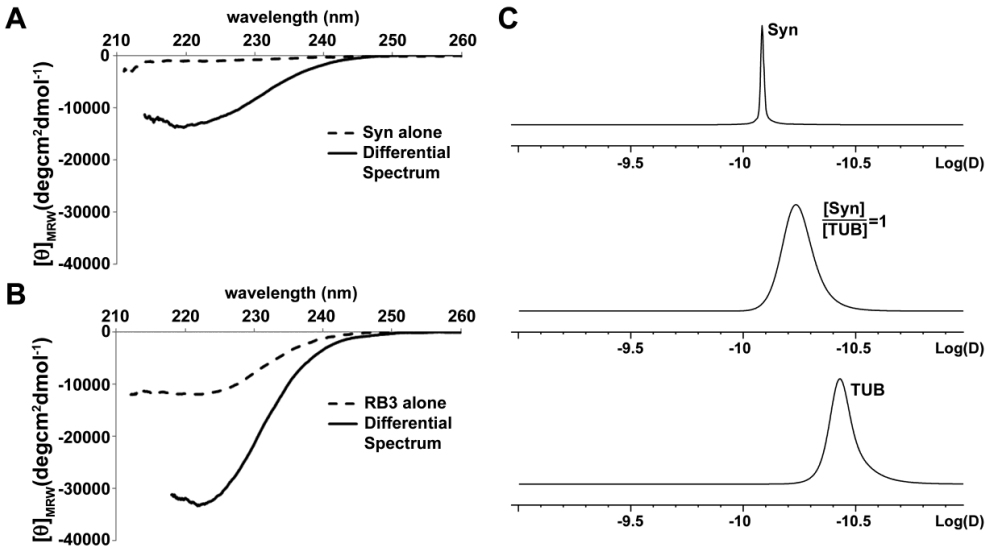
A
wavelength (nm)
210
220
230
240
250
260
0
-10000
-20000
-30000
-40000
[θ]MRW(degcm2dmol-1)
Syn alone
Differential Spectrum
B
wavelength (nm)
RB3 alone
Differential Spectrum
C
Syn
-9.5
-10
-10.5
Log(D)
[Syn]/[TUB]=1
TUB

**FIGURE 6**

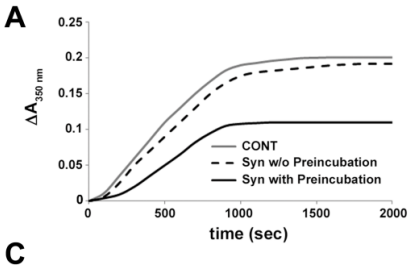


**B**

| Kinetic parameters | CONT | Syn w/o Preincubation | Syn with Preincubation | |
|---|---|---|---|---|
| *P* value | 2.76±0.26 | 3.08±0.3 | 2.08±0.2 | *,# |
| Vi (ΔA/min) | 0.01±0.001 | 0.012±0.001 | 0.005±0.001 | *,# |
| ΔA | 0.196±0.015 | 0.192±0.021 | 0.11±0.02 | *,# |

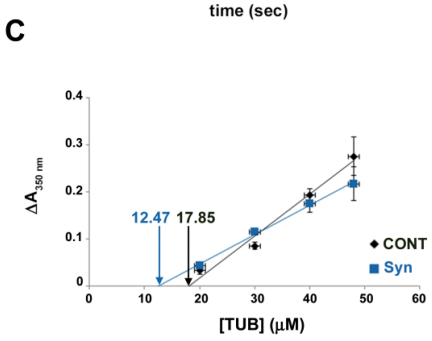


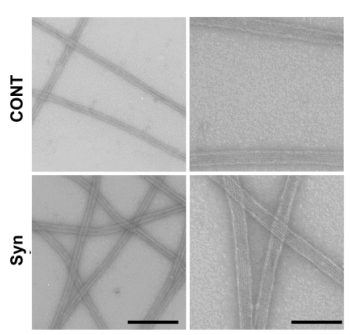


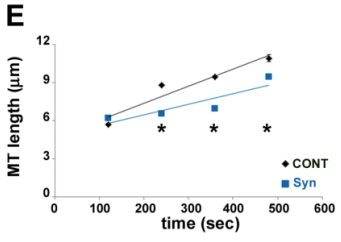


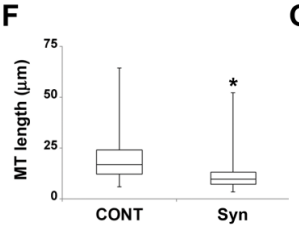


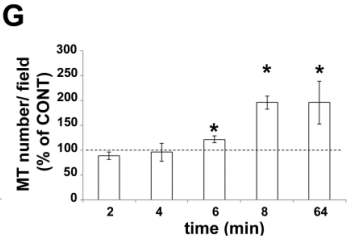


**FIGURE 7**

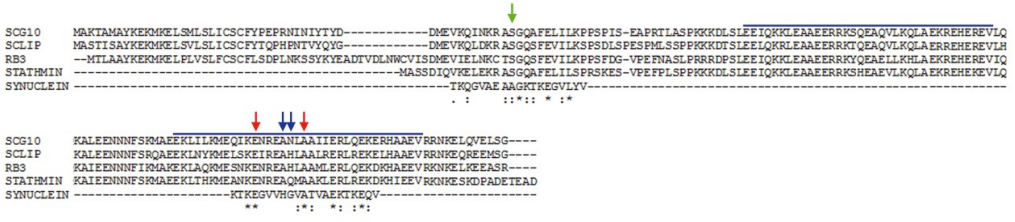

**FIGURE 8**

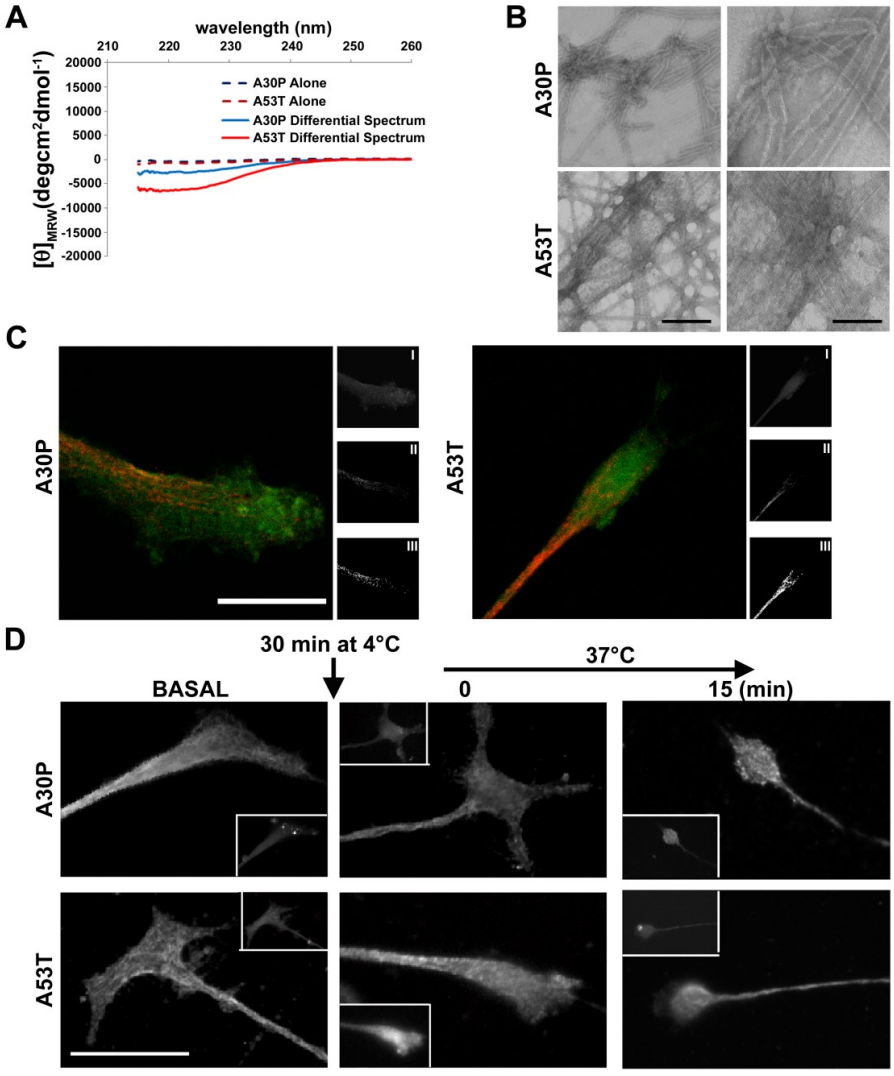
A
wavelength (nm)
210
220
230
240
250
260
20000
15000
10000
5000
0
-5000
-10000
-15000
-20000
[θ]MRW(degcm2dmol-1)
A30P Alone
A53T Alone
A30P Differential Spectrum
A53T Differential Spectrum
B
A30P
A53T
C
A30P
A53T
I
II
III
D
30 min at 4°C
37°C
BASAL
0
15 (min)
A30P
A53T

**FIGURE 9**

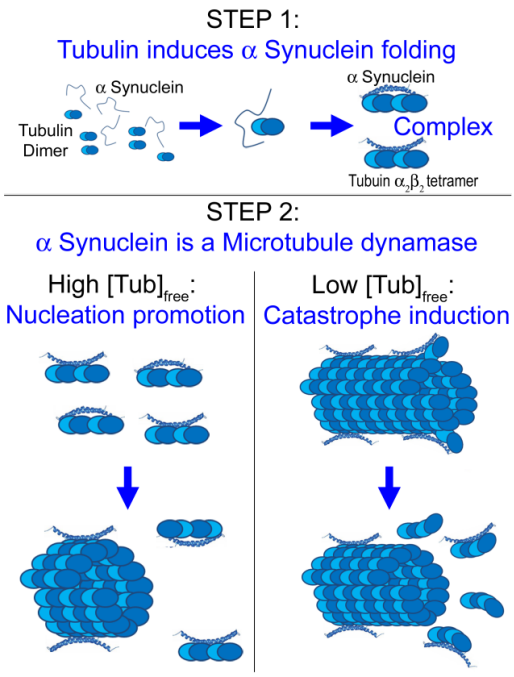
STEP 1:
Tubulin induces α Synuclein folding
α Synuclein
Tubulin Dimer
α Synuclein
Complex
Tubuin α2β2 tetramer
STEP 2:
α Synuclein is a Microtubule dynamase
High [Tub]free:
Nucleation promotion
Low [Tub]free:
Catastrophe induction

**FIGURE S1**

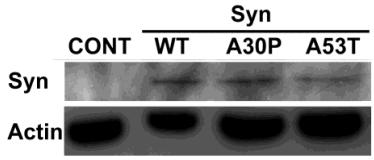


**FIGURE S2**

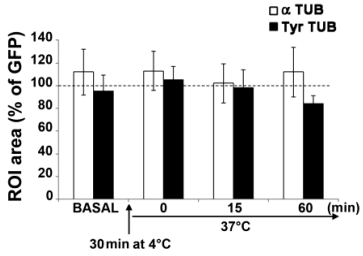


**FIGURE S3**

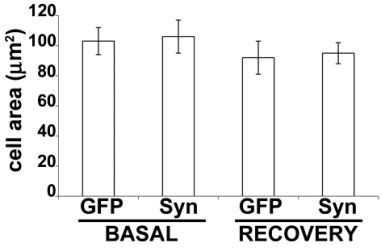

FIGURE S4

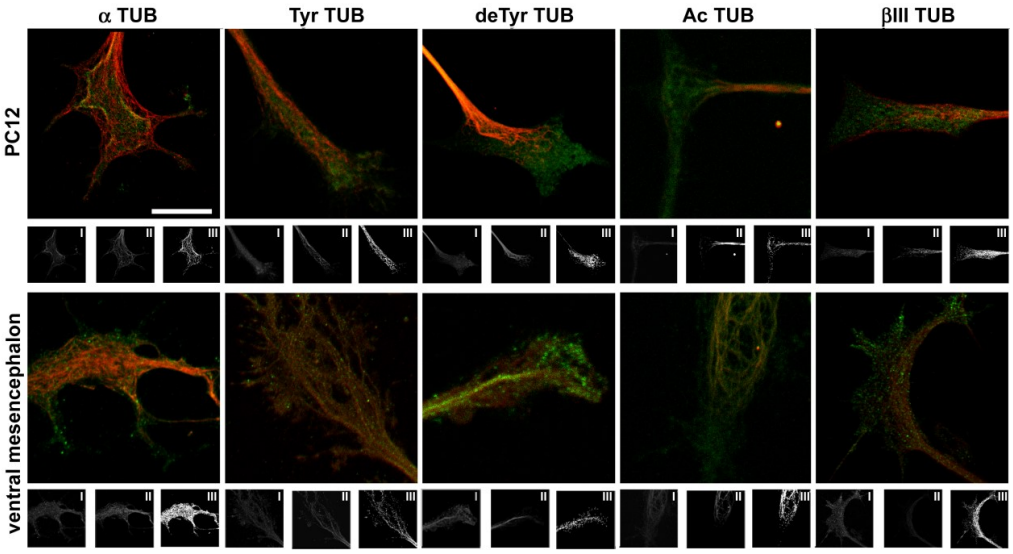


**FIGURE S5**

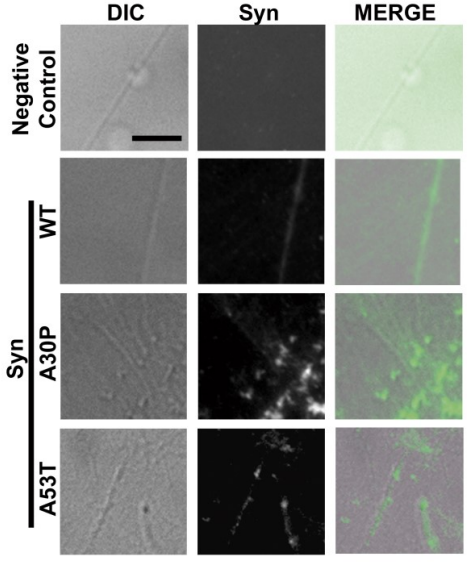

**FIGURE S6**

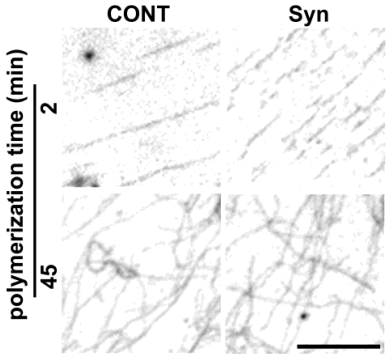


**FIGURE S7**

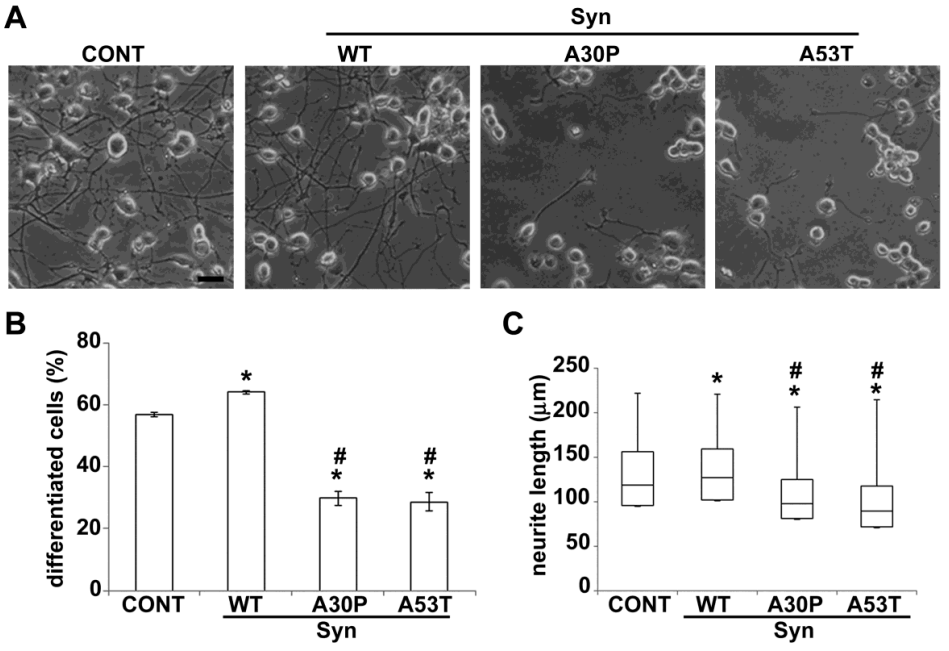

| | PC12 cells | | | ventral mesencephalon neurons |
|---|---|---|---|---|
| | WT | A30P | A53T | |
| α TUB | 0.89±0.04 | 0.68±0.05 (*) | 0.77±0.05 (*) | 0.70±0.07 |
| Tyr TUB | 0.89±0.07 | 0.88±0.05 | 0.82±0.07 | 0.72±0.02 |
| deTyr TUB | 0.55±0.03 | 0.60±0.01 | 0.61±0.03 | 0.54±0.05 |
| Ac TUB | 0.72±0.02 | 0.59±0.07 | 0.47±0.02 (*) | 0.68±0.06 |
| βIII TUB | 0.84±0.01 | 0.84±0.02 | 0.86±0.01 | 0.68±0.05 |

**Table 1.** Syn co-localizes with MTs in neuronal cells**.** Manders' coefficient representing the overlapping between transfected GFP-Syn (PC12 cells) or endogenous Syn (ventral mesencephalon neurons from mouse embryo) and total α tubulin (α TUB), its posttranslational modifications (Tyr TUB, deTyr TUB and Ac TUB) and βIII tubulin (βIII TUB), calculated according to Bolte and Cordelieres [17] and using a threshold-based approach. *$p<0.05$ vs WT according to ANOVA, Dunnett *post hoc* test.

| | Tub 10µM | | | Tub 15µM | | | |
|---|---|---|---|---|---|---|---|
| | Syn 0µM | Syn 5µM | Syn 10µM | Syn 0µM | Syn 5µM | Syn 10µM | Syn 15µM |
| $V_{growth}$ (µm/min) | 1.2 ± 0.1<br>n=1097 | 1.38 ± 0.5<br>n=362 | 1.08 ± 0.18<br>n=395 | 1.1 ± 0.086<br>n=1420 | 1.17 ± 0.14<br>n=663 | 1.38 ± 0.14*<br>n=695 | 1.32 ± 0.24*<br>n=973 |
| $V_{shrinkage}$ (µm/min) | 8.7 ± 2.24<br>n=357 | 7.35 ± 2.1<br>n=209 | 7.5 ± 1.65<br>n=309 | 11 ± 1.77<br>n=287 | 8.6 ± 2<br>n=216 | 11.7 ± 2.6<br>n=298 | 8.5 ± 2.24<br>n=336 |
| $F_{catastrophe}$ ($min^{-1}$) | 0.16 ± 0.05<br>n=9 | 1.04 ± 0.3<br>n=12 | 0.69 ± 0.17<br>n=15 | 0.09 ± 0.03<br>n=9 | 0.27 ± 0.07<br>n=14 | 0.26 ± 0.07<br>n=12 | 0.22 ± 0.06<br>n=11 |
| $F_{rescue}$ ($min^{-1}$) | 0.15<br>n=1 | 0.67 ± 0.33<br>n=4 | 0.33 ± 0.19<br>n=3 | 0.1<br>n=1 | 0.6 ±0.26<br>n=5 | 0.44 ± 0.22<br>n=4 | 1.26 ± 0.44<br>n=8 |
| Growth Duration (s) | 3327 | 692 | 1304 | 5797 | 3056 | 2751 | 2944 |
| Shrinkage Duration (s) | 382 | 356 | 537 | 594 | 512 | 540 | 380 |
| MT number | 32 | 14 | 16 | 41 | 22 | 25 | 20 |

**Table 2.** Folded Syn increases MT dynamics *in vitro***.** Dynamic parameters were determined by VE-DIC light microscopy for MTs assembled from purified axonemes in the presence of tubulin (10 and 15 µM) and increasing concentrations of Syn (0-15 µM). Velocities are expressed as mean ± SEM. The total growth and shrinkage times analysed, as well as the number of MTs used for each condition, are given in the last three rows. Catastrophe and rescue frequencies were calculated by dividing the total number of events by the time spent in growth and shrinkage, respectively. The standard deviation is calculated by dividing $F_{catastrophe}$ or $F_{rescue}$ by $\sqrt{n}$ assuming a Poisson distribution [27]. (*n*) represents the total number of measurements for the growth and shrinkage rates, and the total number of observed events for the catastrophe and rescue frequencies. *$p<0.05$ vs Syn 0µM, according to ANOVA, Dunnett *post hoc* test.